Spatial variations in the geochemistry of arc volcanism in Central America

Dissertation

zur Erlangung des Doktorgrades

der Mathematisch-Naturwissenschaftlichen Fakultät

der Christian-Albrechts-Universität

zu Kiel

Vorgelegt von

Ken Heydolph

Kiel

2010

Für Janne und ihre unendliche Geduld!

Für Ronja, Bente und Mads.

Referent/in.....Prof. Kaj Hoernle, Ph.D.

Koreferent/in.....PD Dr. Thor Hansteen, Ph.D.

Tag der mündlichen Prüfung.....27.04.2010

Zum Druck genehmigt: Kiel,.....27.04.2010

Prof. Dr. Gerhard Fouquet (Präsident)

Hiermit erkläre ich, dass ich die vorliegende Doktorarbeit selbstständig und ohne unerlaubte Hilfen erstellt habe. Ferner habe ich weder diese noch eine ähnliche Arbeit an einer anderen Abteilung oder Hochschule im Rahmen eines Prüfungsverfahrens vorgelegt, veröffentlicht oder zur Veröffentlichung vorgelegt.

Kiel, den.....

Ken Heydolph

Zusammenfassung

Der Vulkanismus in Mittelamerika ist eine Folge der Subduktion der Cocosplatte unter die Karibische Platte. Die dadurch entstehende mittelamerikanische Vulkankette (im Englischen: Central American Volcanic Arc – CAVA) erstreckt sich über fast 1500 km parallel zum Mittelamerikanischen Graben von Guatemala im Nordwesten bis nach Costa Rica im Südosten. Charakteristisch für die mittelamerikanische Vulkankette ist eine systematische Änderung der tektonischen Parameter (z.B. Subduktionswinkel der Cocosplatte) und der geochemischen Zusammensetzung der subduzierenden Platte und der darüber liegenden Kruste. Entlang und quer zu dieser vulkanischen Front, befinden sich zahlreiche z.T. noch aktive Vulkane und Vulkanzentren, die in den letzten Jahren das Ziel intensiver Forschung waren. Daraus entstanden eine Vielzahl häufig unvereinbarer unterschiedlicher Modelle, die verschiedene magmatische Quellen für den Ursprung der Vulkanite in Mittelamerika postulieren.

Im Rahmen dieser Dissertation entstanden neue Modelle, um die magmatischen Quellen der Vulkanite im Nordwesten und Südosten der mittelamerikanischen Vulkankette besser zu bestimmen. Dazu wurde ein neuer, umfassender Datensatz aus Haupt- und Spurenelement Konzentrationen, sowie verschiedener Isotopenverhältnisse (Sr-Nd-Pb und zum ersten Mal für mittelamerikanische Vulkanite Hf) von mafischen vulkanischen Gesteinsproben und verschiedener möglicher magmatischer Endglieder der subduzierenden Cocosplatte und der darüber liegenden Karibischen Platte erstellt. Systematische geochemische Variationen entlang und quer zur Vulkankette von Spurenelement Konzentrationen und Verhältnissen, besonders aber der Hf und Pb Isotopenverhältnisse zeigen deutlich, dass die Sedimente der subduzierenden Cocosplatte nicht zur magmatischen Quellzusammensetzung der Vulkanite im Nordwesten beitragen, wie in mehreren bereits publizierten Modellen angenommen wird. Mit Hilfe der neuen Daten kann vielmehr ein System aus drei magmatischen Endgliedern beschrieben werden, dass die beobachteten systematischen geochemischen Variationen für den Vulkanismus in NW Mittelamerika erklärt. Eine angereicherte (d.h. radiogene Pb und Sr, aber unradiogene Hf und Nd Isotopenverhältnisse) magmatische Quelle in der Lithosphäre unterhalb von Guatemala

bildet dabei das nordwestliche magmatische Endglied für die Vulkanite der mittelamerikanischen Vulkankette. Der südöstliche Teil der Vulkankette ist charakterisiert durch die Subduktion des Cocos Rückens und einer angrenzenden submarinen Vulkanprovinz vor Costa Rica. Diese, durch den Galapagos Hotspot geprägten tektonischen Erhebungen, zeigen eine besondere, angereicherte Isotopen-Signatur, die Galapagos Ozeaninseln Basalt (OIB) Signatur (d.h. radiogene Pb und Hf Isotopenverhältnisse). Die im Rahmen dieser Dissertation neugewonnenen Daten von mafischen Vulkaniten aus Costa Rica und Panama zeigen einen von Zentral-Costa Rica nach Nicaragua systematisch abnehmenden aber anfänglich sehr starken Einfluß der subduzierenden Galapagos-Hotspot submarine Vulkanprovinz auf die Quelle für die Vulkanite.

.

Abstract

Volcanism in Central America results from the subduction of the Cocos plate beneath the Caribbean plate. The resulting central American Volcanic arc (CAVA) extends for ~1500 km parallel to the Middle American Trench from Guatemala in the northwest to Costa Rica in the southeast. Characteristic for the CAVA are systematic variations in tectonic parameters (e.g. subducting angle of the Cocos plate), the composition of the subducting plate and the overlying crust. Various partly still active volcanoes and volcanic centers are located along and across the arc and have been subject to intensive research for the past years. The numerous and often contradicting individual models for the origin of arc volcanics in Central America propose a variety of distinct magmatic sources.

This dissertation provides new models for the magmatic sources of northwestern and southeastern CAVA rocks. A new and comprehensive dataset of main and trace elements concentrations and ratios, and isotope ratios (Sr-Nd-Pb and for the first time for Central American volcanics Hf) of mafic volcanics und potential magmatic endmembers from the subducting Cocos plate and the overlying Caribbean Plate has been established. Systematic along and across arc geochemical variations of trace element concentrations and ratios and isotope ratios (in particular of Hf and Pb) clearly show that subducting Cocos plate sediments have no influence on the magmatic source components for NW CAVA rocks, as has been proposed by several already published models. The new dataset provides a system of three magmatic endmember components which can explain the observed systematic geochemical variations of NW CAVA rocks. The northwestern CAVA endmember is an enriched magmatic component in the lithosphere beneath Guatemala. The southeastern part of the arc is characterized by the offshore Costa Rica subducting Cocos and Coiba ridges and a neighboring subducting seamount province, which all show an enriched Galapagos hotspot influenced ocean island basalt (OIB) signature (i.e. radiogenic Pb and Hf but unradiogenic Sr and Nd isotopic ratios). New data from mafic volcanics from Costa Rica and Panama show a strong, though systematically from Costa Rica to Nicaragua

decreasing influence of the subducting Galapagos hotspot seamount province on the magmatic source composition of the volcanic

Vorwort

Diese Arbeit stellt in ihrer Gesamtheit eine monographische Dissertation dar, die aus vier unabhängigen Kapiteln besteht. Diese sind zum Teil zur Veröffentlichung vorgesehen.

Diese Dissertation entstand auf Anregung von Prof. Dr. Kaj Hoernle, im Rahmen des durch die Deutsche Forschungsgemeinschaft (DFG) geförderten Sonderforschungsbereiches 574 - Volatile und Fluide in Subduktionszonen: Klimarückkopplungen und Auslösemechanismen von Naturkatastrophen. Ihm gilt mein besonderer Dank für die Vergabe dieser Arbeit, sowie seine Unterstützung, sowohl im Gelände als auch im Institut, durch zahlreiche Diskussionen und wichtige Denkanstösse. Ich habe viel gelernt!

Ebenfalls danke ich Thor Hansteen für das Koreferat.

Mein weiterer besonderer Dank gilt Dr. P.v.d. Bogaard für seine umfassende Hilfe bei der Geländearbeit, die den Grundstein zu dieser Arbeit bildete; Dr. F. Hauff, Dr. J. Fietzke, Dipl.-Ing. J. Sticklus und S. Hauff für ihre Assistenz und unschätzbare Hilfe bei der Einarbeitung und Durchführung in die Isotopenanalytik, ohne die diese Dissertation nicht durchführbar gewesen wäre. Ich danke D. Rau für die RFA Analytik, die die Basis für die weiteren Verlauf der Probenauswahl bildete.

Dr. J. Geldmacher, Dr. M. Portnyagin und Dr. S. Duggen danke ich für ihre Diskussionsbereitschaft und hilfreichen Kommentare. Ich danke Dr. R. Werner für seine langjährige Unterstützung im Hintergrund, die mir immer wieder geholfen hat.

Desweiteren danke ich Dr. D. Garbe-Schönberg, Heidi Blaschek, Petra Fiedler, Ulrike Westernströer und Inge Dold für ihre Unterstützung bei der ICP-MS Analytik.

Meinen Hiwis Julia, Philipp und Carina danke ich für immer zuverlässige Probenaufbereitung.

Heidi Wehrmann, Christian Timm, Nikolaus Bigalke, Rieka Harders, Cosima Burkert Steffen Kutterolf, Mathias Marquardt, Seth Sadofsky, Britta Lissin (und natürlich allen anderen vom SFB 574 und IFM-GEOMAR die dabei waren) danke ich für die vielen netten Mensabesuche und Kaffeepausen, guten und unterhaltsamen Gespräche und Zerstreuungen.

Mein größter Dank geht an Janne und die Kleinen (Ronja, Bente und Mads). Ohne sie wäre ich niemals in der Lage gewesen, meine Arbeit in dieser Form durchzuführen. Vielen Dank!

Contents

Table of Figures

1 Chapter 1: Introduction

1.1 Geological background

Subduction zones (Figure 1) mark the one side on the earth where oceanic lithosphere is recycled back into the mantle (e.g. Stern, 2002; Tatsumi, 2005;). Here one oceanic lithosphere is being subducted beneath another one or continental lithosphere. Consisting of oceanic sediments (pelagic, carbonate and/ or terrigenous) and basaltic oceanic crust (altered/ hydrated or fresh), the lithospheric plate transports material from various geochemical distinct sources in the subduction zone. The release of hydrous fluids or melts from the downgoing plate into the overlying mantle wedge causes partial melting, which results in arc volcanism. In general the subducting slab contributes to the overlying arc volcanism (e.g. Morris, 1991; Plank and Langmuir, 1993). Arc volcanoes therefore provide excellent opportunities on detailed geochemical information on the various contributing source components of the subduction zone (e.g. subducting plate, mantle wedge and overlying crust).

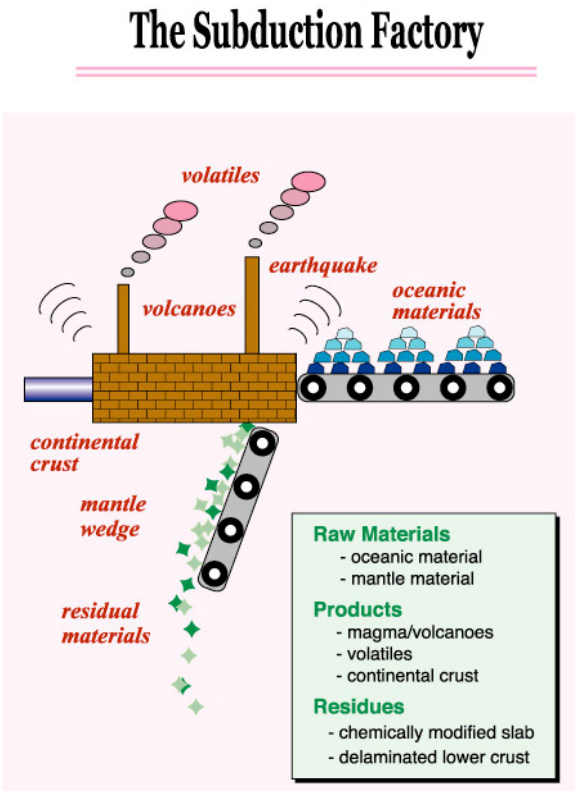

Figure 1.1. Cartoon illustration of the subduction factory, after Tatsumi (JAMSTEC).

Igneous rocks from arc volcanoes in subduction zones are generally enriched in large ion lithophile elements (LILE) relative to light rare earth elements (LREE) and high field strength elements (HFSE) (e.g. Arculus, 1994). Ratios of more to less fluid mobile trace elements (e.g. Ba/La, Ba/ Nb, U/Th, Sr/Ce) are therefore sensitive to the intensity of fluid flux from subducting slab-derived fluids (e.g. Patino et al., 2000; Sadofsky et al., 2008). Other trace element ratios can be used to estimate the degree of partial melting (e.g. La/Yb and Zr/ Hf), however trace element ratios can generally be modified by physical processes like partial melting or magma differentiation. Radiogenic isotope ratios on the other hand are not affected by those processes and therefore can be used to determine the contribution of distinct magmatic sources to arc magmatism. Though considering the elements for which isotope data is available in this dissertation, Pb generally is the most fluid-mobile in subduction systems, followed by Sr, whereas Nd and Hf are considered to be relatively fluid-immobile (e.g. Pearce et al., 2007). Hence high fluid flux in subduction zones and the resulting subduction input can dominate the isotopic composition of e.g. lead.

1.2 Thesis outline

The main reason for this dissertation was to study spatial geochemical evolution along and across the Central American Volcanic Arc. In Central America several systematically varying tectonic parameters (e.g. subduction angle and velocity of the subducting Cocos plate, thickness of the lithosphere) and chemical composition of the overlying Caribbean plate coincide with systematic geochemical variations along the volcanic front from Guatemala to Costa Rica and Panama. The large number of existing models for the Central American Arc volcanism, which are sometimes quite contradicting, cannot explain the new data presented by this thesis. A new model, which is based on the new dataset and tested against existing models, led to surprising results about the feasibility of already suggested magmatic sources.

The work is presented here in three independent chapter (II, III, IV), which are designed for future publication or are already published. The chapters deal with the different parts

of the Central American Volcanic Arc. Chapter II describes the northwestern part, extending from Guatemala to NW Nicaragua. Chapter III and IV describe the southeastern part of the arc, extending from Panama and Costa Rica to NW Nicaragua, which forms the centers of the arc. All chapters give an overview of previous work and existing models in the respective working areas.

2 Chapter

Along- and across-arc geochemical variations in northwestern Central America: Increased contribution of enriched lithosphere to lavas along the volcanic front from Nicaragua to Guatemala and behind the volcanic front

Ken Heydolph[1], Kaj Hoernle[1,2], Paul van den Bogaard[2], Folkmar Hauff[2]*

1 Sonderforschungsbereich 574, University of Kiel, Wischhofstr. 1-3, D-24148 Kiel, Germany;
2 Leibniz-Institut für Meereswissenschaften IFM-GEOMAR,
Wischhofstr. 1-3, D-24148 Kiel, Germany;
**Corresponding author*

In preparation for GCA

2.1 Abstract

The Central American Volcanic Arc (CAVA) has been subject of intensive research over the past years, leading to a variety of distinct models for the origin of CAVA lavas with various source components. We present a new model for the NW Central American Volcanic Arc based on a comprehensive new geochemical data set (major and trace element and Sr-Nd-Pb-Hf isotope ratios) of mafic volcanic front (VF), behind the volcanic front (BVF) and back-arc (BA) lava and tephra samples from NW Nicaragua, Honduras, El Salvador and Guatemala, subducting Cocos Plate sediments (from DSDP Leg 67 Sites 495 and 499) and igneous oceanic crust (from DSDP Leg 67 Site 495), and Guatemalan (Chortis Block) granitic and metamorphic continental basement. Although there are no systematic variations in Sr isotope ratios along the arc, Pb isotope ratios increase and Nd and Hf isotope ratios decrease systematically from NW

Nicaragua to Guatemala. Behind the volcanic front lavas have more radiogenic Pb and less radiogenic Nd and Hf isotopic compositions than related volcanic front lavas. We distinguish three endmembers for the volcanism in NW Central America: (1) NW Nicaraguan volcanic front (VF) samples with very high Ba/(La, Th) and U/Th, low La/Yb, relatively radiogenic Sr, Nd and Hf but unradiogenic Pb, 2) NW Guatemalan VF and Guatemalan and Honduran BVF samples with low Ba/(La, Th) and U/Th, high La/Yb, radiogenic Sr and Pb but unradiogenic Nd and Hf, and 3) Honduran and Nicaraguan behind the volcanic front (BVF) samples with low Ba/(La, Th) and U/Th, high La/Yb, unradiogenic Sr but radiogenic Nd, Hf and Pb. We interpret the NW Nicaragua VF endmember to be dominated by a largely serpentinite-derived fluid flux from the subducting slab, possibly with small amounts (<1 wt. %) of sediment melts, to a depleted N-MORB type of mantle wedge, resulting in large degrees of melting of primarily peridotitic material. The isotopically enriched Guatemala VF and BVF endmember could be derived from parental magmas for plutonic rocks in NW Central America, which crystallized pyroxenitic cumulates in the lithospheric mantle (and possibly lower crust) that were melted and contributed to Quaternary subduction-related volcanism. The presence of the enriched Guatemala endmember correlates largely with the presence of continental crust and crustal (and presumably lithospheric) thickness, i.e. the most enriched compositions occur where the crust is thickest. The isotopically depleted Honduras and Caribbean BA endmember could be derived from melting of young, recycled, oceanic crust in the asthenosphere upwelling in the back-arc, based on the OIB-like major and trace element but relatively depleted isotopic compositions of these samples. Mixing between these three endmember types of magmas can explain the observed systematic geochemical variations along and across the NW Central American Arc.

2.2 Introduction

Subduction zones mark the sites where an oceanic plate is subducted beneath an oceanic or continental plate, transferring lithospheric material back into the Earth's mantle. The release of fluids or hydrous melts from the subducting slab causes partial

melting in the mantle wedge resulting in arc volcanism. Therefore samples from arc volcanoes provide detailed geochemical information on various geochemically distinct source components contributing to subduction-related arc volcanism (e.g. subducting plate, mantle wedge and overlying crust).

Along the Central American subduction zone, where the Cocos Plate subducts beneath the Caribbean Plate, there are systematic variations in tectonic parameters, such as the subduction angle, thickness of the lithosphere and crust of the over-riding plate and the composition of the subducting Cocos Plate and the crust of the over-riding plate (e.g. Carr et al., 1984, 2003; Patino et al., 2000; Rüpke et al., 2004; Auger et al., 2006; Syracuse and Abers, 2006; Abers et al., 2007; Hoernle et al., 2008; MacKenzie et al., 2008). An exceptionally broad geochemical database for Central American volcanism has led to a large number of, in some cases conflicting, models for the generation of Central American arc volcanism, invoking a combination of diverse tectonic parameters, varying crustal compositions and potential source components. Below we briefly summarize the previous work and models proposed to explain geochemical variations along and across the arc in Central America.

Geochemical studies along the CAVA have identified several geochemically distinct endmembers. Carr et al. (1990) argued that Sr and Nd isotopic ratios of Central American volcanic rocks can be explained by mixing of four components: marine sediments from DSDP Site 495, MORB-source mantle (DM), EMORB-source mantle (EM) and continental crust. Mixing between DM and less than 0.5% marine sediments or fluids, form a modified mantle (MM) component. Most of the isotopic data form a trend between EM and MM, which is also well defined in the incompatible-element data e.g. Ba/La vs. La/Yb.

Feigenson and Carr (1993) used inverse modeling to calculate rare earth element patterns of Central American lava sources. Guatemalan and Costa Rican sources display high modal garnet contents and moderate-to-strong light rare earth element (LREE) enrichment, whereas Nicaraguan sources are defined by a slight LREE depletion and little to no modal garnet in the residuum. They propose that a broadly homogeneous but locally heterogeneous mantle wedge could contain relatively

enriched small-sized garnet-bearing veins surrounded by an isotopically depleted mantle peridotite matrix. Melting of distinct sources can be explained by the varying dip of the subducting lithosphere beneath the volcanic arc, which causes varying amounts of flux melting beneath the different arc segments.

Leeman et al. (1994, 1996) showed systematic along-arc variations in B/La ratio and strong correlations between B/La and $^{10}Be/^{9}Be$ ratios They proposed that a decrease in B/La and $^{10}Be/^{9}Be$ ratios along the volcanic front from Nicaragua to Guatemala reflect a decreasing subduction contribution to arc magma sources toward Guatemala.

Using lithium concentrations and isotopic compositions and their strong correlations with other fluid-mobile elements (e.g. B, ^{10}Be, U, $^{87}Sr/^{86}Sr$, LILE) from basaltic Central American Volcanic Arc lavas, Chan et al. (1999, 2000, 2002) provided more evidence for subduction-related modification of subarc mantle by slab-derived fluids. They argued that the low $\delta^{6}Li$ values for the fluids overlap with altered oceanic crust and marine sediment compositions and that Li and Sr isotopic systematics can be explained by small additions of fluids from these sources to depleted or enriched mantle sources for the CAVA magmas.

Patino et al. (2000) used incompatible trace element ratios to demonstrate the role of two different Cocos Plate sediment units (i.e. carbonate and hemipelagic) on both local and regional geochemical variations in Central American arc lavas. Local geochemical variations in all arc segments, defined by trace element ratios with large differences between the stratigraphic units (e.g. Ba/Th and U/La), are a result of the relative variation in the amount of hemipelagic to carbonate sediment input into the magma generation process and in the flux of hydrous fluids (e.g. Ba/La and U/Th) from the subducting slab. In summary, the slab signal is strongest in the Nicaragua volcanic front lavas and decreases to the northwest and southeast along the volcanic arc and into the back arc.

Based on Sr-Nd-Pb isotope data, Feigenson et al. (2004) suggested that a combination of crustal contamination and subducted Cocos Plate sediments contribute

to the Guatemalan and Honduran magmas. Using oxygen isotope data, Eiler et al. (2005) also argued that partial melts of subducted Cocos Plate sediments contribute to Guatemalan magma sources, whereas dehydration of hydrothermally-altered rocks and/or serpentinites contribute to central Nicaraguan magma sources. Walker et al. (2007) linked variations in uranium and thorium disequilibria to crustal contamination of mafic central Guatemalan lavas but proposed that Nicaraguan magmas contain a maximum contribution of subducted Cocos Plate sediments, consistent with the high $^{10}Be/^{9}Be$ isotope ratios in the central Nicaraguan lavas (Morris et al. 1990).

Sadofsky et al. (2008) reported large heterogeneity of CAVA magma sources on local and regional scales using olivine melt inclusion compositions (i.e. major and trace elements and volatile components) from CAVA samples from Guatemala to Costa Rica. They relate these variations to variable contributions of various crustal and mantle components involved in magma genesis. Correlations of water and trace elements (e.g. Ti, Y and Na) and trace element ratios (e.g. Ba/La, B/La) indicate melting in the mantle wedge, fluxed by Ba-, B- and H_2O-rich, possibly serpentinite-derived, fluids, in particular beneath the central (Nicaraguan) part of the arc. On the other hand, components with melt-like properties, e.g. high Cl, S, F, LREE and La/Nb seem to control Guatemalan and Costa Rican magma generation.

Hoernle et al. (2008) argued, based on Pb and Nd isotopic and incompatible trace element (Ba/La and La/Yb), that a component with melt-like properties, derived from the subducting seamount province of the Galapagos hotspot track, is being added to the mantle wedge beneath Central Costa Rica. Systematic variations in isotopic composition of volcanic front volcanoes and arc-parallel seismic velocity anisotropy in the mantle wedge were interpreted to reflect northwestward flow of mantle from beneath Central Costa Rica to northwesternmost Nicaragua. Transfer of material from the slab beneath Nicaragua was interpreted to occur primarily through hydrous fluids derived from the subducting oceanic crust and/or serpentinites in the down-going slab +/- small amounts of sediment melting. Using trace element modeling, Gazel et al. (2009) also demonstrated that the Galapagos hotspot contribution decreases systematically along the volcanic front from central Costa Rica to NW Nicaragua and that small amounts of

sediment melts (≤0.6 wt. %) also contribute to the trace element signatures.

In this study, we present a comprehensive, new geochemical (major and trace elements and Sr-Nd-Pb-Hf isotope ratios) data set, in order to evaluate the different models for the origin of mafic VF and BVF lava and tephra samples from volcanic centers along and across the Central American Volcanic Arc in Guatemala through El Salvador and Honduras to NW-Nicaragua. We note that our study is the first to present Hf isotope data from Central America. Our data confirm systematic along- and across-arc variations in isotopic compositions and major and trace elements (e.g. Carr et al., 1990, 2003; Feigenson et al. 1993, 2004; Sadofsky et al., 2008). We also present new geochemical data from potential geochemical endmembers in the Central American subduction system: subducting Cocos Plate sediments (from DSDP Leg 67 Sites 495 and 499), igneous oceanic crust (from DSDP Leg 67 Site 495) and Guatemalan (Chortis Block) continental basement (granitic and metamorphic). Combined, the our extensive new geochemical datasets for volcanic rocks and subduction zone endmembers allow us to place further strong constraints on the sources involved in magma generation beneath northwestern Central America, allowing us to rule out some of the previous models and to propose some new models for the origin of some endmembers.

2.2.1 Geological overview

Subduction of the Cocos Plate beneath the Central America (Caribbean Plate) creates a chain of volcanoes extending for more than 1400 km from Tacaná Volcano near the Guatemalan-Mexican border to western Panama (Figure 1). These subduction-related volcanic centers can be divided into volcanic front (VF) – making up the main chain of volcanoes - and generally smaller behind the volcanic front (BVF) volcanic centers (Carr et al., 1984), up to 350 km from the trench. Several back-arc volcanic centers (BA) occur in Honduras (e.g. Yojoa and Utila Island) at a distance of 350 to 520 km from the trench. An extensive overview of the Central American geology can be found in e.g. Auboin et al. (1982); Carr et al. (1990, 2003); Protti et al. (1995). Below we summarize the Central American geology pertinent to this study.

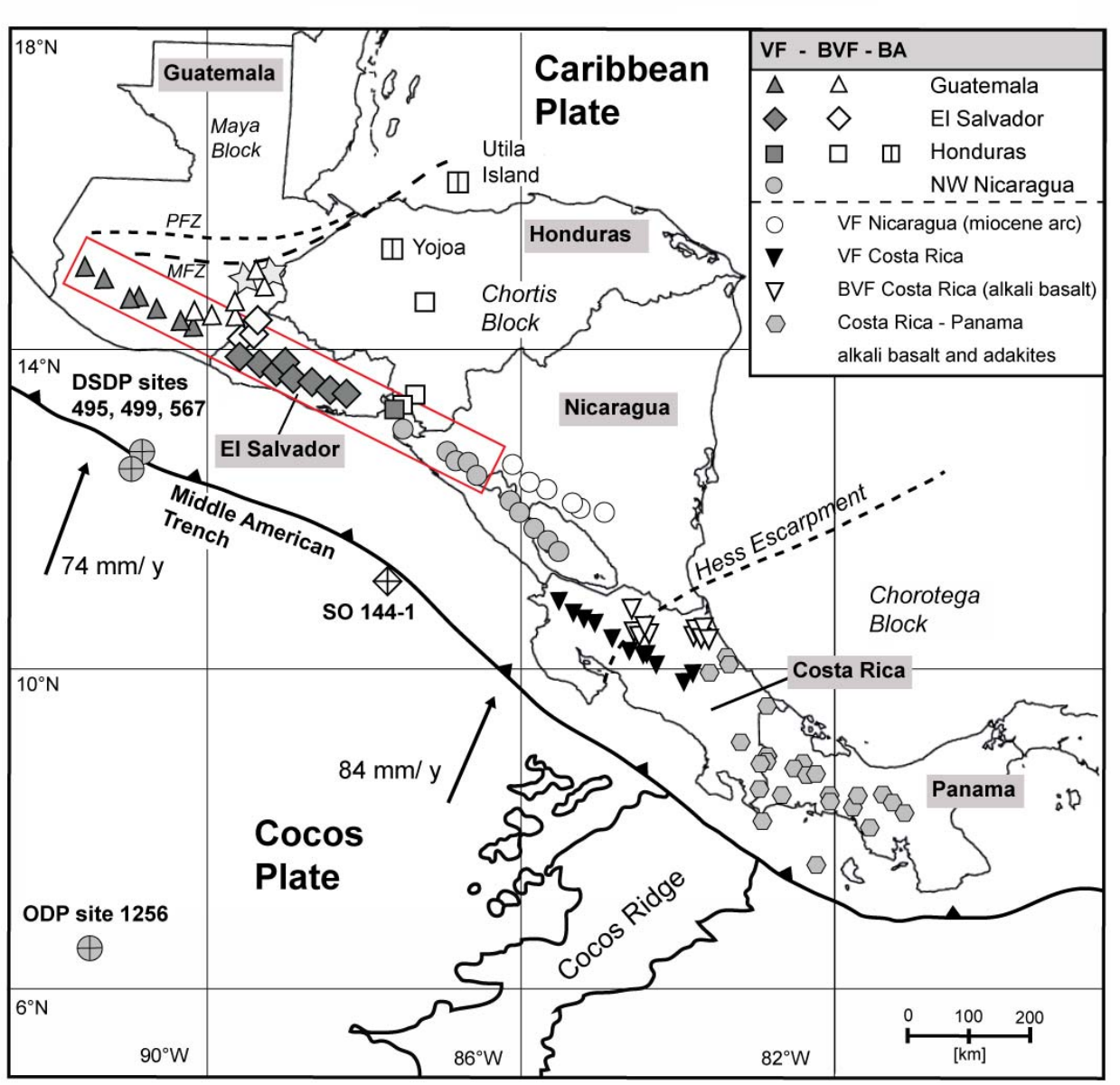

Figure 2.1

Overview map of Central America, showing the subduction of the Cocos Plate beneath the Caribbean Plate. Black arrows indicate direction of Cocos Plate motion and relative velocities to the Caribbean Plate (in mm per year) after DeMets (2001). Solid/shaded symbols mark volcanic front (VF) volcanoes, open symbols mark behind the volcanic front volcanoes (BVF) respectively. Back-arc (BA) samples from Lake Yojoa and Utila Island (both Honduras) marked with divided squares define a separate group. Guatemala basement samples from the Chiquimula pluton (unfilled stars). DSDP leg 67 and 84 drill sites (495, 499 and 567) and ODP leg 206 drill site 1256, marked with gray stars, provide samples for the subduction input (subducting sediments and altered oceanic crust and Guatemalan forearc basement). Data for samples from a seamount on the incoming plate outboard of Nicaragua obtained during the SO144 cruise are from Werner et al. (2003). The rectangle indicates the part of the VF investigated during this study. Data for BVF and BA samples from the northwestern Central American volcanic arc are also reported here.

In this paper, we concentrate on Quaternary subduction-related volcanism in the northwestern part of Central America, extending along the volcanic front from Momotombo Volcano in northwest Nicaragua to Santa Maria Volcano in northwest Guatemala to Utila Island (Caribbean) in the back-arc (Figure 1). The velocity of the north-northeast (~22°) subducting Cocos Plate, generated at the East Pacific Rise, ranges from 74 ± 5 mm/y offshore Guatemala to 84 ± 5 mm/y offshore Nicaragua (Figure 2.1) (DeMets, 2001). The age (~25 Ma; Protti et al., 1995) and composition of the Cocos Plate outboard of NW Nicaragua to Guatemala is similar, suggesting a similar subduction input for this part of the subduction system. The sediment input, which has been well-defined at Deep Sea Drilling Project (DSDP) Site 495 (Figure 1), can be divided into a lower, ~250 m thick, unit of carbonate ooze and an overlying, ~200 m thick, unit of hemipelagic clay (Auboin et al., 1982; Plank and Langmuir, 1998; Patino et al., 2000; Sadofsky et al., 2008). The upper oceanic lithospheric mantle appears to be extensively serpentinized, most likely due to the presence of bend faults cutting through the entire crust into the upper mantle (Rüpke et al., 2002; Abers et al., 2003; Ranero et al., 2003; Grevemeyer et al., 2007; Ivandic et al., 2008; Syracuse et al., 2008). The subduction margin along the Pacific margin of Central America has been shown to be erosional (Ranero and von Huene, 2000; Vannucchi et al., 2001; Vannucchi et al., 2004). The forearc from Guatemala to NW Costa Rica is likely to have a crudely similar composition, consisting of accreted intraplate and older arc assemblages (Hauff et al., 2000; Hoernle and Hauff, 2007; Geldmacher et al., 2008).

The composition of the overlying Caribbean Plate beneath the volcanic arc (Chortis Block) is variable, ranging from accreted oceanic igneous complexes beneath the VF in Nicaragua to continental crust beneath the Guatemala VF and the BVF regions in El Salvador, Honduras and Guatemala (Figure 2.1). In Central Guatemala, the Motagua-Polochic transform fault system, a 110 Ma old convergence zone, marks the transition from the Caribbean Plate (Chortis Block) to the North-American Plate (Maya Block) (Figure 1) (e.g. Donelly et al., 1990; Meschede and Frisch, 1998). From NW Nicaragua to NW Guatemala, the angle of the subducting plate also varies, decreasing from 64° to 48° (Syracuse and Abers, 2006) (Figure 2.2). The overlying crustal thickness increases from ~25 km beneath the

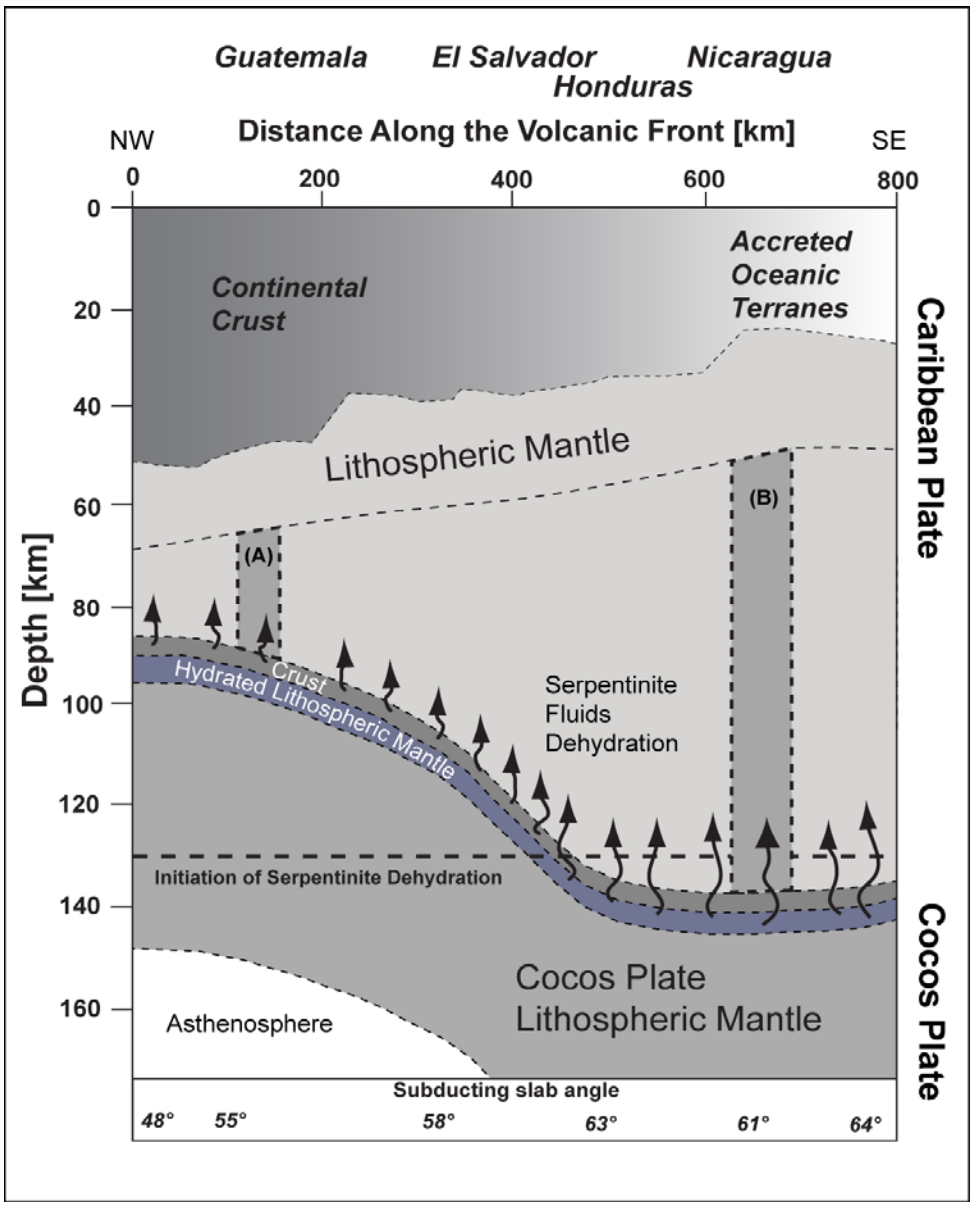

Figure 2.2 Schematic profile parallel to the volcanic front from Guatemala to NW Nicaragua as marked by red box in Figure 1, illustrating increasing crustal thickness and decreasing depth to the subducting slab surface going north from beneath Nicaragua to Guatemala. As a result, the thickness of the mantle wedge (and possible mantle melting columns denoted by a and b) decreases to the NW. Data for crustal thickness after Carr et al. (1984) and MacKenzie et al. (2008). Transition zone between continental and oceanic crust is still unspecified but occurs between NW Nicaragua and Central Guatemala. Values for subducting slab angle and averaged depth to the top of the slab after Syracuse and Abers (2006). The dashed line at ~130 km represents the beginning of serpentinite breakdown after Rüpke et al. (2002). Thickness of hydrated lithospheric mantle after Grevemeyer et al. (2007) and Ivandic et al. (2008) and beneath Nicaragua after MacKenzie et al. (2008).

Nicaraguan VF to ~46 km beneath the Guatemalan VF and with increasing distance behind the VF, for example to ~46 km in the Nicaragua back-arc (e.g. Ligorria & Molina, 1997; Narcia-Lopez et al., 2004; Auger et al., 2006; MacKenzie et al., 2008).

2.3 Analytical Methods

We collected the freshest mafic lava and tephra samples from the youngest volcanic events, historic when possible, from volcanic centers along and across the volcanic arc from Nicaragua to Guatemala, including the back-arc in Honduras. After removal of the altered outer surfaces, the samples were crushed to small rock/glass chips using a steel jaw crusher. The chips were then washed in distilled water in an ultrasonic bath, dried in a drying cabinet at 50°C, hand-picked under a binocular microscope and ground to powder (<63 µm) using an agate mill.

Major elements of whole rock samples (SiO_2, Al_2O_3, MgO, Fe_2O_3, CaO, Na_2O, K_2O, TiO_2, MnO and P_2O_5) were measured on fused glass beads using a Phillips X'Unique PW 1480 X-ray fluorescence spectrometer (XRF) with an Rh-tube at the Leibniz Institute of Marine Sciences, IFM-GEOMAR. Volatiles (H_2O and CO_2) were analyzed using an infrared photometer Rosemount CSA 5003. Analytical accuracy for major element concentrations for international reference standards (JA-2, JB-2, and JB-3) is generally better than 5 %, except for MnO (5 – 12 %) and P_2O_5 (4 – 10 %), of the suggested values by Govindaraju (1994).

Trace elements (Rb, Ba, Th, U, Nb, Ta, Pb, Sr, Ni, Cr, Tl, Li, Sc, V, Co, Cu, Zn, Cs, Sn, Mo, Hf, Zr, Y and the REE) were measured with a VG-Plasmaquad PQ1 inductively coupled plasma-mass spectrometer (ICP-MS) at the Institute of Geosciences, University of Kiel after the methods of Garbe-Schönberg (1993). Analytical accuracy for standard material BHVO-1 for all trace elements is better than 5.5 %, except for Sn and Pb (~12.5 %) and Tl (33 %). Analytical accuracy for standard material for AGV-1 is better than 10 %, except for Cr, Tl and Th (11 – 13%) and Li, Nb, Mo and Tm (21 – 28 %), based on the suggested reference values of Govindaraju (1994) and Jochum et al. (1994).

All isotope analyses were carried out at IFM-GEOMAR using a Thermo Finnigan TRITON (Sr, Nd isotopes) and Finnigan MAT 262-RPQ2+ (Pb, Sr isotopes) thermal ionization mass spectrometers and an AXIOM multiple collector ICP-MS (Hf isotopes), all operating in static mode. Sr-Nd-Pb isotope analyses, carried out in a Class 1000 clean room, were made on a subset of about 100mg whole rock powders of selected samples. The powders were weighed in Teflon beakers and digested in a solution of HF u.p. (ultra-pure) and HNO_3 (5:1) at 150°C for 60 hours. Ion chromatography was carried following the procedure by Hoernle and Tilton (1991), Hoernle et al. (2008) and Geldmacher et al. (2006). Within-run normalization factors were 0.1194 for $^{86}Sr/^{88}Sr$ and 0.7219 for $^{146}Nd/^{144}Nd$. All errors are reported as 2 sigma of the mean. Sr standard NBS 987 averaged during 4 analysis sessions yielded $^{87}Sr/^{88}Sr$ = 0.710234 ± 0.000034 (N=35) and the in-house Nd-monitor SPEX $^{143}Nd/^{144}Nd$ = 0.511720 ± 0.000018 (N=32). Isotope ratios were normalized to 0.710250 (NBS 987) for $^{87}Sr/^{88}Sr$ and 0.511715 (Nd-SPEX; equivalent to a value of 0.511850 for the La Jolla standard) for $^{143}Nd/^{144}Nd$. Lead isotope ratios are normalized to NBS 981 values from Todt et al. (1996). The long-term reproducibility of NBS 981 is $^{206}Pb/^{204}Pb$ = 16.902 ± 0.009, $^{207}Pb/^{204}Pb$ = 15.441 ± 0.012 and $^{208}Pb/^{204}Pb$ = 36.537 ± 0.038 (n=22). Total blanks for Pb chemistry were <100 pg and thus are considered negligible. Hafnium isotope ratios were determined on a subset of samples. 200-500 mg of rock chips were digested for 60 hours at 130˚C in a HF-HNO_3 mixture and chemical separation followed the procedures outlined in Blichert-Toft et al. (1997). For detailed descriptions of MC-ICP-MS setup and analyzing modes see Geldmacher et al. (2006). The JMC 475 Hf-reference standard gave $^{176}Hf/^{177}Hf$ = 0.28216 (n=25) and all measured Hf values were corrected to JMC 475= 0.282163 (Blichert-Toft et al., 1997).

2.4 Results

Seventy-six mafic (MgO >2 wt %) volcanic whole-rock samples (36 lava and 40 tephra samples for which microprobe whole rock and melt inclusion data are reported in Sadofsky et al., 2008 from major volcanic centers along and across the northwestern Central American Volcanic Arc from NW Nicaragua (Momotombo Volcano) through El

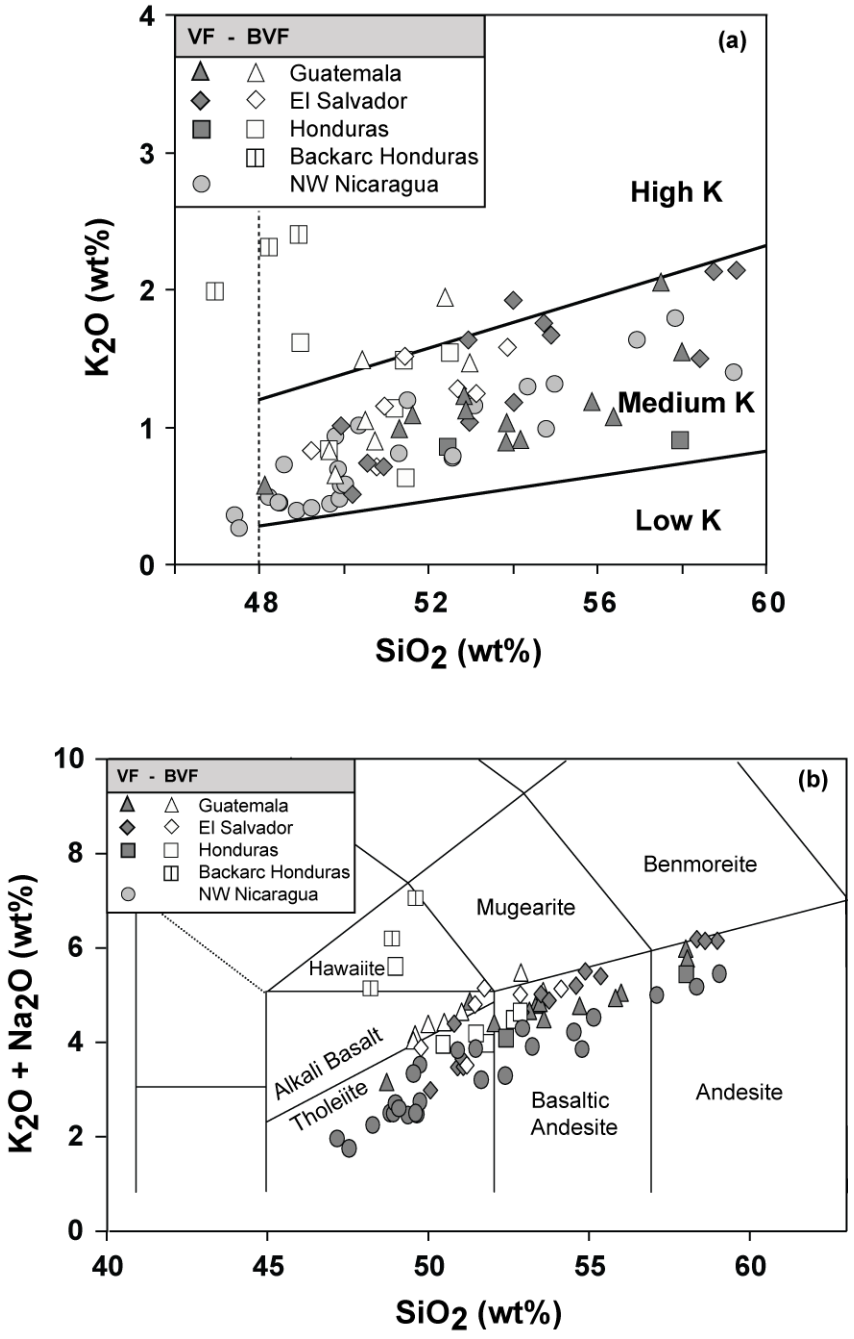

Figure 2.3 Major element classification diagrams for northwestern Central American subduction-related volcanic rocks. (a) SiO2 versus K2O classification diagram (after Le Maitre et al., 1989). Mafic (MgO>2 wt %) volcanic front (VF) rocks plot within the Medium K or calc-alkaline series field, whereas the behind the volcanic front (BVF) and back-arc (BA) samples overlap the VF field and extend into the High K or High-K Calc-alkaline series. (b) Total Alkali versus Silica (TAS) diagram after Le Maitre et al. (2002) with data normalized to 100% on a volatile-free basis, included subdivision line for alkali basalts and tholeiites after MacDonald and Katsura (1964). Solid symbols indicate VF and open symbols BVF and BA samples. See Table 1 for geochemical data in this diagram.

Salvador and Honduras to NW Guatemala have been analyzed for major and trace elements (Table 2.1). All of these samples have also been analyzed for Sr, Nd, Pb (additional data from the NW Nicaragua samples are reported in Hoernle et al., 2008 (Nd and Pb isotope data) and Gazel et al., 2009 (Sr isotope data)) and a subset of 30 samples for Hf isotopes (Table 2.2). Tables 2.1 and 2.2 also include data from samples of the granitic (Chor 8A, P12, G3, G009 L1 and G009 L2) and metamorphic (GU M1, GU M2, 619 and 714A) Guatemalan basement and Cocos Plate sediments and oceanic crust from DSDP Leg 67 Site 495 and ODP Leg 206 Site 1256 offshore Guatemala (Figure 2.1)

2.4.1 Major and Trace element data

On a SiO_2 vs. K_2O classification diagram for subalkalic rocks (Figure 2.3a), VF samples from NW Nicaragua through El Salvador and Honduras to NW Guatemala have compositions within the Medium-K or Calc-alkaline series and BVF samples overlap the VF samples and extend into the High K or High-K Calc-alkaline series. The BA samples have alkalic compositions, similar to hawaiites on a Total Alkali vs. Silica (TAS) diagram (Figure 2.3b).

The most mafic (MgO = 5-8 wt.%) Guatemalan VF whole-rock samples extend to lower FeO_t (total iron as FeO), CaO, MnO and slightly higher SiO_2, TiO_2 and N a_2O contents than samples from Nicaragua with similar MgO content (Figure 2.4a-i), consistent with previous studies of major element concentrations of whole rocks (e.g. Carr et al., 1990, 2003; Patino et al., 2000) and olivine-hosted melt inclusions (Sadofsky et al., 2008). At a given MgO content El Salvador VF and Honduras VF samples show major element concentrations between corresponding VF samples from NW Guatemala and Nicaragua. Behind the volcanic front samples generally show a broader range in major element concentrations at a given MgO content (Figure 2.4 a-i), overlapping with the VF samples and in general extending to lower CaO and FeOt and higher TiO_2, Na_2O, K_2O and P_2O_5 than VF samples. Sc and V show a crude decrease and Pb and Sr a crude increase in the most mafic samples going from NW Nicaragua to Guatemala

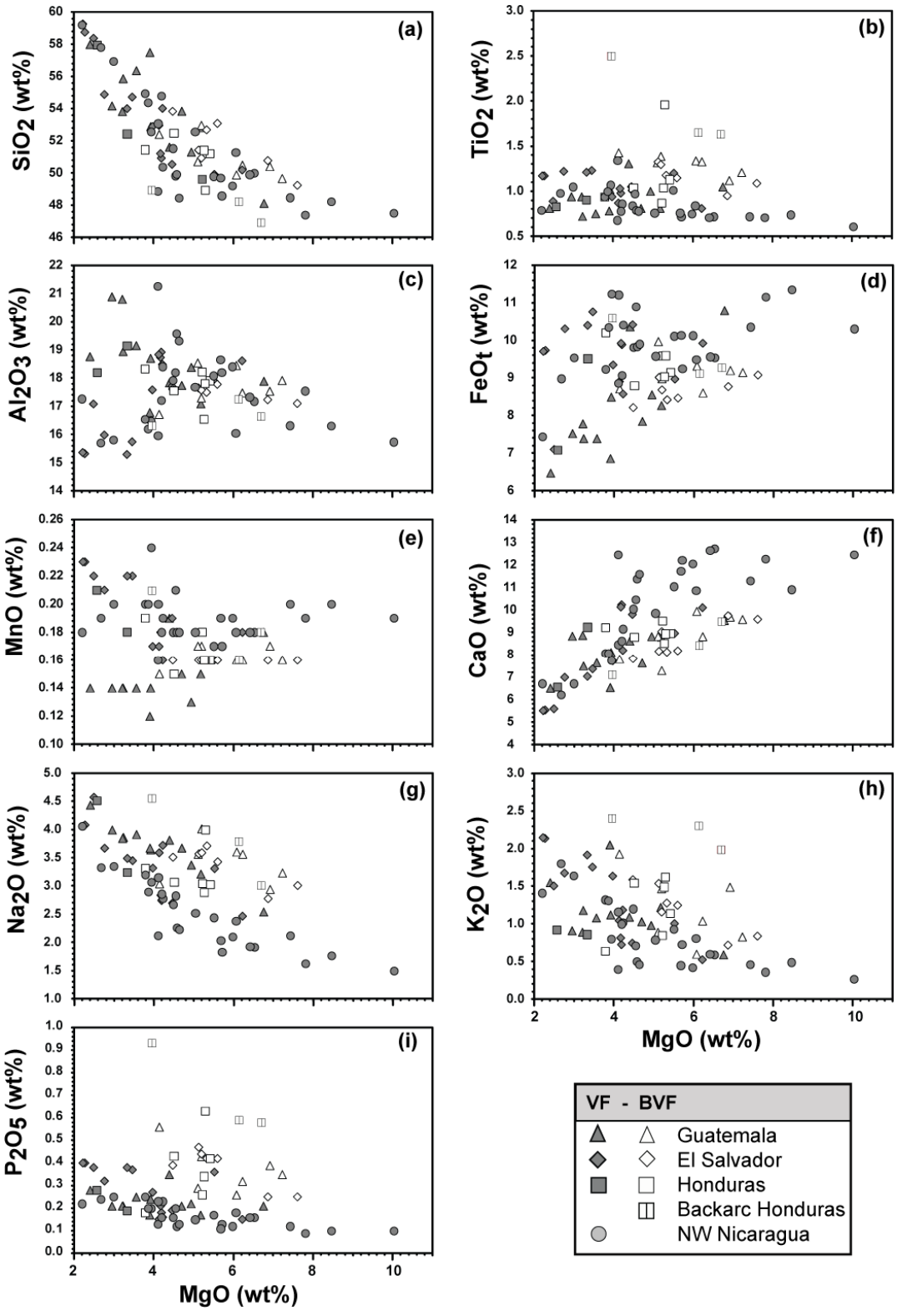

Figure 2.4) (a-i) MgO versus major element oxide variation diagrams for volcanic front (VF) and behind the volcanic front (BVF) and back-arc (BA) mafic volcanic rock samples with MgO > 2wt%.

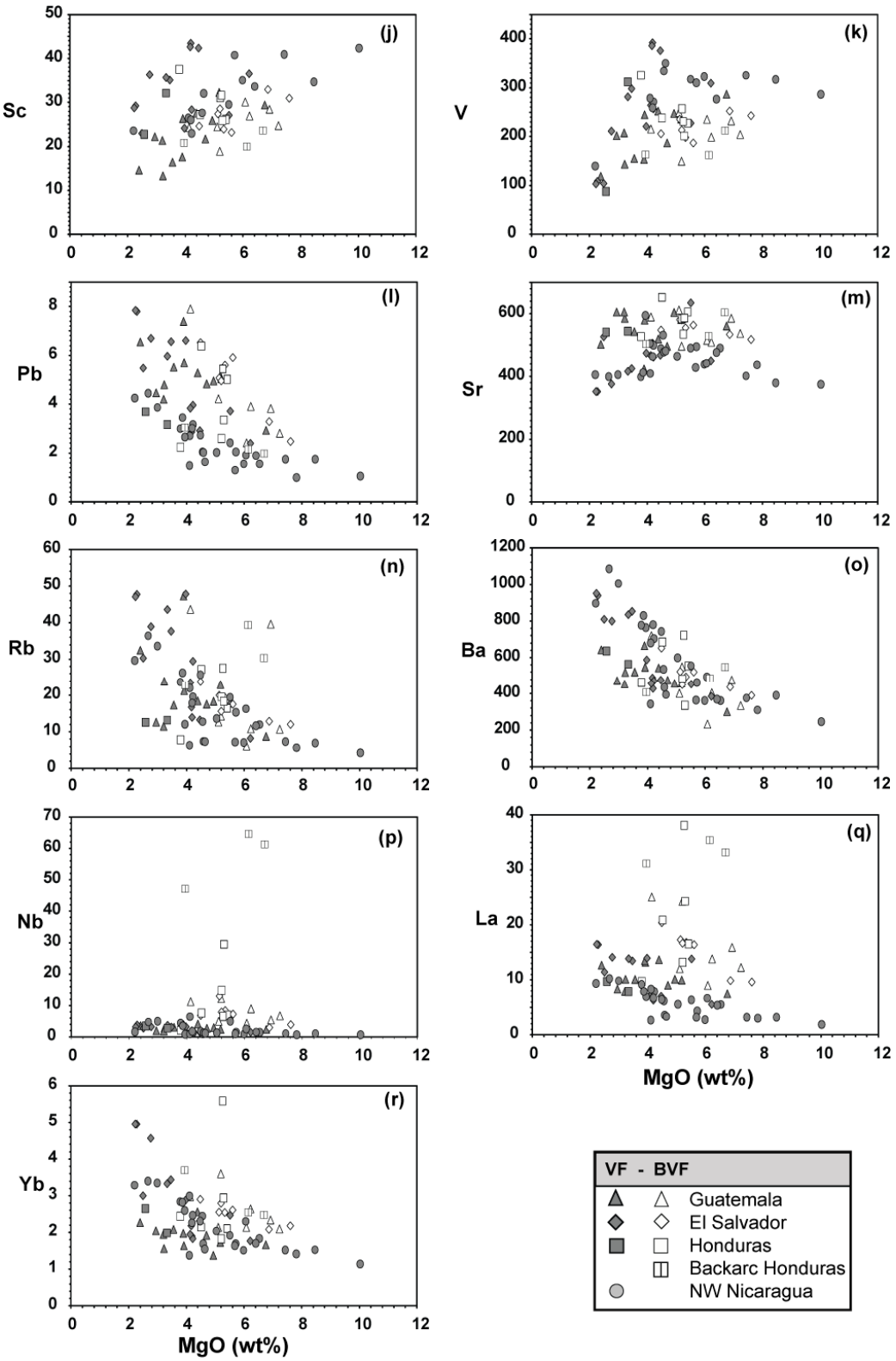

Figure 2.4 (j-r) MgO versus select trace element variation diagrams for volcanic front (VF) and behind the volcanic front (BVF) and back-arc (BA) mafic volcanic rock samples with MgO > 2wt%.

(Figure 2.4 f-r). The most mafic BVF and BA samples generally extend to lower Sc and V but to higher Rb, Nb and the LREE (Figure 2.4 f-r).

On primitive normal (N) MORB normalized multi-element diagrams (Figure 2.5a-d), all samples display enrichment in fluid-mobile large-ion-lithophile elements (LILE; e.g. Ba, K, Pb, Sr) and U, relative to high field strength elements (HFSE; e.g. Nb, Ta, Zr, Hf, Ti) and light rare earth elements (LREE; e.g. La, Ce, Nd) reflecting typical subduction-related trace element abundance patterns (e.g. Arculus, 1994; Pearce, 1995).

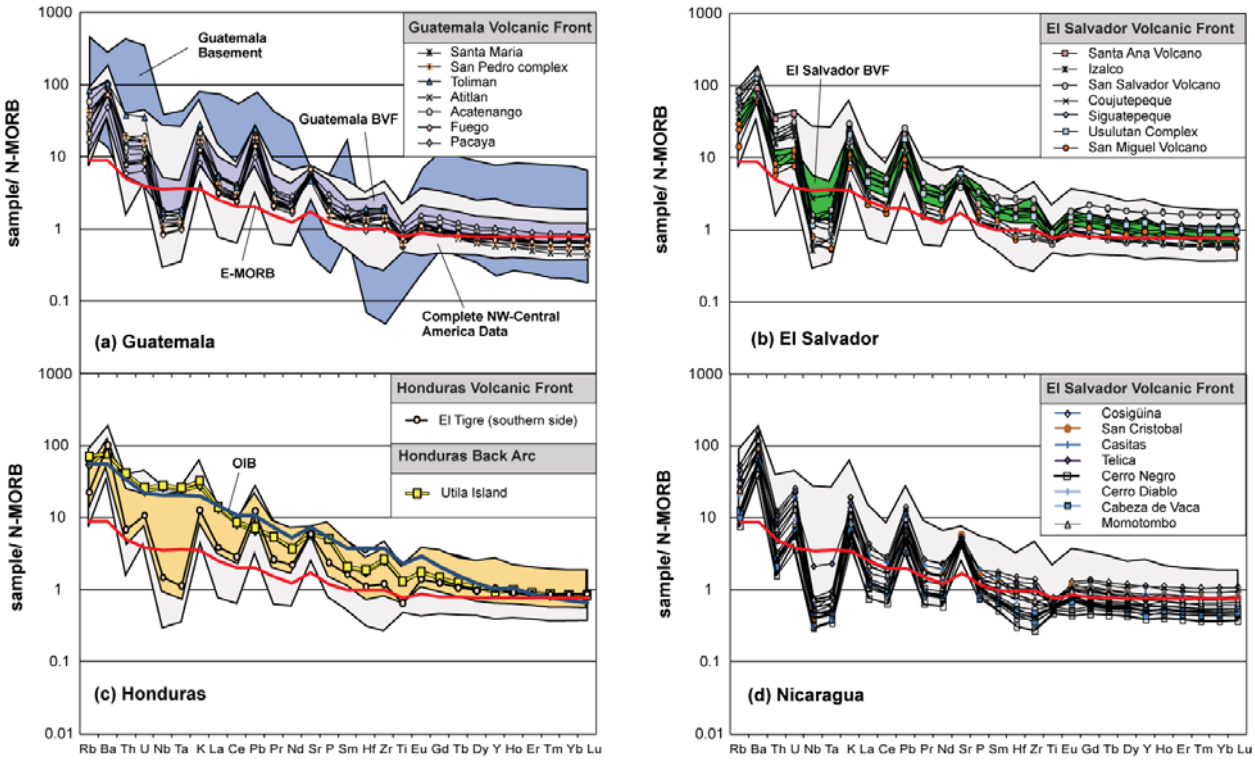

Figure 2.5: Primitive N-MORB normalized (after Sun and McDonough, 1989) multi-element diagram of selected volcanic front (VF) samples (MgO > 2wt %) from Guatemala, El Salvador, Honduras and Nicaragua. The complete range of Central American Arc lava compositions from this study is indicated by underlying grey field, including VF and BVF samples. Colored fields mark BVF sample compositions for respective countries (5a-c). The yellow field (5c) for the Honduras behind the volcanic front (BVF) contains samples from El Tigre to Tegucigalpa. Data for average E-MORB (bold red line) and OIB (bold blue line) compositions after Sun and McDonough (1989).

Systematic variations in trace element compositions and ratios are observed along the volcanic front and between VF, BVF and BA samples. Ratios of fluid mobile to less fluid mobile trace elements (e.g. Ba/La, U/Th, Ba/Th and to a lesser degree Sr/Ce, e.g. Figure 2.6) vary systematically along the volcanic front decreasing from NW Nicaragua to NW Guatemala, consistent with the results of previous studies (e.g. Carr et al., 1990, 2003, 2007; Patino et al., 2000, Sadofsky et al., 2008). BVF and BA samples generally extend to lower fluid mobile to fluid immobile element ratios than associated VF volcanoes lavas with Lake Yojoa and Utila Island rocks extending to the the lowest ratios (Figure 2.6a, b and d). Ratios of more to less incompatible rare earth elements (REE) elements (e.g. La/Yb; Figure 6c) generally increase from Nicaragua to Guatemala, reflecting both generally lower heavy (H) REE and higher LREE contents (steeper negative REE patterns) in the Guatemalan lavas (e.g. Figure 2.5). In general BVF and BA samples have higher LREE/HREE ratios than VF samples along transects perpendicular to the trench and VF. BVF samples have higher HFSE and REE contents than related VF samples with similar MgO contents.

2.4.2 Sr-Nd-Pb-Hf isotopes

The Sr-Nd-Pb-Hf isotope data is presented in Table 2.2. Although $^{87}Sr/^{86}Sr$ isotopic composition doesn't show a clear systematic variation along the VF, there is a broad decrease from NW Nicaragua to central El Salvador (excluding one sample) and then an overall increase from NW El Salvador to Guatemala (Figure 2.7), similar to what has been observed previously (e.g. Carr et al., 2003). On the other hand, the $^{143}Nd/^{144}Nd$ and $^{176}Hf/^{177}Hf$ show a systematic decrease and Pb isotope ratios a systematic increase along the VF from NW Nicaragua through Guatemala (e.g. Figure 2.7). BVF samples have similar or lower Sr, Nd and Hf, but higher Pb isotope ratios thanassociated VF samples. BA samples in Honduras have depleted Sr, Nd, Pb isotopic compositions that fall within the field for Cocos Plate oceanic crust but slightly lower $^{176}Hf/^{177}Hf$. They have distinct endmember compositions on the Sr vs Nd, Pb vs Pb, and Nd vs Hf isotope correlation diagrams. The samples from the BA also have the least

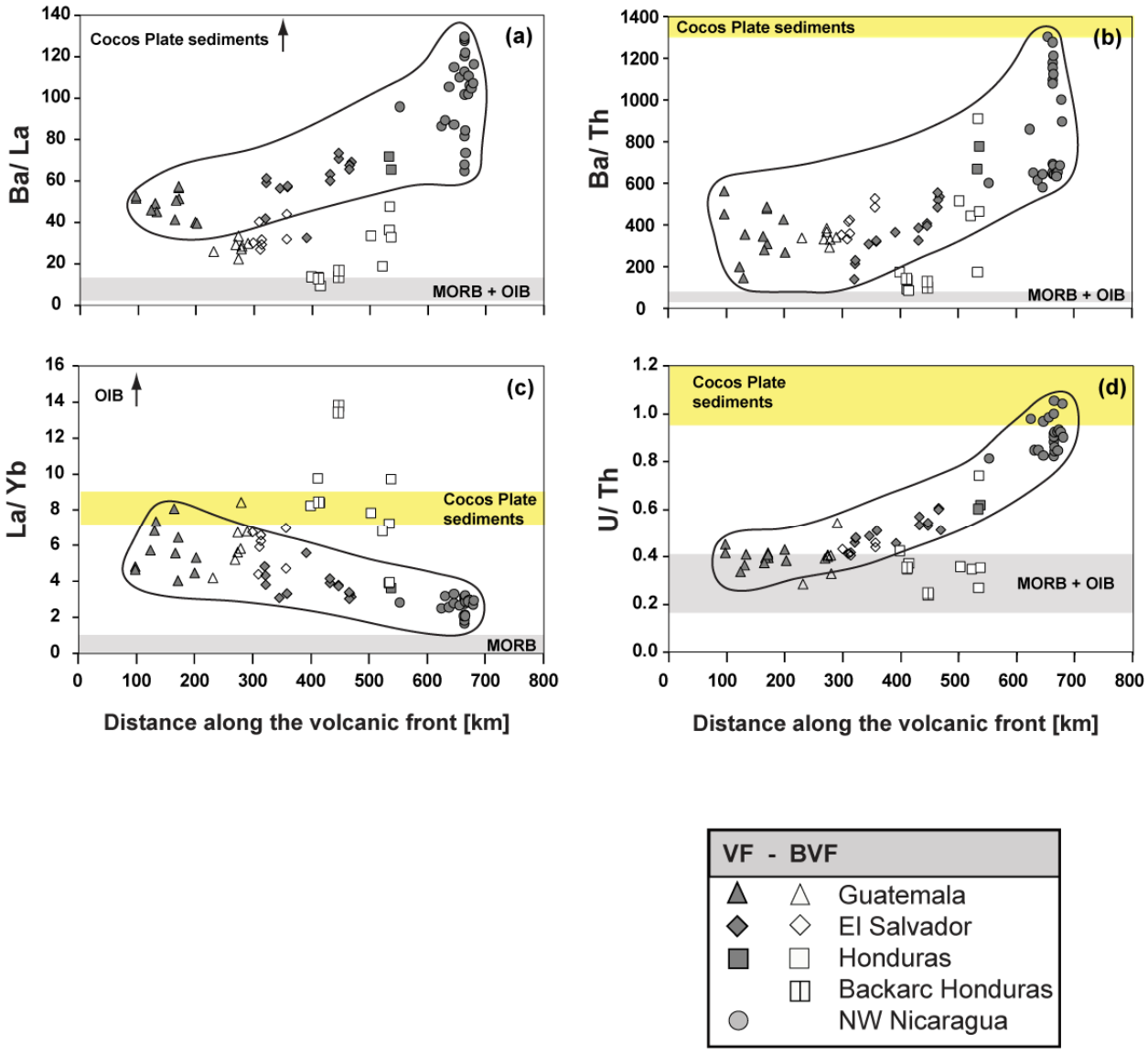

Figure 2.6 **Distance along the volcanic front versus selected trace element ratios of fluid mobile to immobile elements for mafic northwestern CAVA volcanic rock samples from the VF, BVF and the BA. Distance in kilometer is calculated from Tacana Volcano near the Guatemalan-Mexican border. Horizontal grey bars indicate typical trace element ratio values for mid-ocean-ridge basalts (MORB), ocean-island basalts OIB and Cocos Plate sediments (consisting of hemipelagic and carbonate sediments) after Hofmann (1988), Sun & McDonough (1989) and Plank and Langmuir (1998).**

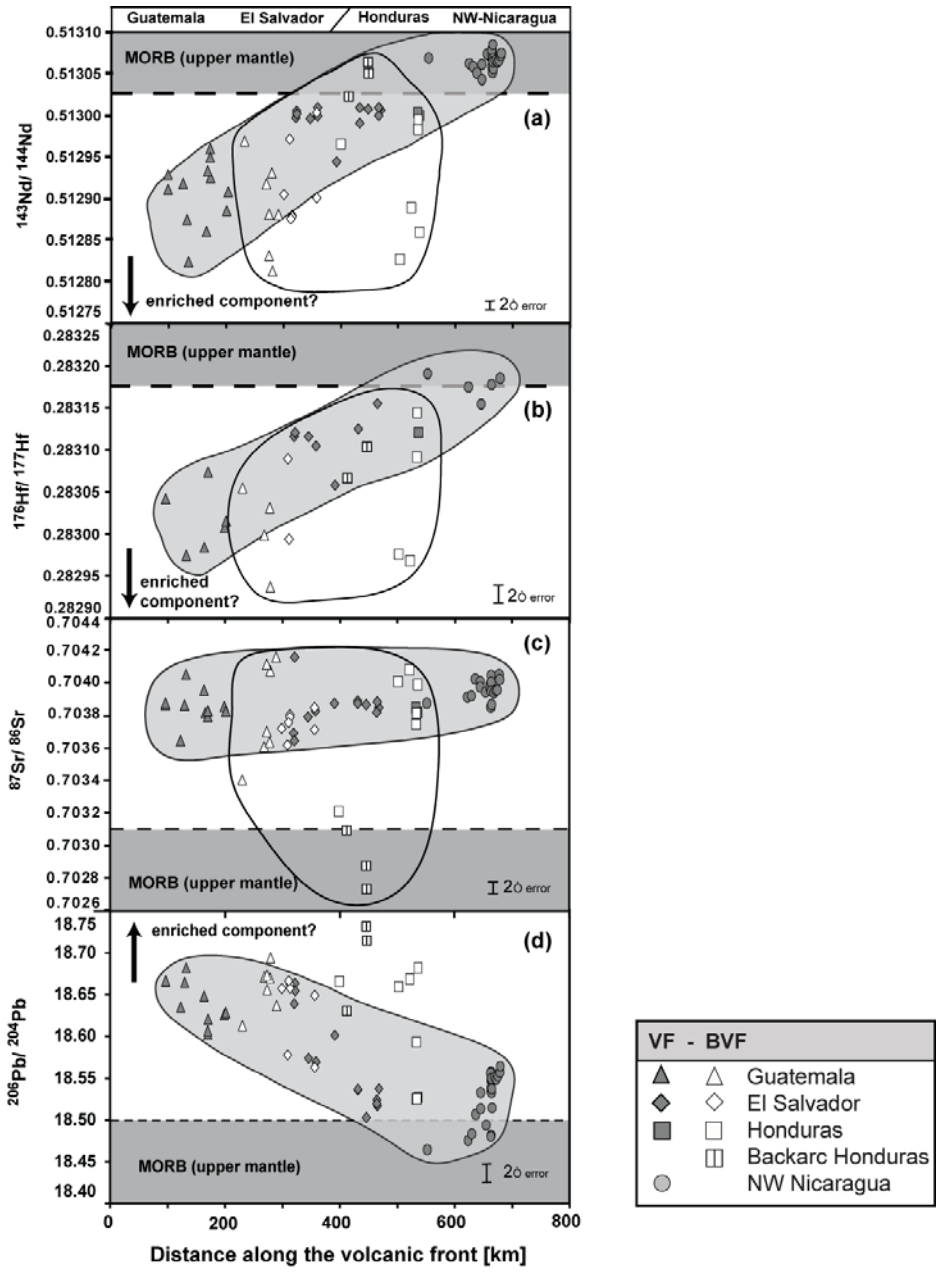

Figure 2.7 Distance along the volcanic front versus 143Nd/144Nd, 176Hf/177Hf, 87Sr/86Sr and 206Pb/204Pb for mafic (MgO > 2 wt %) Central American volcanic samples. Corresponding countries are located on top of the diagrams. Solid symbols represent volcanic front and open symbols behind the volcanic front samples respectively. the geochemistry of selected samples generally vary systematically along the volcanic front and to a lesser extent into the back arc, ranging between depleted MORB/ upper mantle-like isotopic ratios to more enriched isotopic compositions (with the exception of Sr isotopes, which show no systematic variation along the volcanic arc). Grayish fields define the volcanic front array. MORB field includes data from DSDP Leg 67 (offshore Guatemala) after Geldmacher et al., (2008), seamount offshore Nicaragua (SO144-1; Werner et al., 2003), IODP site 1256 MORB (Sadofsky et al., 2008b) and this study. All errors are reported as 2 sigma of the mean.

radiogenic $^{87}Sr/^{86}Sr$ and most radiogenic $^{206}Pb/^{204}Pb$ isotope ratios for all NW Central American subduction-related lavas.

On an $^{87}Sr/^{86}Sr$ vs. $^{143}Nd/^{144}Nd$ isotope correlation diagram (Figure 2.8) for NW Central American volcanics, BVF and BA samples form a crude negative correlation, extending from the MORB field (Honduras BA samples) towards an enriched component with radiogenic Sr and unradiogenic Nd, characterized by BVF samples from Honduras and Guatemala. The VF samples form a crudely vertical array on this diagram. The Guatemala VF samples overlap the BVF/BA array, but the VF samples from El Salvador and NW Nicaragua plot to the right of the BVF/BA array, having more radiogenic Sr isotope ratios for a given Nd isotopic composition. The Pb isotope data from the NW Central American VF samples form good positive correlations with r^2 = 0.77 on the uranogenic Pb isotope diagram (Figure 2.9) and r^2 = 0.93 on the thorogenic Pb isotope diagram, respectively (not shown here). On both Pb isotope diagrams, the array extends from the composition of the crust subducting outboard of Nicaragua, as characterized by the composition of a bend-faulted seamount (Werner et al., 2003), into the Cocos Plate sediment field. With the exception of BA samples from Utila, Honduras, the BVF samples overlap the VF trend, extending to compositions with slightly more radiogenic Pb. On Pb vs. Nd and Hf isotope diagrams, NW Central American VF samples form negative correlations (with r^2 of 0.67 to 0.78 respectively), illustrating coupling between Pb and Nd and Pb and Hf isotopic systems (Figure 2.10).

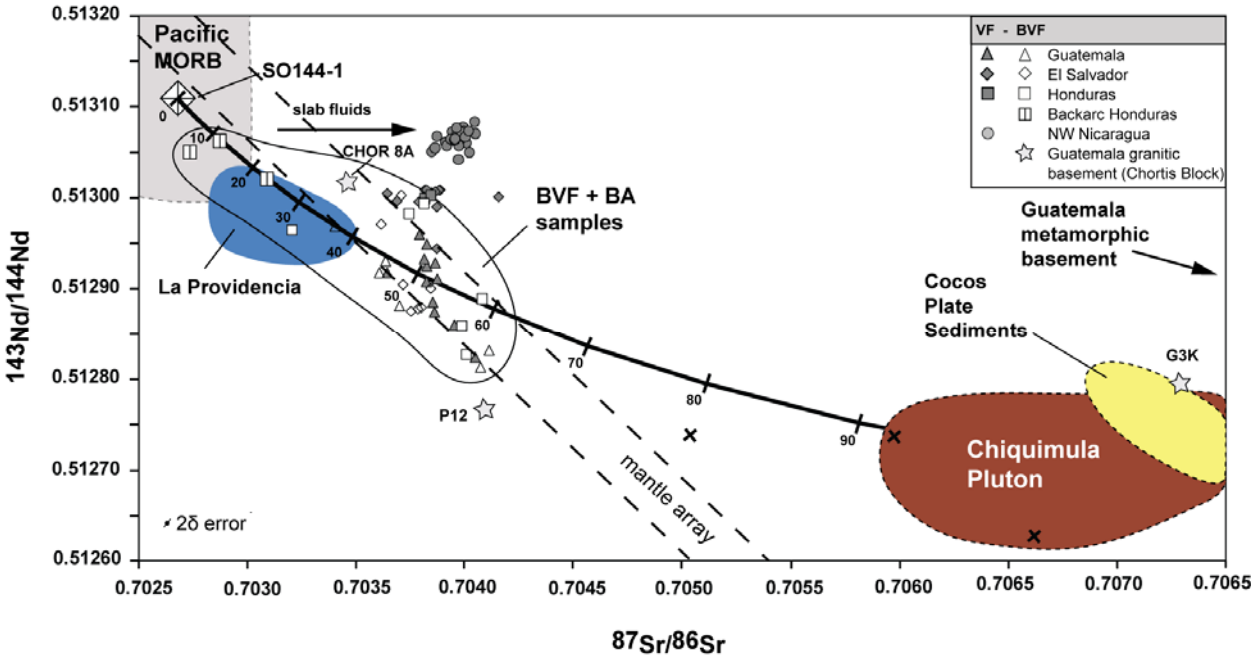

Figure 2.8 Sr-Nd isotope diagram for NW Central American volcanics, with VF samples generally forming a crudely positive to vertical array, whereas BVF samples form a negative array. Pacific MORB (after Stracke et al., 2005; Sadofsky et al., 2008b; Geldmacher et al., 2008; and this study), Cocos Plate Sediments (Feigenson et al., 2004; Sadofsky et al., 2008b; Geldmacher et al., 2008; and this study) and Chiquimula Pluton (after Feigenson et al., 2004) mark potential source component compositions. Black arrow labeled slab fluids indicates Sr isotope enrichment of Nicaraguan samples by slab fluids derived from subducted sediments and seawater-altered oceanic crust, and possibly serpentinite. The black curve represents a binary mixing line between outboard NW Nicaragua subducting crust (Werner et al., 2003) and an average Chiquimula Pluton (Feigenson et al., 2004; and this study). Tick marks indicate the amount of granitic pluton assimilated in melt from the mantle wedge without a slab melt component. All errors are reported as 2 sigma of the mean.

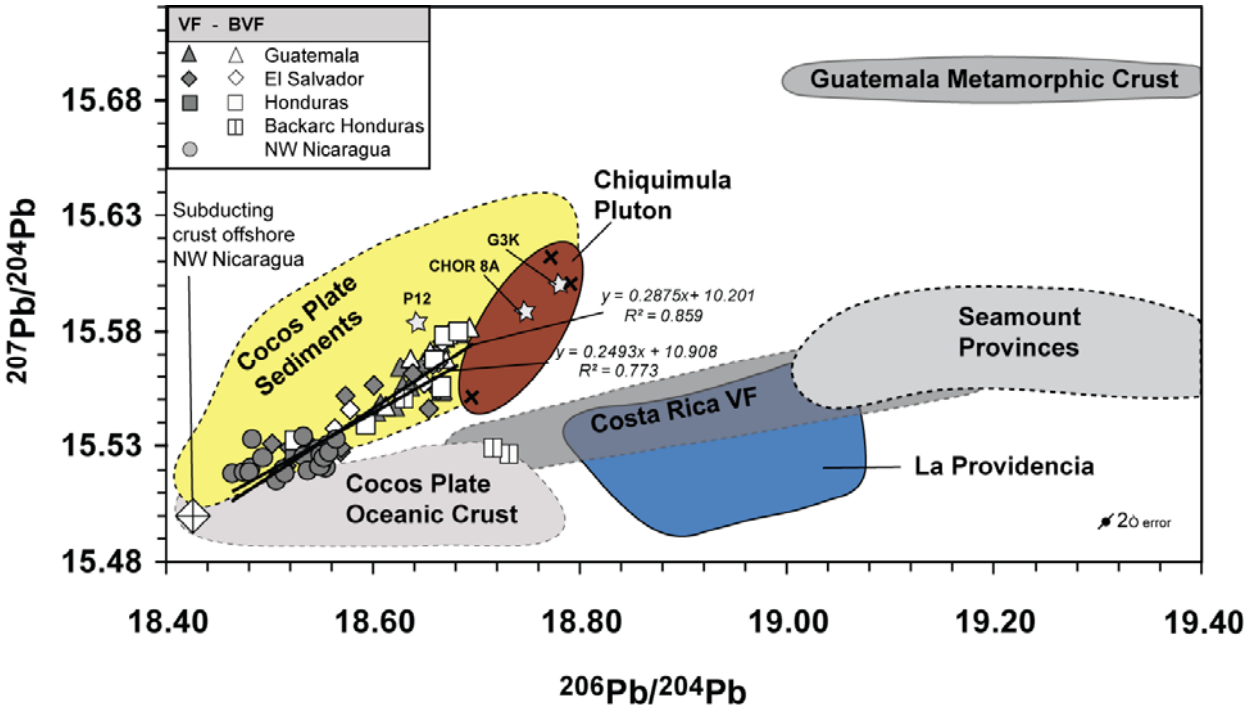

Figure 2.9 Lead isotopic correlation diagram for Central American volcanic rock samples. Northwestern CAVA samples form good linear correlations with r2 = 0.77 (y = 0.2493x + 10.908) on the uranogenic Pb isotope diagram for the VF samples and r2 = 0.86 (y = 0.2875x + 10.201) for VF and BVF samples, excluding back-arc samples from Yojoa and Utila. The Nicaraguan VF samples have the least radiogenic Pb isotopic compositions and overlap with the field for the Cocos Plate. The Guatemalan VF samples and the Guatemala and Honduras BVF samples have the most radiogenic Pb isotopic compositions and overlap the fields for subducting Cocos Plate sediments and Guatemala granitic crust. Subducting crust offshore NW Nicaragua after Werner et al. (2003). Data for Chiquimula Pluton after Feigenson et al. (2004). All errors are reported as 2 sigma of the mean. Fields for Costa Rica VF and Seamount Provinces (after Hoernle et al., 2008) indicate that these components cannot generate the observed data array.

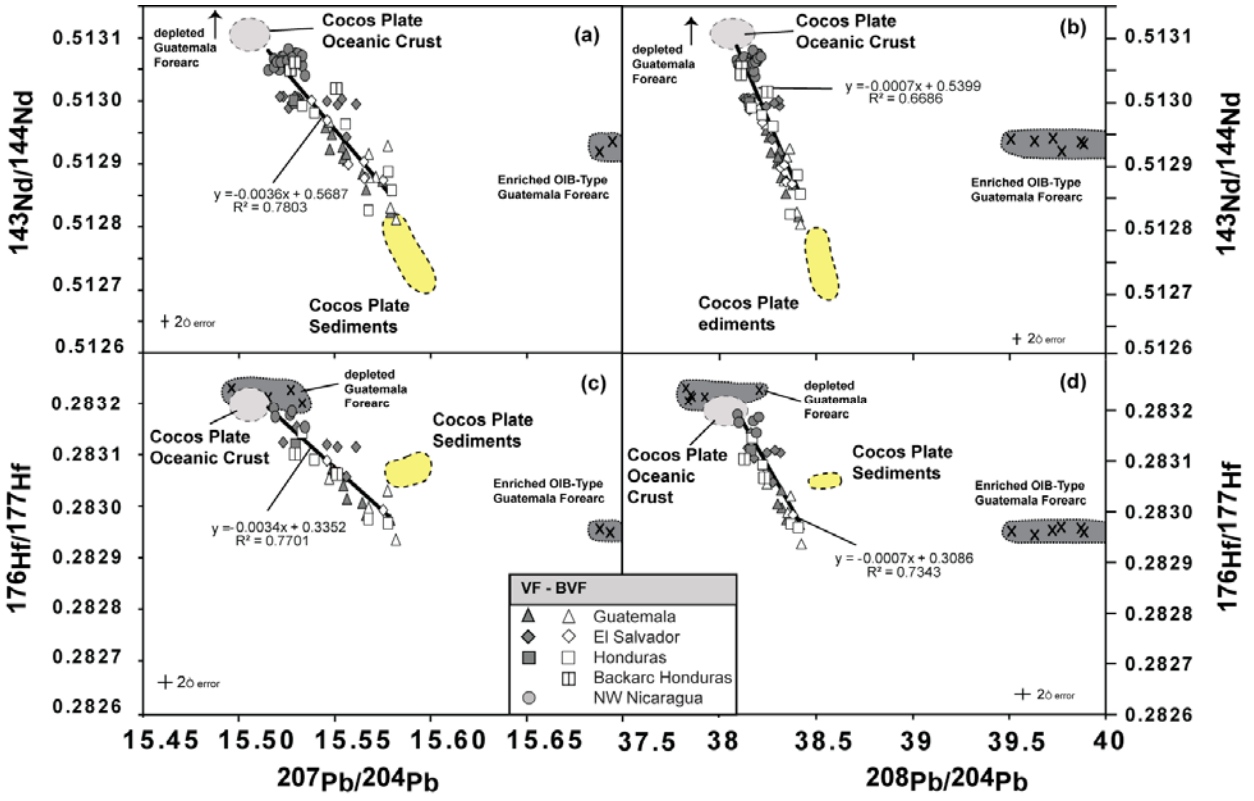

Figure 2.10 (a-d). Lead vs. Nd and Hf isotope correlation diagrams for NW CAVA volcanics with MgO>2%. All samples form negative correlations, ranging from 0.67 to 0.78 for R2 (bold black lines), providing evidence that the Pb isotopic composition are coupled with variations in Nd and Hf isotopic composition. In addition, the Pb vs. Hf isotope correlation diagrams clearly rule out Cocos Plate sediments and enriched OIB-type Guatemalan forearc (Geldmacher et al., 2008) as the enriched endmember for NW Central American volcanism, i.e. Guatemalan VF and Guatemalan and Honduras BVF volcanism. Granitic Guatemalan basement sample G3 however has the appropriate isotopic composition to serve as the enriched endmember. Fields for Cocos Plate Sediments and Oceanic Crust are supplemented by DSDP Leg 67 sample data (offshore Guatemala). Grey oval field indicates Cocos Plate crust subducting offshore NW-Nicaragua (after Hoernle et al., 2008). Additional data from Werner et al. (2003), Feigenson et al. (2004) and Geldmacher et al. (2008). All errors are reported as 2 sigma of the mean.

On the εNd vs. εHf diagram (Figure 2.11), the NW Central American volcanic rocks (VF/BVF/BA) form a good positive correlation (r^2 = 0.89; VF alone has r^2 = 0.98, VF/BVF have r^2 = 0.94 and BVF/BA have r^2 = 0.78). The BVF/BA samples largely overlap with the VF trend but some samples from Guatemala and especially from Honduras fall below the array with the BA samples deviating the most from the array.It is clear from the Pb vs. Hf and the εNd vs. εHf isotope diagrams that the Cocos Plate

sediments cannot serve as the enriched endmember for the VF and the BVF samples. Granitic sample G3 from the Guatemala basement, on the other hand, falls on the enriched end of an extension of the NW Central American array.

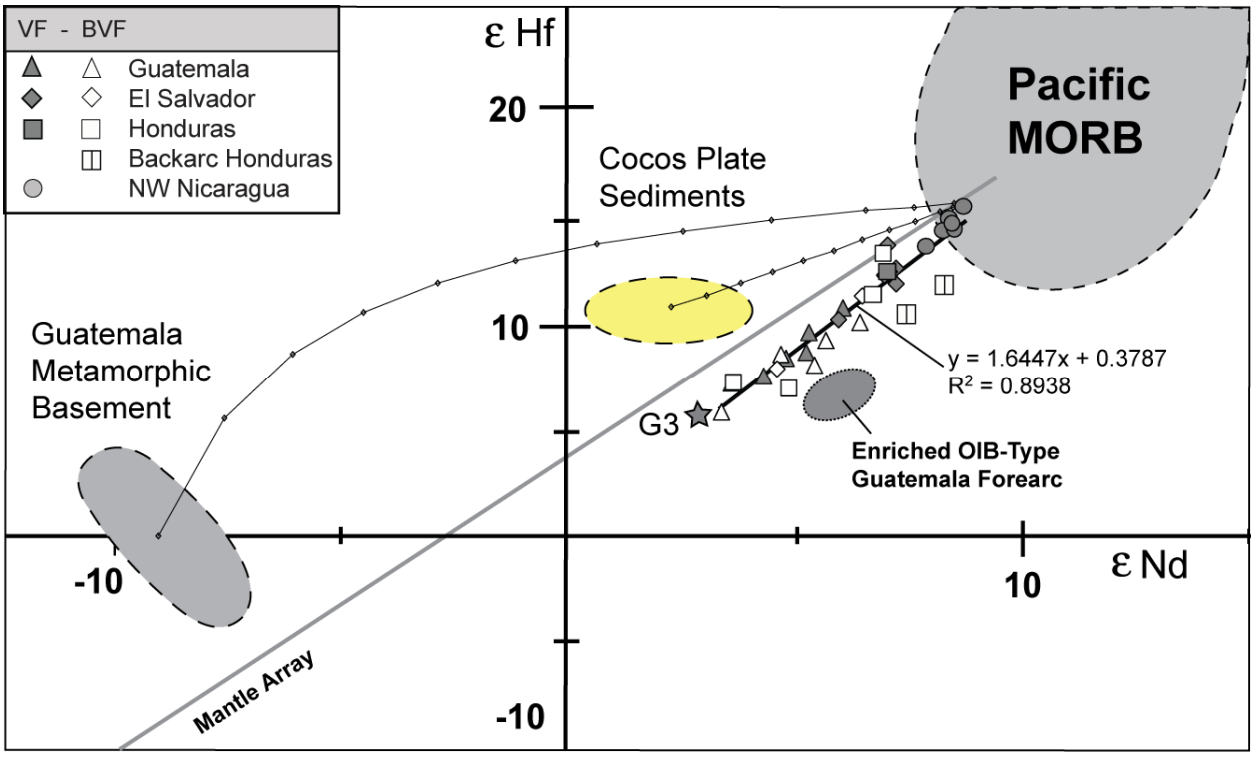

Figure 2.11 eNd versus eHf diagram for Central American volcanic rock samples. Combined VF and BVF samples from the northwestern Central American volcanic arc form a very good positive linear correlation (R2 = 0.8938). Excluding the BA samples, the positive trend can be defined by two components (SO144-1 depleted MORB-type composition and G3 enriched type composition) with Nicaraguan samples having the most Pacific MORB-like compositions and Guatemalan samples trending towards an enriched component. Included are binary mixing lines between a Pacific MORB-like component and several selected source components (e.g. Guatemalan metamorphic basement, Cocos Plate sediments). Diagram modified after Geldmacher et al. (2003) with additional fields for Guatemala Basement, Cocos Plate Sediments (DSDP Leg67 offshore Guatemala) and Guatemala forearc basement (Geldmacher et al., 2008).

2.5 Discussion

As is illustrated on the $^{87}Sr/^{86}Sr$ vs. $^{143}Nd/^{144}Nd$ isotope correlation diagram (Figure 2.8), Quaternary volcanism in NW Central America can be divided into three endmember compositional groups: 1) Volcanic rocks from the NW Nicaragua VF are characterized by high FeO_t, CaO, MnO, Sc, V, Ba/La, Ba/Th, Ba/Nb, U/Th, Sr/Ce, $^{87}Sr/^{86}Sr$, $^{143}Nd/^{144}Nd$ and $^{176}Hf/^{177}Hf$, but low SiO_2, TiO_2, Na_2O, P_2O_5, K_2O, Pb, Sr, Nb, Ta, LREE, La/Yb, Sm/Yb, Zr/Hf and Pb isotope ratios. Differences in major elements are relative to a specific MgO content. Isotopically these rocks represent a depleted endmember in the Central American system, which however display enrichment in $^{87}Sr/^{86}Sr$ compared to Pacific MORB. 2) Volcanic rocks from the Guatemalan VF and from BVF centers are characterized by generally higher SiO_2, TiO_2, Na_2O, P_2O_5, K_2O, Pb, Sr, Nb, Ta, LREE, La/Yb, Sm/Yb, Zr/Hf and Pb isotope ratios but lower FeO_t, CaO, MnO, Sc, V, Ba/La, Ba/Th, Ba/Nb, U/Th, Sr/Ce, $^{143}Nd/^{144}Nd$ and $^{176}Hf/^{177}Hf$, representing an isotopically enriched endmember with enrichments in fluid mobile elements and Sr isotopic composition. 3) Volcanic rocks from the BA (Yojoa in Honduras and Utila Island in the Caribbean) are characterized by high to the highest TiO_2, Na_2O, P_2O_5, K_2O, moderately to highly incompatible trace element abundances (except Pb), ratios of more to less incompatible elements (e.g. La/Yb and La/Sm, Sm/Yb), Zr/Hf, $^{143}Nd/^{144}Nd$ and $^{206}Pb/^{204}Pb$, but low to the lowest SiO_2, CaO, fluid-mobile to less-fluid-mobile element ratios, e.g. Ba/La, Ba/Th, Ba/Nb, U/Th, Sr/Ce, $^{87}Sr/^{86}Sr$, $^{207}Pb/^{204}Pb$ and $^{208}Pb/^{204}Pb$, also representing a depleted endmember isotopically, similar in composition to Pacific MORB.

The incompatible element geochemistry of the Quaternary VF and BVF rocks in NW Central America clearly indicate a subduction zone affinity for these volcanic rocks: relative enrichment of fluid-mobile elements, such as LILEs and Pb (which form peaks on multi-element diagrams, (Figure 2.5), and relative depletion of HFSE, such as Nb, Ta and Ti (which form troughs on multi-element diagrams), and generally high fluid-mobile to less fluid-mobile elements above those commonly found in MORB and OIB, e.g. Ba/La, Ba/Th, Ba/Nb, U/Th and Sr/Ce. The good correlations between Pb, Nd and Hf isotope ratios further suggest that the geochemistry of these volcanic rocks are largely

controlled by two endmembers as defined above. The incompatible element geochemistry of the BA volcanic rocks, however, is characteristic of intraplate or OIB-type volcanism, i.e. enrichment in moderately to highly incompatible elements with relative enrichment (peak on multi-element diagram; Figure 2.5c) in Nb and Ta and relative depletion (trough; Figure 2.5c) in Pb. Below we will discuss the origin of these three endmember compositions in Quaternary NW Central American volcanism.

2.5.1 NW Nicaragua VF Endmember

The high FeO_t but low SiO_2 of the Nicaraguan rocks is likely to reflect deeper average depths of peridotite melting beneath Nicaragua than other parts of the Central American arc (Figure 2.2), due to the deeper depth of the slab beneath Nicaragua than beneath the rest of the Central American VF (Sadofsky et al., 2008). The thinner crust and deeper slab depth also imply that the longest mantle melting column is located beneath Nicaragua. A long melting column will favor large extents of melting and dilution of incompatible elements (e.g. Ti, Na, P, K, Pb, Sr, Nb, Ta, LREE) and more to less incompatible element ratios (e.g. La/Yb, La/Sm) during melting.

High ratios of fluid-mobile to less-fluid-mobile incompatible elements, e.g. Ba/La, Ba/Th, Ba/Nb, U/Th and Sr/Ce, are consistent with the highest flux of subducting slab-derived fluids being added to the mantle wedge beneath Nicaragua (e.g. Carr et al., 1990; Leeman et al., 1994; Patino et al., 2000; Abers and Plank, 2003; Eiler et al., 2005; Sadofsky et al., 2008). It has been shown that outer-rise faulting, related to the bending of the plate, outboard of NW Central America extends into the upper mantle (Ranero et al., 2003) and that the upper mantle in the bend-faulted areas has lower seismic velocities than the upper mantle further to the west, consistent with hydration and serpentinization of the uppermost lithospheric mantle, to a depth of ~4km (Grevemeyer et al., 2007; Ivandic et al., 2008). Although bend-faulting has been mapped along the Cocos Plate outboard of the entire NW Central America (Nicaragua to Guatemala), the steeper subducting angle results in the subducting slab being at the deepest depths beneath the Nicaraguan VF, placing the upper mantle of the down-going plate within the zone of serpentinite dehydration (Figure 2.2). Due to the shallower subduction angle

and shallower depths to the subducting plate to the north, the amount of serpentinite dehydration beneath the VF will decrease to the NW beneath El Salvador and Guatemala. The lowest $\delta^{18}O$, well below typical mantle values, in olivine phenocrysts from Nicaragua are consistent with a greater flux of hydrous fluids from hydrothermally-altered lower oceanic crust and upper mantle serpentinite (Eiler et al., 2005). Greater fluid flux beneath Nicaragua will also enhance the degree of melting, contributing to the dilution of Na and other incompatible elements at a given MgO content (e.g. Eiler et al., 2005).

Considering the elements for which isotope data is available, Pb generally is the most fluid-mobile in subduction systems, followed by Sr, whereas Nd and Hf are considered to be relatively fluid-immobile (e.g. Pearce et al., 2007). If the highest fluid flux occurs beneath Nicaragua (e.g. Carr et al., 1990, 2003; Patino et al., 2000; Rüpke et al., 2002; Eiler et al., 2005; Sadofsky et al., 2008), then the Pb and Sr isotope ratios of Nicaraguan volcanic rocks will be dominated by the subduction input (slab signal), whereas Nd and Hf should provide information about the composition of the mantle wedge. Assuming that the mantle wedge beneath Nicaragua has a composition similar to N-MORB (e.g. Gazel et al., 2009), we compare the average concentrations of Nb, Ta, Pb, Sr, Nd and Hf of the two most mafic Nicaragua VF samples (with MgO 10.03 and 8.46) with average N-MORB of Sun and McDonough (1989). Since MgO is similar for average N-MORB of Sun and McDonough (1989) and the two Nicaraguan VF samples, the 2.5 times lower Nb, Ta and Hf of the Nicaraguan VF rocks indicates derivation through higher degrees of melting (up to 2.5 times higher) and/or derivation from a more depleted source, possibly through multiple episodes of melt extraction. The Nd concentration of the Nicaragua VF rocks is only 1.4 times lower than in MORB, possibly suggesting an increase in the Nd concentration of the Nicaragua VF melts by as much as 75% from a slab component (hydrous fluid and/or melt). In contrast, Sr shows an increase compared to MORB of ~4.2 times and Pb of ~4.7 times. Assuming 2.5 times higher degrees of melting to form the Nicaragua VF melts than average N-MORB, then the enrichment from a slab component could be as much as 6.7 times enrichment for Sr and 7.2 times enrichment for Pb through the addition of a slab component. Therefore the relative enrichment increasing from Hf to Nd to Sr to Pb is consistent with increasing

fluid mobility being the major factor controlling the abundance and thus isotopic composition of these elements in the Nicaraguan VF volcanic rocks. In conclusion, the Hf and Nd isotopic composition should primarily reflect the composition of the mantle wedge, whereas the Sr and Pb isotopic compositions should primarily reflect the composition of the slab fluid (and/or hydrous melt).

We now review the isotope data in order of increasing fluid mobility to better constrain the sources involved in generating the Nicaraguan VF melts. The NW Nicaraguan volcanic rocks have high $^{143}Nd/^{144}Nd$ and $^{176}Hf/^{177}Hf$ ratios, falling within the range observed in Pacific MORB (Figure 2.11). Considering that both Nd and Hf are relatively fluid-immobile, the Nd and Hf isotopic compositions are consistent with the mantle wedge beneath Nicaragua having a MORB-like composition. Since Nd and Hf from the subducting oceanic crust will have similar Nd and Hf isotopic compositions, we cannot rule out a contribution from slab Nd and Hf. A contribution from sediments in the form of a hydrous fluid and/or melt (e.g. Gazel et al., 2009), on the other hand, would have caused a decrease in both Nd and Hf isotopic composition. Therefore the Nd and Hf isotopic ratios of the Nicaraguan melts represent minimum values for the mantle wedge.

On the Sr vs. Nd isotope correlation diagram, the BVF/BA samples form a positive array, extending the Pacific MORB field to more radiogenic Sr and less radiogenic Nd. The BVF/BA array overlaps and is subparallel to the Sr/Nd isotope mantle array. The Nicaraguan samples show the greatest horizontal deviation, i.e. enrichment in $^{87}Sr/^{86}Sr$, from the BVF/BA (or mantle) array and the amount of deviation/enrichment decreases along the VF to Guatemala. The deviation from the best fit line through the BVF/BA array, i.e. difference in $^{87}Sr/^{86}Sr$ ratio between sample and point on the best-fit line with the same $^{143}Nd/^{144}Nd$ isotope ratio ($\Delta^{87}Sr/^{86}Sr = {}^{87}Sr/^{86}Sr(sample) - (({}^{143}Nd/^{144}Nd\ (sample) - 0.6227)/ -0.156) * 1000$) forms good positive correlations with ratios of more to less fluid-mobile elements such as Ba/Th, U/Th, Ba/Nb and Ba/La (see e.g. Figure 12 a and c). These correlations are consistent with

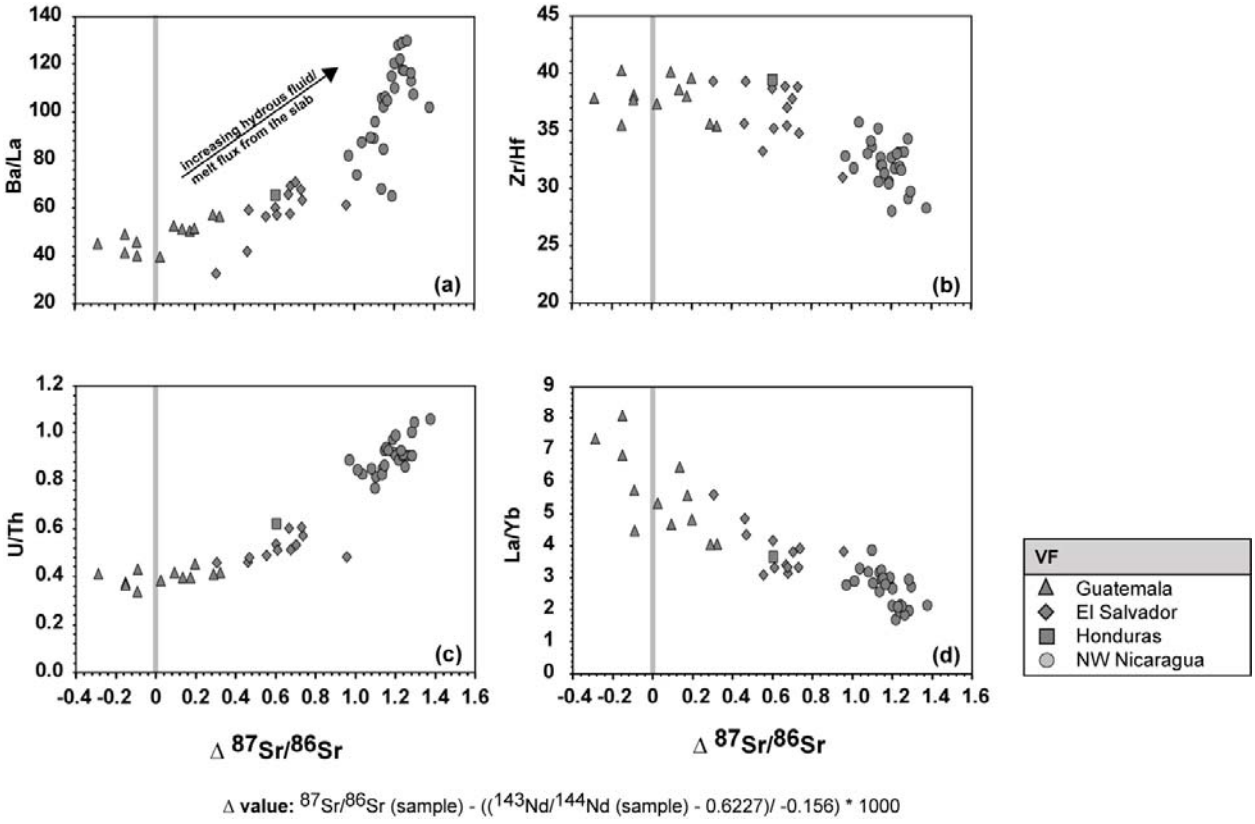

Figure 2.12 (a-d) Fluid flux variation diagram using Δ87Sr/86Sr vs. selected fluid-mobile to less-fluid-mobile element ratios from Central American volcanic rock samples from the volcanic front. The Δ87Sr/86Sr value is based on the horizontal deviation from a best-fit line through the BVF/BA (or mantle) array on the Sr vs. Nd isotope correlation diagram (Figure 8).

$\Delta^{87}Sr/^{86}Sr$ reflecting the magnitude of the hydrous fluid/melt flux from the slab, which determines the degree of decoupling of Sr from Nd and Hf isotope ratios, with Sr being derived from a combination of subducted sediments, seawater-altered oceanic crust and sea-water serpentinized upper lithospheric mantle of the incoming slab. Inverse correlations of $\Delta^{87}Sr/^{86}Sr$ with La/Yb and Zr/Hf ratios are likely to reflect differences in degree of melting and source depletion/enrichment (see Figure 2.12 b and d). Compared to the chondritic ratio of 34.3 +/- 0.3 (Münker et al., 2003), the Nicaraguan magmas exend to lower Zr/Hf, reflecting possible source depletion through repeated melting and melt extraction events, and the Honduras, El Salvador and Guatemala lavas to higher Zr/Hf, possibly reflecting source enrichment by small degree melts. Therefore the mantle beneath the Nicaragua VF appears to have undergone high

degrees of melt extraction and source depletion, whereas the Guatemalan VF have undergone lower extents of melting and possible source enrichment as is also consistent with the Nd and Hf isotopic data.

The NW Nicaraguan samples have the least radiogenic Pb isotopic compositions, which are very similar to the incoming oceanic crust, defined by a small seamount outboard of NW Nicaragua (Hoernle et al., 2008). This similarity in composition indicates that Pb from the subducting oceanic crust and small amounts of subducting sediments (<1%; Gazel et al., 2009) dominates the Pb isotopic composition of the NW Nicaraguan VF lavas. Considering the highly fluid-mobile behavior of Pb in subduction systems and the high fluid flux to the subarc mantle beneath the Nicaraguan VF, it is not surprising that the subduction input completely dominates the Pb isotopic composition.

In conclusion, the incompatible element and Sr-Nd-Pb-Hf isotope geochemistry of the NW Nicaragua lavas appears to be dominated by a largely serpentinite-derived fluid flux from the subducting slab, possibly with small amounts (<1 wt.%) of sediment melts, to a depleted N-MORB type of mantle wedge, resulting in large extents of melting of primarily peridotitic material.

2.5.2 Guatemala VF and general BVF Endmember

Generally lower FeO_t and higher SiO_2 contents in the Guatemala VF and the Guatemala, El Salvador and Honduras BVF lavas (henceforth referred to as the Guatemala endmember) could reflect shallower average melting depths for Guatemala than for Nicaragua VF lavas (see Figure 2.2). Although the thickness of the lithospheric mantle beneath northwestern Central America is not well-constrained, it is clear from the much greater depth to the surface of the slab beneath Nicaragua that lithospheric mantle melting will play a more important relative role beneath the northwesternmost part of the Central American arc (Guatemala) than beneath Nicaragua (see Figure 2.2). The generally lower CaO, MnO, Sc and V and possibly in part the higher SiO_2 in the most mafic Guatemala endmember samples with similar MgO to the Nicaragua VF samples could possibly reflect a greater proportion of pyroxenite contributing to these

melts (e.g. Herzberg and Asimov, 2008), which could also help explain the substantially higher Zr/Hf (up to 52) compared to both the chondritic value (~34) and those of the Nicaraguan lavas in the Guatemala endmember and BA samples (Pertermann et al., 2004). Higher mantle-normalized $(Sm/Yb)_n$ ratios (1.5-2.6) than in the Nicaragua VF lavas (1.2-1.7) suggests that there is more residual garnet in the Guatemala endmember source.

The higher abundances of most incompatible elements, including higher Na_6 (Eiler et al., 2005), and higher ratios of more incompatible to less incompatible elements (e.g. La/Yb, La/Sm) could reflect lower degrees of melting and/or a more enriched source for the Guatemala enriched endmember. Lower degrees of melting are also consistent with a lower fluid flux towards the NW, due to the shallower angle of subduction beneath El Salvador, Honduras and Guatemala as is suggested by lower fluid-mobile to less-fluid-mobile element ratios (e.g. Ba/La, U/Th, Ba/Th, Ba/Nb, Sr/Ce) and $\Delta^{87}Sr/^{86}Sr$. The decreasing thickness of the mantle wedge (i.e. decreasing potential length of the mantle melting column; Figure 2.2) will also favor lower degrees of melting to the NW. In the absence of increased slab melting beneath the aforementioned areas, a lower fluid flux implies that Sr and Pb isotope ratios may also provide information about the composition of the mantle wedge (and possibly overlying crust), similar to Nd and Hf isotopic compositions and not only or preferentially about the subduction input.

The enriched Sr, Nd, Hf and Pb isotopic composition of the Guatemala endmember is not consistent with a major contribution from the subducting plate (sampled at DSDP Site 495) or older accreted arc complexes eroded from the Guatemala forearc by the subduction process (sampled at DSDP Sites 499 and 567) (Geldmacher et al. 2008). The Pb vs. Hf (Figure 2.10) and Nd vs. Hf (Figure 2.11) isotope correlation diagrams rule out subducting Cocos Plate sediments as the enriched Guatemala endmember, primarily because the Hf isotopic compositions are not low enough to serve as this endmember. On the other hand, enriched accreted OIB-type terranes in the forearc can be ruled out as the enriched Guatemala endmember, because their Nd and Hf isotopic ratios are too high (Figure 2.10 and 2.12). Therefore

the subduction input (subducting plate and eroded forearc material) cannot explain the combined Sr-Nd-Pb-Hf isotopic systematics of the enriched Guatemalan endmember.

It has previously been suggested that Guatemalan volcanic rocks may have been crustally contaminated (e.g. Carr et al., 1990, 2003; Walker et al., 1995, 2007, 2009; Patino et al. 2000; Cameron et al., 2002; Feigenson et al., 2004) and therefore we now review whether the basement samples from this and other studies could serve as the possible enriched endmember. To begin with, we will consider dioritic to granodioritic basement samples from the Las Ovejas and Santa Maria areas respectively. Sample Chor 8A from Las Ovejas is too depleted in Sr and Nd isotopic composition to serve as the enriched endmember. Sample P12 from the Las Ovejas area has appropriate Sr and Nd isotopic composition, plotting slightly below the most enriched VF and BVF samples from Guatemala and Honduras (Figure 2.7), but the $^{207}Pb/^{204}Pb$ isotope ratio for this sample is too high to serve as the enriched endmember on the uranogenic Pb isotope diagram. In addition, the Zr/Hf ratios (17-19) of both Las Ovejas samples are too low. The basement samples from the Santa Maria Volcano don't serve as appropriate endmembers either, because their Nd is too radiogenic, Pb not radiogenic enough and the Zr/Hf is again too low (13-25).

Phyllite samples from the metamorphic Chortis Block basement behind the VF in Guatemala have very radiogenic Sr and Pb and unradiogenic Nd and thus could serve as the enriched endmember in these isotopic systems (data from this study and Feigenson et al., 2004). This basement, however, can be ruled out, because it plots above the mantle array on the εNd vs. εHf diagram. The northwestern Central American VF and BVF rocks, however, form a positive correlation below the Nd-Hf mantle array, which has a slightly steeper slope than the mantle array and thus projects to an enriched component beneath the mantle array. Furthermore, mixing between the sample with the most radiogenic Nd and Hf from the Nicaraguan VF with the Guatemalan metamorphic basement forms a convex (or concave down) mixing curve, which does not go through the NW Central American data array (see Figure 2.11). The Zr/Hf ratios of these samples are also too low (27-28) to serve as the enriched endmember. Granodioritic to granitic rocks from the Maya Block, on the other side of

the plate boundary from the NW Central American arc rocks, do not have appropriate Nd-Hf and Pb isotopic compositions (Table 2.2), and their Zr/Hf ratios (17-24) are also too low to serve as the enriched endmember, not to mention the difficulty of getting this material across the plate boundary to the source of the subduction-zone volcanism on the Chortis Block.

Interestingly, only granitic sample G3 from the Chiquimula Intrusive Complex behind the Guatemalan VF on the Chortis Block has a Sr-Nd-Pb-Hf isotopic composition that could serve as the enriched endmember. Chiquimula samples G1 (granite) and G2 (granodiorite) also have appropriate Sr-Nd-Pb isotopic compositions (Feigenson et al., 2004), but no Hf isotope exists for these samples. Nevertheless, in order to model a mixing curve in the Sr and Nd isotope system from the most depleted BA sample (or the composition of the subducting crust, as indicated by sample SO144-1 from Werner et al., 2003) to G3 that goes through the BVF/BA array and the Guatemala VF samples requires a significantly lower Sr/Nd ratio than measured in the Chiquimula samples. In addition, up to ~45 wt. % assimilation is required to generate the Sr and Nd isotopic compositions of the most enriched BVF/VF samples. Such large amounts of assimilation are not only unrealistic based on thermal considerations, but also are not consistent with a basaltic major element composition for these samples rather than a granitic composition. In addition, the oxygen isotope data for the Guatemala VF and the BVF rocks does not allow such a large contribution from granitic rocks, assuming $\delta^{18}O$ values for the granitic basement based on comparison with data for similar types of granites from other areas (Eiler et al., 2005). Finally, the Zr/Hf ratio (27) is also too low for the enriched endmember. In conclusion, although granitic sample G3 has the appropriate Sr-Nd-Pb-Hf isotopic composition to serve as the enriched endmember for northwestern Central America, it does not have an appropriate major and trace element composition to serve as the enriched Guatemalan endmember.

Since the Chiquimula granitic sample (G3) has the appropriate Sr-Nd-Pb-Hf isotopic composition to serve as the enriched endmember, further consideration of this pluton, however, could provide insights into the enriched Guatemala endmember. The Chiquimula plutonic complex consists primarily of gabbro, diorite, granodiorite (~95% by

volume), which yield a whole-rock Rb/Sr age of 50 ± 9 Ma and an initial $^{87}Sr/^{86}Sr$ of ~0.706 (Clemons and Long, 1971), close to the value measured for sample G1 of 0.705960 (Feigenson et al, 2004). On the other hand, a biotite whole-rock Rb/Sr isochron from a granitic sample produced an age of 95 ± 1 Ma (two sigma), whereas a K/Ar age of 84 Ma was obtained on "the same material" (Clemons and Long, 1971). Assuming an initial $^{87}Sr/^{86}Sr$ of 0.706, we get an age of 9.5 Ma for granitic sample G3 using the Rb and Sr concentrations measured by ICP-MS, which generates a very high $^{87}Rb/^{86}Sr$ ratio of 9.56. Assuming an age of 50 Ma, the initial $^{87}Sr/^{86}Sr$ of 0.70050 is clearly too low. Alternatively, assuming an initial identical to the BVF sample with the most radiogenic Sr (0.70415), yields and age of 23 Ma. Therefore, either the G3 granite is relatively young (≤23 Ma), or the sample has not served as a closed system for Rb and/or Sr, both highly mobile elements during weathering, since the formation of the granite. Although the Rb-Sr system is very sensitive to age corrections for sample G3, corrections for radiogenic ingrowth for the other isotopic systems are relatively minor, even if an age of 50 Ma is assumed. The above discussion serves to illustrate that radiogenic ingrowth of ^{87}Sr has played an important role in the evolution of Chiquimula Pluton, and until we have reliable age data for each sample, we will not be able to determine the initial $^{87}Sr/^{86}Sr$ ratios. The measured $^{87}Sr/^{86}Sr$ ratios of the samples (0.70596-0.70729), however, represent maximum initial values and thus maximum source ratios. On the other hand, assuming that parent-daughter ratios for the Sm-Nd, Lu-Hf and (U-Th)/Pb systems, which are low in the samples, were not substantially higher in the source of the Chiquimula Pluton, the Nd, Hf and Pb isotopic compositions could reflect the source composition.

As discussed above, the present subduction input can be ruled out as the source of the Quaternary northwestern Central American enriched endmember. As is illustrated by the Chiquimula plutonic rocks, an enriched component, with an isotopic composition appropriate for the enriched Guatemala endmember, is present within the overriding plate in NW Central America. These granitic crustal rocks, however, do not have the appropriate major and trace element compositions to serve as the enriched endmember. Therefore we favor a lithospheric mantle origin for the enriched component. In accordance with the major and trace element data supporting the

involvement of pyroxenite-derived melts in the generation of the Quaternary Guatemala VF and the BVF volcanic rocks, we propose that the parental magmas for the Chiquimula Pluton, and most likely other plutonic rocks in NW Central America, either froze and formed eclogties or crystallized pyroxenitic cumulates in the lithospheric mantle (and possibly lower crust). A relatively low fluid flux from the subducting crust, combined with a short mantle melting column, resulted in low degrees of melting and preferential sampling of the pyroxenites and eclogites formed in the mantle and lower crust during phases of earlier arc volcanism.

2.5.3 Honduras BA Endmember

The BA samples from Utila Island and Yojoa in Honduras are alkalic (hawaiitic) in composition with similar major element compositions to alkalic ocean island basaltic (OIB) rocks with similar MgO contents. These samples have the highest TiO_2, K_2O, P_2O_5, lowest SiO_2 and similar Al_2O_3, FeOt, MnO, CaO contents compared to the BVF rocks at a given MgO content. They are comparable to the enriched Guatemala endmember samples, suggesting they could also be derived from a pyroxenitic source. The incompatible element characteristics of the BA volcanics are similar to those commonly observed in OIBs, with their multi-element patterns showing relative enrichment in Nb and Ta, relative depletion in Pb and no pronounced peaks at fluid-mobile incompatible elements, in contrast to the VF and most BVF samples. An OIB-type of source is also consistent with the low Ba/La, U/Th and La/Yb ratios.

In contrast to the enriched incompatible element abundances, the Sr-Nd-Hf isotopic compositions of the BA samples are depleted, falling at the enriched end of the Pacific MORB field. The Pb isotopic composition of the Utila and La Providencia samples however are anomalous and fall below the VF/BVF data array on Pb isotope (i.e. have the highest $^{206}Pb/^{204}Pb$ but among the lowest $^{207}Pb/^{204}Pb$ and $^{208}Pb/^{204}Pb$ of all NW CAVA samples) and the Nd vs. Hf isotope diagrams. On the Pb isotope diagrams, these samples plot near the radiogenic end of the field for Cocos Plate Oceanic Crust, exhibiting relatively high $^{206}Pb/^{204}Pb$ but low $^{207}Pb/^{204}Pb$ and $^{208}Pb/^{204}Pb$. Interestingly, the samples with the highest $^{206}Pb/^{204}Pb$ but relatively low

$^{207}Pb/^{204}Pb$ and $^{208}Pb/^{204}Pb$ from the Cocos Plate are the samples that appear to have gained uranium through seafloor alteration processes. Although Pb is relatively immobile during low temperature seafloor alteration, the elevated ^{206}Pb results from radiogenic ingrowth of ^{206}Pb by relatively recent ^{238}U enrichment. ^{207}Pb is derived from ^{235}U, which has largely been exhausted by radioactive decay since the formation of the Earth due to its relatively short half-life of 0.7 Ga. Due to the small amount of ^{235}U relative to ^{238}U, the ^{207}Pb is not significantly affected by relatively recent U enrichment. Since ^{208}Pb is derived from ^{232}Th and Th is relatively immobile during seafloor alteration processes, the composition of ^{208}Pb will also not be significantly affected by low temperature seafloor alteration. Therefore altered seafloor can evolve high ^{206}Pb within relatively short time scales of 10s to 100s of millions of years, while ^{207}Pb and ^{208}Pb show relatively little ingrowth over these time scales (e.g. Thirlwall, 1997). Considering the OIB-like major and trace element compositions of the Utila samples but the relatively depleted isotopic compositions, we propose that the Utila and possibly also La Providencia samples (Feigenson et al., 2004) are derived from melting of young, recycled oceanic crust in the asthenosphere upwelling in the back-arc.

The BVF samples show less pronounced subduction-zone incompatible element signatures than the VF samples, displaying less pronounced Nb and Ta troughs and less pronounced peaks at fluid mobile elements (and lower fluid-mobile to less-fluid-mobile element ratios). In Honduras some of the multi-element patterns approach those of ocean-island-basalt (OIB) – type rocks, displaying neither an relative Nb and Ta depletion (a trough at these elements in the incompatible element patterns) or relative Pb enrichment (a peak in the patterns). Therefore the incompatible elements of the BVF rocks suggest that an OIB-like component, similar to that sampled at Utila and La Providencia, is in the mantle wedge located beneath the BVF localities also. This component however seems to be largely absent in the mantle beneath the VF.

2.6 Conclusions:

We used major and trace elements and Sr-Nd-Pb-Hf isotopic compositions from mafic volcanic front (VF), behind the volcanic front (BVF) and back-arc (BA) lava and tephra samples from NW Nicaragua, Honduras, El Salvador and Guatemala to further constrain the sources for NW Central American Arc volcanism. We distinguished three geochemically distinct endmember components for the prevalent volcanism in NW Central America:

(1) The NW Nicaragua VF endmember, characterized by high FeO^t and low SiO_2, extremely high fluid-mobile-element contents (e.g. LILE) but low N-MORB-like fluid-immobile-element contents (e.g. REE and HFSE), enriched (high) 87Sr/86Sr ratios but depleted (unradiogenic) Pb and (radiogenic) Nd and Hf isotopic compositions. Based also on the results of other published studies, we propose that a very steep slab dip results in serpentinite dehydration and a high fluid flux into the asthenospheric wedge beneath Nicaragua, carrying high contents of fluid-mobile elements. The high fluid flux results in large degrees of melting in the thick mantle mantle wedge (i.e. long melting column), causing dilution of fluid immobile elements. The high Sr isotope ratios are ultimately derived from seawater that altered the crust and upper mantle (converting the peridotite to serpentinite) of the incoming plate and reflect the high fluid flux from dehydration of the serpentinite on the incoming plate. Due to the low Pb concentration of seawater, the elevated (compared to N-MORB) Pb in the Nicaraguan arc magmas is dominated by Pb leached from the subducting ocean crust by the serpentinite-derived fluids with minor amounts of Pb from subducting sediments and or the overriding plate. The high fluid flux from the subducting slab is also responsible for the elevated Pb concentrations, and the high Pb/Nd and Pb/Ce ratios, of the Nicaraguan lavas. The radiogenic Nd and Hf isotopic compositions of the Nicaraguan lavas are largely derived from the mantle wedge, possibly with the addition of small amounts from sediment melts from the subducting plate and/or the overlying lithosphere. In summary, the trace element and Sr-Nd-Pb-Hf isotope ratios of the Nicaraguan lavas appear to be dominated by a largely serpentinite-derived fluid flux from the subducting slab, possibly

with small amounts (<1 wt. %) of sediment melts to a depleted N-MORB type of mantle wedge, resulting in large degrees of melting of primarily peridotitic material.

(2) The enriched Guatemala VF and BVF endmember, characterized by lower FeO^t, CaO, MnO, Sc and V and higher SiO_2 at a given MgO composition than in Nicaraguan VF lavas, high more to less incompatible element ratios, e.g. La/Yb and La/Sm, and Zr/Hf, and enriched Sr, Nd, Hf and Pb isotopic composition. A granitic sample from the Guatemala basement has an appropriate isotopic composition to serve as the enriched endmember, however, requires up to 80% assimilation of the granitic basement which is not consistent with the mafic major element and trace element compositions of the these lavas. We therefore propose that parental magmas for the granitic basement in NW Central America crystallized pyroxenitic cumulates in the lithospheric mantle (and possibly lower crust) that were subsequently melted during Quaternary subduction-related volcanism to generate the enriched Guatemala endmember. The presence of the enriched Guatemala endmember correlates largely with the presence of continental crust and crustal thickness, most likely reflecting more extensive enrichment of the lithosphere through ancient arc volcanism where the crust is thickest.

(3) The Honduras and Caribbean BA endmember, characterized by alkalic lavas with OIB-type trace element compositions and enriched (E)-MORB-type isotopic compositions. We propose that the BA lavas preferentially sample eclogite/pyroxenite in the asthenosphere upwelling in the backarc, derived from relatively young subducted oceanic crust in the upper mantle.

Mixing between these three distinct types of magmas could generate the observed along- and across-arc variations in incompatible trace element and Sr-Nd-Pb-Hf isotope ratios.

Acknowledgements: We would like to thank Carlos Pullinger, Dolores Ferres, Walther Hernadez from SNET, Eddi Sanchez and Otoniel Mathias from INSIVUMEH and Amilcar S. Hernandez from UNAH for field assistance. We thank S. Hauff, D.

Garbe-Schönberg and D. Rau for analytical assistance. We are grateful to M. Carr and U. Martens for generously providing Guatemalan basement samples. This publication is contribution no. 146 of the Sonderforschungsbereich 574 “Volatiles and Fluids in Subduction Zones” of Kiel University.

2.7 References

Abers, G., T. Plank, et al. (2003). "The wet Nicaraguan slab." Geophysical Research Letters **Vol. 30**(No. 2).

Abers, G. A., K. M. Fischer, et al. (2007). "Imaging the arc source in Central America: The TUCAN broadband seismic experiment." Geopysical Research Abstracts **Vol. 9**(10763).

Arculus, R. J. (1994). "Aspects of magma genesis in arcs." Arculus, R **Lithos. 33**(No. 1-3): p. 189-208.

Auboin, J., J.-C. Azéma, et al. (1982). "The middle american trench in the geological framework of central america." DSDP Initial Reports **Vol. 67**: p. 747-755.

Auger, L. S., G. Abers, et al. (2006). "Crustal Thickness Variations Beneath the Central American Arc." American Geophysical Union, Fall Meeting 2006, abstract(T23C-0517).

Blichert-Toft, J. and F. Albarède (1997). "The Lu-Hf isotope geochemistry of chondrites and the evolution of the mantle-crust system." Earth and Planetary Science Letters **Vol. 148**: p. 243-258.

Cameron, B. I., J. A. Walker, et al. (2002). "Flux versus decompression melting at stratovolcanoes in southeastern Guatemala." Journal of Volcanology and Geothermal Research **Vol. 119**: p. 21-50.

Carr, M. J. (1984). "Symmetrical and segmented variation of physical and geochemical characteristics of the Central American volcanic front." J. Volcanol. Geotherm. Res. **Vol. 20**: p. 231-252.

Carr, M. J. and M. D. Feigenson (2003). "Volcanism and Geochemistry in Central America: Progress and Problems." Geophysical Monograph **Vol. 138**(Inside the subduction factory): p. 153-174.

Carr, M. J., M. D. Feigenson, et al. (1990). "Incompatible element and isotopic evidence for tectonic control of source mixing and melt extraction along the Central American arc." Contrib. Mineral. Petrol. **105**: 369-380.

Carr, M. J., I. Saginor, et al. (2007). "Element fluxes from the volcanic front of Nicaragua and Costa Rica." Geochemistry Geophysics Geosystems **Vol. 8**(No. 6): Q06001, doi:10.1029/2006GC001396.

Chan, L.-H. and M. Kastner (2000). "Lithium isotopic compositions of pore fluids and sediments in the Costa Rica subduction zone: implications for fluid processes and sediment contribution to the arc volcanoes." Earth Planet Sci. Let. **183**: 275-290.

Chan, L.-H., W. P. Leeman, et al. (2006). "Correction to "Lithium isotopic composition of marine sediments"." Geochemistry Geophysics Geosystems **Vol. 7**(No. 8): Q08004, doi:10.1029/2006GC001380.

Chan, L.-H., A. Starinsky, et al. (2002). "The behavior of lithium and its isotopes in oilfield brines: Evidence from the Heletz-Kokhav field, Israel." Geochimica et Cosmochimica Acta **66**(4): 615-623.

Chan, L. H., W. P. Leeman, et al. (1999). "Lithium isotopic composition of Central American Volcanic Arc lavas: implications for modification of subarc mantle by slab-derived fluids." Chem. Geol. **160**: 255-280.

Clemons, R. E. and L. E. Long (1971). "Petrologic and Rb-Sr Isotopic Study of the Chiquimula Pluton, Southeastern Guatemala." Geological Society of America Bulletin **82**: 2729-2740.

DeMets, C. (2001). "A new estimate for present-day Cocos-Caribbean plate motion: Implications for slip along the Central American volcanic arc." Geophysical Research Letters **Vol. 28**(No. 21): p. 4043-4046.

Donnelly, T. W., G. S. Horne, et al. (1990). Northern Central America; The Maya and Chortis blocks. The Geology of North America; The Caribbean Region. J. E. Case and G. Dengo. Boulder/Colorado, The Geological Society of America. **Vol. H**.

Eiler, J. M., M. J. Carr, et al. (2005). "Oxygen isotope constraints on the sources of Central American arc lavas." Geochemistry Geophysics Geosystems **Vol. 6**(No. 7): Q07007, doi:10.1029/2004GC000804.

Feigenson, M. and M. J. Carr (1993). "The source of Central American lavas: inferences from geochemical inverse modeling." Contributions to Mineralogy and Petrology **113**(2): 226-235.

Feigenson, M. D., M. J. Carr, et al. (2004). "Lead isotope composition of Central American volcanoes: Influence of the Galapagos plume." Geochemistry Geophysics Geosystems **5**(No.6): Q06001 DOI 10.1029/2003GC000621.

Garbe-Schoenberg, C.-D. (1993). "Simultaneous determination of thirty-seven trace elements in twenty-eight international rock standards by ICP-MS." Geostandards Newsletter **Vol. 17**(No. 1): p. 81-97.

Gazel, E., M. J. Carr, et al. (2009). "Galapagos-OIB signature in southern Central America: Mantle refertilization by arc-hot spot interaction." Geochem. Geophys. Geosyst. **10**(2): 1-32.

Geldmacher, J., K. Hoernle, et al. (2008). "Geochemistry of a new enriched mantle type locality in the northern hemisphere: Implications for the origin of the EM-I source." Earth and Planetary Science Letters **265**(1-2): 167-182.

Geldmacher, J. r., K. Hoernle, et al. (2006). "Origin and geochemical evolution of the Madeira-Tore Rise (eastern North Atlantic)." J. Geophys. Res. **111**.

Govindaraju, K. (1994). "Compilation of working values and sample descriptions for 383 geostandards." Geostandard Newsletters **18**(Special Issue): 158 pp.

Grevemeyer, I., C. R. Ranero, et al. (2007). "Passive and active seismological study of bending-related faulting and mantle serpentinization at the Middle America trench." Earth and Planetary Science Letters **258**(3-4): 528-542.

Hauff, F., K. Hoernle, et al. (2000). "Age and Geochemistry of Basaltic Complexes in Western Costa Rica: Contributions to the Geotectonic Evolution of Central America." Geochemistry Geophysics Geosystems **1**(5): doi:10.1029/1999GC000020.

Herzberg, C. and P. D. Asimow (2008). "Petrology of some oceanic island basalts: PRIMELT2.XLS software for primary magma calculation." Geochem. Geophys. Geosyst. **9**.

Hoernle, K., D. L. Abt, et al. (2008). "Arc-parallel flow in the mantle wedge beneath Costa Rica and Nicaragua." Nature **451**(7182): 1094-1097.

Hoernle, K. and F. Hauff (2004). Oceanic Igneous Complexes in Central America. Central America: Geology, Resources and Hazards. J. Bundschuh and G. Avarado. Lisse, Swets & Zeitlinger**:** accepted with revisions.

Hoernle, K. and G. Tilton (1991). "Sr-Nd-Pb isotope data for Fuerteventura (Canary Islands) basal complex and subaerial volcanics: applications to magma genesis and evolution." Schweizerische mineralogische und petrographische Mitteilungen **71**: 3 - 18.

Ivandic, M., I. Grevemeyer, et al. (2008). "Impact of bending related faulting on the seismic properties of the incoming oceanic plate offshore of Nicaragua." J. Geophys. Res. **113**.

Leeman, W. P. (1996). "Boron and Other Fluid-mobile Elements in Volcanic Arc Lavas: Implications for Subduction Processes." Geophysical Monograph **96**(Subduction: Top to Bottom): 269-276.

Leeman, W. P., M. J. Carr, et al. (1994). "Boron geochemistry of the Central American Volcanic Arc: Constraints on the genesis of subduction-related magmas" Geochimica et Cosmochimica Acta **Vol. 58**(1): pp. 149-168.

Ligorria, J. P. and E. Molina (1997). "Crustal velocity structure of southern Guatemala using refracted and Sp converted waves." Geofísica international.

MacKenzie, L., G. A. Abers, et al. (2008). "Crustal structure along the southern Central American volcanic front." Geochem. Geophys. Geosyst. **9**(8): 1-19.

Meschede, M. (1998). "The impossible Galápagos connection: geometric constraints for a near-American origin of the Caribbean plate." Geologische Rundschau **87**: 200 - 205.

Morris, J. D., W. P. Leeman, et al. (1990). "The subducted components in island arc lavas: constraints from Be isotopes and B-be systematics." Nature **Vol. 344**: p. 31-36.

Narcía-Lopez, R., R. Castro, et al. (2004). "Determination of crustal thickness beneath Chiapas, Mexico using S and Sp waves." Geophysical Journal International **157**(1): 215-228.

Patino, L. C., M. J. Carr, et al. (2000). "Local and regional variations in Central American arc lavas controlled by variations in subducted sediment input." Contrib. Mineral. Petrol. **138**: 265-283.

Pearce, J. A., P. D. Kempton, et al. (2007). "Hf-Nd evidence for the origin and distribution of mantle domains in the SW Pacific." Earth and Planetary Science Letters **Vol. 260**: p. 98-114.

Pearce, J. A. and D. W. Peate (1995). "Tectonic Implications of the Composition of Volcanic Arc Magmas." Annu. Rev. Earth Planet Sci. **23**: 251-285.

Pertermann, M., M. Hirschmann, et al. (2004). "Experimental determination of trace element partitioning between garnet and silica-rich liquid during anhydrous partial melting of MORB-like eclogite." Geochemistry Geophysics Geosystems **5**: doi:10.1029/2003GC000638.

Plank, T. and C. H. Langmuir (1998). "The chemical composition of subducting sediment and its consequences for the crust and mantle." Chemical Geology **145**: 325-394.

Protti, M., F. Güendel, et al. (1995). Correlation between the age of the subducting Cocos plate and the geometry of the Wadati-Benioff zone under Nicaragua and Costa Rica. Geologic and tectonic development of the Caribbean plate boundary in southern Central America. P. Mann. Boulder, Colorado, Gelogical Society of America. **295:** 309 - 326.

Ranero, C. R. and R. Huene von (2000a). "Subduction erosion along the middle America convergent margin." Nature **404**: 748-752.

Ranero, C. R., J. P. Morgan, et al. (2003). "Bending-related faulting and mantle serpentinization at the Middle America trench." Nature **425**: 367-373.

Rüpke, L. H., J. P. Morgan, et al. (2004). "Serpentine and the subduction zone water cycle." Earth and Planetary Science Letters **223**(1-2): 17-34.

Rüpke, L. H., J. Phipps Morgan, et al. (2002). "Are the regional variations in Central American arc lavas due to differing basaltic versus peridotitic slab sources of fluids?" Geology **30**(11): 1035-1038.

Sadofsky, S., M. Portnyagin, et al. (2008). "Subduction cycling of volatiles and trace elements through the Central American volcanic arc: evidence from melt inclusions." Contributions to Mineralogy and Petrology **155**(4): 433-456.

Sun, S.-S. and W. F. McDonough (1989). Chemical and isotopic systematics of oceanic basalts: implications for mantle composition and processes. Magmatism in the Ocean Basins. A. D. Saunders and M. J. Norry. London, Blackwell. **42:** 313 - 345.

Syracuse, E. M. and G. A. Abers (2006). "Global compilation of variations in slab depth beneath arc volcanoes and implications." Geochem. Geophys. Geosyst. **7**(5): 1-18.

Syracuse, E. M., G. A. Abers, et al. (2008). "Seismic tomography and earthquake locations in the Nicaraguan and Costa Rican upper mantle." Geochem. Geophys. Geosyst. **9**(7): 1-22.

Thirlwall, M. F. (1997). "Pb isotopic and elemental evidence for OIB derivation from young HIMU mantle." Chemical Geology **139**: 51-74.

Todt, W., R. A. Cliff, et al. (1996). Evaluation of a ^{202}Pb-^{205}Pb Double Spike for High-Precision Lead Isotope Analysis. Earth Processes: Reading the Isotopic Code. A. Basu and S. Hart. Washington, D.C., AGU Geophysical Monograph. **Vol. 95:** p. 429-437.

Vanucchi, P., D. W. Scholl, et al. (2001). "Tectonic erosion and consequent collapse of the Pacific margin of Costa Rica: combined implications from ODP Leg 170, seismic offshore data and regional geology of the Nicoya Peninsula." Tectonics **20**: 649-668.

Vannucchi, P., S. Galeotti, et al. (2004). "Long-term subduction-erosion along the Guatemalan margin of the Middle America Trench." Geology **Vol.32**(No.7): p. 617-620.

Walker, J. A., M. J. Carr, et al. (1995). "Abrupt change in magma generation processes across the Central American arc in southeastern Guatemala: flux-dominated melting near the base of the wedge to decompression melting near the top of the wedge." Contrib Mineral Petrol **120**: p. 378-390.

Walker, J. A., J. E. Mickelson, et al. (2007). "U-series disequilibria in Guatemalan lavas, crustal contamination and implications for magma genesis along the Central American subduction zone." J. Geophys. Res. **Vol.112**(B06205).

Werner, R., K. Hoernle, et al. (2003). "Geodynamic evolution of the Galapagos hot spot system (Central East Pacific) over the past 20 m.y.: Constraints from morphology, geochemistry, and magnetic anomalies." Geochemistry Geophysics Geosystems **Vol. 4**(No. 12): 1108, doi:10.1029/2003GC000576.

Table 2.1 Major (wt%) and trace elements (ppm) and isotopic ratios of selected Central American Arc volcanics from Volcanic Front (VF), Behind the Volcanic Front (BVF) and Back-arc (BA) samples. Volcanics major and trace element data for samples marked with (*) from Sadofsky et al. (2008).

Note Guatemalan basement sample GU G3K is sample G3 from Feigenson et al. (2004) reanalyzed for this study.

Table 1

sample #	Sample Location	Rock Type	Rock Classification	Lat (N)	Long (W)	DAA	SiO2 wt%	TiO2 wt%	AL2O3 wt%	Fe2O3 wt%	MnO wt%	MgO wt%	CaO wt%	Na2O wt%	K2O wt%	P2O5 wt%	H2O wt%	CO2 wt%	SUM wt%
Guatemala Volcanic Front																			
GU2A	Pacaya complex	tephra	calc-alkaline basalt	14.4090	-90.6153	198.80	48.12	1.05	17.89	12.00	0.18	6.76	9.54	2.54	0.59	0.21	0.32	0.00	98.88
GU4	Acatenango	bomb	calc-alkaline basaltic andesite	14.5398	-90.8452	170.60	55.87	0.72	18.94	8.21	0.14	3.23	7.49	3.86	1.18	0.21	0.62	0.01	99.85
GU5	Acatenango (NW-flank)	bomb	calc-alkaline basaltic andesite	14.5335	-90.9022	165.70	57.99	0.81	18.76	7.19	0.14	2.40	6.50	4.43	1.55	0.28	0.55	0.02	100.05
GU6	Acatenango (NW-flank)	tephra	calc-alkaline basaltic andesite	14.5235	-90.9307	163.60	52.89	1.02	18.70	9.44	0.14	3.92	8.11	3.64	1.12	0.24	0.50	0.07	99.22
GU8A	Pacaya	lava flow	calc-alkaline basalt	14.3821	-90.6023	201.40	51.62	1.31	17.83	11.52	0.19	4.39	8.62	3.81	1.09	0.35	0.10	0.01	100.73
GU15A	Santa Maria (N-flank)	lava flow	calc-alkaline basaltic andesite	14.7528	-91.5242	96.60	56.37	0.75	19.15	8.21	0.14	3.56	7.64	3.91	1.08	0.25	0.18	0.01	101.06
GU17A	Santa Maria (N-flank)	block and ash flow	calc-alkaline basaltic andesite	14.7546	-91.5239	96.60	53.85	0.81	17.74	8.72	0.15	4.70	7.63	3.67	1.03	0.21	0.62	0.03	98.51
GU22	Toliman Volcano (NW-flank)	lava flow	calc-alkaline basaltic andesite	14.6501	-91.2248	129.70	57.50	0.78	16.78	7.62	0.12	3.90	6.53	3.67	2.05	0.17	0.71	0.02	99.12
GU23A	Atitlan Volcano (NW-flank)	bomb	calc-alkaline basalt	14.6016	-91.2251	132.30	51.31	1.00	18.38	9.51	0.13	4.94	8.82	3.37	0.98	0.22	0.41	0.05	98.66
GU26	San Pedro complex	lava flow	calc-alkaline basaltic andesite	14.6540	-91.2976	122.80	52.83	0.81	17.09	9.19	0.15	5.18	8.80	3.21	1.22	0.17	0.66	0.05	98.65
OTO I	Fuego Volcano	lava flow	calc-alkaline basaltic andesite	14.4830	-90.8830	170.10	54.18	0.94	20.88	8.36	0.14	2.95	8.84	3.99	0.91	0.21	0.10	0.00	101.40
OTO II	Fuego Volcano	lava flow	calc-alkaline basaltic andesite	14.4830	-90.8830	170.10	53.83	0.94	20.79	8.65	0.14	3.21	8.87	3.84	0.89	0.21	0.13	0.01	101.37
Guatemala Behind the Volcanic Front																			
GU14A	Barberena-Cuilapa	lava flow	calc-alkaline basalt	14.2942	-90.3410	230.20	49.89	1.34	18.45	10.36	0.16	6.08	9.94	3.60	0.60	0.26	0.26	0.01	100.68
GU29	Coraacaste town	lava flow	calc-alkaline basalt	14.8566	-89.5960	268.30	50.49	1.33	17.48	9.57	0.16	6.23	8.82	3.56	1.04	0.32	0.25	0.02	99.00
GU30	Coraacaste town (SSE)	lava flow	calc-alkaline basaltic andesite	14.8245	-89.5639	273.00	52.95	1.39	17.30	9.99	0.17	5.20	7.29	4.01	1.47	0.43	0.43	0.01	100.20
GU32	Quezaltepeque (SSE)	lahar deposit	calc-alkaline basaltic andesite	14.7447	-89.5461	278.90	52.39	1.43	16.72	9.69	0.15	4.14	7.81	3.04	1.93	0.56	1.71	0.15	97.86
GU35B	Los Gemeloz	lava flow	calc-alkaline basalt	14.5953	-89.6460	277.90	49.67	1.21	17.92	10.17	0.16	7.23	9.58	3.23	0.83	0.35	0.50	0.03	100.35
GU38	Cerro Gordo (W cone)	lava flow	calc-alkaline basalt	14.4427	-89.6110	289.30	50.41	1.12	17.54	10.23	0.17	6.92	9.69	2.94	1.49	0.39	0.30	0.01	100.90
GU39	San Miguel Chapron Graben	bomb	calc-alkaline basalt	14.5113	-89.7499	272.90	50.71	1.32	18.54	11.08	0.17	5.11	8.83	3.56	0.89	0.29	0.61	0.03	100.50
El Salvador Volcanic Front																			
ES002	Siguatepeque Volcano (E)	scoria	calc-alkaline basaltic andesite	13.6150	-88.5556	431.30	54.72	1.23	15.75	11.96	0.22	3.46	7.36	3.45	1.76	0.37	0.86	0.03	100.28
ES003	Siguatepeque Volcano (E)	lava flow	calc-alkaline basaltic andesite	13.6200	-88.5600	431.30	54.00	1.21	15.30	11.56	0.22	3.33	7.03	3.49	1.92	0.38	1.14	0.03	98.44
ES005	Santa Ana Volcano	tephra	calc-alkaline basaltic andesite	13.8451	-89.6291	320.00	52.89	0.94	17.59	10.39	0.17	3.97	7.72	3.32	1.64	0.27	0.74	0.08	98.90
ES009	Laguna Caldera	bomb	calc-alkaline basaltic andesite	13.8399	-89.3609	345.00	54.88	1.22	15.99	11.46	0.21	2.76	6.99	3.67	1.68	0.32	0.36	0.01	99.18
ES019	Coujutepeque, Cerro de Las Pavas	bomb	calc-alkaline basalt	13.7124	-88.9365	391.00	49.92	1.20	17.90	9.97	0.16	5.52	8.96	3.31	1.01	0.36	0.96	0.03	98.31
ES027B	San Miguel Volcano	lava flow	calc-alkaline basalt	13.5028	-88.2217	468.10	50.19	0.81	18.62	11.03	0.18	6.22	10.10	2.47	0.53	0.15	0.46	0.01	100.30
ES028B	San Miguel Volcano (NW)	lava flow	calc-alkaline basalt	13.5112	-88.2478	465.30	50.93	0.98	18.93	10.99	0.18	4.19	10.23	2.75	0.73	0.18	0.33	0.03	100.09
ES 031	San Miguel Volcano	lava flow	calc-alkaline basalt	13.4180	-88.3142	464.30	51.21	1.03	18.74	11.03	0.18	4.17	10.13	2.84	0.82	0.21	0.35	0.02	100.36
ES035A	Usulutan Complex	bomb	calc-alkaline basaltic andesite	13.5538	-88.4314	446.10	58.37	0.89	17.09	7.89	0.22	2.49	5.59	4.57	1.51	0.38	1.26	0.02	99.00
ES036C	Izalco (northern flank)	tephra	calc-alkaline basaltic andesite	13.8184	-89.6312	321.30	54.02	0.85	18.49	9.53	0.16	4.22	8.20	3.72	1.19	0.16	0.20	0.01	100.54
ES038	Izalco (western flank)	lava flow	calc-alkaline basaltic andesite	13.8188	-89.6276	321.70	52.96	0.87	18.84	9.90	0.17	4.13	8.47	3.59	1.05	0.15	0.31	0.01	100.13
ES SSI	San Salvador Volcano	lava flow	calc-alkaline basaltic andesite	13.8045	-89.3296	358.00	58.75	1.17	15.33	10.82	0.23	2.27	5.54	4.08	2.14	0.40	0.19	0.01	100.73
ES SSII	San Salvador Volcano	lava flow	calc-alkaline basaltic andesite	13.8045	-89.3296	358.00	59.26	1.17	15.37	10.79	0.23	2.22	5.51	4.06	2.15	0.40	0.23	0.03	101.16
El Salvador Behind the Volcanic Front																			
ES013	cinder cone close to Cerrito Ojo de Agua	bomb	calc-alkaline basalt	13.8572	-89.2287	356.20	50.78	0.95	17.24	9.75	0.16	6.86	9.76	2.78	0.72	0.25	0.52	0.02	99.25
ES014	Cerrito Ojo de Agua	lava flow	calc-alkaline basaltic andesite	13.8572	-89.2287	356.20	53.85	1.01	17.61	9.13	0.16	4.48	7.83	3.51	1.59	0.39	0.72	0.02	99.56
ES015	Cerro Quemado	tephra	calc-alkaline basaltic andesite	14.2422	-89.4706	313.10	53.10	1.15	17.78	9.41	0.16	5.60	8.19	3.43	1.25	0.42	0.42	0.06	100.49
ES016	Cerro Quemado	bomb	calc-alkaline basaltic andesite	14.2422	-89.4706	313.10	52.70	1.18	17.50	9.36	0.16	5.33	8.13	3.71	1.28	0.42	0.38	0.01	99.77
ES017	Junquillo and Rio Ostija	lava flow	calc-alkaline basalt	14.3180	-89.5836	298.60	51.44	1.33	17.65	10.02	0.16	5.13	8.17	3.57	1.54	0.47	0.83	0.02	99.48
ES018B	San Diego Volcano	lava flow	calc-alkaline basalt	14.2750	-89.4772	310.70	50.94	1.30	17.58	9.65	0.16	5.20	9.05	3.59	1.16	0.44	0.45	0.03	99.07
ES024B	El Singüil	tephra	calc-alkaline basalt	14.0488	-89.6317	308.70	49.24	1.09	17.11	10.09	0.16	7.60	9.60	3.01	0.84	0.25	0.41	0.03	98.99
Honduras Volcanic Front																			
H3B	El Tigre Island (S)	bomb	trachybasalt	13.2526	-87.6304	536.20	57.93	0.83	18.20	7.88	0.21	2.58	6.55	4.51	0.92	0.28	0.47	0.01	99.89
Honduras Behind the Volcanic Front																			
H1	El Tigre Island (N)	bomb	calc-alkaline basalt	13.2896	-87.6418	533.10	49.64	0.87	18.22	10.66	0.18	5.21	9.51	3.05	0.85	0.26	1.11	0.07	98.45
H4B	El Tigre Island (N)	bomb	calc-alkaline basaltic andesite	13.2724	-87.6561	532.80	52.43	0.90	19.15	10.58	0.18	3.33	9.23	3.24	0.86	0.19	0.51	0.01	100.09
H5	Sacate Grande - SE-flank	lava flow	calc-alkaline basalt	13.3202	-87.6171	533.70	51.46	0.94	18.33	11.33	0.19	3.79	9.23	3.31	0.64	0.18	0.59	0.02	99.40
H9	near Zambrano town	lava flow	calc-alkaline basalt	14.2658	-87.3960	501.90	51.21	1.13	17.91	10.17	0.16	5.41	8.96	3.03	1.14	0.42	0.86	0.01	99.54
H13	S of Pore Rios (Sula Graben)	lava flow	calc-alkaline basalt	15.2066	-87.9612	398.70	48.95	1.96	17.81	10.66	0.16	5.29	8.95	3.99	1.62	0.63	0.57	0.48	100.02
H14	Cerro Las Crucitas (W of Tegucigalpa)	lava flow	calc-alkaline basalt	14.0168	-87.3333	521.40	51.42	1.04	16.54	10.04	0.16	5.26	8.54	2.89	1.49	0.34	1.32	0.02	97.72
H16	SW of Tegucigalpa	lava flow	calc-alkaline basaltic andesite	13.9551	-87.2091	536.20	52.49	1.04	17.55	9.78	0.15	4.51	8.80	3.07	1.54	0.43	1.02	0.02	99.36
Honduras Backarc																			
H10	Laguna de Yojoa (N)	lava flow	Hawaiite	14.9297	-87.9801	412.10	48.92	2.50	16.34	11.77	0.21	3.96	7.12	4.55	2.41	0.93	1.01	0.05	98.71
H17A	Utila Island	tuff	Hawaiite	16.1207	-86.8832	446.20	46.93	1.63	16.64	10.31	0.18	6.69	9.49	3.01	1.99	0.58	2.62	0.06	97.45
H18A	Utila Island	clasts	Hawaiite	16.1226	-86.8815	446.30	48.20	1.65	17.25	10.14	0.16	6.14	8.44	3.79	2.31	0.59	1.71	0.09	98.67

Table 1 continued

sample #		Sample Location	Rock Type		Lat (N)	Long (W)	DAA	SiO2 wt%	TiO2 wt%	AL2O3 wt%	Fe2O3 wt%	MnO wt%	MgO wt%	CaO wt%	Na2O wt%	K2O wt%	P2O5 wt%	H2O wt%	CO2 wt%	SUM wt%
NW Nicaragua Volcanic Front																				
P-58A		Cosigüina	lava block	calc-alkaline basaltic andesite	13.0336	-87.5918	551.80	59.20	0.79	17.27	8.27	0.18	2.20	6.70	4.06	1.41	0.22	0.41	0.02	100.30
P-27A		San Cristobal	block from lahar	calc-alkaline basalt	12.6811	-87.0278	623.10	49.82	0.97	18.20	12.10	0.21	4.55	10.45	2.83	0.71	0.20	0.32	0.02	100.24
P-13		Casitas	lava block	calc-alkaline basalt	12.6857	-86.9553	629.60	50.36	0.86	18.41	11.56	0.19	4.22	9.15	2.78	1.02	0.23	1.38	0.04	98.98
P2-16	(*)	Telica/ San Cristobal	tephra	calc-alkaline basalt	12.5965	-86.9322	636.60	48.57	0.72	18.21	10.27	0.17	5.71	12.21	1.83	0.73	0.13	0.57	0.09	98.55
P-7A		Telica	bomb	calc-alkaline basalt	12.6073	-86.8332	645.10	51.52	0.84	17.93	10.90	0.18	4.48	10.04	2.67	1.20	0.16	0.31	0.02	100.15
P-9		Telica	lava flow	calc-alkaline basalt	12.6051	-86.8361	645.00	49.78	1.01	18.09	11.23	0.17	5.51	11.03	2.44	0.93	0.17	0.29	0.01	100.56
P-43		Cone3	bomb	calc-alkaline basaltic andesite	12.5334	-86.6774	663.50	53.07	1.34	15.96	12.45	0.20	4.11	8.45	3.15	1.16	0.23	0.31	0.03	100.33
P-51		Cone2	bomb	calc-alkaline basalt	12.4696	-86.7232	662.90	49.98	0.72	17.18	10.60	0.18	6.53	12.71	1.92	0.59	0.16	0.34	0.02	100.74
P-56G		C. Las Palmitas	tuff	calc-alkaline basaltic andesite	12.6072	-86.7329	654.40	52.57	1.07	16.48	12.48	0.24	3.94	7.73	3.07	0.80	0.20	1.75	0.08	98.82
P-4		C. Negro	bomb	calc-alkaline basalt	12.5076	-86.7009	662.80	49.69	0.76	18.66	11.26	0.19	5.68	11.72	2.04	0.45	0.11	0.17	0.00	100.73
P-6		C. Negro	lava flow	calc-alkaline basalt	12.5023	-86.7005	663.10	49.91	0.79	19.59	10.93	0.18	4.58	11.37	2.26	0.50	0.12	0.22	0.01	100.41
P2-3a	(*)	C. Negro	tephra	calc-alkaline basalt	12.4987	-86.7035	663.10	47.50	0.61	15.74	11.45	0.19	10.03	12.44	1.50	0.27	0.10	0.16	0.04	99.99
P2-3b	(*)	C. Negro	tephra	calc-alkaline basalt	12.4987	-86.7035	663.10	48.86	0.68	21.26	9.84	0.16	4.10	12.45	2.12	0.40	0.13	0.19	0.03	100.15
P2-3d	(*)	C. Negro	tephra	calc-alkaline basalt	12.4987	-86.7035	663.10	49.19	0.75	18.41	11.25	0.19	5.98	12.05	2.10	0.42	0.12	0.16	0.02	100.65
P2-11		C. Negro	lava flow	calc-alkaline basalt	12.4984	-86.7058	662.90	48.44	0.78	19.32	11.00	0.18	4.64	11.59	2.23	0.46	0.13	0.22	0.02	98.96
P2-13		C. Negro	lava flow	calc-alkaline basalt	12.5105	-86.7075	662.10	48.46	0.72	16.32	11.50	0.20	7.43	11.29	2.12	0.46	0.12	0.19	0.03	98.78
P-50		C. Diablo	bomb	calc-alkaline basalt	12.4726	-86.7236	662.70	49.90	0.71	17.33	10.62	0.18	6.41	12.64	1.93	0.60	0.16	0.30	0.02	100.66
P-19		Las Pilas	bomb	calc-alkaline basalt	12.4933	-86.6861	665.00	51.28	0.84	16.05	10.54	0.18	6.06	10.86	2.38	0.81	0.18	0.24	0.00	99.37
P-40A		Cabeza de Vaca	bomb	calc-alkaline basalt	12.5195	-86.6815	663.90	47.39	0.71	17.55	12.39	0.19	7.81	12.25	1.63	0.36	0.09	0.26	0.04	100.55
P-42		Cabeza de Vaca	bomb	calc-alkaline basalt	12.5198	-86.6807	664.00	48.22	0.74	16.31	12.60	0.20	8.46	10.90	1.77	0.49	0.10	0.32	0.04	99.96
P-23		Ojo de Agua	lava flow	calc-alkaline basaltic andesite	12.5145	-86.6806	664.30	54.95	0.94	16.54	10.26	0.20	3.78	8.06	3.20	1.32	0.25	0.27	0.00	99.72
P-46A		Laguna Asos	bomb	calc-alkaline basaltic andesite	12.4402	-86.6716	669.20	56.93	1.05	15.82	10.60	0.20	2.99	6.70	3.35	1.64	0.25	0.71	0.02	99.76
P-47A		C. Buena vista	tephra	calc-alkaline basaltic andesite	12.4005	-86.6643	672.10	57.82	0.98	15.71	9.98	0.19	2.67	6.21	3.33	1.80	0.24	0.90	0.03	99.16
P-48B		Cone4	bomb	calc-alkaline basaltic andesite	12.3727	-86.6500	675.00	54.38	1.00	16.20	11.49	0.20	3.86	8.07	2.90	1.31	0.20	0.69	0.02	99.80
P-32		Momotombo	lava flow	calc-alkaline basaltic andesite	12.4278	-86.5808	678.30	52.57	0.76	17.69	10.64	0.18	5.04	9.85	2.52	0.79	0.15	0.21	0.02	100.40
P-34		Momotombo	lava flow	calc-alkaline basaltic andesite	12.4565	-86.5560	679.00	54.78	0.78	17.21	10.08	0.18	4.19	8.61	2.86	1.00	0.16	0.21	0.01	100.05
Guatemala Basement																				
G 009 L1		Santa Maria basement	basement	granodiorite	14.72	-91.62	89.50	52.87	1.11	16.58	11.05	0.17	5.02	7.97	3.43	1.69	0.15	1.09	0.04	100.26
G 009 L2		Santa Maria basement	basement	granodiorite	14.72	-91.62	89.50	57.60	2.04	16.22	8.88	0.14	2.42	4.08	4.98	3.14	0.47	0.79	0.03	100.32
Chor 8A		Las Ovejas complex	basement	amphibolite/ diorite	14.92	-89.71	254.60	49.97	1.13	19.61	7.46	0.12	5.73	11.85	3.07	0.50	0.17	1.30	0.01	99.72
P12		Las Ovejas complex	basement	diororite	14.89	-89.81	246.60	49.83	1.58	17.73	10.56	0.13	4.37	7.69	3.63	1.86	0.43	1.35	0.03	98.06
GU G3K		near Chiquimula	basement	granitc	14.95	-89.54	268.40	76.27	0.14	12.95	1.17	0.03	0.11	0.45	3.95	4.70	0.03	0.35	0.01	99.80
GU M1		North of Jocotan Fault	basement	phyllite	14.69	-89.63	274.20	55.98	1.71	25.71	2.08	0.01	0.79	0.12	0.22	6.43	0.27	4.54	0.18	93.32
GU M2		North of Jocotan Fault	basement	phyllite	14.71	-89.62	274.00	81.46	0.95	10.65	0.38	0.00	0.24	0.00	0.03	2.36	0.03	2.15	0.02	96.10
619		Rio Hondo (Maya Block)	basement	mylonitc gneiss	15.07	-89.60	256.30	68.46	0.46	14.79	4.24	0.06	1.56	3.03	3.22	2.93	0.16	1.23	0.05	98.91
714A		Concul (Maya Block)	basement	mylotinized orthogneiss	15.06	-90.52	172.90	57.33	2.51	15.43	8.52	0.12	1.54	5.23	1.84	5.65	0.65	1.65	0.06	98.82
Cocos Plate Sediments																				
67_0495_009R_02W_73-75		ODP site 495	hemipelagic sediment	diatomaceous mud	12.4963	-91.0376	262.20	56.89	0.60	12.82	6.01	0.16	2.86	2.09	3.48	1.75	0.13	8.88	1.53	86.79
67_0499_019R_05W_80-82		ODP site 499	hemipelagic sediment	diatomaceous mud	12.6705	-90.9446	261.50	56.31	0.74	15.70	6.86	0.06	2.42	1.65	2.96	1.67	0.14	7.79	1.09	88.51
Cocos Plate MORB																				
67_0495_048R_04W_82-84		ODP site 495	MORB	tholeiite	12.4963	-91.0376	262.20	50.60	1.48	15.93	9.45	0.15	7.22	11.86	2.88	0.09	0.15	1.57	0.14	99.81
206_1256C_10R2_103-105		IODP Site 1256C	MORB	tholeiite	6.7360	-91.9340	486.20	50.13	1.89	12.93	14.99	0.21	6.72	10.29	2.65	0.49	0.15	0.69	0.07	100.57
206_1256D_74R2_102-111		IODP Site 1256D	MORB	tholeiite	6.7360	-91.9340	486.20	50.02	1.36	13.16	12.97	0.25	7.14	10.51	2.95	0.05	0.10	0.49	0.05	98.64

Table 1 continued

sample #	Li ppm	Sc ppm	V ppm	Cr ppm	Co ppm	Ni ppm	Cu ppm	Zn ppm	Ga ppm	Rb ppm	Sr ppm	Y ppm	Zr ppm	Nb ppm	Mo ppm	Sn ppm	Sb ppm	Cs ppm	Ba ppm	La ppm	Ce ppm	Pr ppm	Nd ppm	Sm ppm	Eu ppm	Gd ppm	Tb ppm	Dy ppm	Ho ppm	Er ppm	Tm ppm	Yb ppm	Lu ppm	Hf ppm	Ta ppm	W ppm	Tl ppm	Pb ppm	Th ppm	U ppm
Guatemala Vo																																							
GU2A	5.88	29.38	287.17	28.89	40.26	28.50	59.89	90.44	18.62	8.81	560.34	18.00	73.54	2.46	0.45	0.77	0.13	0.38	300.59	7.48	17.50	2.62	11.95	3.01	1.06	3.16	0.51	3.15	0.63	1.73	0.25	1.67	0.25	1.93	0.14	0.20	0.04	2.93	0.70	0.30
GU4	12.48	13.29	143.38	1.87	20.06	4.22	47.57	85.60	20.00	23.95	584.43	18.22	110.19	2.89	1.12	0.86	0.31	1.21	518.96	10.11	22.34	3.28	14.46	3.40	1.05	3.37	0.51	2.97	0.58	1.59	0.24	1.56	0.24	2.85	0.15	0.38	0.05	4.80	1.67	0.66
GU5	15.29	14.59	118.63	0.85	14.77	2.09	44.58	83.97	19.75	32.49	502.02	25.92	142.62	3.64	1.41	1.16	0.47	1.66	642.79	12.69	28.54	4.25	18.82	4.59	1.27	4.61	0.71	4.19	0.85	2.30	0.34	2.27	0.35	3.75	0.19	0.50	0.12	6.54	2.29	0.91
GU6	9.98	26.31	244.89	13.69	25.34	10.69	74.69	93.41	20.61	21.32	579.01	18.01	129.77	3.46	0.88	1.00	0.19	0.79	547.14	13.23	29.66	4.03	16.79	3.72	1.15	3.54	0.55	3.20	0.63	1.72	0.25	1.64	0.24	3.22	0.21	0.41	0.07	5.70	1.58	0.59
GU8A	9.19	27.54	252.42	12.16	26.91	8.59	96.06	103.16	20.68	18.51	518.78	28.36	119.82	4.18	0.79	1.23	0.12	0.79	543.21	13.70	30.69	4.57	20.69	5.11	1.55	5.24	0.81	4.82	0.97	2.65	0.39	2.56	0.38	3.21	0.21	0.31	0.05	5.29	2.02	0.78
GU15A	9.04	16.39	155.23	34.67	21.21	19.60	40.58	95.18	19.91	17.38	542.46	20.92	135.15	3.12	0.95	0.94	0.21	0.49	520.57	10.08	22.85	3.38	15.26	3.67	1.09	3.74	0.59	3.61	0.73	2.05	0.31	2.08	0.32	3.41	0.18	0.38	0.06	5.52	0.92	0.42
GU17A	10.44	21.66	186.99	61.60	26.20	28.18	55.52	90.25	18.76	17.64	495.77	19.74	123.33	2.82	0.95	0.85	0.23	0.84	475.09	9.01	21.19	3.08	13.65	3.33	1.03	3.39	0.54	3.35	0.67	1.89	0.28	1.92	0.30	3.07	0.16	0.41	0.07	4.83	1.05	0.44
GU22	11.54	17.59	153.31	35.70	19.70	14.13	33.14	69.40	16.87	47.33	424.23	19.94	140.39	3.96	1.85	1.19	0.31	1.92	665.29	13.53	28.89	3.92	16.47	3.74	0.97	3.73	0.58	3.44	0.70	1.95	0.29	1.98	0.30	3.95	0.24	0.75	0.17	7.39	4.55	1.66
GU23A	9.42	25.89	247.66	48.83	28.45	24.00	70.09	91.06	20.25	18.42	603.23	16.14	99.08	3.01	0.70	0.89	0.16	0.81	457.30	10.12	23.01	3.29	14.16	3.27	1.04	3.26	0.50	2.89	0.56	1.48	0.21	1.38	0.20	2.62	0.18	0.37	0.08	4.95	1.28	0.53
GU26	7.53	32.26	236.01	68.12	29.50	18.08	55.21	87.59	19.12	23.03	581.10	18.32	103.60	2.44	0.73	0.88	0.11	0.87	458.29	9.96	22.11	3.20	13.81	3.27	0.99	3.24	0.52	3.13	0.64	1.77	0.26	1.73	0.26	2.74	0.15	0.31	0.08	5.15	2.29	0.78
OTO I	10.87	22.17	201.96	3.90	19.70	6.74	79.26	87.66	20.75	12.70	604.70	20.75	84.09	2.01	0.84	0.87	0.16	0.59	472.29	8.33	19.03	2.91	13.71	3.53	1.17	3.73	0.60	3.70	0.75	2.07	0.31	2.05	0.31	2.37	0.13	0.29	0.17	4.47	0.98	0.41
OTO II	10.91	21.33	207.76	4.01	21.21	7.84	80.98	87.91	20.58	11.55	604.79	19.77	80.98	1.93	0.78	0.85	0.15	0.57	453.18	7.91	18.13	2.77	13.15	3.37	1.13	3.56	0.58	3.54	0.72	1.97	0.29	1.95	0.29	2.27	0.13	0.29	0.05	4.20	0.93	0.38
Guatemala Be																																								
GU14A	6.69	30.16	235.02	105.36	34.07	48.62	64.90	78.54	18.37	6.12	515.24	24.92	129.41	4.38	0.53	1.03	0.05	0.08	234.08	8.98	21.60	3.21	14.45	3.76	1.29	4.11	0.66	4.04	0.82	2.23	0.33	2.14	0.32	2.77	0.23	0.11	0.02	2.42	0.69	0.20
GU29	8.88	26.97	198.64	159.64	33.31	76.60	39.66	82.17	17.56	10.82	509.03	27.33	155.35	8.97	1.02	1.12	0.06	0.30	405.30	13.80	30.17	4.25	18.92	4.55	1.52	4.87	0.79	4.77	0.97	2.68	0.40	2.64	0.40	3.55	0.57	0.29	0.06	3.91	1.21	0.48
GU30	7.96	18.92	148.94	125.03	28.25	68.88	31.34	87.98	18.10	14.27	496.37	40.60	181.14	12.21	1.37	1.26	0.07	0.43	548.97	24.29	43.87	6.92	29.52	6.90	2.10	7.34	1.14	6.80	1.37	3.69	0.54	3.60	0.53	4.37	0.61	2.68	0.10	5.04	1.42	0.57
GU32	6.80	24.30	215.24	90.50	28.78	41.29	43.65	106.88	19.16	43.59	589.08	32.55	230.15	11.21	1.32	1.37	0.07	0.81	719.01	25.07	54.81	7.60	31.95	6.91	2.01	6.58	1.01	5.87	1.15	3.11	0.45	2.97	0.44	5.38	0.58	0.52	0.27	7.90	2.16	0.71
GU35B	5.64	24.77	203.90	290.17	34.08	76.69	45.34	72.01	16.48	10.71	536.92	23.46	136.75	6.75	0.90	0.97	0.08	0.37	335.25	12.24	27.48	3.87	16.73	3.98	1.33	4.17	0.65	3.89	0.79	2.14	0.32	2.10	0.31	2.93	0.35	0.18	0.02	2.81	1.14	0.46
GU38	7.53	28.48	231.69	238.49	34.14	65.91	42.03	77.30	16.81	39.57	584.89	28.38	139.50	5.43	0.87	0.97	0.12	1.03	476.34	15.90	34.31	5.09	22.31	5.25	1.65	5.35	0.79	4.55	0.91	2.44	0.36	2.34	0.35	3.22	0.25	0.39	0.13	3.83	1.38	0.75
GU39	7.70	24.47	249.09	29.41	28.97	9.80	30.99	93.76	19.66	12.70	610.95	25.00	116.42	5.00	0.65	1.02	0.10	0.42	402.86	12.04	26.86	3.95	17.65	4.32	1.40	4.40	0.68	4.05	0.82	2.22	0.33	2.14	0.32	2.78	0.24	0.21	0.06	4.22	1.09	0.45
El Salvador Vo																																							
ES002	11.95	35.11	297.92	1.91	25.93	3.94	237.52	121.94	18.98	37.65	425.79	34.44	132.60	3.12	1.41	1.42	0.47	1.74	852.59	13.46	31.17	4.89	23.05	5.98	1.62	6.25	1.01	6.17	1.26	3.47	0.52	3.44	0.52	3.81	0.20	0.86	0.09	6.55	2.20	1.25
ES003	10.12	35.68	281.11	1.20	25.57	3.55	245.98	122.31	20.19	43.60	416.89	38.34	147.18	3.68	1.48	1.32	0.52	1.84	834.23	13.86	32.50	5.00	23.17	5.98	1.62	6.25	0.98	5.99	1.22	3.42	0.50	3.33	0.50	3.80	0.17	0.56	0.09	5.96	2.55	1.36
ES005	10.25	24.14	220.47	9.11	29.12	9.17	100.82	93.06	19.10	47.85	474.28	27.22	147.10	3.21	1.57	1.40	0.38	2.56	586.32	13.96	31.50	4.59	20.34	4.93	1.31	5.05	0.82	5.01	1.03	2.86	0.42	2.88	0.44	4.13	0.24	1.09	0.17	6.60	4.19	1.93
ES009	11.11	36.31	210.83	1.92	23.20	2.24	183.06	114.79	19.09	38.92	376.90	42.86	169.78	3.22	1.49	1.71	0.37	1.97	798.65	14.11	33.90	5.28	24.97	6.63	1.78	7.33	1.24	7.81	1.63	4.54	0.68	4.57	0.68	5.11	0.22	0.75	0.17	6.69	2.57	1.26
ES019	5.05	27.08	227.21	131.16	28.31	45.20	49.56	72.34	16.84	17.55	634.08	24.67	125.90	6.42	0.87	1.05	0.06	0.65	452.23	13.81	31.58	4.49	20.17	4.66	1.59	4.76	0.76	4.51	0.92	2.51	0.37	2.47	0.37	3.20	0.41	0.27	0.06	3.71	1.23	0.56
ES027B	7.70	36.55	309.16	35.79	38.34	27.76	148.01	91.40	19.05	8.16	449.94	20.07	55.95	1.47	0.49	0.60	0.18	0.38	384.28	5.55	12.90	2.08	10.01	2.78	0.90	3.05	0.49	3.07	0.64	1.77	0.27	1.76	0.26	1.51	0.07	0.18	0.07	2.39	0.71	0.37
ES028B	8.64	43.46	392.10	18.62	31.36	8.51	243.81	96.63	20.76	13.90	505.80	22.91	63.59	1.57	0.65	0.67	0.26	0.58	427.30	6.30	14.68	2.35	11.05	3.11	1.00	3.43	0.55	3.39	0.70	1.93	0.29	1.90	0.29	1.64	0.07	0.25	0.06	2.98	0.82	0.50
ES 031	10.95	42.63	385.86	20.82	32.07	8.93	263.94	100.38	21.13	16.72	505.34	26.35	76.99	1.91	0.78	0.78	0.32	0.74	487.10	7.41	17.28	2.77	13.25	3.63	1.11	3.96	0.64	3.93	0.81	2.22	0.33	2.18	0.32	1.98	0.09	0.29	0.05	2.85	1.00	0.60
ES035A	13.28	22.96	103.60	3.54	13.03	2.15	19.60	104.25	19.68	30.27	526.29	34.83	114.82	2.74	1.21	1.52	0.40	1.33	808.89	11.42	27.04	4.20	19.83	5.20	1.57	5.56	0.88	5.34	1.10	3.03	0.45	3.00	0.45	3.04	0.13	0.44	0.07	5.48	1.97	1.05
ES036C	12.71	28.36	256.45	11.60	31.50	12.67	128.08	82.80	19.90	29.42	461.62	21.06	74.98	1.60	0.96	0.64	0.21	1.28	469.87	7.94	17.09	2.54	11.16	2.95	1.00	3.15	0.51	3.16	0.65	1.80	0.27	1.83	0.28	1.91	0.09	0.40	0.13	3.96	2.19	1.05
ES038	7.67	26.02	263.88	9.92	29.37	10.78	110.81	76.55	18.15	23.48	466.59	18.00	59.86	1.24	0.84	0.59	0.17	1.24	455.71	7.42	16.50	2.41	11.14	2.86	1.05	3.14	0.53	3.28	0.68	1.91	0.28	1.94	0.30	1.93	0.10	0.47	0.06	3.83	1.97	0.95
ES SSI	16.22	29.24	107.86	0.34	18.34	1.03	61.78	123.21	18.73	47.77	352.70	48.57	195.30	3.80	1.70	1.68	0.41	2.17	938.61	16.42	38.72	6.00	28.31	7.48	1.86	8.16	1.35	8.45	1.76	4.91	0.74	4.95	0.74	5.55	0.25	0.83	0.17	7.79	2.92	1.49
ES SSII	12.84	28.76	102.64	0.36	17.77	0.91	55.88	121.21	18.57	47.10	352.82	48.56	196.53	3.15	1.64	0.85	0.38	1.84	950.81	16.49	38.86	6.00	28.34	7.50	1.85	8.15	1.35	8.44	1.76	4.91	0.74	4.95	0.75	5.54	0.16	0.69	0.18	7.84	2.92	1.49
El Salvador Ba																																							
ES013	4.96	32.97	251.96	220.90	35.01	76.12	65.20	81.66	17.27	12.84	534.06	21.29	92.77	3.03	0.59	0.72	0.11	0.41	436.50	9.89	22.28	3.34	15.25	3.73	1.19	3.88	0.62	3.74	0.76	2.11	0.31	2.08	0.32	2.46	0.19	0.25	0.07	3.29	0.90	0.41
ES014	9.02	24.60	205.78	68.63	27.99	31.95	69.73	93.73	19.64	23.71	547.84	39.09	205.16	6.88	1.26	1.11	0.10	0.49	652.62	20.38	41.04	6.02	25.68	5.59	1.59	5.73	0.86	5.13	1.07	2.99	0.44	2.91	0.46	4.42	0.29	0.31	0.13	6.53	1.23	0.54
ES015	10.73	23.14	186.92	155.12	28.03	62.37	45.13	84.64	17.40	17.52	563.54	26.88	183.49	7.29	1.01	1.30	0.12	0.53	520.91	16.39	37.52	5.34	23.43	5.23	1.58	5.22	0.81	4.77	0.96	2.65	0.39	2.61	0.39	4.26	0.43	0.32	0.10	5.91	1.22	0.51
ES016	11.39	23.89	198.19	142.65	27.79	53.47	48.17	84.73	18.45	19.26	554.89	29.65	193.51	8.43	1.08	1.26	0.13	0.53	494.01	16.79	38.12	5.38	23.05	5.23	1.56	5.20	0.79	4.66	0.93	2.57	0.38	2.55	0.38	4.21	0.38	0.28	0.09	5.60	1.37	0.56
ES017	13.41	27.38	235.29	147.75	32.79	66.61	52.78	93.82	19.96	19.94	580.83	31.44	201.01	13.00	1.59	1.26	0.07	0.43	522.90	17.28	38.00	5.33	22.82	5.28	1.65	5.31	0.81	4.79	0.96	2.62	0.39	2.56	0.39	4.04	0.58	0.26	0.10	5.08	1.48	0.64
ES018B	7.65	28.56	213.21	94.19	26.59	35.95	47.56	80.47	17.71	15.58	580.14	27.94	188.67	7.95	0.99	1.24	0.10	0.45	450.12	16.66	39.37	5.64	24.66	5.51	1.76	5.49	0.87	5.19	1.05	2.86	0.42	2.80	0.42	4.54	0.48	0.28	0.07	4.96	1.08	0.45
ES024B	5.62	30.97	242.62	232.39	36.80	98.35	55.74	73.85	16.50	12.00	518.00	21.15	95.19	3.96	0.64	0.78	0.07	0.45	390.24	9.64	22.11	3.25	14.92	3.65	1.26	3.86	0.64	3.93	0.81	2.21	0.32	2.18	0.33	2.63	0.27	0.19	0.02	2.48	1.17	0.48
Honduras Vol																																							
H3B	10.54	22.77	87.72	0.86	12.16	2.12	23.79	98.49	19.32	12.60	540.66	29.13	89.96	3.47	0.76	0.91	0.26	0.45	635.60	9.71	21.84	3.44	16.27	4.30	1.42	4.62	0.73	4.48	0.93	2.60	0.39	2.65	0.40	2.28	0.15	1.01	0.06	3.69	0.82	0.51
Honduras Bel																																							
H1	5.58	31.09	256.94	45.77	30.59	22.06	95.56	82.70	17.97	19.59	584.29	18.46	69.58	14.84	1.16	0.78	0.15	0.52	481.44	13.22	24.17	3.15	13.56	3.21	1.11	3.33	0.53	3.23	0.66	1.83	0.27	1.82	0.27	1.87	0.75	1.19	0.03	2.60	2.75	0.75
H4B	8.41	32.11	312.32	3.05	26.21	4.64	173.48	104.91	21.96	13.19	543.55	22.58	77.78	2.77	0.67	0.71	0.17	0.43	563.55	7.84	17.33	2.63	12.26	3.25	1.09	3.49	0.55	3.43	0.71	1.98	0.30	1.99	0.30	1.94	0.13	0.19	0.05	3.17	0.84	0.51
H5	7.82	37.52	325.43	4.44	27.66	5.64	148.22	93.68	20.16	7.81	526.78	39.35	58.93	2.19	0.50	0.62	0.11	0.20	461.56	9.70	15.15	3.05	14.64	3.87	1.42	4.73	0.73	4.51	0.98	2.69	0.38	2.44	0.37	1.48	0.10	0.18	0.03	2.24	0.51	0.37
H9	6.35	26.15	227.17	107.93	31.73	45.06	66.66	99.37	19.36	16.45	605.28	26.39	147.39	6.97	0.91	1.00	0.09	0.40	553.96	16.53	34.24	5.05	22.10	4.89	1.52	4.84	0.71	4.11	0.83	2.22	0.33	2.11	0.32	3.29	0.29	0.25	0.07	5.02	1.07	0.38
H13	8.61	25.92	201.21	93.32	30.87	44.82	29.02	86.47	19.31	18.40	586.26	35.13	278.04	29.48	2.29	1.70	0.05	0.24	335.78	24.29	50.47	6.67	27.40	6.15	1.94	6.25	0.96	5.62	1.13	3.06	0.45	2.94	0.44	5.30	1.42	0.27	0.07	3.35	1.91	0.81
H14	8.02	31.62	230.96	174.17	33.77	61.70	71.09	93.43	18.17	27.59	535.06	73.55	148.69	6.52	0.67	0.95	0.08	0.38	721.31	38.10	59.91	11.48	50.11	11.91	3.70	12.42	1.91	11.15	2.21	5.88	0.86	5.58	0.81	3.42	0.35	0.35	0.08	5.45	1.62	0.57
H16	7.89	27.25	238.09	64.50	26.57	28.51	74.79	94.54	18.61	27.19	652.01	22.35	167.00	7.61	1.06	1.17	0.06	0.58	685.24	20.89	44.69	6.14	26.05	5.55	1.54	5.09	0.74	4.29	0.84	2.26	0.33	2.14	0.33	3.94	0.42	0.25	0.12	6.38	1.46	0.52
Honduras Bac																																							
H10	7.87	20.83	163.68	15.08	23.25	11.20	18.68	109.21	21.62	22.70	504.86	41.67	275.37	47.12	3.41	1.82	0.07	0.30	408.36	31.19	66.29	8.75	37.04	8.33	3.08	8.38	1.30	7.62	1.49	3.97	0.56	3.69	0.54	5.62	2.73	0.58	0.06	3.03	2.98	1.05
H17A	4.64	23.66	212.89	242.26	34.46	90.34	56.44	72.93	17.00	30.40	602.80	27.50	185.27	61.32	2.33	1.36	0.05	0.29	544.97	33.21	60.83	7.06	26.37	5.25	1.80	5.15	0.81	4.79	0.95	2.56	0.37	2.48	0.37	3.54	3.15	0.87	0.10	1.98	4.45	1.09
H18A	9.51	19.91	162.64	175.35	28.65	58.50	47.85	70.85	17.36	39.32	527.87	25.84	196.12	64.47	3.42	1.43	0.06	0.31	482.14	35.28	64.11	7.12	27.28	5.43	1.76	5.36	0.83	4.93	0.98	2.67	0.39	2.56	0.38	3.83	3.37	0.44	0.07	2.16	4.93	1.20

Table 1 continued

sample #	Li ppm	Sc ppm	V ppm	Cr ppm	Co ppm	Ni ppm	Cu ppm	Zn ppm	Ga ppm	Rb ppm	Sr ppm	Y ppm	Zr ppm	Nb ppm	Mo ppm	Sn ppm	Sb ppm	Cs ppm	Ba ppm	La ppm	Ce ppm	Pr ppm	Nd ppm	Sm ppm	Eu ppm	Gd ppm	Tb ppm	Dy ppm	Ho ppm	Er ppm	Tm ppm	Yb ppm	Lu ppm	Hf ppm	Ta ppm	W ppm	Tl ppm	Pb ppm	Th ppm	U ppm
NW Nicaragua																																								
P-58A	14.12	23.57	139.74	1.22	15.92	2.06	86.62	89.79	19.21	29.64	406.29	31.89	104.59	1.68	1.11	1.00	0.81	1.48	897.26	9.34	21.80	3.52	17.04	4.65	1.33	5.17	0.86	5.49	1.15	3.21	0.49	3.29	0.50	3.11	0.11	0.39	n.d.	4.25	1.49	1.22
P-27A	6.04	n.d.	n.d.	n.d.	n.d.	n.d.	214.20	n.d.	n.d.	12.77	531.27	21.50	52.10	0.99	0.50	0.69	0.07	0.45	536.21	6.17	14.44	2.40	12.06	3.46	1.21	3.96	0.66	4.19	0.88	2.35	0.37	2.45	0.37	1.81	0.06	0.16	0.03	2.05	0.62	0.61
P-13	4.85	22.97	271.18	4.28	27.64	6.93	117.05	91.12	18.74	19.61	499.10	24.86	66.37	1.41	0.59	0.68	0.11	0.21	703.97	7.86	18.37	2.97	14.25	3.87	1.17	4.09	0.68	4.25	0.88	2.50	0.37	2.47	0.37	2.01	0.08	0.18	0.24	3.16	1.08	0.92
P2-16	5.99	40.77	309.95	24.02	34.83	22.60	133.99	67.85	16.19	15.37	494.70	16.72	48.30	1.58	0.56	0.52	0.32	0.66	461.94	4.37	11.00	1.81	8.68	2.50	0.82	2.93	0.48	3.04	0.62	1.71	0.25	1.69	0.25	1.58	0.10	0.27	0.07	2.05	0.75	0.64
P-7A	8.24	n.d.	n.d.	n.d.	n.d.	n.d.	183.37	n.d.	n.d.	25.76	489.43	20.38	77.01	1.86	0.92	0.77	0.49	1.12	742.98	6.45	14.82	2.38	11.51	3.27	1.09	3.74	0.62	3.90	0.81	2.19	0.34	2.31	0.34	2.52	0.13	0.37	0.12	2.74	1.15	1.12
P-9	6.41	29.52	317.62	31.39	34.46	25.59	151.11	78.18	18.24	19.48	490.45	20.47	78.46	5.01	0.84	0.79	0.32	0.78	555.04	6.34	14.56	2.32	11.27	3.23	1.06	3.48	0.58	3.57	0.73	2.00	0.29	1.92	0.29	2.19	0.31	0.23	0.06	2.42	0.95	0.79
P-43	8.64	n.d.	n.d.	n.d.	n.d.	n.d.	185.27	n.d.	n.d.	22.08	409.60	26.42	107.86	6.45	1.19	1.07	0.40	0.99	680.42	8.30	19.39	2.97	14.50	4.15	1.42	4.85	0.82	5.16	1.08	2.87	0.45	2.99	0.45	3.29	0.40	0.36	0.11	2.70	1.05	0.93
P-51	4.87	n.d.	n.d.	n.d.	n.d.	n.d.	122.48	n.d.	n.d.	11.98	490.45	16.35	51.41	1.49	0.53	0.60	0.14	0.42	361.72	5.55	12.83	2.05	9.95	2.75	0.95	3.15	0.51	3.24	0.67	1.79	0.28	1.84	0.28	1.69	0.10	0.15	0.07	1.56	0.52	0.48
P-56G	7.13	n.d.	n.d.	n.d.	n.d.	n.d.	167.93	n.d.	n.d.	12.02	594.99	22.63	49.91	0.86	0.54	0.70	0.09	0.48	764.09	6.93	15.73	2.59	12.92	3.70	1.48	4.23	0.70	4.44	0.92	2.47	0.39	2.60	0.40	1.78	0.06	0.15	0.11	2.66	0.59	0.58
P-4	4.87	n.d.	n.d.	n.d.	n.d.	n.d.	140.75	n.d.	n.d.	7.19	428.88	14.22	32.80	0.98	0.45	0.41	0.17	0.37	364.85	3.23	7.43	1.22	6.28	1.96	0.81	2.43	0.42	2.77	0.58	1.57	0.24	1.64	0.25	1.13	0.07	0.15	0.04	1.30	0.31	0.31
P-6	5.31	27.61	334.47	18.71	31.09	15.33	173.54	80.99	19.46	7.37	477.51	16.57	39.78	1.30	0.54	0.50	0.19	0.35	435.53	3.61	8.60	1.40	7.12	2.17	0.83	2.52	0.44	2.87	0.60	1.70	0.25	1.69	0.25	1.22	0.11	0.13	0.04	2.02	0.40	0.36
P2-3a	3.06	42.33	286.74	142.31	49.72	64.98	111.57	67.37	14.10	4.31	374.78	11.18	20.50	0.69	0.27	0.28	0.12	0.23	246.78	1.93	4.90	0.86	4.38	1.40	0.46	1.74	0.31	1.99	0.41	1.16	0.17	1.14	0.17	0.65	0.05	0.09	0.02	1.06	0.19	0.17
P2-3b	4.00	26.49	278.73	10.97	26.11	11.51	126.11	67.08	17.80	6.35	504.84	13.18	28.17	0.93	0.37	0.40	0.15	0.32	344.09	2.67	6.52	1.13	5.61	1.70	0.52	2.06	0.35	2.30	0.48	1.35	0.20	1.37	0.20	0.85	0.06	0.11	0.03	1.49	0.30	0.27
P2-3d	4.11	35.09	323.01	49.64	34.63	24.50	152.67	74.68	16.91	7.08	438.83	14.64	30.99	0.95	0.41	0.37	0.17	0.36	362.30	2.79	6.85	1.18	5.96	1.84	0.55	2.26	0.39	2.54	0.53	1.51	0.22	1.51	0.23	0.93	0.06	0.13	0.04	1.56	0.34	0.30
P2-11	5.15	32.08	350.28	11.29	31.89	12.98	162.94	85.70	18.15	7.28	480.68	15.08	32.47	1.15	0.46	0.45	0.19	0.37	394.64	3.35	7.77	1.28	6.50	1.98	0.78	2.37	0.41	2.65	0.56	1.56	0.23	1.55	0.24	1.02	0.07	0.10	0.04	1.64	0.33	0.30
P2-13	5.33	40.95	325.63	75.29	44.34	40.39	145.59	85.34	16.03	7.31	401.93	14.58	32.09	1.10	0.48	0.43	0.19	0.37	376.06	3.20	7.45	1.24	6.22	1.92	0.75	2.30	0.40	2.58	0.54	1.53	0.23	1.52	0.23	1.02	0.07	0.10	0.03	1.75	0.33	0.29
P-50	4.97	33.66	276.77	101.86	35.06	30.80	142.49	69.37	15.82	11.69	476.93	17.57	53.28	1.57	0.53	0.58	0.14	0.41	369.09	5.42	12.61	2.03	9.69	2.63	0.87	2.86	0.48	3.00	0.61	1.72	0.25	1.70	0.25	1.51	0.10	0.14	0.05	1.90	0.57	0.47
P-19	6.79	n.d.	n.d.	n.d.	n.d.	n.d.	113.49	n.d.	n.d.	16.33	442.07	20.39	73.90	2.52	0.66	0.75	0.23	0.68	493.24	6.67	15.46	2.44	11.75	3.26	1.10	3.80	0.64	3.98	0.82	2.20	0.34	2.30	0.34	2.33	0.16	0.24	0.05	1.92	0.77	0.65
P-40A	3.80	n.d.	n.d.	n.d.	n.d.	n.d.	165.41	n.d.	n.d.	5.70	437.29	12.35	26.98	0.72	0.24	0.43	0.10	0.25	310.92	3.05	6.80	1.13	5.79	1.78	0.72	2.17	0.38	2.46	0.51	1.37	0.21	1.42	0.22	0.95	0.05	0.09	0.04	0.99	0.26	0.27
P-42	3.79	34.71	317.07	63.14	47.85	38.39	129.57	78.63	15.98	6.96	380.22	15.11	35.40	1.10	0.42	0.45	0.17	0.33	391.21	3.20	7.46	1.25	6.28	1.91	0.71	2.24	0.39	2.56	0.54	1.53	0.23	1.53	0.23	1.07	0.06	0.11	0.05	1.76	0.35	0.32
P-23	8.57	n.d.	n.d.	n.d.	n.d.	n.d.	90.29	n.d.	n.d.	23.68	399.17	25.61	105.00	4.46	1.15	0.98	0.37	1.05	777.89	9.19	20.93	3.27	15.36	4.18	1.33	4.74	0.78	4.88	1.02	2.74	0.42	2.84	0.44	3.21	0.28	0.35	0.14	3.00	1.13	0.98
P-46A	10.55	n.d.	n.d.	n.d.	n.d.	n.d.	60.74	n.d.	n.d.	33.59	406.40	29.23	127.03	4.99	1.53	1.17	0.67	1.63	1005.05	9.83	22.48	3.47	16.36	4.60	1.47	5.28	0.88	5.59	1.16	3.17	0.50	3.34	0.51	3.97	0.32	0.51	0.10	3.87	1.54	1.43
P-47A	11.48	n.d.	n.d.	n.d.	n.d.	n.d.	52.77	n.d.	n.d.	36.42	399.77	30.01	132.71	4.78	1.64	1.14	0.73	1.76	1085.39	10.20	23.28	3.58	16.98	4.71	1.49	5.37	0.89	5.71	1.19	3.24	0.50	3.40	0.52	4.15	0.31	0.54	0.16	4.45	1.66	1.55
P-48B	8.55	n.d.	n.d.	n.d.	n.d.	n.d.	173.09	n.d.	n.d.	26.26	412.58	24.47	98.28	3.56	1.30	0.93	0.56	1.29	830.03	7.91	17.97	2.80	13.39	3.80	1.25	4.38	0.74	4.72	0.99	2.69	0.42	2.82	0.43	3.14	0.23	0.41	0.16	3.45	1.21	1.12
P-32	6.75	n.d.	n.d.	n.d.	n.d.	n.d.	135.54	n.d.	n.d.	13.64	464.09	17.59	52.57	1.34	0.67	0.56	0.25	0.62	598.73	5.57	12.45	2.00	9.70	2.79	1.01	3.21	0.53	3.41	0.72	1.92	0.30	2.04	0.31	1.77	0.09	0.21	0.10	2.03	0.60	0.62
P-34	8.69	26.03	259.05	10.44	26.33	8.70	153.46	76.15	17.36	17.88	463.58	22.83	71.64	1.76	0.84	0.65	0.34	0.83	780.53	6.70	15.17	2.41	11.50	3.24	1.01	3.52	0.60	3.80	0.79	2.28	0.33	2.26	0.34	2.09	0.11	0.23	0.10	3.02	0.87	0.79
Guatemala Ba																																								
G 009 L1	22.12	33.96	249.49	95.79	30.58	41.97	98.69	105.11	17.91	38.69	346.14	24.33	5.43	4.00	0.51	0.94	0.24	2.46	589.66	9.88	20.75	3.15	14.36	3.84	1.26	4.20	0.71	4.47	0.93	2.59	0.40	2.65	0.40	0.40	0.25	0.62	0.07	5.36	1.51	0.47
G 009 L2	12.18	17.21	147.76	13.46	19.00	15.25	99.99	101.45	20.18	63.14	367.11	27.04	10.81	13.68	2.85	1.15	0.11	0.83	1639.45	20.62	45.69	6.42	27.81	6.19	1.83	5.91	0.88	5.09	1.00	2.67	0.38	2.38	0.34	0.43	0.76	0.49	0.13	7.82	2.81	0.63
Chor 8A	31.00	25.30	196.09	106.87	29.18	77.34	3.18	60.93	17.58	11.89	303.22	19.19	8.63	6.50	0.37	2.34	0.07	1.44	85.83	6.07	14.93	2.21	10.41	2.84	1.06	3.29	0.56	3.47	0.72	1.96	0.29	1.89	0.28	0.50	0.37	0.32	0.08	5.04	0.44	0.20
P12	11.35	22.87	250.61	22.66	28.46	12.74	164.26	108.75	23.56	35.73	582.45	17.78	21.47	10.08	1.13	1.16	0.03	0.42	721.09	20.83	41.27	5.38	22.54	4.77	1.38	4.47	0.64	3.50	0.66	1.70	0.23	1.48	0.21	1.16	0.52	0.15		5.57	0.92	0.45
GU G3K	8.21	2.05	4.64	0.37	0.54	0.26	3.32	21.95	14.57	128.91	39.01	8.95	18.85	10.27	1.07	1.34	0.06	2.19	589.23	14.37	27.45	3.31	11.85	2.22	0.26	1.95	0.29	1.65	0.33	0.92	0.14	0.97	0.15	0.70	0.87	0.67	0.64	10.29	8.77	1.44
GU M1																																								
GU M2	11.31	10.67	62.89	42.24	0.30	28.32	4.06	9.24	14.01	96.48	36.77	6.39	11.10	13.93	0.45	1.86	2.27	5.23	1321.16	24.92	51.85	6.05	22.10	3.92	0.76	2.96	0.38	1.71	0.28	0.70	0.09	0.62	0.08	0.39	0.86	4.43	1.09	3.12	5.20	1.47
619	32.09	10.72	81.68	14.86	7.50	5.21	7.14	55.47	18.47	137.19	177.66	14.90	3.42	12.65	0.32	4.59	0.01	3.84	431.50	31.77	64.02	7.50	27.62	5.47	0.96	4.96	0.70	3.52	0.59	1.35	0.16	0.92	0.12	0.14	0.87	0.32	0.89	14.11	13.58	1.78
714A	9.09	13.82	61.63	1.58	9.45	2.13	7.64	179.05	36.95	259.56	392.12	205.63	16.96	86.66	4.07	10.45	0.03	0.48	906.19	180.41	400.83	55.21	214.85	46.42	6.79	42.82	6.93	41.18	7.96	21.84	3.33	21.89	2.98	0.98	5.63	0.62	1.54	22.44	51.90	16.73
Cocos Plate S																																								
[illegible]	[illegible]	[illegible]	[illegible]	[illegible]	[illegible]	[illegible]	[illegible]	[illegible]	[illegible]	[illegible]	[illegible]	[illegible]	[illegible]	[illegible]	[illegible]	[illegible]	[illegible]	[illegible]	[illegible]	[illegible]	[illegible]	[illegible]	[illegible]	[illegible]	[illegible]	[illegible]	[illegible]	[illegible]	[illegible]	[illegible]	[illegible]	[illegible]	[illegible]	[illegible]	[illegible]	[illegible]	[illegible]	[illegible]	[illegible]	[illegible]

Table 1 continued

sample #	Selected Trace element ratios	Ba/La	Ba/Th	U/Th	Sr/Ce	La/Yb	Zr/Hf
Guatemala Vo							
GU2A		40.18	427.85	0.43	32.02	4.49	38.15
GU4		51.34	311.08	0.40	26.16	6.47	38.61
GU5		50.64	281.30	0.40	17.59	5.59	38.02
GU6		41.36	347.06	0.38	19.52	8.08	40.26
GU8A		39.64	269.10	0.38	16.90	5.35	37.37
GU15A		51.62	565.15	0.45	23.74	4.84	39.60
GU17A		52.74	454.03	0.42	23.40	4.68	40.14
GU22		49.16	146.34	0.37	14.69	6.84	35.55
GU23A		45.20	356.40	0.41	26.21	7.36	37.88
GU26		45.99	199.83	0.34	26.28	5.75	37.74
OTO I		56.72	480.04	0.42	31.78	4.07	35.47
OTO II		57.31	488.65	0.41	33.36	4.06	35.64
Guatemala Be							
GU14A		26.06	339.82	0.29	23.85	4.21	46.72
GU29		29.37	333.98	0.39	16.87	5.23	43.79
GU30		22.60	386.83	0.40	11.31	6.75	41.48
GU32		28.68	332.39	0.33	10.75	8.44	42.81
GU35B		27.39	294.60	0.41	19.54	5.84	46.67
GU38		29.97	344.02	0.54	17.05	6.80	43.29
GU39		33.46	370.23	0.41	22.75	5.63	41.87
El Salvador V							
ES002		63.35	387.86	0.57	13.66	3.92	34.79
ES003		60.19	327.38	0.53	12.83	4.16	38.69
ES005		42.01	139.85	0.46	15.05	4.85	35.63
ES009		56.59	310.16	0.49	11.12	3.09	33.22
ES019		32.74	366.81	0.46	20.08	5.60	39.31
ES027B		69.25	538.45	0.51	34.88	3.14	37.02
ES028B		67.77	522.35	0.61	34.45	3.32	38.82
ES 031		65.74	487.31	0.60	29.25	3.40	38.86
ES035A		70.83	409.73	0.53	19.46	3.81	37.79
ES036C		59.21	214.81	0.48	27.02	4.34	39.30
ES038		61.40	231.87	0.48	28.28	3.82	30.94
ES SSI		57.18	321.77	0.51	9.11	3.31	35.22
ES SSII		57.66	326.17	0.51	9.08	3.33	35.45
El Salvador B							
ES013		44.14	486.00	0.46	23.97	4.75	37.77
ES014		32.02	528.85	0.44	13.35	7.01	46.37
ES015		31.78	425.65	0.42	15.02	6.27	43.04
ES016		29.42	360.22	0.41	14.56	6.60	45.98
ES017		30.26	354.38	0.43	15.28	6.76	49.77
ES018B		27.02	417.60	0.41	14.74	5.95	41.60
ES024B		40.48	333.33	0.41	23.43	4.42	36.21
Honduras Vol							
H3B		65.49	778.73	0.62	24.75	3.66	39.40
Honduras Bel							
H1		36.40	175.23	0.27	24.17	7.26	37.29
H4B		71.91	670.38	0.60	31.36	3.95	40.05
H5		47.57	913.08	0.74	34.77	3.97	39.71
H9		33.51	518.22	0.36	17.68	7.85	44.74
H13		13.82	175.82	0.43	11.62	8.25	52.47
H14		18.93	444.97	0.35	8.93	6.83	43.50
H16		32.81	468.13	0.36	14.59	9.74	42.34
Honduras Bac							
H10		13.09	137.02	0.35	7.62	8.45	49.03
H17A		16.41	122.57	0.24	9.91	13.41	52.36
H18A		13.66	97.89	0.24	8.23	13.77	51.16

Table 1 continued

sample #	Selected Trace element ratios	Ba/La	Ba/Th	U/Th	Sr/Ce	La/Yb	Zr/Hf
NW Nicaragua							
P-58A		96.06	602.25	0.82	18.64	2.84	33.60
P-27A		86.92	860.59	0.98	36.78	2.52	28.83
P-13		89.60	652.01	0.85	27.17	3.18	33.04
P2-16		105.81	615.68	0.85	44.99	2.58	30.59
P-7A		115.18	645.72	0.97	33.02	2.79	30.60
P-9		87.50	582.06	0.83	33.68	3.30	35.77
P-43		81.99	646.02	0.89	21.12	2.78	32.82
P-51		65.13	692.91	0.92	38.24	3.02	30.40
P-56G		110.23	1304.92	0.99	37.82	2.67	28.02
P-4		113.01	1180.36	1.00	57.69	1.97	29.10
P-6		120.51	1097.05	0.91	55.55	2.14	32.67
P2-3a		127.98	1278.72	0.89	76.49	1.70	31.74
P2-3b		129.01	1155.81	0.91	77.48	1.94	33.15
P2-3d		129.87	1079.81	0.91	64.06	1.84	33.18
P2-11		117.65	1198.40	0.91	61.84	2.17	31.90
P2-13		117.41	1127.48	0.86	53.96	2.11	31.60
P-50		68.13	653.16	0.83	37.81	3.18	35.21
P-19		73.90	644.38	0.85	28.60	2.90	31.78
P-40A		102.01	1212.89	1.06	64.35	2.15	28.29
P-42		122.12	1126.38	0.93	50.95	2.10	33.00
P-23		84.61	686.28	0.86	19.07	3.24	32.70
P-46A		102.24	650.55	0.93	18.08	2.94	32.03
P-47A		106.40	654.82	0.94	17.17	3.00	31.99
P-48B		105.00	686.67	0.93	22.96	2.80	31.31
P-32		107.50	1002.40	1.04	37.27	2.73	29.73
P-34		116.53	897.47	0.91	30.55	2.96	34.32
Guatemala Ba							
G 009 L1		59.70	391.45	0.32	16.68	3.73	13.48
G 009 L2		79.49	582.81	0.23	8.03	8.65	25.11
Chor 8A		14.14	193.66	0.45	20.31	3.20	17.26
P12		34.62	787.41	0.49	14.11	14.09	18.58
GU G3K		41.00	67.22	0.16	1.42	14.85	26.85
GU M1							
GU M2		53.01	253.99	0.28	0.71	40.38	28.50
619		13.58	31.77	0.13	2.77	34.48	23.64
714A		5.02	17.46	0.32	0.98	8.24	17.28
Cocos Plate S							
67_0495_009R_0		20.26	103.75	1.97	13.21	5.79	41.07
67_0499_019R_0		144.17	564.45	2.61	14.21	5.96	37.48
Cocos Plate M							
67_0495_048R_0		1.35	38.82	2.06	11.08	0.97	39.72
206_1256C_10R2		3.15	49.35	0.33	6.56	0.93	36.11
206_1256D_74R2		2.64	41.42	0.31	9.85	0.64	34.56

Table 2.2 Sr-Nd-Pb-Hf isotopic compositions for Central American Arc volcanics from Volcanic Front (VF), Behind the Volcanic Front (BVF) and Back-arc (BA) samples with MgO>2 wt%. Note Pb and Nd isotope data for Nicaraguan samples marked with (**) from Hoernle et al. (2008).

Table 2

sample #	$^{87}Sr/^{86}Sr$	2 σ	$^{143}Nd/^{144}Nd$	2 σ	εNd	$^{206}Pb/^{204}Pb$	2 σ	$^{207}Pb/^{204}Pb$	2 σ	$^{208}Pb/^{204}Pb$	2 σ	$^{176}Hf/^{177}Hf$	2 σ	εHf
Guatemala Volcanic Front														
GU2A	0.703852	0.000002	0.512885	0.000003	4.82	18.625	0.007	15.564	0.006	38.321	0.014	0.2830082	0.000005	8.35
GU 4	0.703824	0.000003	0.512925	0.000002	5.59	18.620	0.001	15.547	0.001	38.268	0.003			
GU 5	0.703812	0.000002	0.512932	0.000003	5.74									
GU6	0.703951	0.000004	0.512860	0.000002	4.33	18.647	0.000	15.566	0.000	38.345	0.001	0.2829846	0.000004	7.52
GU 8A	0.703823	0.000003	0.512908	0.000002	5.26	18.628	0.001	15.556	0.001	38.300	0.003	0.2830159	0.000008	8.63
GU 15A	0.703863	0.000002	0.512928	0.000002	5.66	18.665	0.001	15.554	0.001	38.313	0.002			
GU17A	0.703872	0.000003	0.512911	0.000002	5.32	18.666	0.001	15.554	0.001	38.319	0.002	0.2830423	0.000009	9.56
GU 22	0.703859	0.000005	0.512874	0.000003	4.61	18.664	0.001	15.575	0.001	38.381	0.001			
GU23A	0.704046	0.000003	0.512824	0.000003	3.63	18.681	0.001	15.579	0.001	38.412	0.002	0.2829751	0.000009	7.18
GU26	0.703643	0.000002	0.512917	0.000003	5.45	18.634	0.001	15.556	0.001	38.304	0.002			
OTO I	0.703790	0.000002	0.512959	0.000003	6.26	18.602	0.001	15.545	0.000	38.243	0.001			
OTO II	0.703824	0.000003	0.512949	0.000002	6.06	18.606	0.000	15.548	0.000	38.257	0.001	0.2830743	0.000008	10.69
Guatemala Behind the Volcanic Front														
GUA 14A	0.703401	0.000002	0.512968	0.000003	6.45	18.612	0.002	15.547	0.001	38.244	0.003	0.2830550	0.000007	10.01
GU 29	0.703604	0.000003	0.512917	0.000003	5.45	18.670	0.001	15.567	0.001	38.352	0.001	0.2829988	0.000007	8.02
GU 30	0.703697	0.000003	0.512881	0.000003	4.74	18.655	0.002	15.571	0.001	38.351	0.003			
GU32	0.704071	0.000005	0.512813	0.000003	3.41	18.693	0.001	15.582	0.001	38.423	0.002	0.2829369	0.000007	5.83
GU 35B	0.703633	0.000003	0.512930	0.000003	5.70	18.669	0.002	15.577	0.002	38.367	0.006	0.2830314	0.000008	9.17
GU 38	0.704154	0.000003	0.512880	0.000002	4.73	18.636	0.000	15.568	0.000	38.337	0.001			
GU 39	0.704110	0.000003	0.512831	0.000002	3.77	18.672	0.000	15.579	0.000	38.404	0.001			
El Salvador Volcanic Front														
ES002	0.703886	0.000003	0.513009	0.000003	7.23	18.535	0.000	15.523	0.000	38.143	0.001	0.2831259	0.000007	12.52
ES003	0.703871	0.000002	0.512990	0.000003	6.87	18.536	0.001	15.526	0.001	38.157	0.003			
ES005	0.703689	0.000002	0.512997	0.000003	6.99	18.638	0.001	15.561	0.001	38.313	0.002	0.2831168	0.000006	12.19
ES009	0.703788	0.000003	0.512996	0.000003	6.97	18.573	0.001	15.551	0.001	38.243	0.002	0.2831168	0.000005	12.19
ES019	0.703871	0.000003	0.512944	0.000003	5.97	18.601	0.001	15.556	0.001	38.274	0.002	0.2830586	0.000006	10.14
ES 027B	0.703846	0.000002	0.513006	0.000002	7.17	18.537	0.002	15.531	0.002	38.173	0.004			
ES 028B	0.703881	0.000003	0.513008	0.000003	7.23	18.516	0.002	15.521	0.001	38.126	0.003			
ES 031	0.703816	0.000005	0.513009	0.000005	7.23	18.519	0.002	15.529	0.001	38.153	0.004			
ES 035A	0.703863	0.000005	0.513007	0.000002	7.20	18.502	0.001	15.531	0.001	38.139	0.001			
ES 036C	0.703643	0.000004	0.513005	0.000003	7.15	18.663	0.000	15.554	0.000	38.307	0.001			
ES038	0.704154	0.000003	0.513001	0.000003	7.08	18.654	0.001	15.546	0.000	38.285	0.001	0.2831215	0.000005	12.36
ES SSI	0.703824	0.000002	0.512998	0.000004	7.03	18.568	0.000	15.527	0.000	38.173	0.001			
ES SSII	0.703824	0.000003	0.513009	0.000002	7.23	18.569	0.000	15.529	0.000	38.176	0.001	0.2831056	0.000008	11.80
El Salvador Behind the Volcanic Front														
ES013	0.703708	0.000003	0.513002	0.000003	7.11	18.562	0.001	15.538	0.001	38.189	0.001			
ES014	0.703844	0.000003	0.512900	0.000003	5.12	18.648	0.001	15.557	0.001	38.318	0.002			
ES015	0.703801	0.000003	0.512879	0.000003	4.71	18.662	0.001	15.566	0.001	38.349	0.001			
ES016	0.703785	0.000003	0.512878	0.000002	4.68	18.657	0.001	15.565	0.000	38.347	0.001			
ES017	0.703716	0.000003	0.512905	0.000002	5.20	18.657	0.001	15.565	0.001	38.338	0.002			
ES018B	0.703753	0.000003	0.512875	0.000002	4.63	18.666	0.001	15.575	0.001	38.378	0.003	0.2829940	0.000007	7.85
ES024B	0.703615	0.000002	0.512971	0.000003	6.49	18.577	0.001	15.546	0.001	38.225	0.003	0.2830902	0.000007	11.25
Honduras Volcanic Front														
H3B	0.703815	0.000003	0.512999	0.000003	7.04	18.527	0.002	15.529	0.001	38.162	0.003	0.2831216	0.000010	12.36
Honduras Behind the Volcanic Front														
H1	0.703743	0.000002	0.512982	0.000002	6.72	18.593	0.001	15.539	0.001	38.221	0.003	0.2830922	0.000004	11.32
H4B	0.703844	0.000002	0.513002	0.000003	7.11	18.525	0.001	15.528	0.001	38.156	0.002			
H5	0.703811	0.000002	0.512994	0.000003	6.94	18.525	0.002	15.533	0.001	38.168	0.003	0.2831452	0.000007	13.20
H9	0.704006	0.000003	0.512827	0.000003	3.69	18.659	0.001	15.567	0.001	38.367	0.002	0.2829762	0.000007	7.22
H13	0.703206	0.000003	0.512965	0.000003	6.37	18.665	0.001	15.555	0.001	38.278	0.002			
H14	0.704078	0.000002	0.512889	0.000002	4.89	18.668	0.002	15.578	0.001	38.406	0.003	0.2829685	0.000007	6.95
H16	0.703985	0.000003	0.512859	0.000002	4.32	18.681	0.001	15.580	0.001	38.421	0.004			

Table 2 continued

sample #		$^{87}Sr/^{86}Sr$	2 σ	$^{143}Nd/^{144}Nd$	2 σ	εNd	$^{206}Pb/^{204}Pb$	2 σ	$^{207}Pb/^{204}Pb$	2 σ	$^{208}Pb/^{204}Pb$	2 σ	$^{176}Hf/^{177}Hf$	2 σ	εHf
Honduras Backarc															
H10		0.703089	0.000003	0.513021	0.000003	7.47	18.630	0.001	15.550	0.001	38.227	0.002	0.2830667	0.000008	10.42
H17A		0.702870	0.000003	0.513062	0.000002	8.28	18.714	0.002	15.529	0.002	38.126	0.004	0.2831040	0.000006	11.74
H18A		0.702730	0.000002	0.513050	0.000003	8.03	18.731	0.001	15.527	0.001	38.119	0.003			
NW Nicaragua Volcanic Front															
P-58A	(**)	0.703872	0.000002	0.513068	0.000003	8.38	18.464	0.001	15.518	0.001	38.091	0.002	0.2831921	0.000004	14.86
P-27A	(**)	0.703909	0.000002	0.513061	0.000002	8.26	18.475	0.002	15.519	0.002	38.099	0.005	0.2831760	0.000008	14.29
P-13	(**)	0.703917	0.000002	0.513057	0.000003	8.18	18.483	0.001	15.533	0.001	38.140	0.002			
P2-16	(**)	0.704019	0.000003	0.513050	0.000002	8.04	18.506	0.001	15.515	0.001	38.118	0.002			
P-7A	(**)	0.704005	0.000002	0.513060	0.000002	8.23	18.513	0.001	15.520	0.001	38.139	0.003			
P-9	(**)	0.703971	0.000002	0.513042	0.000003	7.88	18.532	0.001	15.534	0.001	38.188	0.002	0.2831557	0.000007	13.57
P-43	(**)	0.703849	0.000002	0.513051	0.000002	8.05	18.554	0.001	15.521	0.001	38.180	0.003			
P-51	(**)	0.703965	0.000006	0.513067	0.000006	8.36	18.481	0.001	15.520	0.001	38.114	0.002			
P-56G	(**)	0.703941	0.000006	0.513073	0.000004	8.48	18.493	0.001	15.525	0.001	38.131	0.002			
P-4	(**)	0.703991	0.000006	0.513078	0.000006	8.57	18.557	0.002	15.529	0.001	38.205	0.003			
P-6	(**)	0.703983	0.000002	0.513066	0.000003	8.34	18.546	0.003	15.529	0.002	38.195	0.006			
P2-3a	(**)	0.703965	0.000003	0.513071	0.000003	8.45									
P2-3b	(**)	0.703978	0.000003	0.513072	0.000002	8.47	18.538	0.002	15.522	0.002	38.171	0.005			
P2-3d	(**)	0.703994	0.000003	0.513074	0.000003	8.50	18.533	0.002	15.526	0.002	38.172	0.005	0.2831790	0.000007	14.39
P2-11	(**)	0.703982	0.000005	0.513072	0.000003	8.47	18.549	0.002	15.523	0.001	38.184	0.003			
P2-13	(**)	0.703961	0.000009	0.513077	0.000004	8.56	18.555	0.001	15.530	0.001	38.205	0.002			
P-50	(**)	0.703971	0.000003	0.513057	0.000002	8.18	18.480	0.001	15.519	0.001	38.107	0.002			
P-19	(**)	0.703864	0.000003	0.513055	0.000002	8.13	18.514	0.003	15.518	0.002	38.133	0.006			
P-40A	(**)	0.704044	0.000007	0.513084	0.000006	8.69	18.532	0.001	15.526	0.001	38.175	0.002			
P-42	(**)	0.704001	0.000002	0.513067	0.000003	8.37	18.549	0.002	15.526	0.002	38.187	0.005			
P-23	(**)	0.703943	0.000004	0.513063	0.000003	8.30	18.537	0.002	15.520	0.001	38.157	0.003			
P-46A	(**)	0.703936	0.000003	0.513065	0.000002	8.32	18.550	0.001	15.523	0.001	38.180	0.002			
P-47A	(**)	0.703952	0.000002	0.513063	0.000002	8.30	18.548	0.001	15.521	0.001	38.176	0.002			
P-48B	(**)	0.703954	0.000003	0.513065	0.000002	8.33	18.552	0.001	15.525	0.001	38.188	0.002			
P-32	(**)	0.704046	0.000003	0.513071	0.000003	8.44	18.557	0.001	15.527	0.001	38.202	0.003	0.2831865	0.000007	14.66
P-34	(**)	0.704017	0.000002	0.513073	0.000003	8.49	18.564	0.001	15.533	0.001	38.217	0.002			
Guatemala Basement															
G 009 L1		0.703699	0.000001	0.512977	0.000003	6.61	18.588	0.001	15.536	0.000	38.231	0.001	0.2831810	0.000006	14.46
G 009 L2		0.704004	0.000003	0.512947	0.000001	6.03	18.728	0.000	15.554	0.000	38.397	0.001	0.2830864	0.000004	11.12
Chor 8A		0.703455	0.000002	0.513017	0.000003	7.40	18.781	0.001	15.604	0.001	38.554	0.002	0.2831157	0.000004	12.15
P12		0.704093	0.000003	0.512764	0.000003	2.46	18.643	0.001	15.588	0.001	38.349	0.002			
G3		0.707295	0.000002	0.512795	0.000003	3.06	18.747	0.001	15.593	0.001	38.514	0.002	0.2829273	0.000005	5.49
M1		0.737244	0.000003	0.512166	0.000003	-9.20	19.006	0.001	15.699	0.001	38.803	0.002			
M2		0.742724	0.000002	0.512131	0.000003	-9.89	19.782	0.001	15.697	0.001	39.874	0.001	0.2828454	0.000007	2.60
619		0.723420	0.000002	0.512219	0.000003	-8.18	18.815	0.0007	15.634	0.0007	38.795	0.0020	0.282654	0.000006	-4.19
714A		0.734146	0.000002	0.512158	0.000002	-9.36	23.759	0.0012	15.947	0.0009	43.934	0.0031	0.284771	0.000006	70.69
Cocos Plate Sediments															
67_0495_009R_02W_73-75		0.707689	0.000002	0.512716	0.000002	1.53	18.755	0.001	15.595	0.001	38.540	0.002	0.2830736	0.000003	10.67
67_0499_019R_05W_80-82		0.706951	0.000002	0.512801	0.000002	3.18	18.727	0.000	15.581	0.000	38.491	0.001	0.2830673	0.000005	10.44
Cocos Plate MORB															
67_0495_048R_04W_82-84		0.702793	0.000003	0.513120	0.000002	9.40	18.476	0.001	15.502	0.001	38.012	0.003	0.2831809	0.000005	14.46
206_1256C_10R2_103-105		0.702995	0.000002	0.513095	0.000003	8.91	18.478	0.009	15.510	0.008	38.086	0.019	0.2831893	0.000004	14.76
206_1256D_74R2_102-111		0.703077	0.000002	0.513095	0.000002	8.91	18.513	0.005	15.502	0.005	38.110	0.011	0.2832090	0.000003	15.45

3 Chapter:

Along-arc geochemical variations in southwestern Central America (Panama to Nicaragua): Source constraints from Hf isotopes

Ken Heydolph[1], Kaj Hoernle[1,2], Joerg Geldmacher[3]*

1Sonderforschungsbereich 574, University of Kiel, Wischhofstr. 1-3, D-24148 Kiel, Germany;
2Leibniz-Institut für Meereswissenschaften IFM-GEOMAR, Wischhofstr. 1-3, D-24148 Kiel, Germany;
3 Integrated Ocean Drilling Program, Texas A&M University, 1000 Discovery Drive, College Station, Texas 77845-9547

**Corresponding author*

In preparation for GCA or G-Cubed

3.1 Abstract

The Central American Volcanic Arc (CAVA) results from the subduction of the Cocos Plate beneath the Caribbean plate, with normal oceanic crust formed at the East Pacific Rise (EPR) subducting beneath Guatemala to northwestern Costa Rica, whereas crust formed at the Cocos-Nazca spreading centre (CNS) with the Galapagos hotspot track on it is being subducted beneath central Costa Rica to Panama. We present here a comprehensive new geochemical data set of major and trace element and Sr and Hf isotope ratios of mafic volcanic front (VF), behind the volcanic front (BVF) and back-arc (BA) lava and tephra samples from SW Nicaragua, Costa Rica and Panama. Our new geochemical data demonstrates the influence of the subducting Galapagos hotspot Seamount province, the subducting crust and to a lesser degree the subducting Cocos

and Coiba ridges on the source composition of SW CAVA lavas. $^{87}Sr/^{86}Sr$ and $^{176}Hf/^{177}Hf$ isotopic ratios increase and $^{206}Pb/^{204}Pb$ and $^{207}Pb/^{204}Pb$ decrease systematically from central Costa Rica to NW Nicaragua. Though lavas from Masaya volcano (SW Nicaragua) form a local maximum having the highest $^{87}Sr/^{86}Sr$ (and $^{176}Hf/^{177}Hf$ is just based on one value) isotopic ratios, probably reflect a local sediment component addition to their magma source. Lavas with high Nb and Nb/La from Nejapa volcano (Nicaragua), unradiogenic Sr and Hf isotope ratios probably represent local OIB-like component contributions to Nicaraguan magmas. Combined Nd and Hf isotope data from SW CAVA lavas also form a good linear correlation (r^2 = 0.828; VF alone, VF/ alkali basalts/ adakites have r^2 = 0.6588). Combined Nd, Hf and Pb isotopic data for SW CAVA lavas from Nicaragua to central Costa Rica define an endmember for NW Nicaraguan with radiogenic Nd and Hf and unradiogenic Pb isotope ratios, represented by a mixture of the incoming plate (igneous and sedimentary portions) and the mantle wedge, and a central Costa Rican endmember with unradiogenic Nd and Hf and radiogenic Pb isotope ratio, represented by the subducting seamount province. Alkali basalt and adakite samples from southern Costa Rica and Panama with unradiogenic to intermediate Nd and Hf and radiogenic Pb define a third endmember, represented by the subducting Cocos and Coiba Ridges.

3.2 Introduction

In subduction zones an oceanic plate subducts beneath an oceanic or continental plate, transferring lithospheric material back into the Earth's mantle. Fluid release or hydrous melts from the subducting slab cause partial melting in the overlying mantle wedge which results in arc volcanism. Therefore samples from arc volcanoes provide detailed geochemical information on various geochemically distinct source components contributing to the subduction-related arc volcanism (e.g. subducting plate, mantle wedge and overlying crust).

The Central American Volcanic Arc (CAVA), resulting from the subduction of the Cocos Plate beneath the Caribbean Plate, extends for 1100 km from the Mexico-

Guatemala border to central Costa Rica, parallel to the Middle American Trench (Figure 1). The systematic variations of subduction parameters, such as the subduction angle, thickness of the subducting lithosphere and the convergence rate of the Cocos Plate, as well as the thickness and composition of the overriding Caribbean Plate have been extensively described by several authors (e.g. Carr et al., 1984, 2003; Patino et al., 2000; Rüpke et al., 2004; Auger et al., 2006; Syracuse and Abers, 2006; Abers et al., 2007; MacKenzie et al., 2008). The resulting number of varying subduction parameters and potential source components has led to a number of distinct and sometimes contradicting models for the generation of Central American Arc volcanism.

Geochemical studies along the CAVA identified several geochemically distinct endmembers. Carr et al. (1990) argued that Sr and Nd isotopic ratios of Central American volcanic rocks can be explained by mixing of four components: marine sediments from DSDP Site 495, MORB-source mantle (DM), EMORB-source mantle (EM) and continental crust. Mixing between DM and less than 0.5% marine sediments or fluids, form a modified mantle (MM) component. Most of the calc-alkaline VF samples can be explained as a result of mixing between MM and EM components, which is also well defined in the incompatible-element data e.g. Ba/La vs. La/Yb.

Feigenson and Carr (1993) used inverse modeling to calculate rare earth element patterns of Central American lava sources. Costa Rican sources have high modal garnet content and moderate-to-strong light rare earth element (LREE) enrichment, whereas Nicaraguan sources are defined by a slight LREE depletion and little to no modal garnet in the residuum. They propose a broadly homogeneous but locally heterogeneous mantle wedge which could contain relatively enriched small-sized garnet-bearing veins surrounded by an isotopically depleted mantle peridotite matrix. Melting of distinct sources can be explained by the varying dip of the subducting lithosphere beneath the volcanic arc, which causes varying amounts of flux melting beneath the different arc segments.

Leeman et al. (1994, 1996) showed systematic along-arc variations in B/La ratio and strong correlations between B/La and $^{10}Be/^{9}Be$ ratios. Based on low B/La and ^{10}Be values for the Costa Rican lavas and a low subduction angle of the Cocos Ridge off Costa Rica, they deduced a minimal subduction contribution to arc magma sources

below Costa Rica.

Chan et al. (1999, 2000, 2002) used lithium concentrations and isotopic compositions and their strong correlations with other fluid-mobile elements from basaltic Central American Volcanic Arc lavas (e.g. B, ^{10}Be, U, ^{87}Sr/^{86}Sr, LILE) to demonstrate a subduction-related modification of the subarc mantle beneath Nicaragua to Costa Rica from slab-derived fluids. Both mantle endmembers from Nicaragua and Costa Rica have MORB-like δ^6Li values (-4.5‰). They estimated slab fluids with low δ^6Li values (-8‰ to -10‰), which overlapping with altered oceanic crust and marine sediment compositions, and imply small additions of these fluids from these sources to depleted or enriched mantle sources could explain Li and Sr isotopic systematics in the CAVA magmas.

Patino et al. (2000) showed that ratios of more to less fluid mobile trace elements (e.g. Ba/La and U/Th) reflect the flux of hydrous fluids from the subducting Cocos plate the mantle wedge. The highest flux is beneath the volcanic front of NW Nicaragua and decrease to northern Costa Rica, both along the volcanic front and into the back arc.

Abratis and Wörner (2001) used geochronological, trace element and Pb isotope data of adakitic and alkalic backarc lavas from southern central Costa Rican back-arc to demonstrate that the enriched OIB-type Costa Rican lavas originate from OIB-type asthenospheric mantle derived from the Galapagos plume. They proposed that a slab-window in the subducting lithosphere allowed the flux of Pacific asthenosphere into the mantle wedge beneath central Costa Rica. An age progression and isotopic signatures of Holocene Central American arc volcanics to the north suggest that the flow in the upper mantle beneath Costa Rica migrates northward at a rate of 40 mm/yr.

Feigenson et al. (2004) showed that Central Costa Rica volcanic front and back-arc lavas have Sr-Nd-Pb isotope data overlapping with the Galapagos Islands and hot spot tracks. They argued that the geographically restricted enriched mantle signature, traceable into the back-arc region, correlates well with the Galapagos hotspot track over the past 90 Ma. They argue that the enriched signal in back arc lavas can be derived by remelting Galapagos hotspot influenced mantle and doesn't require any subducting component.

Goss and Kay (2006) reported steep rare earth element (REE) patterns and

distinctively enriched Pb isotope compositions, when compared to older Miocene lavas, from southern Costa Rica and Panama Pliocene adakitic magmas. They suggested that this signature could result from incorporation and subsequent partial melting of ophiolitic forearc crust by forearc subduction erosion into the mantle wedge beneath southern Costa Rica. High-pressure metamorphism in the subduction channels could explain the steep REE patterns in the adakitic lavas.

Using oxygen isotope data, Eiler et al. (2005) argued that dehydration of hydrothermally-altered rocks and/or serpentinites on the down-going plate contribute to central Nicaraguan magma sources. Walker et al. (2007) proposed that Nicaraguan magmas contain a maximum contribution of subducted Cocos Plate sediments, consistent with the high $^{10}Be/^{9}Be$ isotope ratios in the central Nicaraguan lavas (Morris et al. 1990).

Large heterogeneity of CAVA magma sources on local and regional scales have been reported by Sadofsky et al. (2008), using olivine melt inclusion compositions (i.e. major and trace elements and volatile components) from CAVA samples from Costa Rica to Guatemala. They relate these variations to variable contributions of various crustal and mantle components involved in magma genesis. The magma generation in the central Nicaraguan part of the arc seems to be dominated by melting in the mantle wedge, fluxed by Ba-, B- and H_2O-rich, possibly serpentinite-derived, fluids based on correlations of water and trace elements (e.g. Ti, Y and Na) and trace element ratios (e.g. Ba/La, B/La). Whereas Costa Rican magma generation seem to be controlled by components with melt-like properties, e.g. high Cl, S, F, LREE and La/Nb.

Based on combined Pb and Nd isotopic, incompatible trace element (Ba/La and La/Yb) and seismic velocity anisotropy data, Hoernle et al. (2008) argued that Costa Rican VF and BA lavas isotopic compositions can only be explain by the addition of the subducting seamount province to their magma source. They interpreted systematic variations in isotopic composition of volcanic front volcanoes and arc-parallel seismic velocity anisotropy in the mantle wedge to reflect northwestward flow in the mantle beneath Central Costa Rica to northwest Nicaragua. They proposed that primarily hydrous fluids derived from the subducting oceanic crust and/or serpentinites in the down-going slab +/- small amounts of sediment melts could account for the material

transfer from the slab beneath Nicaragua. Recent trace element modeling by Gazel et al. (2009) demonstrated that the Galapagos hotspot contribution decreases systematically along the volcanic front from central Costa Rica to NW Nicaragua and that small amounts of sediment melts (≤0.6 wt. %) also contribute to the trace element signatures. Central Costa Rica VF and BA lavas have a Galapagos-OIB-like isotopic signature and trace element ratios (e.g. Ba/La <40, La/Yb >10), which has an Late Miocene (~6 Ma) origin most likely resulting from the subduction of the Galapagos hotspot seamount province.

In this study, we present a new geochemical (major and trace elements and Sr-Hf isotope ratios) data set, in order to put new constraints on sources for mafic VF and BVF lavas from volcanic centers along and across the Central American Volcanic Arc in Panama, Costa Rica and Nicaragua. We note that our data, since it is based in part on the same sample material, is complementary to the Hoernle et al. (2008) and Gazel et al. (2009) papers. We further note that our study is the first to present Hf isotope data for mafic volcanic rock samples from Panama, Costa Rica and Nicaragua. Our data confirm systematic along- and across-arc variations in isotopic compositions and major and trace elements (e.g. Carr et al., 1990, 2003; Feigenson et al. 1993, 2004; Sadofsky et al., 2008; Hoernle et al., 2008; Gazel et al., 2009). We also present new geochemical data for the influence of the Galapagos hotspot derived magmas on volcanic arc lavas in Costa Rica and their decreasing influence towards Nicaragua. We evaluate data on potential geochemical endmembers in the southwestern part of the Central American subduction system: subducting Cocos Plate sediments (from DSDP Sites 495 and 499) and seamount province (from SO144 cruise), Cocos and Coiba ridges (SO144 cruise) igneous oceanic crust (from DSDP Site 495 and IODP site 1256). Integrating the new geochemical dataset for volcanic rocks and subduction zone endmembers with available geochemical data on the same samples allow us to place further strong constraints on the sources involved in magma generation beneath southwestern Central America and present a comprehensive model for the southern CAVA.

3.2.1 Geological overview

Subduction of the Cocos Plate beneath the Central America (Caribbean Plate) creates a chain of volcanoes extending for more than 1400 km from Tacaná Volcano near the Guatemalan-Mexican border to western Panama (Figure 1). These subduction-related volcanic centers can be divided into volcanic front (VF) – making up the main chain of volcanoes - and generally smaller behind the volcanic front (BVF) volcanic centers (Carr et al., 1984), up to 350 km from the trench. An extensive overview of the Central American geology can be found in e.g. Auboin et al. (1982); Carr et al. (1990, 2003); Protti et al. (1995). Below we summarize the Central American geology relevant to this study.

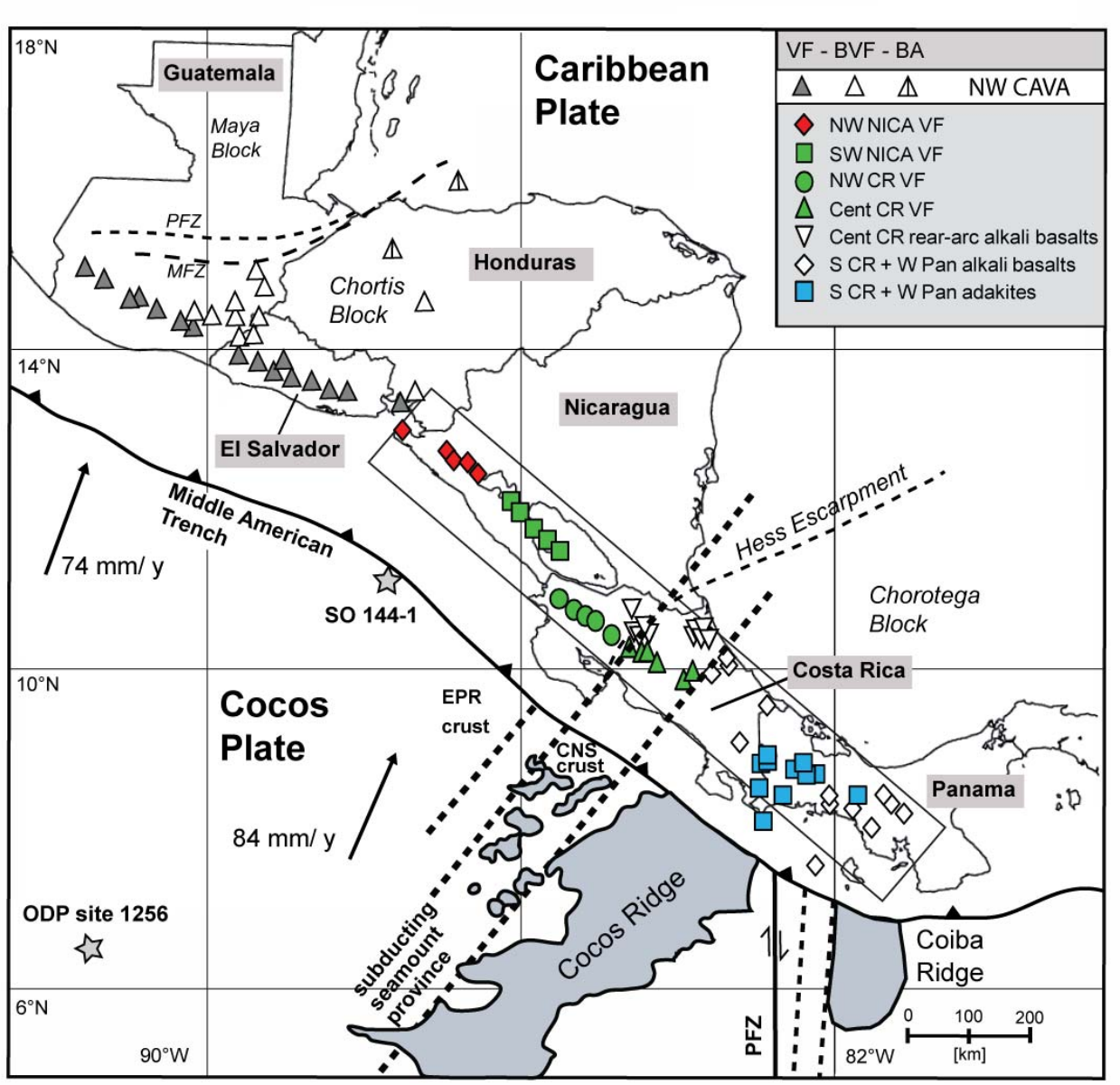

Figure 3.1 Overview map of Central America, with black arrows indicating the subduction direction and relative velocity (in mm per year, after DeMets, 2001) of the Cocos Plate beneath the Caribbean. Dredge site SO 144-1 (after Werner et al., 2003) and ODP site 1256 mark sample locations for Cocos Plate oceanic crust. The heavy dashed lines denote the boundaries of the Galapagos hotspot track seamount province, Cocos and Coiba ridges, and its projection beneath Central America, i.e. central Costa Rica and Panama. Line with longer dashes marks the boundary between crust formed at the East Pacific Rise (EPR) and the Cocos Nazca spreading centre (CNS).

In this study, we concentrate on Quaternary subduction-related volcanism in the southwestern part of Central America, extending along the volcanic front from Cosigüina Volcano in northwest Nicaragua to Turrialba Volcano in central Costa Rica and Tortuguero in the back-arc (Figure 1). We further concentrate on Pliocene to Quaternary subduction-related adakite and alkali basalt bearing volcanism from the Talamanca mountain range in southern Costa Rica to Chiriqui and Sona in Panama.

The volcanism in Central America results from the subduction of the Cocos Plate beneath the Caribbean Plate. While the convergence rate between the two tectonic plates is almost constant with ~84 ± 5 mm/a offshore Nicaragua to southern Costa Rica (DeMets, 2001), the angle of the subducting Plate decreases from an arc-wide maximum of 64° beneath Nicaragua to ~59° in central Costa Rica and ~30° in southern Costa Rica (Graefe et al., 2002; Syracuse and Abers, 2006). The subducting Cocos Plate crust north of the Nicoya Peninsula (Figure 1), generated at the East Pacific Rise spreading center, has an average age of ~25 Ma (Protti et al., 1995). Here the subducting upper lithospheric mantle appears to be extensively serpentinized, most likely due to the presence of faults related to the bending of the plate outboard of the trench. These faults cut through the entire crust and extend into the upper mantle, where they have allowed hydration and serpentinization of the uppermost mantle of the incoming plate (Rüpke et al., 2002; Abers et al., 2003; Ranero et al., 2003; Grevemeyer et al., 2007; Ivandic et al., 2008; Syracuse et al., 2008). The crust subducting south of the Nicoya Peninsula (Figure 1) has been generated between approximately 15-20 Ma ago at the slow spreading Cocos Nazca spreading center (Protti et al., 1995; Werner et al., 1999, 2003). The seamount province of the NE-trending Galapagos Hotspot track, located NW of the Cocos Ridge, subducts beneath Central Costa Rica, whereas the Cocos & Coiba Ridges subduct beneath southern Costa Rica and western Panama (e.g. Hoernle et al., 2002). The Galapagos Hotspot subducting beneath Costa Rica ranges in age between 13.0 and 14.5 Ma and the Coiba Ridge 15-20 Ma (Werner et al., 1999, 2003) and is geochemically zoned with the seamount province and Cocos/Coiba Ridges having distinct compositions (Hoernle et al., 2000, 2008).

In general the Pacific subduction margin of Central America has been shown to be erosional (Ranero and von Huene, 2000; Vannucchi et al., 2001; Vannucchi et al., 2004). The large accreted oceanic complexes along the Pacific coast of Central America and the intrusive Talamanca complex (southern Costa Rica) represent an earlier episode of plate convergence associated with accretionary processes (e.g. Drummond et al., 1995; Hauff et al., 2000; Denyer et al., 2006; Hoernle and Hauff, 2007; Geldmacher et al., 2008). The thickness of the Cocos crust increases from 5 to 7 km offshore Nicaragua to 12 km offshore SE Costa Rica on the flank of the Cocos Ridge (von Huene et al., 2000) to 21 km at the thickest part of the Cocos Ridge (Walther et al., 2000). The overlying crustal thickness is the thinnest directly beneath the Nicaraguan arc (24.6 ± 3.5 km) and the thickest beneath the back arc of Nicaragua (43.5 ± 2.5 km) and the Costa Rican arc (37.9 ± 5.2 km) (e.g. Auger et al., 2006; MacKenzie et al., 2008). The top to the downgoing plate ranges along the volcanic front from less than ~150 km beneath Nicaragua to ~60 km beneath Costa Rica (Syracuse et al., 2006, 2008).

3.3 Analytical Methods

We collected the freshest Quaternary mafic lava and tephra samples from the youngest volcanic events, historic when possible, from volcanic centers along and across the volcanic arc in Nicaragua, Costa Rica and Panama. After removal of the altered outer surfaces, the samples were crushed to small rock chips using a steel jaw crusher. The chips were then washed in distilled water in an ultrasonic bath, dried in a drying cabinet at 50°C, hand-picked under a binocular microscope and ground to powder (<63 µm) using an agate mill.

Major elements of whole rock samples (SiO_2, Al_2O_3, MgO, Fe_2O_3, CaO, Na_2O, K_2O, TiO_2, MnO and P_2O_5) were measured on fused glass beads using a Phillips X'Unique PW 1480 X-ray fluorescence spectrometer (XRF) with an Rh-tube at Leibniz Institute of Marine Sciences, IFM-GEOMAR. Volatiles (H_2O and CO_2) were analyzed using an infrared photometer Rosemount CSA 5003. Analytical accuracy for major

element concentrations for international reference standards (JA-2, JB-2, and JB-3) is generally better than 5 %, except for MnO (5 – 12 %) and P_2O_5 (4 – 10 %), of the suggested values by Govindaraju (1994).

Trace elements (Rb, Ba, Th, U, Nb, Ta, Pb, Sr, Ni, Cr, Tl, Li, Sc, V, Co, Cu, Zn, Cs, Sn, Mo, Hf, Zr, Y and the REE) were measured with a VG-Plasmaquad PQ1 inductively coupled plasma-mass spectrometer (ICP-MS) at the Institute of Geosciences, University of Kiel after the methods of Garbe-Schönberg (1993). Analytical accuracy for standard material BHVO-1 for all trace elements is better than 5.5 %, except for Sn and Pb (~12.5 %) and Tl (33 %). Analytical accuracy for standard material for AGV-1 is better than 10 %, except for Cr, Tl and Th (11 – 13%) and Li, Nb, Mo and Tm (21 – 28 %), based on the suggested reference values of Govindaraju (1994) and Jochum et al. (1994).

Isotope analyses were carried out at IFM-GEOMAR using a Thermo Finnigan TRITON (Sr isotopes) and Finnigan MAT 262-RPQ2+ (Sr isotopes) thermal ionization mass spectrometers and an AXIOM multiple collector ICP-MS (Hf isotopes), all operating in static mode. Sr isotope analyses, carried out in a Class 1000 clean room, were made on a subset of about 100mg whole rock powders of selected samples. The powders were weighted into Teflon beakers and digested in a solution of HF u.p. (ultra-pure) and HNO_3 (5:1) at 150°C for 60 hours. Ion chromatography was carried following the procedure by Hoernle and Tilton (1991), Hoernle et al. (2008) and Geldmacher et al. (2006). Within-run normalization factors were 0.1194 for $^{86}Sr/^{88}Sr$. All errors are reported as 2 sigma of the mean. Sr standard NBS 987 averaged during 4 analysis sessions yielded $^{87}Sr/^{88}Sr$ =0.710233 ± 0.000036 (N=36). Isotope ratios were normalized to 0.710250 (NBS 987) for $^{87}Sr/^{88}Sr$. Hafnium isotope ratios were determined on a subset of 20 samples. 200-500 mg of rock chips were digested for 60 hours at 130˚C in a HF-HNO_3 mixture and chemical separation followed the procedures outlined in Blichert-Toft et al. (1997). For detailed descriptions of MC-ICP-MS setup and analyzing modes see Geldmacher et al. (2006). The JMC 475 Hf-reference standard gave $^{176}Hf/^{177}Hf$ = 0.282132 (n=24) and all measured Hf values were corrected to JMC 475= 0.282163 (Blichert-Toft et al., 1997).

3.4 Results

Seventy-six mafic (MgO >3.5 wt %, with the exception of 3 Costa Rica VF samples having 2.6 – 3.5 wt%) volcanic whole-rock samples (36 lava and 40 tephra samples) from major volcanic centers along and across the southwestern Central American Volcanic Arc from SW Nicaragua (Nejapa Volcano) through Costa Rica to Panama have been analyzed for major and trace elements (Table 1). All of these samples have also been analyzed for Sr and a subset of 20 samples for Hf isotopes (Table 2). Note additional Pb and Nd isotope data from these samples are reported in Hoernle et al. (2008).

3.4.1 Major and Trace element data

On a SiO_2 vs. K_2O classification diagram for subalkalic rocks (Figure 2), VF samples from SW Nicaragua to NW and Central Costa Rica have compositions within the Medium-K or calc-alkaline series with few Central Costa Rica samples extending into the High K or High-K calc-alkaline and few NW Costa Rica and SW Nicaragua into the Low K or tholeiitic series. The alkali basalts from S Costa Rica and W Panama have High-K calc-alkaline compositions extending into calc-alkaline series. Adakite samples from S Costa Rica and W Panama have calk-alkaline to High-K calc-alkaline compositions largely overlapping with C Costa Rica VF sample compositions. In summary Central Costa Rica VF and Backarc, southern Costa Rica and western Panama volcanic rocks have generally higher K values, extending from the Medium into the High K field, whereas Nicaragua and northwest Costa Rica samples range from Low to Medium K values. This confirms Gazel et al. (2009).

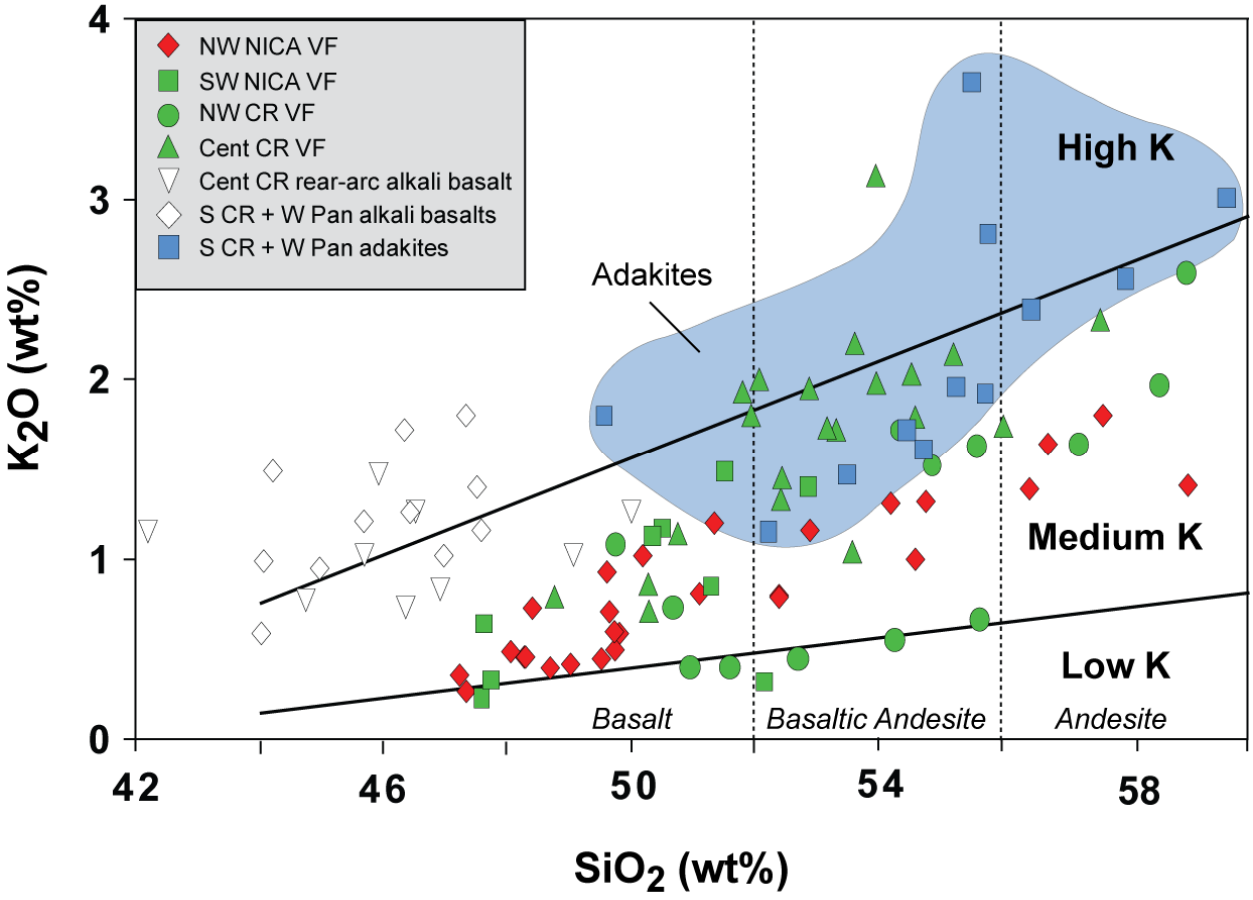

Figure 3.2 SiO_2 versus K_2O major element classification diagram (after Le Maitre et al., 1989) for southwestern Central American subduction-related volcanic rocks. Mafic (MgO>3.15 wt %) volcanic front (VF) rocks from SW Nicaragua to central Costa Rica plot within the Medium K or calc-alkaline series field. Most of the southern Costa Rica and western Panama alkali basalts samples plot within the High K or High-K Calc-alkaline series and adakite samples (blue field) within the High K series and largely overlapping with the Medium K series. Central Costa Rican rear-arc samples have intermediate to high K compositions, with generally lower SiO_2 content. Data for NW Nicaraguan VF samples is also shown (Heydolph et al., to be submitted). Vertical dashed lines indicate transitions between basalt to basaltic andesite and andesite compositions for volcanics (modified after Le Maitre et al., 2001). See Table 1 for geochemical data in this diagram.

Volcanic front samples from Nicaragua and NW Costa Rica usually have higher FeOt (total iron as FeO), MnO, CaO, Al_2O_3, Sc, V and Yb, but lower SiO_2, TiO_2, Na_2O, P_2O_5, K_2O, Pb, Sr, Rb, Ba, Nb and La contents at a given MgO content (Figure 3a-t) than Central Costa Rica to western Panama samples. Central Costa Rica BVF samples

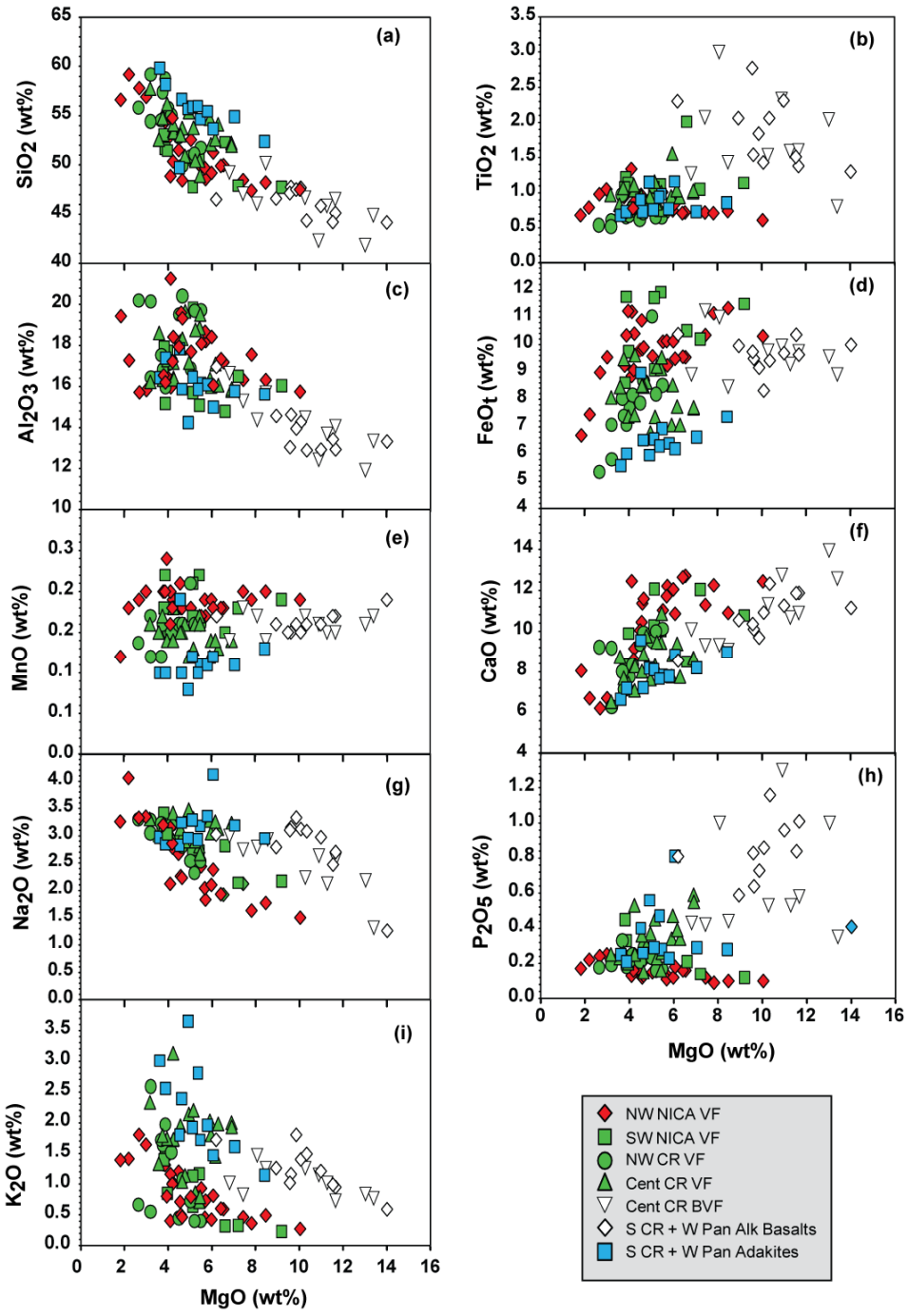

Figure 3.3 (a-i) MgO versus major element oxide variation diagrams for volcanic front (VF) and behind the volcanic front (BVF), adakite and alkali basalt mafic volcanic rock samples with MgO > 3.15 wt%. (j-r) MgO versus select trace elements variation diagrams for volcanic front (VF) and behind the volcanic front (BVF), adakite and alkali basalt mafic volcanic rock samples with MgO > 3.15 wt%.

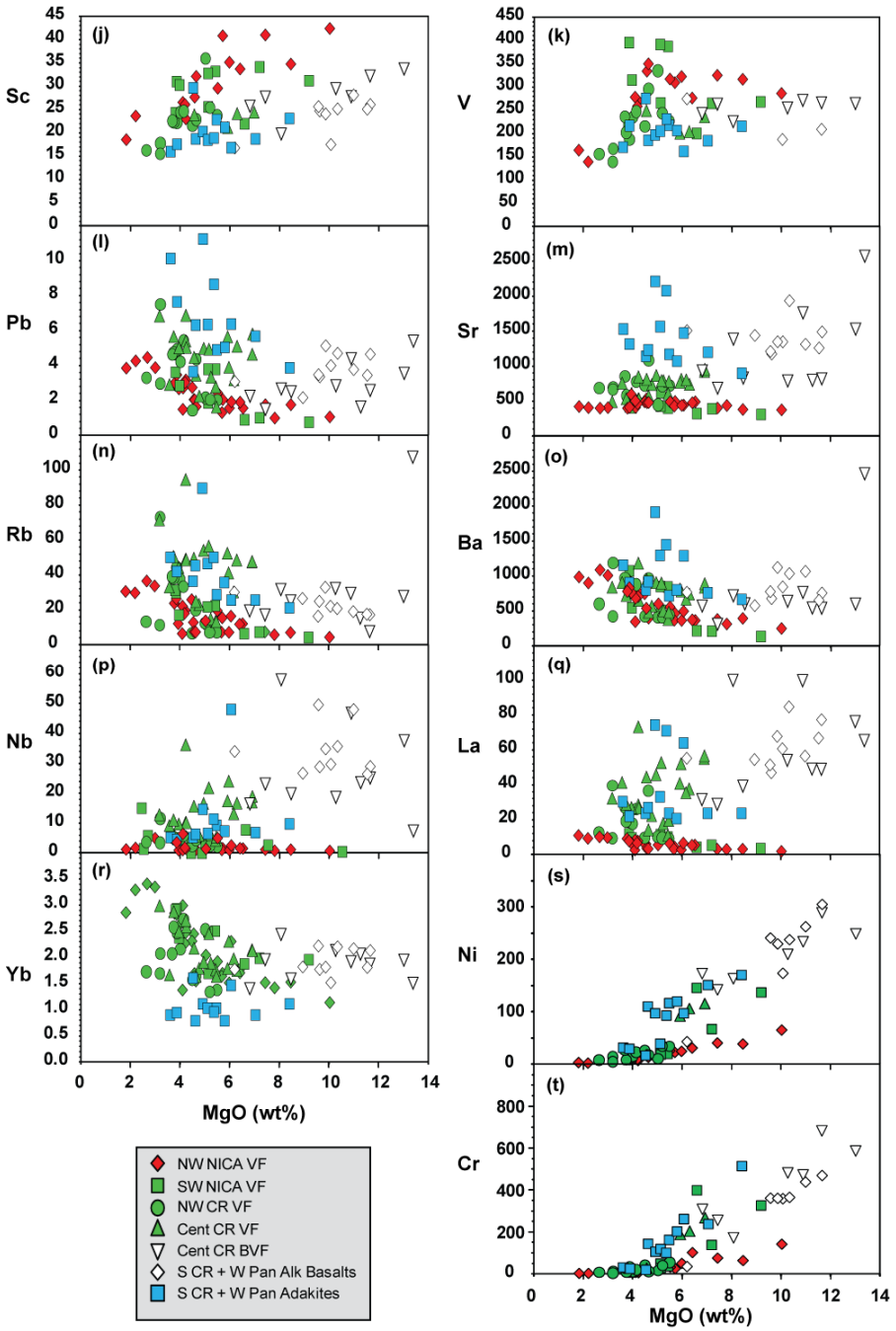

having the highest MgO values (MgO = 6.81-13.39 wt%.) show similar concentrations to southern Costa Rica and Panama alkali basalt samples with generally lower SiO_2, Al_2O_3 and higher TiO_2 than VF samples from Costa Rica and Nicaragua (Figure 3a-c). Adakite samples from southern Costa Rica and Panama have higher SiO_2 and K_2O and lower FeOt, MnO and CaO than VF samples from Costa Rica and Nicaragua (Figure 3a, c, d,

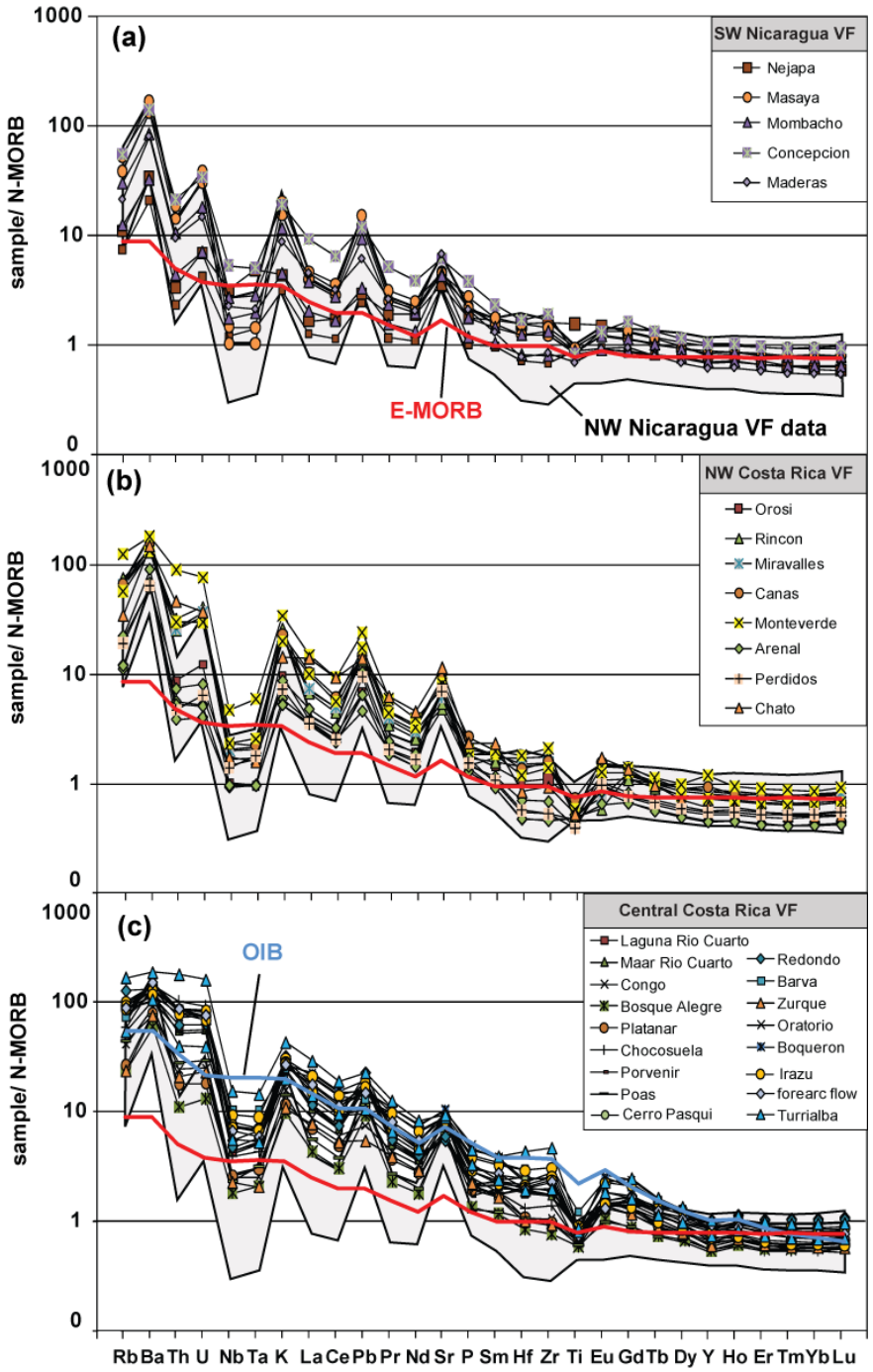

Figure 3.4 (a-f) Primitive N-MORB normalized (after Sun and McDonough, 1989) multi-element diagrams of selected volcanic front (VF) and behind the volcanic front (BVF) samples (MgO > 3.15 wt %) from Nicaragua, Costa Rica and alkali basalt and adakite samples from Costa Rica and Panama. The complete range of southwestern Central American volcanic front arc lava compositions from this study is indicated by underlying grey field, including VF, BVF, alkali basalt and adakite samples. Data for average E-MORB (bold red line) and OIB (bold blue line) compositions after Sun and McDonough (1989).

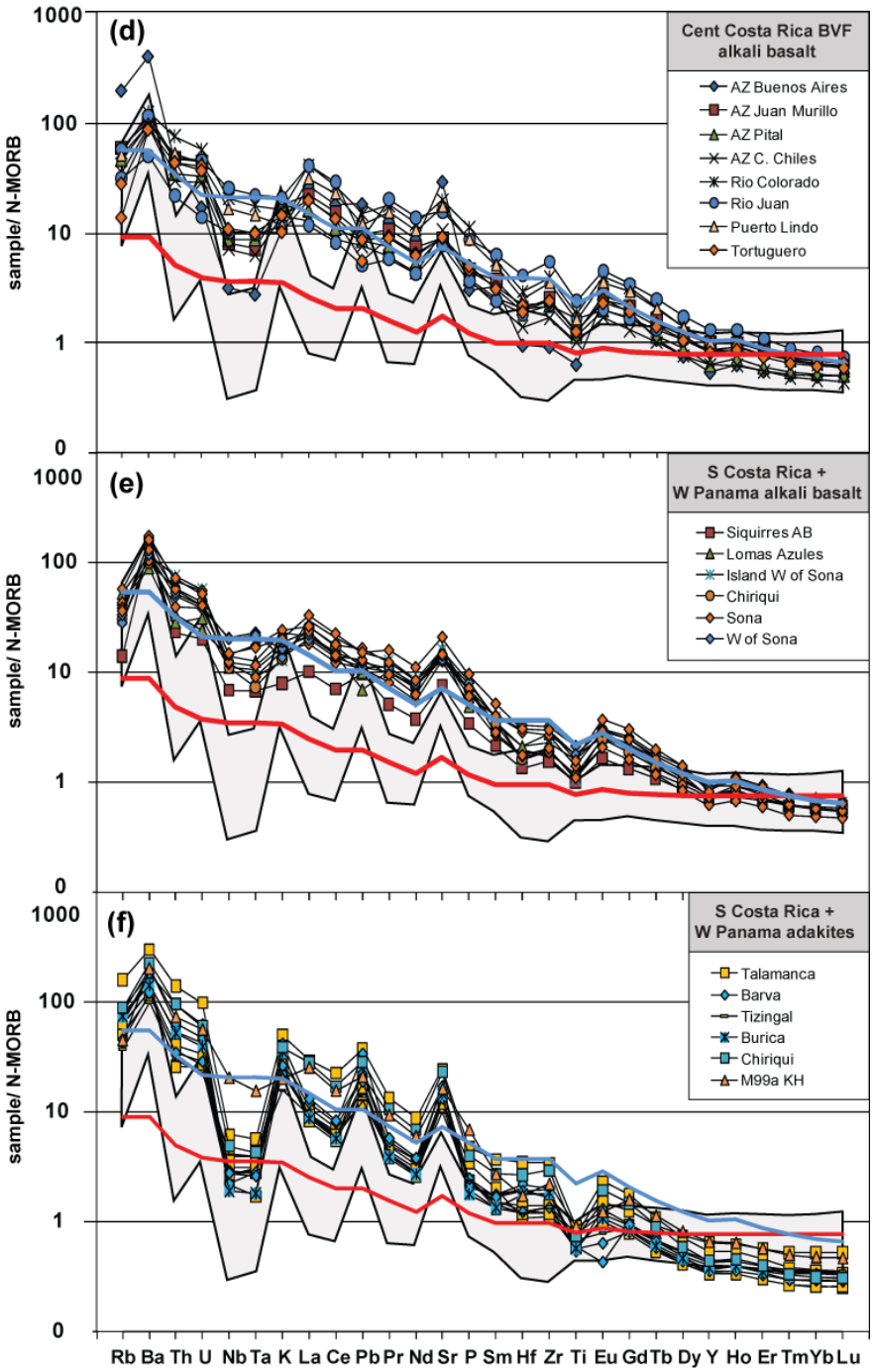

e, f, i). Sc and V show a crude decrease and Pb and Sr a crude increase in the most mafic VF samples going from NW Nicaragua to central Costa Rica (Figure 3j-m). The most mafic central Costa Rica BVF samples generally extend to intermediate Sc, V, Pb, Rb, Ba and Yb but higher Sr, Nb and La, when compared to VF samples from

Nicaragua and Costa Rica (Figure 3j-r). Alkali basalt samples from southern Costa Rica and Panama have higher Sr, Nb and La and intermediate Sc, V, Pb, Rb, Ba and Yb than VF samples from Nicaragua and Costa Rica.

On primitive N-MORB normalized multi-element diagrams (Figure 4a-f), all samples display enrichment in fluid-mobile large-ion-lithophile elements (LILE; e.g. Ba, K, Pb, Sr) and U, relative to high field strength elements (HFSE; e.g. Nb, Ta, Zr, Hf, Ti) and light rare earth elements (LREE; e.g. La, Ce, Nd) reflecting typical subduction-related trace element abundance patterns (e.g. Arculus, 1994; Pearce, 1995).

Trace element compositions and ratios vary systematically along the volcanic front, between VF and adakite samples from southern Costa Rica and western Panama and between VF/adakite and BVF S Costa Rica and western Panama alkali basalt samples. Ratios of more to less fluid mobile trace elements (e.g. Ba/La, U/Th, Ba/Th and to a lesser degree Sr/Ce, Figure 5j-m) vary systematically along the volcanic front decreasing from NW Nicaragua to Panama, consistent with the results of previous studies (e.g. Carr et al., 1990, 2003, 2007; Patino et al., 2000, Sadofsky et al., 2008). Central Costa Rica VF and BVF samples generally extend to the lowest more to less fluid mobile element ratios (Figure 4j-m), with southern Costa Rica and Panama adakite and alkali basalt samples showing similar compositions. Ratios of more to less incompatible rare earth elements (REE) elements (e.g. La/Yb) (Figure 5n) generally increase from Nicaragua to central Costa Rica, reflecting both generally lower heavy (H) REE and higher LREE contents in the central Costa Rican lavas (e.g. Figure 5n). Zr/Hf ratio shows broad increase from NW Nicaragua to Central Costa Rica. (Figure 5o). Southern Costa Rica and western Panama have similar La/Yb and Zr/Hf to central Costa Rica. In general central Costa Rican BVF samples have higher LREE/HREE ratios than VF volcanoes along transects in central Costa Rica perpendicular to the trench and VF. BVF samples have higher HFSE and REE contents than related VF samples with similar MgO contents.

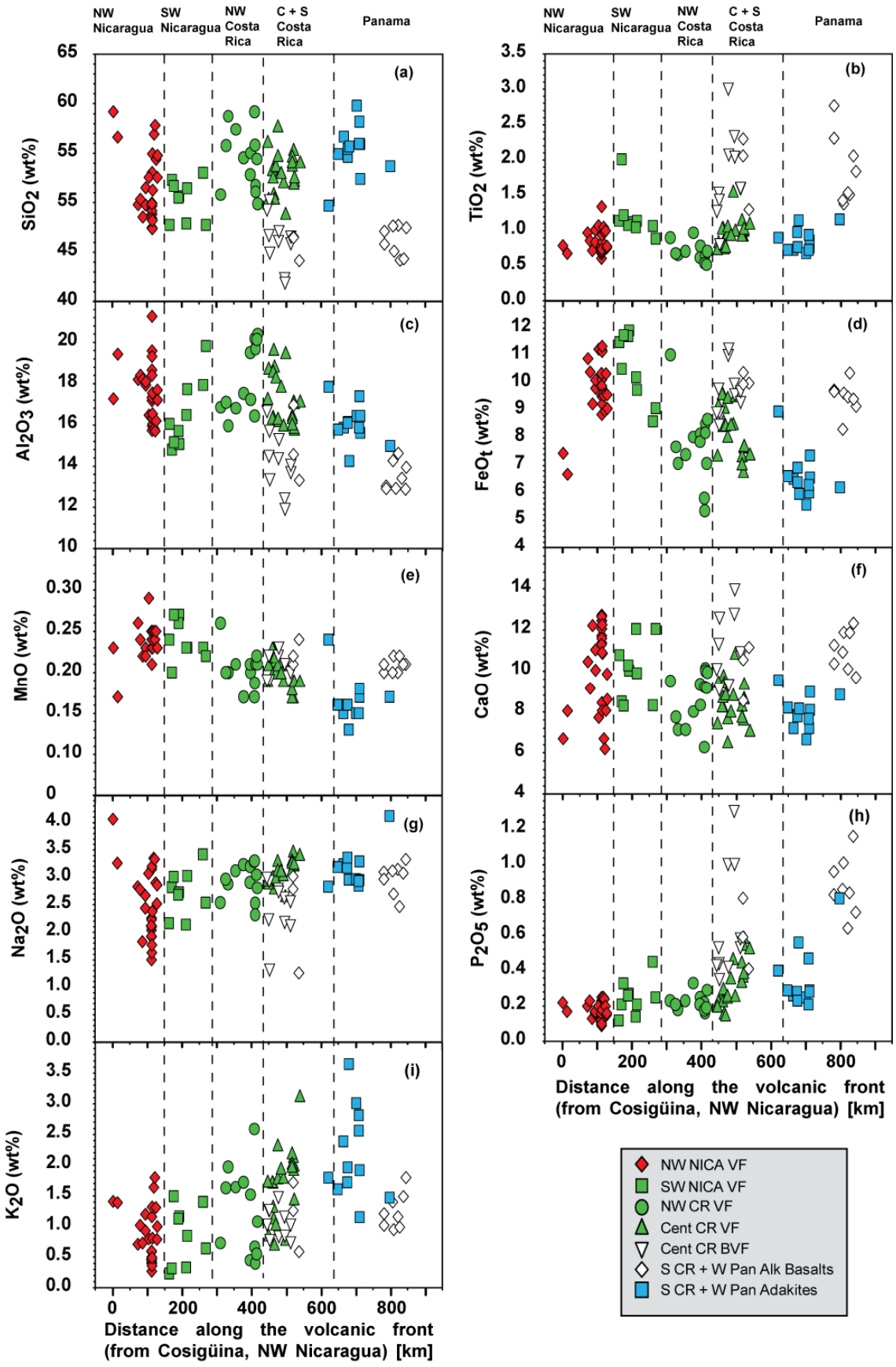
NW Nicaragua
SW Nicaragua
NW Costa Rica
C + S Costa Rica
Panama
(a)
(b)
(c)
(d)
(e)
(f)
(g)
(h)
(i)
SiO2 (wt%)
TiO2 (wt%)
Al2O3 (wt%)
FeOt (wt%)
MnO (wt%)
CaO (wt%)
Na2O (wt%)
P2O5 (wt%)
K2O (wt%)
Distance along the volcanic front (from Cosigüina, NW Nicaragua) [km]
NW NICA VF
SW NICA VF
NW CR VF
Cent CR VF
Cent CR BVF
S CR + W Pan Alk Basalts
S CR + W Pan Adakites

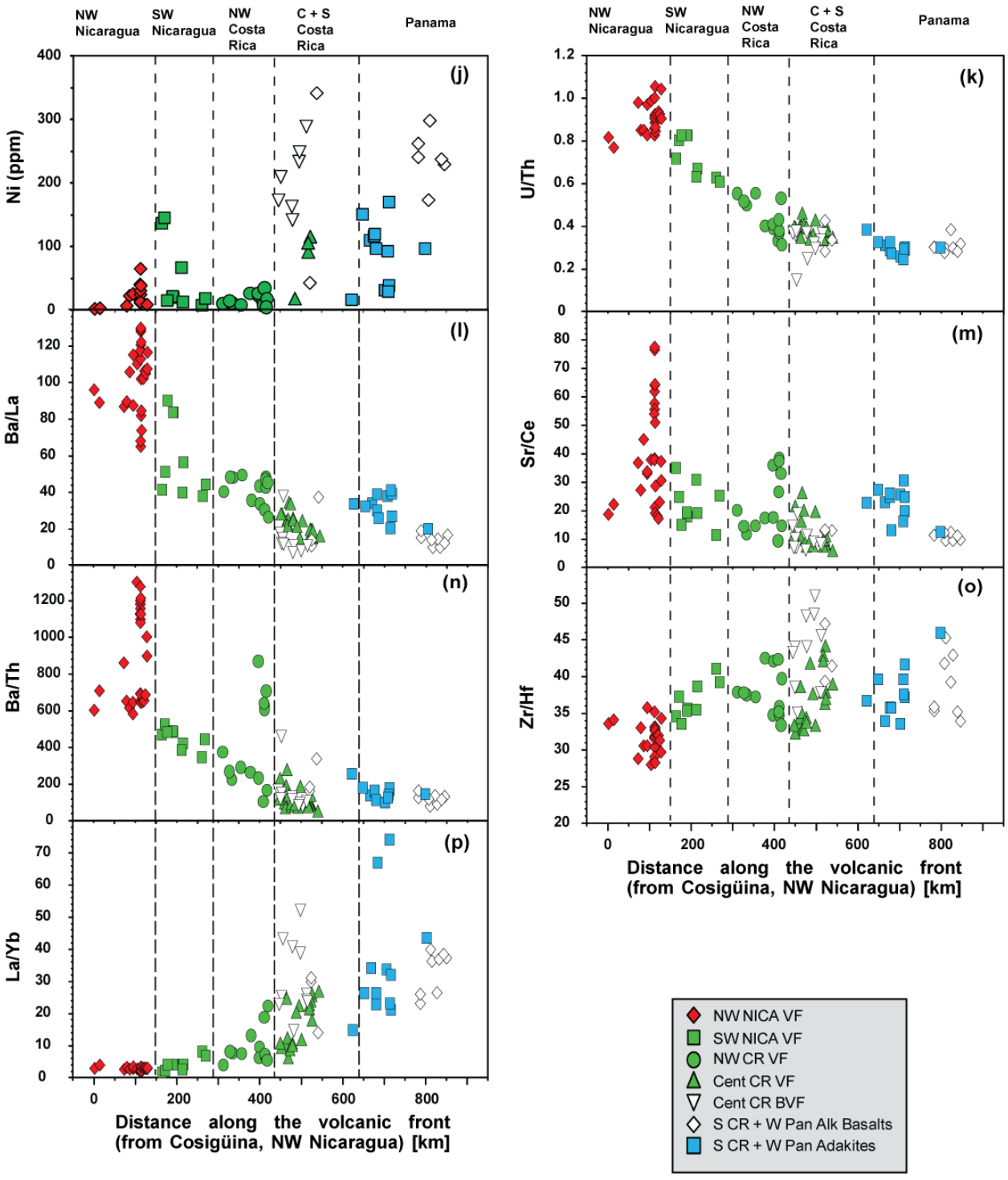

Figure 3.5 Distance along the volcanic front versus major (a-i) and selected trace element ratios (j-o) of fluid mobile to immobile elements for mafic southwestern CAVA volcanic rock samples from the VF, BVF. Also shown are data for southwestern Costa Rica and western Panama alkali basalt and adakite samples. Dashed vertical lines mark the respective country borders. Distance in kilometer is calculated from Cosigüina Volcano in NW Nicaraguan near the border to Honduras at the Gulf of Fonseca.

3.4.2 Sr-Nd-Pb-Hf isotopes

The Sr and Hf isotope data is presented in Table 2. The $^{87}Sr/^{86}Sr$ isotopic composition shows an initial increase along the VF from NW Nicaragua (Cosigüina Volcano) to Central Nicaragua (with a maximum $^{87}Sr/^{86}Sr$ of 0.7042 for Masaya Volcano) and then a systematic decrease through central Costa Rica to western Panama (Figure 6a). Two samples from the Nejapa volcanic centers with $^{87}Sr/^{86}Sr$ of 0.7037 form a local minimum. Southern Costa Rica and western Panama adakite and alkali basalt samples continue the decreasing trend observed in the VF samples to $^{87}Sr/^{86}Sr$ as low as 0.7033, similar to what has been observed previously (e.g. Carr et al., 2003). Backarc Central Costa Rica samples show a larger range in Sr isotope ratios than the Central Costa Rica VF samples, completely overlapping with the Central Costa Rica VF samples but extending the Sr isotopic composition to generally lower values. Southern Costa Rica and Panama adakite samples extend to the least radiogenic Sr isotope ratios. As noted previously (Hoernle et al., 2008), the Pb isotope ratios (e.g. Figure 6b) increase systematically along the VF from NW Nicaragua ($^{206}Pb/^{204}Pb$ = 18.4) to central Costa Rica, where after a slight decrease, the Pb isotope ratios increase to their maximum values (e.g. $^{206}Pb/^{204}Pb$ = 19.3) in the westernmost Panama adakites before decreasing again slightly in the central Panama alkali basalts ($^{206}Pb/^{204}Pb$ = 19.1). The Central Costa Rica backarc alkali basalts also extend to similar Pb isotopic ratios as the western Panama adakites. The variation in Nd isotopic composition is not as tight as for the Pb isotope ratios, but overall Nd isotope variations form a mirror image of the Pb isotope variations with the lowest Nd isotope ratios ($^{143}Nd/^{144}Nd$ = 0.51293) being present in the Central Costa Rica backarc alkali basalts and the westernmost Panama adakites (Figure 6c). The $^{176}Hf/^{177}Hf$ isotope data (Figure 6d) show a crudely similar variation along the southern part of the Central American arc to the variations in Nd isotopic composition, although the Hf isotope data shows greater variability than the Nd isotopic variation, in particular for samples from southwestern Nicaragua (Nejapa, Mombacho and Concepcion). BVF samples from central Costa Rica have the lowest $^{176}Hf/^{177}Hf$ isotope ratios along the arc. Southern Costa Rica and Panama adakite and alkali basalt samples show a broad scatter largely overlapping with the Central Costa Rica volcanic front samples. Central Costa Rica BVF samples in

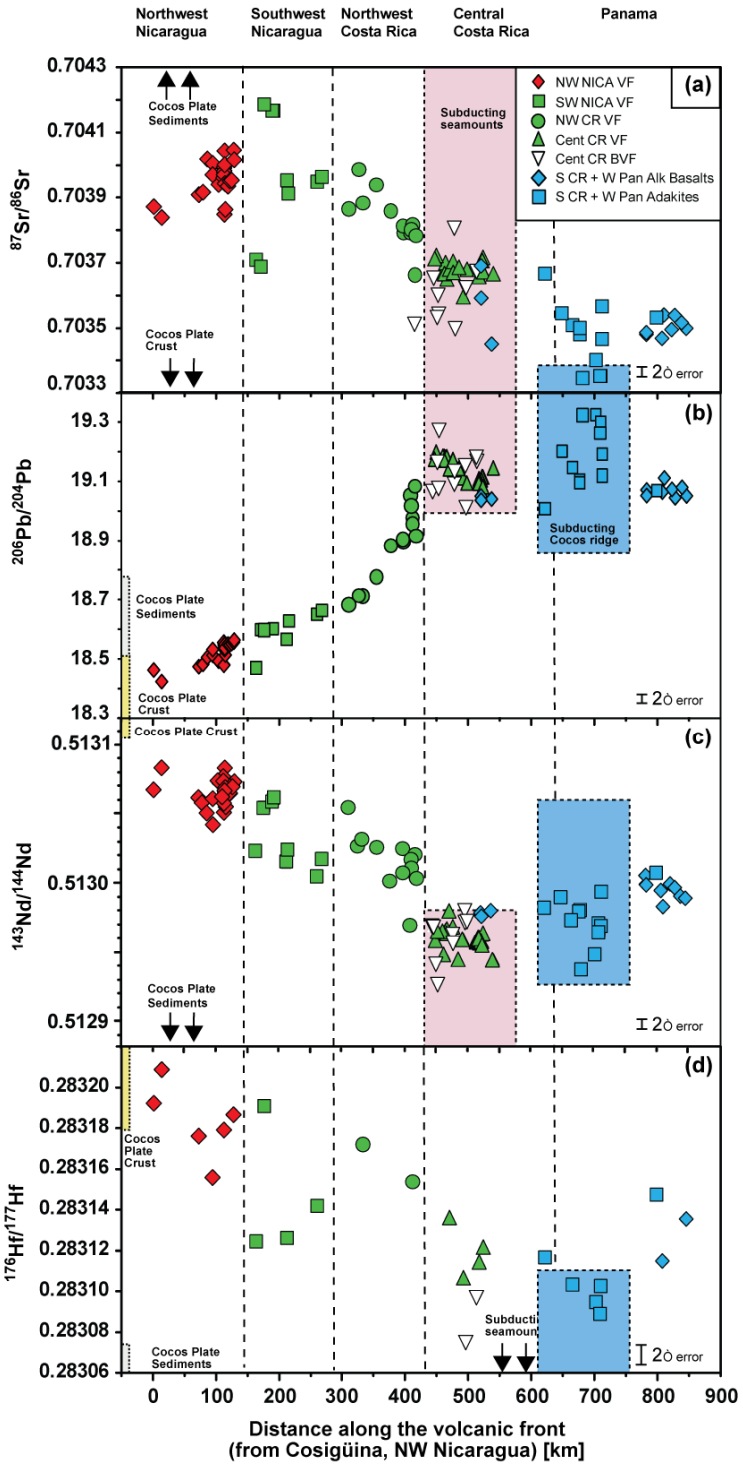

Figure 3.6 (a-d)Distance along the volcanic front versus $^{87}Sr/^{86}Sr$, $^{206}Pb/^{204}Pb$, $^{207}Pb/^{204}Pb$ and $^{176}Hf/^{177}Hf$ for mafic (MgO > 3.15 wt %) southwestern Central American volcanic samples from the VF and BVF. Also shown are data for southwestern Costa Rica and western Panama alkali basalt and adakite samples. Data for subducting seamounts, Cocos Plate sediments and crust from Feigenson et al. (2004), Werner et al. (2003), Geldmacher et al. (2003, 2008), Heydolph et al. (to be submitted). All errors are reported as 2 sigma of the mean. Distance in kilometer is calculated from Cosigüina Volcano in NW Nicaraguan near the border to Honduras at the Gulf of Fonseca.

central Costa Rica extend to the most enriched, subducting seamount province-like compositions, with less radiogenic $^{87}Sr/^{86}Sr$, 143Nd/144Nd and $^{176}Hf/^{177}Hf$ but more radiogenic Pb isotope ratios than associated VF samples.

On $^{206}Pb/^{204}Pb$, $^{207}Pb/^{204}Pb$ and $^{208}Pb/^{204}Pb$ vs. $^{176}Hf/^{177}Hf$ isotope correlation diagrams (Figure 7) for SW Central American volcanics, VF and BVF samples from Nicaragua and Costa Rica form a crude negative correlation, extending from Cocos Plate crust-like composition with unradiogenic Pb and radiogenic Hf towards an enriched component with radiogenic Pb and unradiogenic Hf. The northwestern Nicaragua VF samples have the most depleted i.e. enriched MORB (E-MORB) like compositions. The southern Costa Rica and Panama alkali basalt and adakite samples overlap with central Costa Rica BVF samples though they have slightly more radiogenic Hf isotope ratios (with the exception of 2 samples from Barva and Chiriqui, which have less radiogenic Hf isotope ratios for a given Pb isotopic composition). On the Pb versus 176Hf/177Hf isotope diagrams, the samples from SW Nicaragua form a vertical trend. Addition of sediments to these lavas cannot explain the low Pb and Hf isotope ratios, as is clear from the $^{207}Pb/^{204}Pb$ and $^{208}Pb/^{204}Pb$ vs. $^{176}Hf/^{177}Hf$ isotope diagrams (Fig. 7 b, c).

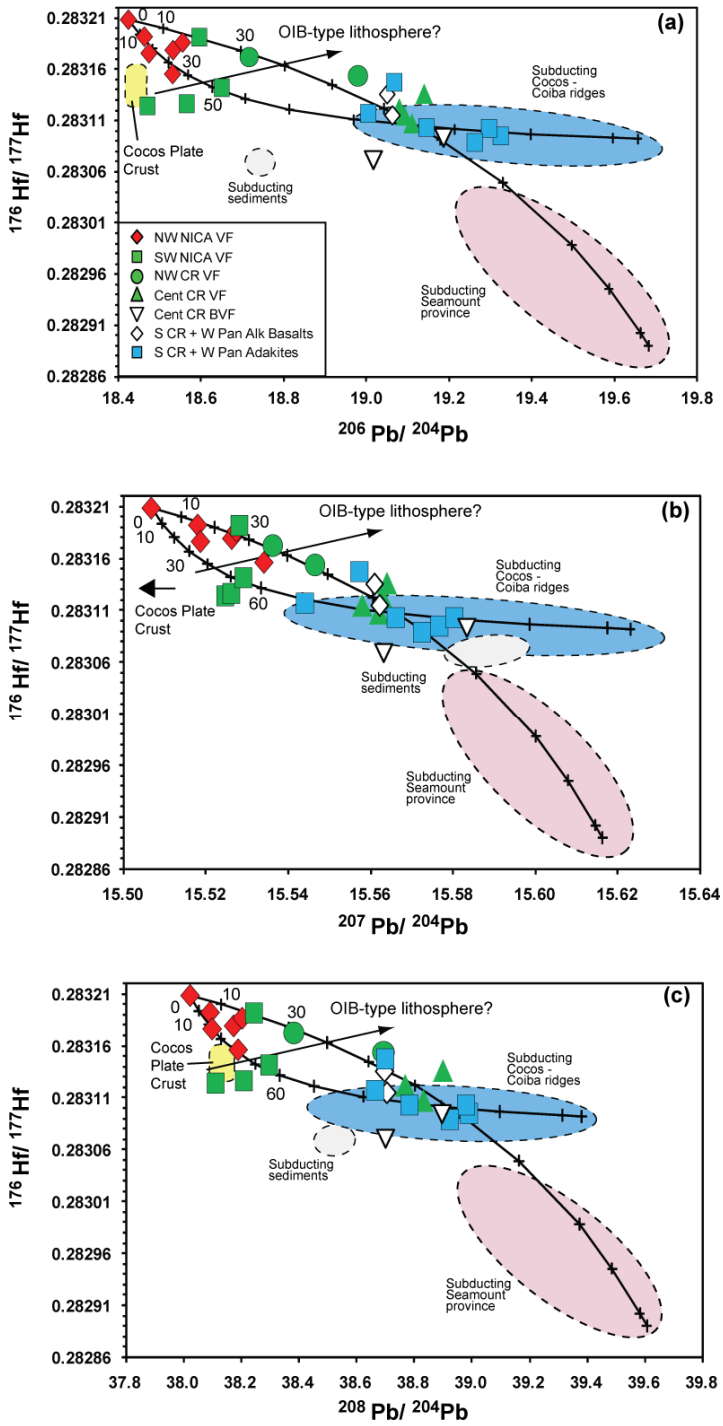

Figure 3.7 (a-c) Pb vs. Hf isotope data for mafic (MgO > 3.15 wt %) southwestern Central American volcanic rock samples from the VF and BVF. Also shown are data for southwestern Costa Rica and western Panama alkali basalt and adakite samples. Data for subducting Seamount province, subducting Cocos and Coiba ridges, Cocos Plate sediments and crust from Feigenson et al. (2004), Werner et al. (2003), Geldmacher et al. (2003, 2008), Heydolph et al. (to be submitted). All errors are reported as 2 sigma of the mean.

On the εNd vs. εHf diagram (Figure 8), the SW Central American rocks form a good positive correlation if only the VF (r^2 = 0.83) or if all arc-related rocks are considered (r^2 = 0.66). The SW Central American VF array falls on top of the mantle array and has a similar slope. The alkali basalt and adakite samples largely overlap with the VF trend but overall are shifted to slightly lower εHf values, forming a trend with a slightly shallower slope than the VF array.

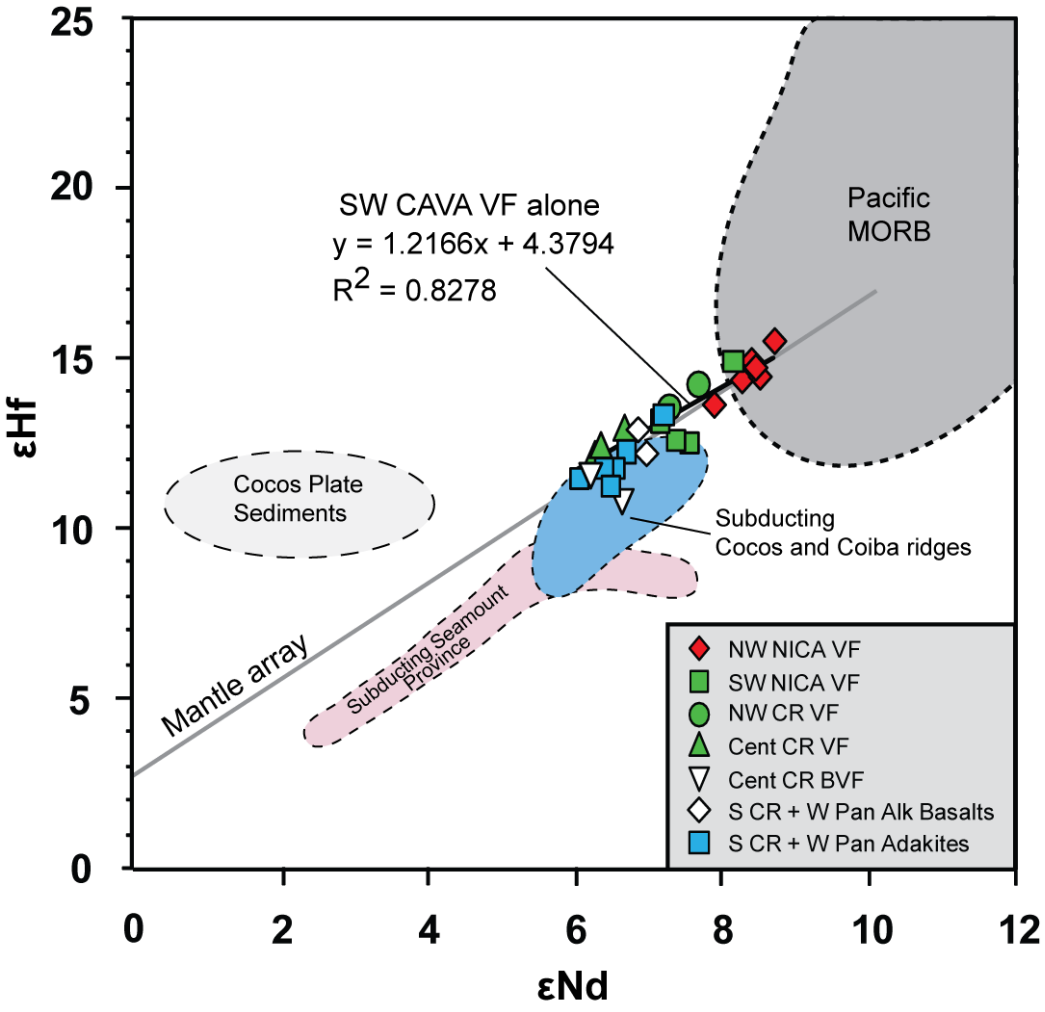

Figure 3.8 eNd vs. eHf diagram for mafic southwestern Central American VF and BVF volcanic rock samples. Combined VF and BVF samples from the southwestern Central American volcanic arc form a good positive linear correlation (R^2 = 0.8278). Excluding the central Costa Rica BVF and southern Costa Rica and western Panama samples, the positive trend can be defined by two components (SO144-1/ Pacific MORB-type composition and subducting Seamount province enriched type composition) with Nicaraguan samples having the most Pacific MORB-like compositions and central Costa Rica samples trending towards an enriched component. Diagram modified after Geldmacher et al. (2003) with additional fields for Cocos Plate Sediments (DSDP Leg67 offshore Guatemala), subducting Cocos and Coiba ridges and subducting Seamount province (Geldmacher et al., 2003, 2008).

3.5 Discussion

Various authors suggested distinct models for the origin of the enriched OIB-like signature in southwestern CAVA volcanic rocks (e.g. Abratis and Wörner, 2001; Goss and Kay, 2005; Hoernle et al., 2008; Gazel et al., 2009). We will now briefly discuss the most recent models and further evaluate with our new geochemical dataset.

Enriched isotopic signatures in Costa Rican volcanic rocks have been reported by various authors (e.g. Carr et al., 1990, 2003; Abratis and Wörner, 2001; Feigenson, 2004; Goss and Kay, 2005; Hoernle et al., 2008; Gazel et al., 2009). However the origin of this signature has been intensively debated. The OIB-like signature in central Costa Rican lavas could result from melting of the upwelling Pacific upper mantle through a slab window in the mantle wedge beneath southern Costa Rica and Panama (Abratis and Wörner, 2001). Though, as Gazel et al. (2009) pointed out by their new data, this model does not account for the more intermediate isotopic values of some of the Early Middle Miocene Talamanca Range samples. Feigenson et al. (2004) suggested that remelting of Galapagos influenced mantle during modern subduction beneath central Costa Rica could generate the OIB-like trace element and isotopic signatures of all erupted lavas above the hot spot track. New isotopic data for tertiary lavas and shallow intrusion from Costa Rica show that the OIB-like signature is of Late Miocene origin (Gazel et al., 2009). That contradicts the remelting Galapagos influenced mantle model from Feigenson et al. (2004), which would rather result in an OIB-like signature since the Oligocene. Another model by (Goss and Kay, 2006) suggests that incorporating parts of the accreted fore-arc oceanic complexes by tectonic erosion. These complexes are associated with Caribbean large igneous province (CLIP) remnants. However, this is only plausible if the tectonic erosion started with beginning of the Galapagos hotspot tracks and new data on late Miocene lavas from Costa Rica (Gazel et al., 2009) show more enriched 208Pb/204Pb and lower $^{143}Nd/^{144}Nd$ isotopic compositions at a given $^{206}Pb/^{204}Pb$ when compared to Costa Rican fore-arc CLIP complexes. On the other hand new models from Hoernle et al. (2008) and Gazel et al. (2009) suggest, based on Pb and Nd isotopic compositions that the offshore central Costa Rica subducting Galapagos hotspot seamount province could explain the radiogenic Pb with high

$^{208}Pb/^{204}Pb$ of Costa Rican VF and BA lavas. The subducting Cocos and Coiba ridges could explain the volcanic rocks from southern Costa Rica and western Panama, which have radiogenic Pb but intermediate $^{208}Pb/^{204}Pb$ and $^{143}Nd/^{144}Nd$, Other potential source components for the Costa Rica and Panama volcanic rocks (e.g. CLIP-like Costa Rica fore-arc or Galapagos hotspot influenced mantle have isotopic composition distinct from the subducting seamount province and therefore cannot explain the Pb and Nd isotopic data (Hoernle et al., 2008), or would result in enriched signatures for longer periods than the middle Miocene (Gazel et al., 2009).

Generally all volcanic front samples from Nicaragua and Costa Rica show an incompatible element geochemistry which clearly indicates a subduction zone affinity for these volcanic rocks: relative enrichment of fluid-mobile elements, such as LILEs and Pb (which form peaks on multi-element diagrams, (Figure 4), and relative depletion of HFSE, such as Nb, Ta and Ti (which form troughs on multi-element diagrams). Ratios of high to less fluid-mobile trace elements i.e. Ba/La, Ba/Th, Ba/Nb, U/Th and Sr/Ce (Figure 5 j-o) range for all NW and some SW Nicaraguan above those commonly found in MORB and OIB and rather reflect the influence of a sediment component to their magma sources. Lavas from Costa Rica and Panama have generally Ba/La values <40 (with a few exceptions in NW Costa Rica having Ba/La ~49), which could reflect the derivation from an enriched source. Ratios of La/Yb, indicative for lower degress of partial melting or an enriched source contribution to the magmas sources are highest from central Costa Rica to Panama (ranging from ~10 to ~74). Compared $^{206}Pb/^{204}Pb$ isotope data and La/Yb show that high $^{206}Pb/^{204}Pb$ and La/Yb data coincide, indicating an enriched source contribution.

Combined $^{87}Sr/^{86}Sr$, $^{206}Pb/^{204}Pb$, $^{207}Pb/^{204}Pb$, $^{208}Pb/^{204}Pb$, $^{143}Nd/^{144}Nd$ and $^{176}Hf/^{177}Hf$ isotopic data demonstrate the noticeable influence of distinct subducting Cocos Plate components (Cocos Plate crust, subducting sediments, subducting Seamount province and subducting Cocos and Coiba ridges) on the SW CAVA lava compositions. We identify at least three compositional endmembers: 1) NW Nicaraguan VF rocks have high Ba/La, Ba/Th and U/Th but low La/Yb and Zr/Hf, unradiogenic Pb but radiogenic Sr, Nd and Hf isotope ratios, comparable to offshore NW Nicaragua subducting Cocos

plate crust (e.g. Figure 7, 8, Isos II (appendix)). Isotopically these rocks represent a depleted endmember in the Central American system, although they are enriched in $^{87}Sr/^{86}Sr$ when compared to Pacific MORB. 2) Central Costa Rica VF rocks have low Ba/La, Ba/Th and U/Th but high La/Yb and Zr/Hf, radiogenic Pb but unradiogenic Sr, Nd and Hf isotope ratios. These rocks show similar isotopic compositions to the offshore central Costa Rica subducting Seamount Province (Figure 6, 7, Isos II (appendix)). 3) Southern Costa Rica and western Panama alkali basalt and adakite rocks have low Ba/La, Ba/Th and U/Th but high La/Yb and Zr/Hf (similar to central Costa Rican rocks),unradiogenic Sr and $^{176}Hf/^{177}Hf$ but high $^{206}Pb/^{204}Pb$ and $^{207}Pb/^{204}Pb$ isotope ratios. The source component of these rocks could be influenced by the subducting Cocos and Coiba ridges (Figure 6, 7, Isos I, II (appendix)) or the subducting seamount province. An additional and distinct source from subducting crust source component is required for SW Nicaragua lavas from Masaya volcano with high Ba/La, $^{87}Sr/^{86}Sr$ and $^{176}Hf/^{177}Hf$ but unradiogenic Pb. Sadofsky et al. (2009) inferred from low Ba/Th and δ18O and higher U/La and correlation with H_2O from melt inclusion studies, that a subducting hemipelagic sediment is contributing to the magma source of Masaya volcano.

Our new major and trace element and Sr and Hf isotope data supplement data from Hoernle et al. (2008), who demonstrate the influence of the subducting Galapagos hot spot track (seamount province) on the chemistry of the erupted rocks in southwestern Central America. Below we will compare our new data with existing models for the origin of the source compositions for southwestern Central American arc lavas. Ratios indicative for an enriched mantle component (e.g. Zr/Hf, La/Yb) show high values ~20 and ~40 respectively for central Costa Rican lavas and decrease systematically to Nicaragua. Whereas ratios of Ba/La and Ba/Th, which are almost constant within the sediment column of the Cocos plate, clearly show a strong sediment contribution to the magma source for NW Nicaragua. This signal decrease systematically along the arc to Costa Rica and Panama.

3.5.1 The subducting Cocos plate offshore central Costa Rica and Panama

As illustrated on distance along the volcanic front vs. Sr, Pb and Hf isotope ratios diagrams (Figure 6) and the Pb vs. Hf isotope correlation diagrams (Figure 7), all volcanic front samples from NW Nicaragua to Central Costa Rica vary systematically along the volcanic front and additionally form crude negative trends between the Cocos Plate crust and subducting Seamount province and Cocos and Coiba ridges. SW CAVA VF rocks form a good positive linear correlation on an Nd vs. Hf isotope diagram (Figure 8, 9) between subducting Cocos plate crust/ Pacific MORB and subducting Seamount province. Combined Sr vs. Nd and Hf isotopic data (Figure Isos I and II) show positive correlation for SW VF CAVA lavas, ranging from subducting Cocos and Coiba ridges-like compositions to a more radiogenic one with elevated Sr isotope ratios (most likely reflecting seawater alteration). Binary mixing curves between a Pacific MORB (or the composition of the subducting crust, as indicated by sample SO144-1 from Werner et al., 2003, although we don't have Hf isotope data on this sample) endmember and an enriched subducting Seamount province endmember requires assimilation of ~10 to 15 % of the enriched component to generate our observed Nd and Hf isotopic compositions of the most enriched VF samples from central Costa Rica. Other potential source components e.g. Cocos Plate sediments, do not have appropriate isotopic compositions and mixing between a Pacific MORB like endmember and these components cannot explain our observed correlation of volcanic rocks from NW Nicaragua to Central Costa Rica VF samples. Binary mixing curves require the addition of ~50% of the subducting Cocos and Coiba ridge component to generate our observed trends. Cocos plate sediments, which have unradiogenic Hf and radiogenic Nd, clearly lie above the mantle array and cannot explain our correlation

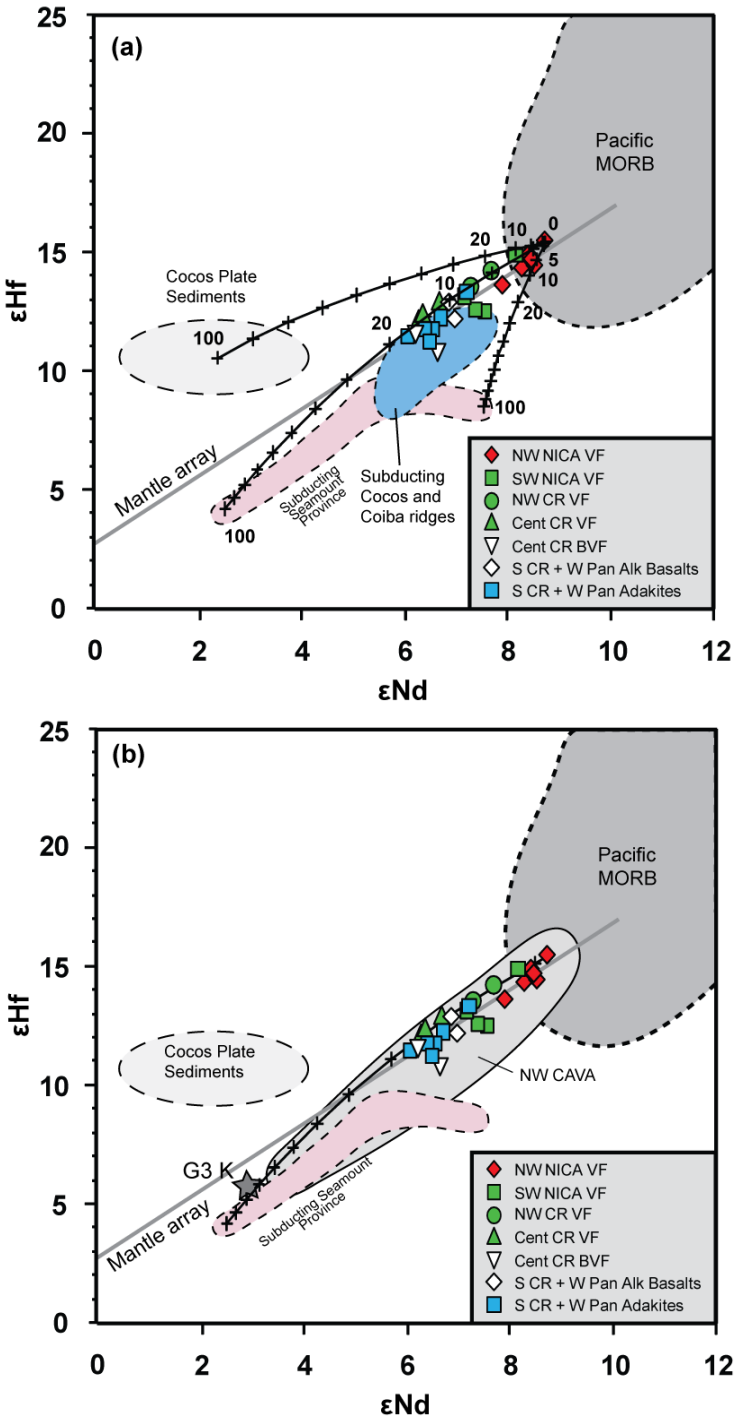

Figure 3.9 (a, b) **(a) eNd vs. eHf diagram for mafic southwestern Central American VF and BVF volcanic rock samples. For data on additional sources see Figure 8. Also shown are binary mixing lines for mixing between a depleted Cocos plate crust/ MORB-like component and Cocos plate sediments, subducting Cocos and Coiba ridges and subducting Seamount province. Numbers indicate the mixing ratios. (b) eNd vs. eHf diagram for mafic southwestern Central American VF and BVF volcanic rock samples. Additional field for NW CAVA VF and BVF and G3K Guatemalan basement sample from Heydolph et al. (to be submitted).**

Nd and Hf isotopic compositions of the entire VF and BVF NW CAVA with VF SW CAVA lavas (Figure 9b) and modeled binary mixing curves show positive trends for both NW CAVA and SW volcanic rocks, with Nicaragua being the common radiogenic endmember for both trends. While the magma sources for NW CAVA rocks are dominated by a three component system, consisting of (1) an enriched lithospheric mantle component with high more to less incompatible element ratios, e.g. La/Yb and La/Sm, and Zr/Hf, and enriched Sr, Nd, Hf and Pb isotopic composition for NW Guatemalan lavas. (2) A Honduras and Caribbean BA endmember, characterized by alkalic lavas with OIB-type trace element compositions and enriched (E)-MORB-type isotopic compositions. Probably resulting from sampling eclogite/pyroxenite veins in the asthenosphere upwelling in the backarc, derived from relatively young subducted oceanic crust in the upper mantle. And (3) a NW Nicaraguan endmember with trace element and Sr-Nd-Pb-Hf isotope ratios being largely dominated by serpentinite-derived fluid flux from the subducting slab, possibly with small amounts (<1 wt. %) of sediment melts to a depleted N-MORB type of mantle wedge, resulting in large degrees of melting of primarily peridotitic material. The trends for SW CAVA rocks can largely be explained with mixing of three subducting Galapagos hotspot track components. The offshore central Costa Rica subducting seamount province with radiogenic Pb and high $^{206}Pb/^{204}Pb$, low $^{87}Sr/^{86}Sr$ and $^{143}Nd/^{144}Nd$ and intermediate to low $^{176}Hf/^{177}Hf$ serves as an endmember for central Costa Rican lavas. The subducting Cocos and Coiba ridges, having radiogenic Pb, but intermediate $^{208}Pb/^{204}Pb$, $^{143}Nd/^{144}Nd$ and $^{176}Hf/^{177}Hf$ could serve as endmember for southern Costa Rica and western Panama lavas. The Nicaraguan endmember with unradiogenic Pb and radiogenic Nd, Hf and Sr is dominated by fluid flux from the subducting plate (serpentinite and magmatic crust)

3.6 Conclusions:

The combined Sr, Nd, Hf and Pb isotope data from mafic volcanic front (VF), behind the volcanic front (BVF) and back-arc (BA) lava and tephra samples from NW Nicaragua, Costa Rica and Panama confirm the influence of distinct subduction components of the subducting Cocos plate on the source compositions for SW Central American Arc volcanism. We distinguished three geochemically distinct endmember components for the prevalent volcanism in SW Central America:

(1) The NW Nicaragua VF endmember which is characterized by radiogenic Sr and Hf but unradiogenic Pb isotopic compositions, low ratios of La/Yb and Zr/Hf but high more to less fluid mobile element ratios (e.g. Ba/La, Ba/Th, U/Th), most likely is represented by a sediment component. An enriched mantle source addition to the lavas source would result in high La/Yb and Zr/Hf and low Ba/La und U/Th and could not be explained by our observed variations in the data. This coincides with the steepest subduction angle and the thinnest overlying crust along the whole Central American Volcanic Arc. The high fluid flux resulting from the dehydration of serpentinite in the subducting plate, causes melting in the depleted mantle wedge. Cocos Plate sediments seem to have minor influence on this endmember composition.

(2) The central Costa Rica VF endmember has unradiogenic Sr and Hf and radiogenic Pb isotopic compositions, intermediate to high ratios of La/Yb and Zr/Hf but low more to less fluid mobile element ratios (e.g. Ba/La, Ba/Th, U/Th). This clearly demonstrates the influence of the subducting Seamount province on the source component for SW CAVA lavas.

(3) Southern Costa Rica and western Panama adakites and alkali basalts with high ratios of Zr/Hf and La/Yb and radiogenic Pb but unradiogenic and (to a lesser degree) Hf isotopic compositions define another endmember. We suggest an enriched mantle component as represented by the subducting Cocos and Coiba ridges. Combined Sr vs Hf and Nd, and Nd vs. Hf data show positive correlation for SW VF CAVA, elevated Sr isotopic composition could result from seawater alteration. The subducting Cocos and

Coiba ridges have radiogenic Pb and unradiogenic Hf isotopic compositions and could serve as an endmember for our observed trends.

Acknowledgements

We thank S. Hauff, D. Garbe-Schönberg and D. Rau for analytical assistance and Paul van den Bogaard, Guillermo Alvarado, Holly Nichols and Britta Lissinna for assistance in collecting and preparing samples for analyses.

This publication is contribution no. XXX of the Sonderforschungsbereich 574 “Volatiles and Fluids in Subduction Zones” of Kiel University.

3.7 References:

Abers, G. A., K. M. Fischer, et al. (2007). "Imaging the arc source in Central America: The TUCAN broadband seismic experiment." Geopysical Research Abstracts **Vol. 9**(10763).

Abratis, M. and G. Worner (2001). "Ridge collision, slab window formation, and the flux of Pacific asthenosphere into the Caribbean realm." Geol. Soc. Am. **Vol.29**(No.2): 127-130.

Auger, L. S., G. Abers, et al. (2006). "Crustal Thickness Variations Beneath the Central American Arc." American Geophysical Union, Fall Meeting 2006, abstract(T23C-0517).

Barckhausen, U., C. R. Ranero, et al. (2001). "Revised tectonic boundaries in the Cocos Plate off Costa Rica: Implications for the segmentation of the convergent margin and for plate tectonic models." Journal Geophysical Research **Vol. 106**(No. B9): p. 19207-19220.

Blichert-Toft, J. and F. Albarède (1997). "The Lu-Hf isotope geochemistry of chondrites and the evolution of the mantle-crust system." Earth and Planetary Science Letters **Vol. 148**: p. 243-258.

Blichert-Toft, J. and W. M. White (2001). "Hf isotope geochemistry of the Galápagos islands." Geochemistry Geophysics Geosystems **Vol. 2**(No. 9): doi:10.1029/2000GC000138.

Carr, M. J. (1984). "Symmetrical and segmented variation of physical and geochemical characteristics of the Central American volcanic front." J. Volcanol. Geotherm. Res. **Vol. 20**: p. 231-252.

Carr, M. J. and M. D. Feigenson (2003). "Volcanism and Geochemistry in Central America: Progress and Problems." Geophysical Monograph **Vol. 138**(Inside the subduction factory): p. 153-174.

Feigenson, M. D., M. J. Carr, et al. (2004). "Lead isotope composition of Central American volcanoes: Influence of the Galapagos plume." Geochemistry Geophysics Geosystems **5**(No.6): Q06001 DOI 10.1029/2003GC000621.

Garbe-Schoenberg, C.-D. (1993). "Simultaneous determination of thirty-seven trace elements in twenty-eight international rock standards by ICP-MS." Geostandards Newsletter **Vol. 17**(No. 1): p. 81-97.

Gazel, E., M. J. Carr, et al. (2009). "Galapagos-OIB signature in southern Central America: Mantle refertilization by arc-hot spot interaction." Geochem. Geophys. Geosyst. **10**(2): 1-32.

Geist, D. J., W. M. White, et al. (1988). "Plume-asthenosphere mixing beneath the Galapagos archipelago." Nature **333**: 657-660.

Geldmacher, J., B. Hanan, et al. (2003). "Hafnium isotopic variations in volcanic rocks from the Caribbean Large Igneous Province and Galápagos hotspot tracks." Geochemistry Geophysics Geosystems **4**(7).

Geldmacher, J. r., K. Hoernle, et al. (2006). "Origin and geochemical evolution of the Madeira-Tore Rise (eastern North Atlantic)." J. Geophys. Res. **111**.

Govindaraju, K. (1994). "Compilation of working values and sample descriptions for 383 geostandards." Geostandard Newsletters **18**(Special Issue): 158 pp.

Harpp, K. S. and W. M. White (2001). "Tracing a mantle plume: Isotopic and trace element variations of Galápagos seamounts." Geochemistry Geophysics Geosystems **2**: 2000GC000137.

Herrstrom, E. A., M. K. Reagan, et al. (1995). "Variations in lava composition associated with flow of asthenosphere beneath southern Central America." Geology **27, no.7**: 617 - 620.

Hoernle, K., D. L. Abt, et al. (2008). "Arc-parallel flow in the mantle wedge beneath Costa Rica and Nicaragua." Nature **451**(7182): 1094-1097.

Hoernle, K. and G. Tilton (1991). "Sr-Nd-Pb isotope data for Fuerteventura (Canary Islands) basal complex and subaerial volcanics: applications to magma genesis and evolution." Schweizerische mineralogische und petrographische Mitteilungen **71**: 3 - 18.

Hoernle, K., R. Werner, et al. (2000). "Existence of complex spatial zonation in the Galapagos plume for at least 14 m.y." Geology **Vol. 28**(No. 5): p. 435-438.

Jochum, K. P. and G. Jenner (1994). "Trace element analysis of Geological Survey of Japan silicate reference materials: Comparison of SSMS with ICP-MS data an a critical discussion of compiled values." Fresenius Journal of Analytical Chemistry **350**: 310-318.

Le Maitre, R. W. (1989). A classification of igneous rocks and glossary of terms. Oxford, Blackwell Scientific Publications.

MacKenzie, L., G. A. Abers, et al. (2008). "Crustal structure along the southern Central American volcanic front." Geochem. Geophys. Geosyst. **9**(8): 1-19.

Patino, L. C., M. J. Carr, et al. (2000). "Local and regional variations in Central American arc lavas controlled by variations in subducted sediment input." Contrib. Mineral. Petrol. **138**: 265-283.

Reagan, M. K. and J. B. Gill (1989). "Coexisting Calcalkaline and High-Niobium Basalts from Turrialba Volcano, Costa Rica: Implications for Residual Titanates in Arc Magma Sources." Journal of Geophysical Research **Vol. 94**(No. B4): p. 4619-4633.

Rüpke, L. H., J. P. Morgan, et al. (2004). "Serpentine and the subduction zone water cycle." Earth and Planetary Science Letters **223**(1-2): 17-34.

Rusby, R. I. and R. C. Searle (1995). "A history of the Easter microplate, 5.25 Ma t present." Journal Geophysical Research **100**(B7): 12617-12640.

Russell, R. D. (1971). "The systematics of double spiking." Journal Geophysical Research **76**(20): 4949-4955.

Syracuse, E. M. and G. A. Abers (2006). "Global compilation of variations in slab depth beneath arc volcanoes and implications." Geochem. Geophys. Geosyst. **7**(5): 1-18.

Todt, W., R. A. Cliff, et al. (1996). Evaluation of a ^{202}Pb-^{205}Pb Double Spike for High-Precision Lead Isotope Analysis. Earth Processes: Reading the Isotopic Code. A. Basu and S. Hart. Washington, D.C., AGU Geophysical Monograph. **Vol. 95:** p. 429-437.

von Huene, R., C. R. Ranero, et al. (2000). "Quarternary convergent margin tectonics of Costa Rica, segmentation of the Cocos Plate, and Central American volcanism." Tectonics **Vol. 19**(No. 2): p. 314-334.

Walther, C. H. E., E. R. Flueh, et al. (2000). "Crustal structure across the Pacific margin of Nicaragua: evidence for ophiolithic basement and a shallow mantle sliver." Geophysical Journal International **141**: 759-777.

Werner, R., K. Hoernle, et al. (2003). "Geodynamic evolution of the Galapagos hot spot system (Central East Pacific) over the past 20 m.y.: Constraints from morphology, geochemistry, and magnetic anomalies." Geochemistry Geophysics Geosystems **Vol. 4**(No. 12): 1108, doi:10.1029/2003GC000576.

White, W. M. and A. W. Hofmann (1978). "Geochemistry of the Galápagos islands: Implications for mantle dynamics and evolution." Carnegie Institution Yearbook(77): 596-606.

White, W. M., A. R. McBirney, et al. (1993). "Petrology and geochemistry of the Galápagos Islands: Portrait of a pathological mantle plume." Journal of Geophysical Research **98, No B11**: 19.533 - 19.563.

Table 3.1. Major (wt%) and trace elements (ppm) and selected trace element ratios data of southwestern Central American Arc volcanics extending from southwestern Nicaragua to central Costa Rica for Volcanic Front (VF) and Behind the Volcanic Front (BVF) samples. Also shown are southern Costa Rica and western Panama Pliocene to quaternary alkali basalt and adakite samples.

Table 3.1. Major (wt%) and trace elements (ppm) and selected trace element ratios data of southwestern Central American Arc volcanics extending from southwestern Nicaragua to central Costa Rica for Volcanic Front (VF) and Behind the Volcanic Front (BVF) samples. Also shown are southern Costa Rica and western Panama Pliocene to quaternary alkali basalt and adakite samples.

sample #	Sample Location	Lat (N)	Long (W)	DAA	SiO2 wt%	TiO2 wt%	AL2O3 wt%	Fe2O3 wt%	MnO wt%	MgO wt%	CaO wt%	Na2O wt%	K2O wt%	P2O5 wt%	H2O wt%	CO2 wt%	SUM wt%
NW Nicaragua VF																	
P-58A	Cosigüina	13.03	-87.59	551.80	59.20	0.79	17.27	8.27	0.18	2.20	6.70	4.06	1.41	0.22	0.41	0.02	100.73
P-60	Cosigüina	12.87	-87.56	564.40	56.63	0.68	19.43	7.42	0.12	1.82	8.05	3.26	1.39	0.17	1.11	0.05	100.13
P-27A	San Cristobal	12.68	-87.03	623.10	49.82	0.97	18.20	12.10	0.21	4.55	10.45	2.83	0.71	0.20	0.32	0.02	100.38
P-13	Casitas	12.69	-86.96	629.60	50.36	0.86	18.41	11.56	0.19	4.22	9.15	2.78	1.02	0.23	1.38	0.04	100.20
P2-16	Telica	12.60	-86.93	636.60	48.57	0.72	18.21	10.27	0.17	5.71	12.21	1.83	0.73	0.13	0.57	0.09	99.21
P-7A	Telica	12.61	-86.83	645.10	51.52	0.84	17.93	10.90	0.18	4.48	10.04	2.67	1.20	0.16	0.31	0.02	100.25
P-9	Telica	12.61	-86.84	645.00	49.78	1.01	18.09	11.23	0.17	5.51	11.03	2.44	0.93	0.17	0.29	0.01	100.66
P-43	Cone3	12.53	-86.68	663.50	53.07	1.34	15.96	12.45	0.20	4.11	8.45	3.15	1.16	0.23	0.31	0.03	100.46
P-51	Cone2	12.47	-86.72	662.90	49.98	0.72	17.18	10.60	0.18	6.53	12.71	1.92	0.59	0.16	0.34	0.02	100.93
P-56G	C. Las Palmitas	12.61	-86.73	654.40	52.57	1.07	16.48	12.48	0.24	3.94	7.73	3.07	0.80	0.20	1.75	0.08	100.41
P-4	C. Negro	12.51	-86.70	662.80	49.69	0.76	18.66	11.26	0.19	5.68	11.72	2.04	0.45	0.11	0.17	0.00	100.73
P-6	C. Negro	12.50	-86.70	663.10	49.91	0.79	19.59	10.93	0.18	4.58	11.37	2.26	0.50	0.12	0.22	0.01	100.46
P2-3a	C. Negro	12.50	-86.70	663.10	47.50	0.61	15.74	11.45	0.19	10.03	12.44	1.50	0.27	0.10	0.16	0.04	100.03
P2-3b	C. Negro	12.50	-86.70	663.10	48.86	0.68	21.26	9.84	0.16	4.10	12.45	2.12	0.40	0.13	0.19	0.03	100.22
P2-3d	C. Negro	12.50	-86.70	663.10	49.19	0.75	18.41	11.25	0.19	5.98	12.05	2.10	0.42	0.12	0.16	0.02	100.64
P2-11	C. Negro	12.50	-86.71	662.90	48.44	0.78	19.32	11.00	0.18	4.64	11.59	2.23	0.46	0.13	0.22	0.02	99.01
P2-13	C. Negro	12.51	-86.71	662.10	48.46	0.72	16.32	11.50	0.20	7.43	11.29	2.12	0.46	0.12	0.19	0.03	98.84
P-50	C. Diablo	12.47	-86.72	662.70	49.90	0.71	17.33	10.62	0.18	6.41	12.64	1.93	0.60	0.16	0.30	0.02	100.80
P-19	Las Pilas	12.49	-86.69	665.00	51.28	0.84	16.05	10.54	0.18	6.06	10.86	2.38	0.81	0.18	0.24	0.00	99.42
P-40A	Cabeza de Vaca	12.52	-86.68	663.90	47.39	0.71	17.55	12.39	0.19	7.81	12.25	1.63	0.36	0.09	0.26	0.04	100.67
P-42	Cabeza de Vaca	12.52	-86.68	664.00	48.22	0.74	16.31	12.60	0.20	8.46	10.90	1.77	0.49	0.10	0.32	0.04	100.15
P-23	Ojo de Agua	12.51	-86.68	664.30	54.95	0.94	16.54	10.26	0.20	3.78	8.06	3.20	1.32	0.25	0.27	0.00	99.77
P-46A	Laguna Asos	12.44	-86.67	669.20	56.93	1.05	15.82	10.60	0.20	2.99	6.70	3.35	1.64	0.25	0.71	0.02	100.26
P-47A	C. Buena vista	12.40	-86.66	672.10	57.82	0.98	15.71	9.98	0.19	2.67	6.21	3.33	1.80	0.24	0.90	0.03	99.86
P-48B	Cone4	12.37	-86.65	675.00	54.38	1.00	16.20	11.49	0.20	3.86	8.07	2.90	1.31	0.20	0.69	0.02	100.32
P-32	Momotombo	12.43	-86.58	678.30	52.57	0.76	17.69	10.64	0.18	5.04	9.85	2.52	0.79	0.15	0.21	0.02	100.42
P-34	Momotombo	12.46	-86.56	679.00	54.78	0.78	17.21	10.08	0.18	4.19	8.61	2.86	1.00	0.16	0.21	0.01	100.07
SW Nicaragua VF																	
P2-32d	Nejapa crater	12.23	-86.32	713.50	47.75	1.14	16.04	12.77	0.19	9.19	10.78	2.17	0.23	0.12	0.33	0.02	100.73
P2-53	Nejapa	12.08	-86.32	721.00	52.32	2.01	14.79	11.68	0.15	6.60	8.50	2.82	0.32	0.21	0.47	0.01	99.88
P-68B	Masaya	12.01	-86.14	741.50	50.67	1.12	15.08	13.24	0.22	5.42	10.03	2.73	1.17	0.27	0.34	0.02	100.31
P-71A	Masaya	12.00	-86.17	739.70	50.52	1.08	15.70	13.02	0.21	5.12	10.27	2.69	1.13	0.26	0.38	0.03	100.41
P2-47	Masaya	12.09	-86.26	726.60	51.69	1.22	15.17	13.05	0.22	3.86	8.30	3.01	1.49	0.33	0.38	0.09	98.81
P-63	Cone near Mombacho	11.84	-86.00	764.90	51.47	1.14	17.73	10.83	0.18	3.96	9.89	3.03	0.85	0.21	0.64	0.01	99.94
P2-58	Cone near Mombacho	11.89	-85.99	762.20	47.90	1.05	16.49	11.34	0.18	7.20	12.04	2.14	0.33	0.14	0.44	0.01	99.26
P-86A	Concepcion	11.56	-85.67	810.40	53.04	1.07	17.94	9.56	0.18	3.81	8.33	3.42	1.40	0.45	0.61	0.00	99.81
P-80A	Maderas	11.50	-85.62	818.20	47.78	0.89	19.82	10.09	0.17	5.13	12.06	2.54	0.64	0.25	0.32	0.01	99.70
NW Costa Rica VF																	
CR-44	Orosi	11.06	-85.43	860.80	50.83	0.90	16.86	12.26	0.21	5.02	9.51	2.54	0.73	0.23	0.82	0.08	99.99
CR-35	Rincon	10.75	-85.37	882.90	58.74	0.66	15.96	7.86	0.15	3.87	7.13	2.88	1.97	0.18	1.11	0.05	100.56
CR-56	Rincon	10.90	-85.35	876.70	55.78	0.68	17.10	8.53	0.15	4.01	7.75	2.97	1.63	0.21	0.69	0.00	99.50
P2-118	Miravalles	10.71	-85.17	904.50	57.42	0.71	16.81	8.22	0.16	3.74	7.14	3.12	1.64	0.23	0.66	0.01	99.86
CR-30	Canas	10.47	-85.07	927.30	54.53	0.97	17.53	8.93	0.12	3.68	8.01	3.23	1.72	0.33	1.15	0.15	100.35
CR-51B	Monteverde	10.38	-84.90	947.30	55.05	0.78	17.23	9.06	0.15	4.14	8.33	3.20	1.52	0.25	0.78	0.03	100.52
CR-55	Monteverde	10.30	-84.83	958.50	59.18	0.61	16.43	6.45	0.12	3.20	6.28	3.29	2.59	0.22	0.88	0.00	99.25
CR-58	Arenal	10.48	-84.85	946.40	52.85	0.62	19.50	8.74	0.16	4.49	9.35	2.91	0.45	0.21	0.29	0.00	99.57
CR-61B	Arenal	10.48	-84.69	961.50	51.74	0.65	19.71	9.46	0.16	5.49	10.12	2.53	0.40	0.17	0.39	0.00	100.82
CR-61C	Arenal	10.48	-84.69	961.50	51.10	0.65	19.69	9.10	0.16	5.20	10.01	2.32	0.40	0.16	0.55	0.02	99.36
CR-64	Arenal	10.46	-84.72	959.90	55.82	0.54	20.19	5.94	0.14	2.64	9.22	3.30	0.67	0.18	0.25	0.02	98.90
CR-71	Chato	10.46	-84.64	967.30	49.91	0.71	20.41	9.64	0.16	4.64	9.94	2.81	1.08	0.29	0.48	0.00	100.07
CR-84	Perdidos	10.43	-84.68	965.50	54.43	0.52	20.14	7.86	0.17	3.19	9.17	3.05	0.55	0.19	0.29	0.01	99.57
Central Costa Rica VF																	
P-118	Laguna Rio Cuarto	10.35	-84.22	1012.10	53.49	1.05	16.42	10.68	0.18	4.23	8.29	2.93	1.72	0.25	0.64	0.02	99.90
P-122	Maar Rio Cuarto	10.36	-84.24	1010.10	53.34	1.04	16.35	10.68	0.18	4.25	8.28	2.91	1.73	0.25	0.87	0.02	99.90
P-123A	Congo	10.27	-84.25	1014.00	50.92	0.86	19.66	9.58	0.16	4.77	9.78	2.90	1.14	0.30	0.27	0.01	100.35
P-124	Bosque Alegre	10.30	-84.21	1016.20	50.45	0.76	18.85	10.13	0.17	5.43	9.45	2.81	0.71	0.16	0.53	0.01	99.46
P-151D	Platanar	10.30	-84.39	999.40	50.44	0.85	18.75	10.22	0.16	5.24	9.47	2.90	0.86	0.23	0.53	0.01	99.66

Table 3.1. Major (wt%) and trace elements (ppm) and selected trace element ratios data of southwestern Central American Arc volcanics extending from southwestern Nicaragua to central Costa Rica for Volcanic Front (VF) and Behind the Volcanic Front (BVF) samples. Also shown are southern Costa Rica and western Panama Pliocene to quaternary alkali basalt and adakite samples.

sample #	Sample Location	Lat (N)	Long (W)	DAA	SiO2	TiO2	AL2O3	Fe2O3	MnO	MgO	CaO	Na2O	K2O	P2O5	H2O	CO2	SUM
					wt%	wt%	wt%	wt%	wt%	wt%	wt%	wt%	wt%	wt%	wt%	wt%	wt%
P-119A	Chocosuela	10.28	-84.26	1012.30	52.59	0.83	18.60	9.39	0.15	3.57	8.74	3.02	1.33	0.23	0.99	0.15	99.59
P-169	Porvenir	10.29	-84.42	996.80	56.20	0.75	17.29	8.19	0.14	3.95	7.45	2.96	1.74	0.20	0.85	0.00	99.72
P-109	Poás	10.20	-84.23	1020.10	53.75	0.78	18.32	9.41	0.15	4.64	8.87	3.00	1.04	0.15	0.26	0.03	100.40
P-112	Redonda cone 2	10.12	-84.21	1026.00	57.77	0.97	16.22	8.96	0.16	3.17	6.53	3.31	2.33	0.25	0.33	0.03	100.03
P-113	Redonda cone 3	10.11	-84.21	1026.10	54.77	1.07	16.33	10.53	0.17	3.74	7.70	3.14	1.79	0.26	0.64	0.04	100.18
P-171	Barva	10.03	-84.09	1042.10	52.11	1.56	16.00	9.47	0.14	5.96	8.84	3.05	1.80	0.47	0.26	0.01	99.67
P-102C	Zurque	10.07	-84.01	1048.10	48.92	1.01	19.50	10.60	0.16	5.46	10.87	2.67	0.79	0.26	0.32	0.01	100.57
P-139	Cone Oratorio	9.90	-83.84	1073.40	52.24	1.01	15.80	8.52	0.14	6.90	8.69	3.23	2.00	0.59	0.53	0.01	99.66
P-140	Cone Boqueron	9.89	-83.85	1072.20	51.97	1.03	15.89	8.56	0.14	6.91	8.67	3.23	1.93	0.55	0.58	0.01	99.47
P-143	Cerro Pasquí	9.93	-83.84	1071.10	55.39	0.94	17.16	7.53	0.12	4.95	7.64	3.48	2.14	0.37	0.54	0.02	100.28
P-160A	Irazú	9.98	-83.85	1067.30	53.79	1.16	16.49	8.17	0.13	5.16	8.32	3.32	2.20	0.45	0.17	0.01	99.37
P-162	Irazú	9.98	-83.85	1067.30	54.71	0.95	16.36	7.84	0.12	5.91	7.79	3.28	2.03	0.34	0.22	0.01	99.56
P2-72	Irazú	9.98	-83.85	1067.00	54.14	0.94	16.06	7.84	0.13	6.29	7.77	3.13	1.98	0.34	0.36	0.03	99.01
P-96	forearc flow	9.98	-84.20	1035.30	53.05	0.95	17.87	9.44	0.15	4.56	8.03	3.13	1.95	0.36	0.55	0.01	100.05
P-97A	Turrialba	10.02	-83.76	1073.40	52.61	1.04	17.09	8.59	0.14	6.16	9.39	3.26	1.45	0.39	0.24	0.02	100.38
P-149A	Turrialba	10.09	-83.54	1089.90	54.13	1.11	17.16	8.24	0.14	4.23	7.09	3.42	3.13	0.53	0.33	0.01	99.52
Central Costa Rica BVF - Alkaline (≤2 My)																	
P-152	Aquas Zarcas Buenos Aires	10.38	-84.30	1002.80	44.89	0.80	13.33	9.90	0.17	13.39	12.57	1.31	0.77	0.35	1.58	0.02	99.08
P-153	AZ Juan Murillo	10.39	-84.32	1000.40	46.67	1.53	14.47	10.86	0.17	10.27	11.30	2.23	1.26	0.53	0.44	0.02	99.75
P-154B	AZ Pital	10.45	-84.28	1001.80	50.17	1.43	15.69	9.40	0.14	8.47	9.07	2.93	1.26	0.44	0.60	0.01	99.61
P-155A	AZ C. Chiles	10.46	-84.34	994.80	49.23	1.27	16.64	9.90	0.14	6.81	10.07	2.99	1.02	0.43	0.61	0.03	99.14
P-130A	Rio Colorado	10.70	-83.65	1045.10	42.33	2.33	12.41	11.06	0.16	10.89	12.75	2.63	1.15	1.30	2.32	0.18	99.51
P-128	Rio San Juan	10.77	-83.80	1027.50	46.07	3.00	14.36	12.23	0.17	8.07	9.30	2.79	1.47	1.00	1.47	0.04	99.97
P-129	Rio San Juan	10.78	-83.78	1028.90	47.07	2.07	15.28	12.49	0.18	7.43	9.29	2.74	0.83	0.42	2.65	0.04	100.49
P-138	Puerto Lindo	10.59	-83.70	1046.20	41.87	2.04	11.90	10.63	0.16	13.02	13.94	2.18	0.84	1.00	1.98	0.03	99.59
P-132B	Tortugero	10.58	-83.53	1062.80	45.84	1.59	13.68	10.32	0.15	11.27	10.67	2.12	1.02	0.53	1.78	0.25	99.22
P-133	Tortugero	10.58	-83.53	1062.80	46.51	1.60	14.04	10.76	0.15	11.65	10.89	2.56	0.73	0.58	0.36	0.00	99.83
Southern Costa Rica Pliocene-Quaternary Adakite (<5 My)																	
TC-3		9.09	-83.27	1171.60	49.73	0.90	17.84	9.96	0.19	4.52	9.55	2.83	1.80	0.40	1.17	0.08	98.97
TC-5A		8.85	-82.95	1215.60	56.66	0.73	15.87	7.23	0.10	4.62	7.21	3.24	2.39	0.26	0.69	0.06	99.06
TC-6A		8.91	-82.79	1226.50	54.64	0.98	16.15	7.69	0.11	5.47	7.84	3.18	1.72	0.28	0.63	0.03	98.72
TC-7		8.90	-82.79	1227.10	55.44	0.77	16.09	7.10	0.11	5.79	7.78	3.36	1.96	0.23	0.28	0.02	98.93
TC-8		8.62	-82.92	1231.00	55.69	1.15	14.24	6.62	0.08	4.91	8.17	2.96	3.65	0.56	0.58	0.04	98.65
Southern Costa Rica Pliocene-Quaternary BVF Alkaline (<5 My)																	
P-145	Siquirres AB	10.07	-83.58	1087.30	44.16	1.30	13.31	11.10	0.19	14.02	11.14	1.26	0.59	0.41	2.33	0.03	99.84
P-163B	Lomas Azules	10.36	-83.59	1070.50	46.58	2.06	14.56	11.06	0.16	8.94	10.54	2.79	1.26	0.59	1.11	0.02	99.67
P-164	Lomas Azules	10.38	-83.57	1070.70	46.49	2.30	16.96	11.53	0.17	6.19	8.54	3.02	1.72	0.81	2.03	0.12	99.88
Panama Adakites (≤ 1 My)																	
M44KH	Barva	9.67	-82.62	1198.60	54.91	0.73	15.77	7.35	0.11	7.04	8.20	3.19	1.61	0.29	0.23	0.03	99.46
M53KH	Barva	8.79	-82.59	1252.10	59.83	0.68	16.43	6.19	0.10	3.61	6.65	2.97	3.01	0.25	0.14	0.00	99.86
M55KH	Barva	8.80	-82.47	1262.30	55.91	0.76	16.44	7.28	0.12	5.11	8.10	3.29	1.92	0.29	0.34	0.01	99.57
M57aKH	Tizingal Volcanic Complex	8.80	-82.47	1262.30	52.40	0.86	15.62	8.18	0.13	8.41	8.98	2.95	1.15	0.28	0.44	0.00	99.40
M64c KH	Burica	8.18	-82.88	1260.10	58.18	0.73	17.38	6.68	0.10	3.87	7.20	2.85	2.56	0.21	0.23	0.01	100.00
M65a KH	Chiriquí	8.47	-82.71	1259.20	55.96	0.94	15.86	6.99	0.10	5.36	7.66	2.93	2.81	0.47	0.41	0.03	99.52
M99a KH		8.34	-81.83	1348.60	53.67	1.16	14.99	6.88	0.12	6.06	8.84	4.12	1.47	0.81	1.20	0.04	99.36
Panama Pliocene-Quaternary Alkaline (<5 My)																	
3-12-4-03	island west of Sona	7.47	-82.24	1360.60	45.11	1.38	12.92	10.70	0.17	11.66	11.87	2.70	0.95	1.01	0.39	0.01	98.87
CP97-1	Chiriquí	8.22	-81.59	1377.80	44.20	1.51	13.41	11.51	0.17	11.54	11.86	2.47	0.99	0.84	1.07	0.02	99.59
SO96-1	Sona	8.07	-81.73	1372.70	47.74	1.54	14.62	10.54	0.15	9.62	10.09	3.15	1.16	0.64	0.51	0.05	99.81
M36KH	west of Sona	8.27	-82.04	1332.70	47.13	2.77	13.03	10.82	0.15	9.57	10.35	3.10	1.02	0.83	1.18	0.02	99.97
M37KH	west of Sona	8.27	-82.04	1332.70	45.83	2.31	12.91	10.76	0.16	10.99	11.25	2.97	1.21	0.96	0.54	0.05	99.94
M105 KH	Sona	8.24	-81.79	1357.50	47.67	1.43	14.26	9.24	0.15	10.07	10.91	3.12	1.40	0.86	0.59	0.11	99.81
M 118aKH	Sona	8.13	-81.45	1395.80	47.49	1.84	13.94	10.17	0.16	9.86	9.68	3.33	1.80	0.73	0.57	0.09	99.66
M121aKH	Sona	8.19	-81.49	1388.60	44.35	2.06	12.88	10.46	0.16	10.34	12.32	3.08	1.49	1.16	0.65	0.08	99.03

Table 3.1 continued

sample #	Li	Sc	V	Cr	Co	Ni	Cu	Zn	Ga	Rb	Sr	Y	Zr	Nb	Mo	Sn	Cs	Ba	La	Ce	Pr	Nd	Sm	Eu	Gd	Tb
	ppm	ppm	ppm	ppm	ppm	ppm	ppm	ppm	ppm	ppm	ppm	ppm	ppm	ppm	ppm	ppm	ppm	ppm	ppm	ppm	ppm	ppm	ppm	ppm	ppm	ppm
NW Nicaragua VF																										
P-58A	14.12	23.57	139.74	1.22	15.92	2.06	86.62	89.79	19.21	29.64	406.29	31.89	104.59	1.68	1.11	1.00	1.48	897.26	9.34	21.80	3.52	17.04	4.65	1.33	5.17	0.86
P-60	7.54	18.50	164.79	1.32	15.04	3.06	144.38	67.30	18.95	30.46	422.43	32.31	92.05	1.16	1.01	0.65	1.10	984.42	11.05	19.07	3.54	16.72	4.25	1.24	4.89	0.78
P-27A	6.04	n.d.	n.d.	n.d.	n.d.	n.d.	214.20			12.77	531.27	21.50	52.10	0.99	0.50	0.69	0.45	536.21	6.17	14.44	2.40	12.06	3.46	1.21	3.96	0.66
P-13	4.85	22.97	271.18	4.28	27.64	6.93	117.05	91.12	18.74	19.61	499.10	24.86	66.37	1.41	0.59	0.68	0.21	703.97	7.86	18.37	2.97	14.25	3.87	1.17	4.09	0.68
P2-16	5.99	40.77	309.95	24.02	34.83	22.60	133.99	67.85	16.19	15.37	494.70	16.72	48.30	1.58	0.56	0.52	0.66	461.94	4.37	11.00	1.81	8.68	2.50	0.82	2.93	0.48
P-7A	8.24	n.d.	n.d.	n.d.	n.d.	n.d.	183.37			25.76	489.43	20.38	77.01	1.86	0.92	0.77	1.12	742.98	6.45	14.82	2.38	11.51	3.27	1.09	3.74	0.62
P-9	6.41	29.52	317.62	31.39	34.46	25.59	151.11	78.18	18.24	19.48	490.45	20.47	78.46	5.01	0.84	0.79	0.78	555.04	6.34	14.56	2.32	11.27	3.23	1.06	3.48	0.58
P-43	8.64	n.d.	n.d.	n.d.	n.d.	n.d.	185.27			22.08	409.60	26.42	107.86	6.45	1.19	1.07	0.99	680.42	8.30	19.39	2.97	14.50	4.15	1.42	4.85	0.82
P-51	4.87	n.d.	n.d.	n.d.	n.d.	n.d.	122.48			11.98	490.45	16.35	51.41	1.49	0.53	0.60	0.42	361.72	5.55	12.83	2.05	9.95	2.75	0.95	3.15	0.51
P-56G	7.13	n.d.	n.d.	n.d.	n.d.	n.d.	167.93			12.02	594.99	22.63	49.91	0.86	0.54	0.70	0.48	764.09	6.93	15.73	2.59	12.92	3.70	1.48	4.23	0.70
P-4	4.87	n.d.	n.d.	n.d.	n.d.	n.d.	140.75			7.19	428.88	14.22	32.80	0.98	0.45	0.41	0.37	364.85	3.23	7.43	1.22	6.28	1.96	0.81	2.43	0.42
P-6	5.31	27.61	334.47	18.71	31.09	15.33	173.54	80.99	19.46	7.37	477.51	16.57	39.78	1.30	0.54	0.50	0.35	435.53	3.61	8.60	1.40	7.12	2.17	0.83	2.52	0.44
P2-3a	3.06	42.33	286.74	142.31	49.72	64.98	111.57	67.37	14.10	4.31	374.78	11.18	20.50	0.69	0.27	0.28	0.23	246.78	1.93	4.90	0.86	4.38	1.40	0.46	1.74	0.31
P2-3b	4.00	26.49	278.73	10.97	26.11	11.51	126.11	67.08	17.80	6.35	504.84	13.18	28.17	0.93	0.37	0.40	0.32	344.09	2.67	6.52	1.13	5.61	1.70	0.52	2.06	0.35
P2-3d	4.11	35.09	323.01	49.64	34.63	24.50	152.67	74.68	16.91	7.08	438.83	14.64	30.99	0.95	0.41	0.37	0.36	362.30	2.79	6.85	1.18	5.96	1.84	0.55	2.26	0.39
P2-11	5.15	32.08	350.28	11.29	31.89	12.98	162.94	85.70	18.15	7.28	480.68	15.08	32.47	1.15	0.46	0.45	0.37	394.64	3.35	7.77	1.28	6.50	1.98	0.78	2.37	0.41
P2-13	5.33	40.95	325.63	75.29	44.34	40.39	145.59	85.34	16.03	7.31	401.93	14.58	32.09	1.10	0.48	0.43	0.37	376.06	3.20	7.45	1.24	6.22	1.92	0.75	2.30	0.40
P-50	4.97	33.66	276.77	101.86	35.06	30.80	142.49	69.37	15.82	11.69	476.93	17.57	53.28	1.57	0.53	0.58	0.41	369.09	5.42	12.61	2.03	9.69	2.63	0.87	2.86	0.48
P-19	6.79	n.d.	n.d.	n.d.	n.d.	n.d.	113.49			16.33	442.07	20.39	73.90	2.52	0.66	0.75	0.68	493.24	6.67	15.46	2.44	11.75	3.26	1.10	3.80	0.64
P-40A	3.80	n.d.	n.d.	n.d.	n.d.	n.d.	165.41			5.70	437.29	12.35	26.98	0.72	0.24	0.43	0.25	310.92	3.05	6.80	1.13	5.79	1.78	0.72	2.17	0.38
P-42	3.79	34.71	317.07	63.14	47.85	38.39	129.57	78.63	15.98	6.96	380.22	15.11	35.40	1.10	0.42	0.45	0.33	391.21	3.20	7.46	1.25	6.28	1.91	0.71	2.24	0.39
P-23	8.57						90.29			23.68	399.17	25.61	105.00	4.46	1.15	0.98	1.05	777.89	9.19	20.93	3.27	15.36	4.18	1.33	4.74	0.78
P-46A	10.55						60.74			33.59	406.40	29.23	127.03	4.99	1.53	1.17	1.63	1005.05	9.83	22.48	3.47	16.36	4.60	1.47	5.28	0.88
P-47A	11.48						52.77			36.42	399.77	30.01	132.71	4.78	1.64	1.14	1.76	1085.39	10.20	23.28	3.58	16.98	4.71	1.49	5.37	0.89
P-48B	8.55						173.09			26.26	412.58	24.47	98.28	3.56	1.30	0.93	1.29	830.03	7.91	17.97	2.80	13.39	3.80	1.25	4.38	0.74
P-32	6.75						135.54			13.64	464.09	17.59	52.57	1.34	0.67	0.56	0.62	598.73	5.57	12.45	2.00	9.70	2.79	1.01	3.21	0.53
P-34	8.69	26.03	259.05	10.44	26.33	8.70	153.46	76.15	17.36	17.88	463.58	22.83	71.64	1.76	0.84	0.65	0.83	780.53	6.70	15.17	2.41	11.50	3.24	1.01	3.52	0.60
SW Nicaragua VF																										
P2-32d	4.42	31.20	267.54	326.45	49.25	137.02	137.53	88.66	16.23	4.21	305.72	19.56	51.58	2.82	0.32	0.73	0.10	133.09	3.21	8.74	1.56	8.11	2.58	0.97	3.19	0.55
P2-53	4.25	21.93	200.06	398.21	37.70	144.93	138.45	106.87	17.79	6.27	322.45	22.57	120.74	7.57	0.47	1.24	0.18	215.90	4.22	13.02	2.57	14.13	4.51	1.56	4.86	0.77
P-68B	10.20	33.21	387.21	35.99	34.12	19.78	249.53	101.57	17.79	22.28	392.90	25.31	92.62	2.49	1.08	0.87	0.88	843.37	10.07	21.81	3.38	15.78	4.13	1.26	4.22	0.70
P-71A	9.64	32.75	390.76	47.76	34.14	21.79	238.73	101.99	18.64	21.80	427.34	25.30	92.15	2.45	1.07	0.89	0.85	845.10	10.10	21.97	3.41	15.83	4.14	1.28	4.25	0.70
P2-47	14.66	30.96	395.46	11.02	32.22	14.75	346.41	118.90	18.48	29.64	413.84	28.15	108.21	3.45	1.46	1.09	1.17	1073.31	11.91	27.62	4.19	18.80	4.75	1.37	5.03	0.79
P-63	7.74	30.29	315.15	6.49	30.27	12.97	129.02	95.96	18.97	17.07	406.07	23.87	100.29	6.40	1.41	0.88	0.49	539.12	9.57	21.05	3.14	14.62	3.88	1.26	4.25	0.69
P2-58	4.02	34.13	264.77	138.68	39.32	67.19	129.26	79.28	16.62	7.09	390.18	19.99	60.18	4.14	0.42	0.69	0.20	206.61	5.18	12.67	2.08	9.88	2.78	0.94	3.30	0.56
P-86A	6.61	24.35	216.97	11.49	22.62	7.96	62.68	84.81	19.12	31.06	562.79	29.44	145.19	12.55	1.19	1.16	0.67	889.52	23.38	48.98	6.93	28.59	6.23	1.37	6.09	0.92
P-80A	4.30	25.56	265.95	26.26	31.03	18.50	120.36	69.40	17.89	12.08	616.74	17.47	63.79	5.36	0.49	0.84	0.27	510.59	11.53	24.34	3.52	15.22	3.50	0.96	3.54	0.54
NW Costa Rica VF																										
CR-44	7.98	35.96	334.88	14.46	37.06	10.61	138.36	89.44	16.77	12.36	444.33	25.49	85.95	2.49	1.03	0.69	0.12	407.28	10.06	22.03	3.23	14.84	3.94	1.15	4.31	0.70
CR-35	9.19	22.21	187.32	34.59	20.55	11.27	104.84	67.78	15.91	44.19	458.62	24.06	138.41	4.98	1.96	0.84	1.15	908.37	18.82	38.74	5.33	21.56	4.69	0.63	4.57	0.69
CR-56	12.11	24.41	235.48	10.74	23.96	14.80	126.83	72.86	16.73	37.68	513.43	21.24	117.01	4.05	1.73	0.77	1.02	853.51	17.64	35.57	4.77	19.67	4.38	1.17	4.24	0.64
P2-118	10.18	22.31	202.27	6.72	20.34	8.40	53.58	72.50	17.09	37.87	577.46	25.19	119.83	4.92	1.61	0.81	1.11	950.77	19.23	39.41	5.59	23.09	5.10	0.80	4.85	0.74
CR-30	7.02	22.54	236.30	25.27	23.79	26.41	86.04	80.52	17.87	38.92	850.36	27.50	124.35	5.70	1.40	0.76	0.48	970.29	27.20	48.64	6.39	26.35	5.50	1.67	5.47	0.77
CR-51B	8.95	24.62	247.10	19.53	29.93	22.70	106.50	80.05	17.23	33.26	777.35	35.07	108.04	5.74	1.33	0.67	0.45	877.19	25.99	44.18	6.14	25.16	5.18	1.55	5.44	0.80
CR-55	13.91	17.73	167.68	13.24	17.18	14.23	72.14	67.08	16.78	73.04	687.80	21.59	164.38	11.51	3.48	0.81	1.41	1186.82	38.97	73.08	8.18	30.26	5.46	1.36	4.83	0.68
CR-58	5.97	21.54	215.16	41.50	24.87	26.57	68.84	77.63	18.16	6.49	720.92	15.27	41.50	2.36	0.69	0.37	0.07	421.02	9.68	20.06	2.79	12.19	2.84	1.02	2.91	0.45
CR-61B	4.93	23.68	227.12	53.72	28.10	34.12	96.38	72.48	17.82	7.07	717.57	13.61	36.36	2.27	0.60	0.33	0.18	443.04	9.12	18.62	2.62	11.02	2.57	0.70	2.59	0.41
CR-61C	6.33	25.40	243.45	40.16	28.98	34.51	94.91	74.79	17.83	7.04	711.91	13.32	36.16	2.39	0.74	0.37	0.18	404.40	9.45	19.01	2.56	11.09	2.54	0.92	2.58	0.40
CR-64	9.45	16.25	156.23	6.50	16.88	7.60	78.73	77.69	18.67	13.17	684.51	16.71	54.11	3.62	1.27	0.44	0.32	597.92	12.71	25.74	3.41	14.53	3.25	1.10	3.23	0.50
CR-71	7.11	22.86	295.02	11.00	28.19	17.82	121.54	79.02	19.17	20.07	1079.27	18.14	72.76	4.28	1.01	0.49	0.30	964.03	36.54	73.20	8.64	34.89	6.45	1.85	5.27	0.68
CR-84	8.14	15.49	139.45	2.64	16.93	4.49	46.03	73.75	17.73	11.24	662.14	16.19	41.26	3.41	1.04	0.40	0.26	421.79	9.28	20.00	2.85	12.71	2.99	1.05	2.98	0.47
Central Costa Rica VF																										
P-118	6.68	n.d.	n.d.	n.d.	n.d.	n.d.	172.79			49.09	534.91	24.80	129.14	10.26	2.63	1.02	1.04	655.84	28.44	53.82	6.87	27.31	5.69	1.50	5.78	0.83
P-122	6.83	n.d.	n.d.	n.d.	n.d.	n.d.	161.13			48.77	531.57	23.93	127.70	10.13	2.64	0.99	1.04	649.84	26.65	52.48	6.63	26.57	5.53	1.47	5.57	0.80
P-123A	4.32	n.d.	n.d.	n.d.	n.d.	n.d.	113.12			23.20	738.44	16.86	79.02	5.94	1.06	0.64	0.29	567.67	22.23	45.51	5.79	23.97	4.90	1.57	4.71	0.64
P-124	4.11	n.d.	n.d.	n.d.	n.d.	n.d.	85.04			13.41	607.53	15.33	57.55	4.27	1.03	0.57	0.28	377.06	10.91	23.05	3.05	13.21	3.11	1.09	3.27	0.50
P-151D	4.70	n.d.	n.d.	n.d.	n.d.	n.d.	94.95			14.97	795.43	17.45	72.47	6.10	1.27	0.65	0.32	503.52	17.74	36.77	4.84	20.35	4.40	1.36	4.31	0.61

Table 3.1 continued

sample #	Li	Sc	V	Cr	Co	Ni	Cu	Zn	Ga	Rb	Sr	Y	Zr	Nb	Mo	Sn	Cs	Ba	La	Ce	Pr	Nd	Sm	Eu	Gd	Tb
	ppm	ppm	ppm	ppm	ppm	ppm	ppm	ppm	ppm	ppm	ppm	ppm	ppm	ppm	ppm	ppm	ppm	ppm	ppm	ppm	ppm	ppm	ppm	ppm	ppm	ppm
P-119A	5.12	n.d.	n.d.	n.d.	n.d.	n.d.	31.92			33.20	758.30	15.53	105.02	9.18	2.33	0.62	0.32	907.10	41.23	70.19	7.54	27.10	4.91	1.57	4.79	0.61
P-169	7.36	n.d.	n.d.	n.d.	n.d.	n.d.	73.49			44.44	612.95	22.74	132.75	9.69	2.47	0.84	1.02	760.96	26.89	52.05	6.61	26.19	5.34	1.38	5.28	0.74
P-109	6.78	n.d.	n.d.	n.d.	n.d.	n.d.	97.09			25.05	574.76	14.68	72.69	5.53	1.54	0.68	0.55	480.30	14.18	28.53	3.59	14.65	3.22	1.02	3.29	0.49
P-112	10.67	n.d.	n.d.	n.d.	n.d.	n.d.	158.50			71.52	492.36	26.79	178.08	12.84	3.75	1.20	1.55	841.27	32.20	65.58	8.04	31.23	6.34	1.57	6.36	0.90
P-113	6.53	n.d.	n.d.	n.d.	n.d.	n.d.	185.67			50.75	536.58	26.58	141.61	11.08	2.50	1.01	0.66	720.70	28.85	56.00	7.30	29.11	6.05	1.59	6.14	0.91
P-171	5.71	n.d.	n.d.	n.d.	n.d.	n.d.	88.78			41.28	814.48	24.29	231.25	24.08	2.47	1.38	0.57	784.80	51.96	105.95	12.95	49.69	9.02	2.49	8.16	1.04
P-102C	4.25	n.d.	n.d.	n.d.	n.d.	n.d.	159.33			13.37	784.37	15.49	68.87	5.30	0.78	0.62	0.22	480.37	19.47	39.85	5.15	21.29	4.36	1.43	4.28	0.58
P-139	6.63	n.d.	n.d.	n.d.	n.d.	n.d.	124.97			47.54	927.01	22.92	189.41	17.08	2.57	1.01	0.72	838.50	55.04	114.21	14.21	55.63	10.16	2.72	8.91	1.06
P-140	8.97	24.45	236.61	266.30	31.58	115.96	150.27	84.04	19.84	47.81	957.84	26.35	210.28	18.94	2.66	1.07	0.73	891.75	56.57	117.28	14.19	55.02	9.93	2.56	7.62	1.03
P-143	7.34	n.d.	n.d.	n.d.	n.d.	n.d.	95.71			54.14	870.16	18.73	185.50	16.60	2.85	1.01	0.90	908.13	45.68	89.40	10.66	40.20	7.01	1.91	6.33	0.78
P-160A	6.99	n.d.	n.d.	n.d.	n.d.	n.d.	105.48			56.54	796.00	24.70	229.37	21.86	3.02	1.25	0.84	901.45	52.63	106.36	12.80	48.60	8.67	2.31	7.88	1.00
P-162	9.35	21.16	201.36	187.16	26.56	92.09	133.60	74.55	19.08	52.48	771.96	20.52	189.51	17.45	2.93	0.99	0.85	814.35	40.72	80.62	9.44	35.36	6.25	1.55	4.95	0.71
P2-72	9.78	24.16	204.89	202.85	28.58	106.43	107.77	74.59	17.69	48.64	742.18	18.55	177.55	16.70	2.73	0.91	0.80	741.10	37.62	75.96	9.01	32.98	5.88	1.48	4.94	0.66
P-96	7.08	23.90	249.31	26.44	25.96	18.44	97.88	77.87	19.05	49.63	816.25	24.28	171.84	15.66	2.51	1.03	0.62	950.95	44.39	85.20	10.71	40.35	7.30	1.36	6.22	0.85
P-97A	6.14	n.d.	n.d.	n.d.	n.d.	n.d.	95.01			30.38	806.87	19.44	147.99	13.16	1.66	0.88	0.40	667.16	35.44	72.07	8.83	34.27	6.41	1.90	5.99	0.78
P-149A	8.50	n.d.	n.d.	n.d.	n.d.	n.d.	151.77			94.60	852.00	26.80	348.70	36.30	4.65	1.68	1.14	1186.91	73.14	143.68	16.75	61.08	10.37	2.35	9.16	1.11
Central Costa Rica BVF - Alkaline																										
P-152	3.74	n.d.	n.d.	n.d.	n.d.	n.d.	92.10			107.25	2569.11	14.97	67.62	7.27	0.55	0.56	1.46	2458.70	65.21	133.59	16.57	63.09	8.35	2.52	6.78	0.71
P-153	5.34	29.43	254.88	481.61	43.82	209.71	110.31	88.66	17.13	32.27	784.80	27.68	184.85	18.57	1.03	1.11	0.28	637.63	53.90	113.57	13.83	53.59	9.68	2.74	7.75	1.08
P-154B	3.93	n.d.	n.d.	n.d.	n.d.	n.d.	82.16			25.17	826.03	17.43	158.74	19.77	1.29	1.00	0.22	600.65	39.15	80.13	9.78	37.71	6.67	1.99	6.15	0.76
P-155A	4.84	25.66	242.78	307.48	37.94	173.04	107.56	83.46	19.34	19.42	929.35	17.63	123.42	16.39	1.23	0.86	0.26	571.42	31.46	63.82	7.92	31.05	5.81	1.72	4.72	0.67
P-130A	6.76	27.69	271.22	472.44	48.84	233.83	106.46	107.44	18.69	29.45	1757.08	27.92	287.69	46.80	1.22	1.62	0.34	764.32	99.50	195.56	23.02	86.89	14.56	4.03	11.57	1.40
P-128	7.06	19.70	225.11	171.29	45.42	163.27	101.37	115.16	21.26	31.63	1383.05	36.44	399.60	57.97	1.06	2.02	0.10	715.97	99.68	212.84	25.99	98.65	16.38	4.54	12.40	1.64
P-129	4.73	27.61	262.98	255.04	51.75	142.21	87.34	104.79	19.11	17.08	682.09	24.00	162.72	23.04	0.63	1.30	0.09	309.29	28.71	60.40	7.51	30.52	6.28	2.01	6.01	0.88
P-138	5.11	33.63	264.43	586.82	48.53	248.75	152.76	81.85	16.14	27.70	1525.94	27.76	255.76	37.55	1.26	1.48	0.35	598.44	76.11	167.25	19.74	75.65	13.21	3.57	10.60	1.34
P-132B	2.89	n.d.	n.d.	n.d.	n.d.	n.d.	95.77			15.25	795.21	22.58	167.84	23.49	1.04	1.05	0.27	542.09	48.95	97.74	12.00	46.52	8.49	2.48	7.88	0.99
P-133	5.95	32.14	266.16	682.52	50.83	288.86	101.90	92.47	16.92	7.64	815.78	23.04	177.45	25.03	0.46	1.12	0.59	537.99	48.80	99.67	11.74	45.16	8.07	2.33	7.05	0.93
Southern Costa Rica Pliocene-Qua																										
TC-3	5.95	29.57	275.37	19.90	29.00	16.47	60.44	77.34	16.81	36.34	1141.47	18.12	82.07	5.15	0.39	0.45	0.33	802.24	23.69	50.10	6.56	26.42	5.33	1.57	4.64	0.62
TC-5A	7.33	18.71	186.02	142.65	26.98	109.76	136.57	68.58	19.28	45.20	1232.38	9.63	88.38	6.39	0.42	0.41	0.49	915.46	26.97	53.69	6.42	23.83	4.10	1.12	3.12	0.38
TC-6A	7.50	22.87	217.78	162.16	29.75	116.01	135.65	76.84	19.48	28.64	1164.92	12.66	104.52	9.18	2.27	0.60	0.30	713.62	23.56	46.91	5.81	22.10	4.04	1.20	3.41	0.45
TC-7	7.20	21.14	206.99	201.78	30.46	119.23	151.98	73.51	19.17	35.53	1072.25	9.41	88.60	7.31	1.29	0.76	0.37	802.74	20.66	41.06	5.01	18.90	3.53	1.02	2.88	0.36
TC-8	8.89	20.27	197.54	104.82	27.08	96.96	51.81	67.61	21.72	89.57	2211.98	15.04	254.40	14.54	1.50	0.54	0.43	1914.59	74.21	169.00	17.80	64.66	9.77	2.39	6.53	0.73
Southern Costa Rica Pliocene-Qua																										
P-145	4.29	29.51	281.48	951.20	56.94	341.17	103.72	78.20	16.41	8.09	708.71	20.90	117.25	16.44	0.51	0.93	0.14	970.61	26.00	54.34	6.93	28.27	5.78	1.73	5.07	0.74
P-163B	4.26	n.d.	n.d.	n.d.	n.d.	n.d.	152.50			26.55	1437.46	21.48	174.93	26.65	0.94	1.11	0.75	575.65	54.35	111.91	13.90	53.86	9.55	2.90	8.53	1.03
P-164	5.43	16.81	274.25	35.24	34.56	42.31	70.68	99.17	19.38	30.13	1506.43	22.35	211.15	33.94	1.16	1.32	0.57	766.86	55.11	113.59	13.78	53.18	9.15	2.70	7.55	0.98
Panama Adakites (≤ 1 My)																										
M44KH	6.69	18.71	185.04	237.01	29.06	150.93	128.32	69.03	18.20	25.57	1196.34	10.02	100.22	6.78	1.70	0.54	0.35	759.97	23.50	43.82	5.35	19.85	3.55	0.65	2.99	0.39
M53KH	5.60	15.99	171.02	30.24	17.95	31.14	153.97	59.61	22.57	50.02	1531.61	10.16	151.26	5.19	1.94	0.85	0.62	1152.20	30.33	59.82	7.05	26.59	4.63	1.33	3.53	0.47
M55KH	6.98	18.41	205.50	117.67	23.68	39.34	142.80	71.80	20.18	46.35	1561.59	11.26	145.53	6.51	1.69	0.82	0.40	1291.24	33.02	62.87	7.63	27.90	4.45	0.44	3.49	0.44
M57aKH	7.00	23.09	216.00	514.66	35.79	170.04	123.27	73.40	18.02	21.01	898.15	12.06	101.85	9.65	1.84	0.57	0.33	636.59	23.56	45.24	5.57	20.78	3.75	0.81	3.24	0.45
M64c KH	5.45	17.51	217.24	24.38	20.90	29.61	113.86	65.10	21.71	41.90	1316.78	10.62	136.51	4.48	1.40	0.66	0.51	902.18	21.95	42.97	5.17	19.90	3.55	1.11	3.06	0.41
M65a KH	5.83	18.87	231.63	98.88	26.81	92.40	202.29	73.64	21.66	49.98	2082.51	12.43	219.18	11.44	2.18	1.01	0.51	1445.04	71.04	128.75	14.10	50.14	7.19	2.00	5.46	0.62
M99a KH	8.95	16.81	162.01	260.09	27.57	96.82	67.61	69.61	19.13	25.46	1477.18	18.55	163.92	48.03	0.65	0.84	0.37	1287.93	63.94	118.19	12.41	44.15	7.19	1.27	5.88	0.76
Panama Pliocene-Quaternary Alka																										
3-12-4-03	6.15	26.09	209.18	467.99	50.48	297.90	90.29	91.30	17.88	17.29	1487.93	26.64	152.90	28.91	1.58	1.02	0.23	755.47	77.22	157.72	17.57	64.12	10.55	2.68	8.51	1.12
CP97-1	n.d.	25.11	n.d.	n.d.	n.d.	n.d.	n.d.			17.59	1256.82	22.32	146.34	26.36			0.21	652.33	66.67	133.13	15.26	55.98	9.30	2.61	7.14	0.93
SO96-1	n.d.	24.72	n.d.	n.d.	n.d.	n.d.	n.d.			24.95	1169.69	21.04	142.56	28.79			0.31	677.05	46.81	94.14	10.98	41.19	7.27	2.20	6.08	0.83
M36KH	5.07	25.66		360.12	44.60	240.27	87.58	114.42		16.44	1207.31	25.41	245.83	49.57	0.58	1.57	0.19	775.85	51.28	106.08	13.65	55.97	10.91	3.23	9.76	1.27
M37KH	5.44	28.14		436.78	48.18	261.75	98.77	107.99		19.08	1310.34	25.16	228.41	48.00	1.76	1.51	0.40	1065.66	56.34	115.75	14.73	58.52	10.83	3.13	9.47	1.19
M105 KH	5.07	17.52	187.38	357.53	36.54	172.84	67.32	69.20	17.11	22.12	1345.20	17.88	154.83	29.65	1.50	0.90	0.28	843.66	60.54	109.61	12.90	47.07	7.68	2.17	6.09	0.81
M 118aKH	7.58	24.09		359.59	45.58	228.92	68.70	98.61		32.90	1346.10	21.19	204.71	34.80	1.72	1.49	0.47	1121.58	67.66	138.25	16.77	63.63	10.88	3.07	9.32	1.13
M121aKH	3.95	25.17		363.88	44.88	237.05	99.97	105.94		20.80	1937.24	23.82	228.83	35.65	2.39	1.34	0.31	1033.54	84.58	173.47	21.60	83.46	14.06	3.90	11.51	1.37

Table 3.1 continued

sample #	Dy ppm	Ho ppm	Er ppm	Tm ppm	Yb ppm	Lu ppm	Hf ppm	Ta ppm	Tl ppm	Pb ppm	Th ppm	U ppm	W ppm	Sb ppm	Selected Trace element ratios La/Yb	Ba/La	Ba/Th	U/Th	Ce/Pb	Zr/Hf
NW Nicaragua VF																				
P-58A	5.49	1.15	3.21	0.49	3.29	0.50	3.11	0.11	n.d.	4.25	1.49	1.22	0.39	0.81	2.84	96.06	602.25	0.82	5.13	33.60
P-60	4.89	1.04	2.90	0.43	2.85	0.44	2.70	0.08	n.d.	3.84	1.39	1.07	0.45	0.77	3.87	89.11	708.23	0.77	4.97	34.12
P-27A	4.19	0.88	2.35	0.37	2.45	0.37	1.81	0.06	0.03	2.05	0.62	0.61	0.16	0.07	2.52	86.92	860.59	0.98	7.05	28.83
P-13	4.25	0.88	2.50	0.37	2.47	0.37	2.01	0.08	0.24	3.16	1.08	0.92	0.18	0.11	3.18	89.60	652.01	0.85	5.81	33.04
P2-16	3.04	0.62	1.71	0.25	1.69	0.25	1.58	0.10	0.07	2.05	0.75	0.64	0.27	0.32	2.58	105.81	615.68	0.85	5.37	30.59
P-7A	3.90	0.81	2.19	0.34	2.31	0.34	2.52	0.13	0.12	2.74	1.15	1.12	0.37	0.49	2.79	115.18	645.72	0.97	5.41	30.60
P-9	3.57	0.73	2.00	0.29	1.92	0.29	2.19	0.31	0.06	2.42	0.95	0.79	0.23	0.32	3.30	87.50	582.06	0.83	6.01	35.77
P-43	5.16	1.08	2.87	0.45	2.99	0.45	3.29	0.40	0.11	2.70	1.05	0.93	0.36	0.40	2.78	81.99	646.02	0.89	7.17	32.82
P-51	3.24	0.67	1.79	0.28	1.84	0.28	1.69	0.10	0.07	1.56	0.52	0.48	0.15	0.14	3.02	65.13	692.91	0.92	8.22	30.40
P-56G	4.44	0.92	2.47	0.39	2.60	0.40	1.78	0.06	0.11	2.66	0.59	0.58	0.15	0.09	2.67	110.23	1304.92	0.99	5.91	28.02
P-4	2.77	0.58	1.57	0.24	1.64	0.25	1.13	0.07	0.04	1.30	0.31	0.31	0.15	0.17	1.97	113.01	1180.36	1.00	5.71	29.10
P-6	2.87	0.60	1.70	0.25	1.69	0.25	1.22	0.11	0.04	2.02	0.40	0.36	0.13	0.19	2.14	120.51	1097.05	0.91	4.25	32.67
P2-3a	1.99	0.41	1.16	0.17	1.14	0.17	0.65	0.05	0.02	1.06	0.19	0.17	0.09	0.12	1.70	127.98	1278.72	0.89	4.62	31.74
P2-3b	2.30	0.48	1.35	0.20	1.37	0.20	0.85	0.06	0.03	1.49	0.30	0.27	0.11	0.15	1.94	129.01	1155.81	0.91	4.38	33.15
P2-3d	2.54	0.53	1.51	0.22	1.51	0.23	0.93	0.06	0.04	1.56	0.34	0.30	0.13	0.17	1.84	129.87	1079.81	0.91	4.39	33.18
P2-11	2.65	0.56	1.56	0.23	1.55	0.24	1.02	0.07	0.04	1.64	0.33	0.30	0.10	0.19	2.17	117.65	1198.40	0.91	4.73	31.90
P2-13	2.58	0.54	1.53	0.23	1.52	0.23	1.02	0.07	0.03	1.75	0.33	0.29	0.10	0.19	2.11	117.41	1127.48	0.86	4.25	31.60
P-50	3.00	0.61	1.72	0.25	1.70	0.25	1.51	0.10	0.05	1.90	0.57	0.47	0.14	0.14	3.18	68.13	653.16	0.83	6.64	35.21
P-19	3.98	0.82	2.20	0.34	2.30	0.34	2.33	0.16	0.05	1.92	0.77	0.65	0.24	0.23	2.90	73.90	644.38	0.85	8.06	31.78
P-40A	2.46	0.51	1.37	0.21	1.42	0.22	0.95	0.05	0.04	0.99	0.26	0.27	0.09	0.10	2.15	102.01	1212.89	1.06	6.84	28.29
P-42	2.56	0.54	1.53	0.23	1.53	0.23	1.07	0.06	0.05	1.76	0.35	0.32	0.11	0.17	2.10	122.12	1126.38	0.93	4.25	33.00
P-23	4.88	1.02	2.74	0.42	2.84	0.44	3.21	0.28	0.14	3.00	1.13	0.98	0.35	0.37	3.24	84.61	686.28	0.86	6.98	32.70
P-46A	5.59	1.16	3.17	0.50	3.34	0.51	3.97	0.32	0.10	3.87	1.54	1.43	0.51	0.67	2.94	102.24	650.55	0.93	5.81	32.03
P-47A	5.71	1.19	3.24	0.50	3.40	0.52	4.15	0.31	0.16	4.45	1.66	1.55	0.54	0.73	3.00	106.40	654.82	0.94	5.24	31.99
P-48B	4.72	0.99	2.69	0.42	2.82	0.43	3.14	0.23	0.16	3.45	1.21	1.12	0.41	0.56	2.80	105.00	686.67	0.93	5.20	31.31
P-32	3.41	0.72	1.92	0.30	2.04	0.31	1.77	0.09	0.10	2.03	0.60	0.62	0.21	0.25	2.73	107.50	1002.40	1.04	6.15	29.73
P-34	3.80	0.79	2.28	0.33	2.26	0.34	2.09	0.11	0.10	3.02	0.87	0.79	0.23	0.34	2.96	116.53	897.47	0.91	5.02	34.32
SW Nicaragua VF																				
P2-32d	3.52	0.72	2.00	0.29	1.96	0.29	1.49	0.19	0.02	0.75	0.28	0.20	0.08	0.02	1.64	41.51	471.35	0.72	11.63	34.58
P2-53	4.49	0.84	2.15	0.30	1.88	0.27	3.24	0.63	0.03	0.89	0.41	0.33	0.11	0.04	2.25	51.21	526.32	0.81	14.67	37.27
P-68B	4.30	0.89	2.51	0.37	2.50	0.37	2.60	0.14	0.04	3.77	1.74	1.44	0.23	0.22	4.03	83.77	484.12	0.83	5.78	35.65
P-71A	4.30	0.89	2.49	0.37	2.48	0.37	2.61	0.14	0.03	3.78	1.73	1.42	0.23	0.22	4.07	83.64	489.36	0.82	5.81	35.36
P2-47	4.95	1.02	2.88	0.43	2.93	0.45	3.23	0.19	0.09	4.63	2.22	1.84	0.46	0.32	4.06	90.15	483.61	0.83	5.97	33.53
P-63	4.25	0.88	2.40	0.36	2.38	0.36	2.59	0.37	0.07	2.83	1.28	0.86	0.18	0.10	4.03	56.34	421.03	0.67	7.44	38.70
P2-58	3.57	0.73	2.01	0.30	1.99	0.30	1.69	0.26	0.02	1.00	0.53	0.34	0.10	0.03	2.61	39.88	387.59	0.63	12.61	35.53
P-86A	5.31	1.05	2.91	0.43	2.90	0.43	3.54	0.67	0.14	3.62	2.57	1.62	0.33	0.06	8.07	38.04	345.90	0.63	13.53	41.06
P-80A	3.19	0.64	1.75	0.25	1.70	0.25	1.63	0.28	0.03	1.86	1.15	0.70	0.15	0.03	6.79	44.30	444.81	0.61	13.07	39.21
NW Costa Rica VF																				
CR-44	4.37	0.91	2.53	0.38	2.53	0.39	2.27	0.13	0.02	2.14	1.09	0.60	0.15	0.14						
CR-35	4.13	0.83	2.37	0.36	2.46	0.38	3.69	0.29	0.22	4.89	4.03	2.01	0.44	0.28	7.64	48.26	225.43	0.50	7.92	37.51
CR-56	3.75	0.77	2.13	0.32	2.16	0.34	3.09	0.23	0.15	4.21	3.17	1.64	0.32	0.25						
P2-118	4.32	0.87	2.47	0.37	2.58	0.39	3.22	0.28	0.21	4.74	3.26	1.80	0.45	0.23	7.46	49.45	292.08	0.55	8.31	37.26
CR-30	4.30	0.86	2.30	0.32	2.07	0.32	2.92	0.30	0.10	4.62	3.66	1.47	0.29	0.17						
CR-51B	4.72	1.01	2.84	0.42	2.73	0.44	2.57	0.35	0.09	5.43	3.76	1.46	0.29	0.09						
CR-55	3.71	0.73	2.05	0.30	2.07	0.32	3.88	0.81	0.18	7.50	11.22	3.74	0.95	0.39						
CR-58	2.71	0.55	1.54	0.23	1.57	0.24	1.19	0.13	0.01	1.44	0.48	0.20	0.10	0.07						
CR-61B	2.43	0.49	1.35	0.20	1.38	0.21	1.01	0.13	0.02	2.02	0.70	0.26	0.19	0.08	6.63	48.59	629.98	0.37	9.22	35.89
CR-61C	2.38	0.48	1.33	0.20	1.34	0.20	1.04	0.13	0.02	2.05	0.67	0.25	0.18	0.09						
CR-64	2.98	0.61	1.70	0.26	1.73	0.27	1.54	0.23	0.04	3.30	0.93	0.40	0.28	0.17						
CR-71	3.43	0.64	1.74	0.25	1.63	0.25	1.83	0.22	0.06	4.36	5.77	1.81	0.27	0.08						
CR-84	2.82	0.58	1.63	0.25	1.69	0.27	1.24	0.24	0.02	2.96	0.60	0.32	0.23	0.14						
Central Costa Rica VF																				
P-118	4.90	0.98	2.63	0.40	2.69	0.41	3.83	0.69	0.08	5.42	6.67	2.67	0.75	0.24	10.57	23.06	98.26	0.40	9.92	33.69
P-122	4.70	0.95	2.55	0.39	2.59	0.40	3.71	0.68	0.08	5.05	6.55	2.62	0.76	0.22	10.27	24.39	99.17	0.40	10.38	34.45
P-123A	3.58	0.69	1.80	0.27	1.79	0.27	2.25	0.33	0.04	2.26	2.93	1.18	0.34	0.06	12.41	25.53	193.59	0.40	20.15	35.17
P-124	3.09	0.63	1.69	0.26	1.77	0.27	1.75	0.27	0.04	2.79	1.34	0.62	0.23	0.07	6.18	34.57	281.23	0.46	8.26	32.84
P-151D	3.55	0.71	1.85	0.28	1.89	0.29	2.24	0.39	0.04	3.35	2.16	0.86	0.28	0.08	9.38	28.39	232.75	0.40	10.99	32.31

Table 3.1 continued

sample #	Dy	Ho	Er	Tm	Yb	Lu	Hf	Ta	Tl	Pb	Th	U	W	Sb	Selected Trace element ratios					
	ppm	ppm	ppm	ppm	ppm	ppm	ppm	ppm	ppm	ppm	ppm	ppm	ppm	ppm	La/Yb	Ba/La	Ba/Th	U/Th	Ce/Pb	Zr/Hf
P-119A	3.25	0.63	1.65	0.25	1.67	0.26	2.72	0.57	0.07	2.92	12.41	4.34	1.17	0.12	24.75	22.00	73.08	0.35	24.02	38.62
P-169	4.39	0.90	2.39	0.37	2.50	0.38	3.98	0.67	0.12	5.03	6.31	2.53	0.81	0.26	10.77	28.30	120.59	0.40	10.35	33.39
P-109	2.93	0.60	1.60	0.25	1.64	0.26	2.22	0.42	0.06	3.46	3.36	1.38	0.44	0.14	8.67	33.87	143.01	0.41	8.24	32.76
P-112	5.32	1.07	2.88	0.45	2.99	0.46	5.17	0.87	0.15	6.85	10.08	3.96	1.15	0.36	10.77	26.12	83.46	0.39	9.57	34.43
P-113	5.20	1.06	2.82	0.43	2.88	0.44	4.19	0.75	0.06	5.67	7.44	2.98	0.74	0.21	10.02	24.98	96.87	0.40	9.87	33.80
P-171	5.40	0.99	2.47	0.36	2.31	0.34	6.14	1.34	0.09	3.92	10.46	3.81	0.97	0.17	22.52	15.10	75.01	0.36	27.05	37.67
P-102C	3.30	0.65	1.67	0.25	1.64	0.24	2.06	0.27	0.03	1.64	2.53	1.09	0.22	0.07	11.90	24.67	189.79	0.43	24.32	33.38
P-139	5.21	0.94	2.31	0.33	2.15	0.32	5.00	0.87	0.12	4.66	8.77	3.54	0.87	0.20	25.61	15.24	95.56	0.40	24.49	37.91
P-140	5.08	0.92	2.41	0.32	2.13	0.31	4.76	0.92	0.11	5.82	9.81	3.47	0.79	0.20	26.55	15.76	90.90	0.35	20.15	44.16
P-143	4.07	0.76	1.93	0.29	1.91	0.28	5.10	0.92	0.11	5.00	10.43	3.96	0.97	0.25	23.94	19.88	87.04	0.38	17.88	36.35
P-160A	5.31	1.00	2.55	0.38	2.45	0.37	6.05	1.17	0.12	4.95	10.22	3.92	0.98	0.22	21.44	17.13	88.20	0.38	21.49	37.90
P-162	3.74	0.71	1.91	0.27	1.79	0.27	4.42	0.91	0.11	5.66	10.20	3.46	0.81	0.24	22.78	20.00	79.82	0.34	14.24	42.86
P2-72	3.59	0.68	1.82	0.26	1.75	0.26	4.22	0.89	0.11	5.12	9.39	3.22	1.18	0.25						
P-96	4.46	0.84	2.31	0.33	2.18	0.33	4.11	0.77	0.05	4.48	10.42	3.56	0.88	0.22	20.39	21.42	91.25	0.34	19.01	41.80
P-97A	4.17	0.79	2.05	0.30	1.97	0.30	4.00	0.69	0.05	3.20	4.79	1.85	0.47	0.11	17.96	18.83	139.34	0.39	22.54	37.00
P-149A	5.73	1.06	2.75	0.41	2.71	0.41	8.95	1.89	0.12	6.89	21.62	7.56	1.95	0.37	26.99	16.23	54.89	0.35	20.84	38.96
Central Costa Rica BVF - Alkaline																				
P-152	3.42	0.63	1.63	0.23	1.50	0.23	1.93	0.35	0.03	5.38	5.33	0.79	0.33	0.02	43.34					35.04
P-153	5.45	0.98	2.53	0.34	2.13	0.31	4.18	0.92	0.04	2.84	5.57	2.02	0.33	0.03	25.27	11.83	114.55	0.36	40.03	44.25
P-154B	3.97	0.72	1.77	0.25	1.58	0.23	4.11	1.11	0.06	2.50	4.03	1.52	0.44	0.06	24.74	15.34	149.20	0.38	32.07	38.59
P-155A	3.44	0.63	1.63	0.22	1.40	0.20	2.84	0.80	0.00	2.25	3.49	1.32	0.40	0.07	22.49	18.17	163.80	0.38	28.41	43.46
P-130A	6.26	1.05	2.55	0.32	1.92	0.27	5.92	2.25	0.06	4.38	8.81	2.62	0.40	0.07						
P-128	7.79	1.31	3.23	0.40	2.44	0.34	8.28	2.79	0.03	2.66	5.60	2.10	0.42	0.07	40.88	7.18	127.88	0.37	80.00	48.25
P-129	4.80	0.90	2.29	0.32	1.96	0.28	3.70	1.23	0.01	1.49	2.55	0.64	0.09	0.02						
P-138	6.18	1.02	2.50	0.31	1.94	0.27	5.02	1.84	0.04	3.54	6.15	1.97	0.68	0.05	39.14	7.86	97.27	0.32	47.18	50.92
P-132B	5.14	0.94	2.30	0.32	2.06	0.30	4.45	1.29	0.01	1.63	5.13	1.86	0.54	0.05	23.76	11.07	105.74	0.36	59.79	37.74
P-133	4.77	0.87	2.21	0.30	1.87	0.27	3.90	1.28	0.01	2.58	5.15	1.71	0.17	0.05	23.76	11.07	105.74	0.36	59.79	37.74
Southern Costa Rica Pliocene-Qua																				
TC-3	3.41	0.63	1.71	0.24	1.60	0.24	2.23	0.22	0.07	3.64	3.13	1.20	0.14	0.11	14.80	33.87	255.91	0.38	13.75	36.73
TC-5A	1.90	0.34	0.89	0.12	0.79	0.12	2.60	0.36	0.02	6.32	6.53	2.03	0.09	0.08	34.18	33.94	140.23	0.31	8.50	33.96
TC-6A	2.44	0.44	1.17	0.16	1.03	0.15	2.92	0.51	0.18	4.91	4.44	1.27	0.57	0.19	22.82	30.29	160.63	0.29	9.56	35.81
TC-7	1.88	0.34	0.89	0.12	0.78	0.12	2.48	0.41	0.07	5.05	4.88	1.58	0.32	0.10	26.33	38.86	164.63	0.32	8.14	35.74
TC-8	3.28	0.55	1.38	0.17	1.11	0.15	7.12	0.74	0.07	11.25	16.93	4.63	0.44	0.12	66.91	25.80	113.09	0.27	15.03	35.75
Southern Costa Rica Pliocene-Qua																				
P-145	4.03	0.77	2.06	0.28	1.85	0.27	2.83	0.90	0.04	3.00	2.87	0.96	0.13	0.02	14.04	37.33	338.09	0.34	18.11	41.44
P-163B	5.13	0.90	2.15	0.29	1.82	0.26	4.45	1.40	0.03	2.16	3.53	1.50	0.31	0.04	29.89	10.59	163.06	0.43	51.88	39.34
P-164	4.79	0.85	2.15	0.29	1.77	0.25	4.48	1.69	0.04	3.07	4.15	1.18	0.32	0.04	29.89	10.59	163.06	0.43	51.88	39.34
Panama Adakites (≤ 1 My)																				
M44KH	2.00	0.36	0.98	0.13	0.90	0.13	2.53	0.36	0.05	5.68	4.15	1.35		0.07	2.82	119.35	1225.73	0.14	274.97	50.55
M53KH	2.18	0.40	1.03	0.13	0.90	0.13	4.51	0.37	0.13	10.14	11.41	2.94		0.15	2.19	150.81	1492.18	0.13	382.49	8.83
M55KH	2.20	0.40	1.11	0.15	1.03	0.15	3.91	0.34	0.09	6.34	7.70	2.23		0.06	2.53	138.66	1412.42	0.14	361.10	11.26
M57aKH	2.37	0.44	1.18	0.17	1.11	0.16	2.45	0.52	0.04	3.85	3.54	1.07		0.06	3.22	74.48	764.19	0.14	229.51	52.52
M64c KH	2.11	0.40	1.06	0.15	0.95	0.14	3.63	0.24	0.09	7.65	6.34	1.87	0.18	0.12	2.99	124.02	1247.19	0.14	340.36	9.66
M65a KH	2.71	0.46	1.20	0.15	0.96	0.14	5.53	0.56	0.08	8.64	11.52	2.82	0.39	0.08	1.73	167.55	1736.16	0.13	471.57	16.94
M99a KH	3.72	0.65	1.71	0.23	1.46	0.21	3.57	2.04	0.06	6.36	8.88	2.67		0.07	2.58	79.62	865.03	0.13	251.76	16.46
Panama Pliocene-Quaternary Alka																				
3-12-4-03	5.49	0.97	2.50	0.33	2.13	0.30	3.38	1.21	0.03	4.63	9.36	2.76		0.05	2.53	55.85	595.31	0.13	157.73	34.99
CP97-1	4.81	0.87	2.21	0.29	1.81	0.25	3.41	0.98		3.43	7.13	2.13	0.83		2.40	56.32	568.16	0.13	168.52	0.00
SO96-1	4.45	0.82	2.11	0.29	1.77	0.25	3.63	1.21		3.34	4.88	1.88	0.73		2.90	55.58	554.66	0.14	174.43	0.00
M36KH	6.57	1.15	2.85	0.37	2.22	0.31	6.96	3.09	0.03	3.47	6.13	1.86		0.03	2.33	47.52	423.74	0.13	213.10	24.61
M37KH	6.14	1.08	2.75	0.36	2.17	0.31	6.37	2.90	0.04	3.76	6.47	1.95		0.03	2.32	52.07	476.06	0.13	211.08	27.64
M105 KH	3.94	0.70	1.82	0.24	1.52	0.22	3.71	1.54	0.01	3.99	7.03	1.95		0.05	2.33	75.22	740.39	0.13	221.22	28.38
M 118aKH	5.53	0.96	2.35	0.29	1.81	0.26	6.04	2.35	0.04	5.11	8.42	2.68		0.06	1.95	63.52	571.98	0.13	212.37	24.55
M121aKH	6.61	1.13	2.79	0.35	2.20	0.30	6.50	2.25	0.03	4.69	8.85	2.50		0.03	1.69	81.31	695.14	0.13	202.37	20.59

Table 3.2. Sr and Hf isotopic compositions of southwestern Central American Arc volcanics extending from southwestern Nicaragua to central Costa Rica for Volcanic Front (VF) and Behind the Volcanic Front (BVF) samples. Also shown are southern Costa Rica and western Panama Pliocene to quaternary alkali basalt and adakite samples. Note! Pb isotope data from Hoernle et al. (2008).

Table 3.2. Sr and Hf isotopic compositions of southwestern Central American Arc volcanics extending from southwestern Nicaragua to central Costa Rica for Volcanic Front (VF) and Behind the Volcanic Front (BVF) samples. Also shown are southern Costa Rica and western Panama Pliocene to quaternary alkali basalt and adakite samples. Note! Pb isotope data from Hoernle et al. (2008).

sample #	$^{87}Sr/^{86}Sr$	2 σ	$^{143}Nd/^{144}Nd$	2 σ	εNd	$^{206}Pb/^{204}Pb$	2 σ	$^{207}Pb/^{204}Pb$	2 σ	$^{208}Pb/^{204}Pb$	2 σ	$^{176}Hf/^{177}Hf$	2 σ	εHf
P-58A	0.703872	0.000002	0.513068	0.000003	8.38	18.464	0.001	15.518	0.001	38.091	0.002	0.28	0.00	14.86
P-60	0.703839	0.000002	0.513084	0.000003	8.69	18.425	0.001	15.507	0.001	38.023	0.002	0.28	0.00	15.44
P-27A	0.703909	0.000002	0.513061	0.000002	8.26	18.475	0.002	15.519	0.002	38.099	0.005	0.28	0.00	14.29
P-13	0.703917	0.000002	0.513057	0.000003	8.18	18.483	0.001	15.533	0.001	38.140	0.002			
P2-16	0.704019	0.000003	0.513050	0.000002	8.04	18.506	0.001	15.515	0.001	38.118	0.002			
P-7A	0.704005	0.000002	0.513060	0.000002	8.23	18.513	0.001	15.520	0.001	38.139	0.003			
P-9	0.703971	0.000002	0.513042	0.000003	7.88	18.532	0.001	15.534	0.001	38.188	0.002	0.28	0.00	13.57
P-43	0.703849	0.000002	0.513051	0.000002	8.05	18.554	0.001	15.521	0.001	38.180	0.003			
P-51	0.703965	0.000006	0.513067	0.000006	8.36	18.481	0.001	15.520	0.001	38.114	0.002			
P-56G	0.703941	0.000006	0.513073	0.000004	8.48	18.493	0.001	15.525	0.001	38.131	0.002			
P-4	0.703991	0.000006	0.513078	0.000006	8.57	18.557	0.002	15.529	0.001	38.205	0.003			
P-6	0.703983	0.000002	0.513066	0.000003	8.34	18.546	0.003	15.529	0.002	38.195	0.006			
P2-3a	0.703965	0.000003	0.513071	0.000003	8.45									
P2-3b	0.703978	0.000003	0.513072	0.000002	8.47	18.538	0.002	15.522	0.002	38.171	0.005			
P2-3d	0.703994	0.000003	0.513074	0.000003	8.50	18.533	0.002	15.526	0.002	38.172	0.005	0.28	0.00	14.39
P2-11	0.703982	0.000005	0.513072	0.000003	8.47	18.549	0.002	15.523	0.001	38.184	0.003			
P2-13	0.703961	0.000009	0.513077	0.000004	8.56	18.555	0.001	15.530	0.001	38.205	0.002			
P-50	0.703971	0.000003	0.513057	0.000002	8.18	18.480	0.001	15.519	0.001	38.107	0.002			
P-19	0.703864	0.000003	0.513055	0.000002	8.13	18.514	0.003	15.518	0.002	38.133	0.006			
P-40A	0.704044	0.000007	0.513084	0.000006	8.69	18.532	0.001	15.526	0.001	38.175	0.002			
P-42	0.704001	0.000002	0.513067	0.000003	8.37	18.549	0.002	15.526	0.002	38.187	0.005			
P-23	0.703943	0.000004	0.513063	0.000003	8.30	18.537	0.002	15.520	0.001	38.157	0.003			
P-46A	0.703936	0.000003	0.513065	0.000002	8.32	18.550	0.001	15.523	0.001	38.180	0.002			
P-47A	0.703952	0.000002	0.513063	0.000002	8.30	18.548	0.001	15.521	0.001	38.176	0.002			
P-48B	0.703954	0.000003	0.513065	0.000002	8.33	18.552	0.001	15.525	0.001	38.188	0.002			
P-32	0.704046	0.000003	0.513071	0.000003	8.44	18.557	0.001	15.527	0.001	38.202	0.003	0.28	0.00	14.66
P-34	0.704017	0.000002	0.513073	0.000003	8.49	18.564	0.001	15.533	0.001	38.217	0.002			
SW Nicaragua VF														
P2-32d	0.703710	0.000002	0.513024	0.000003	7.53	18.472	0.001	15.525	0.001	38.111	0.003	0.28	0.00	12.47
P2-53	0.703689	0.000003				18.599	0.004	15.520	0.004	38.215	0.009			
P-68B	0.704167	0.000002	0.513061	0.000003	8.25	18.603	0.003	15.530	0.002	38.251	0.006			
P-71A	0.704167	0.000002	0.513059	0.000002	8.21									
P2-47	0.704187	0.000003	0.513055	0.000002	8.13	18.597	0.000	15.528	0.000	38.244	0.001	0.28	0.00	14.82
P-63	0.703913	0.000004	0.513024	0.000002	7.53	18.628	0.002	15.526	0.002	38.260	0.004			
P2-58	0.703953	0.000003	0.513015	0.000002	7.35	18.567	0.001	15.526	0.001	38.211	0.003	0.28	0.00	12.52
P-86A	0.703949	0.000002	0.513004	0.000002	7.15	18.652	0.002	15.529	0.002	38.295	0.005	0.28	0.00	13.08
P-80A	0.703963	0.000002	0.513018	0.000002	7.41	18.663	0.003	15.538	0.003	38.323	0.007			
NW Costa Rica VF														
CR-44	0.703866	0.000003	0.513054	0.000002	8.12	18.683	0.003	15.528	0.002	38.323	0.005			
CR-35	0.703884	0.000003	0.513031	0.000002	7.67	18.714	0.002	15.536	0.002	38.378	0.005	0.28	0.00	14.15
CR-56	0.703986	0.000003	0.513027	0.000003	7.59	18.714	0.002	15.530	0.002	38.367	0.004			
P2-118	0.703940	0.000002	0.513025	0.000002	7.56	18.777	0.001	15.539	0.001	38.447	0.002			
CR-30	0.703860	0.000002	0.513001	0.000003	7.08	18.882	0.002	15.540	0.002	38.546	0.005			
CR-51B	0.703792	0.000003	0.513007	0.000002	7.20	18.897	0.001	15.539	0.001	38.578	0.002			
CR-55	0.703794	0.000003	0.512969	0.000003	6.46	19.052	0.000	15.554	0.000	38.791	0.001			
CR-58	0.703813	0.000002	0.513025	0.000003	7.55	18.903	0.002	15.540	0.002	38.583	0.005			
CR-61B	0.703814	0.000004	0.513010	0.000004	7.25	18.976	0.007	15.546	0.005	38.686	0.013	0.28	0.00	13.50
CR-61C	0.703816	0.000003	0.513011	0.000002	7.28	18.954	0.001	15.553	0.001	38.673	0.002			
CR-64	0.703802	0.000004	0.513017	0.000004	7.39	19.016	0.004	15.566	0.003	38.768	0.009			
CR-71	0.703784	0.000003	0.513003	0.000003	7.12	18.914	0.001	15.544	0.001	38.605	0.003			
CR-84	0.703663	0.000002	0.513021	0.000003	7.46	19.083	0.001	15.558	0.001	38.840	0.002			
Central Costa Rica VF														
P-118	0.703667	0.000002	0.512963	0.000002	6.34	19.183	0.004	15.569	0.003	38.960	0.007			
P-122	0.703672	0.000002	0.512965	0.000002	6.37	19.184	0.001	15.569	0.001	38.960	0.002			
P-123A	0.703700	0.000003	0.512963	0.000002	6.34	19.181	0.002	15.567	0.002	38.942	0.005			
P-124	0.703651	0.000003	0.512966	0.000003	6.40	19.182	0.001	15.577	0.001	38.981	0.002			
P-151D	0.703722	0.000003	0.512958	0.000003	6.24	19.198	0.004	15.565	0.003	38.966	0.007			
P-119A	0.703667	0.000002	0.512948	0.000002	6.04	19.171	0.002	15.557	0.002	38.908	0.005			
P-169	0.703713	0.000003	0.512967	0.000003	6.42	19.174	0.001	15.565	0.001	38.940	0.002			

Table 3.2. Sr and Hf isotopic compositions of southwestern Central American Arc volcanics extending from southwestern Nicaragua to central Costa Rica for Volcanic Front (VF) and Behind the Volcanic Front (BVF) samples. Also shown are southern Costa Rica and western Panama Pliocene to quaternary alkali basalt and adakite samples. Note! Pb isotope data from Hoernle et al. (2008).

sample #	$^{87}Sr/^{86}Sr$	2 σ	$^{143}Nd/^{144}Nd$	2 σ	εNd	$^{206}Pb/^{204}Pb$	2 σ	$^{207}Pb/^{204}Pb$	2 σ	$^{208}Pb/^{204}Pb$	2 σ	$^{176}Hf/^{177}Hf$	2 σ	εHf
P-109	0.703681	0.000003	0.512979	0.000002	6.65	19.141	0.001	15.564	0.001	38.899	0.003	0.28	0.00	12.88
P-112	0.703704	0.000008	0.512960	0.000002	6.28	19.173	0.001	15.567	0.001	38.879	0.002			
P-113	0.703671	0.000002	0.512967	0.000004	6.42	19.172	0.001	15.562	0.001	38.926	0.003			
P-171	0.703597	0.000002	0.512959	0.000002	6.26	19.111	0.003	15.562	0.003	38.832	0.006	0.28	0.00	11.84
P-102C	0.703680	0.000003	0.512971	0.000003	6.50	19.093	0.004	15.562	0.003	38.790	0.010			
P-139	0.703716	0.000002	0.512957	0.000002	6.21	19.114	0.001	15.570	0.001	38.833	0.002			
P-140	0.703707	0.000002	0.512955	0.000002	6.18	19.115	0.001	15.571	0.001	38.834	0.001			
P-143	0.703683	0.000003	0.512958	0.000002	6.24	19.104	0.001	15.567	0.001	38.814	0.002			
P-160A	0.703680	0.000002	0.512956	0.000002	6.20	19.108	0.001	15.565	0.001	38.809	0.002			
P-162	0.703660	0.000002	0.512961	0.000003	6.30	19.100	0.001	15.566	0.001	38.804	0.002			
P2-72	0.703658	0.000003	0.512958	0.000002	6.24	19.093	0.000	15.558	0.000	38.779	0.001	0.28	0.00	12.11
P-96	0.703686	0.000004	0.512944	0.000004	5.97	19.143	0.001	15.562	0.001	38.877	0.002			
P-97A	0.703672	0.000002	0.512962	0.000002	6.32	19.080	0.002	15.563	0.001	38.769	0.003	0.28	0.00	12.37
P-149A	0.703667	0.000002	0.512944	0.000002	5.97	19.144	0.001	15.560	0.001	38.880	0.002			
Central Costa Rica BVF - Alkaline (≤2 My)														
P-152	0.703532	0.000005	0.512925	0.000002	5.60	19.277	0.001	15.569	0.001	39.096	0.003			
P-153	0.703542	0.000003	0.512940	0.000002	5.89	19.173	0.003	15.570	0.002	38.893	0.005			
P-154B	0.703600	0.000002	0.512964	0.000002	6.36	19.082	0.002	15.556	0.002	38.747	0.005			
P-155A	0.703653	0.000002	0.512968	0.000002	6.44	19.074	0.002	15.569	0.002	38.785	0.005			
P-130A	0.703623	0.000006	0.512971	0.000004	6.49	19.160	0.003	15.580	0.003	38.846	0.007			
P-128	0.703807	0.000002	0.512955	0.000003	6.19	19.099	0.002	15.567	0.002	38.782	0.004			
P-129	0.703497	0.000005	0.512961	0.000004	6.29	19.140	0.003	15.564	0.003	38.830	0.007			
P-138	0.703623	0.000005	0.512978	0.000003	6.63	19.016	0.002	15.563	0.002	38.702	0.005	0.28	0.00	10.72
P-132B	0.703674	0.000003	0.512956	0.000004	6.21	19.189	0.001	15.583	0.001	38.911	0.003	0.28	0.00	11.49
P-133	0.703673	0.000006	0.512957	0.000004	6.23	19.177	0.001	15.566	0.001	38.869	0.002			
Southern Costa Rica Pliocene-Quaternary Adakite (<5 My)														
TC-3	0.703667	0.000003	0.512981	0.000002	6.69	19.006	0.001	15.544	0.001	38.663	0.001	0.28	0.00	12.19
TC-5A	0.703509	0.000005	0.512973	0.000002	6.53	19.145	0.001	15.566	0.001	38.782	0.001	0.28	0.00	11.72
TC-6A	0.703481	0.000003	0.512979	0.000002	6.65	19.103	0.000	15.560	0.000	38.727	0.001			
TC-7	0.703501	0.000004	0.512980	0.000002	6.67	19.095	0.000	15.560	0.000	38.734	0.001			
TC-8	0.703347	0.000003	0.512937	0.000002	5.83	19.322	0.004	15.571	0.000	38.958	0.001			
Southern Costa Rica Pliocene-Quaternary BVF Alkaline (<5 My)														
P-145	0.703450	0.000002	0.512980	0.000002	6.67	19.040	0.003	15.555	0.002	38.673	0.006			
P-163B	0.703690	0.000002	0.512978	0.000002	6.63	19.050	0.001	15.552	0.001	38.692	0.003			
P-164	0.703591	0.000005	0.512976	0.000004	6.60	19.036	0.003	15.558	0.002	38.679	0.006			
Panama Adakites (≤ 1 My)														
M44KH	0.703545	0.000005	0.512989	0.000003	6.85	19.202	0.001	15.574	0.001	38.875	0.001			
M53KH	0.703403	0.000003	0.512948	0.000003	6.04	19.324	0.001	15.577	0.001	38.991	0.002	0.28	0.00	11.41
M55KH	0.703466	0.000005	0.512968	0.000003	6.44	19.191	0.001	15.575	0.001	38.869	0.002			
M57aKH	0.703568	0.000003	0.512993	0.000002	6.93	19.119	0.001	15.561	0.001	38.770	0.003			
M64c KH	0.703354	0.000004	0.512965	0.000002	6.38	19.296	0.001	15.580	0.001	38.980	0.002	0.28	0.00	11.69
M65a KH	0.703352	0.000003	0.512970	0.000002	6.47	19.263	0.001	15.572	0.001	38.925	0.003	0.28	0.00	11.21
M99a KH	0.703533	0.000003	0.513006	0.000002	7.18	19.069	0.001	15.557	0.001	38.697	0.002	0.28	0.00	13.27
Panama Pliocene-Quaternary Alkaline (<5 My)														
3-12-4-03	0.703540	0.000005	0.512983	0.000003	6.72	19.110	0.001	15.572	0.000	38.776	0.001			
CP97-1	0.703538	0.000003	0.512997	0.000003	7.00	19.045	0.001	15.540	0.000	38.648	0.002			
SO96-1	0.703495	0.000003	0.512999	0.000003	7.04	19.073	0.001	15.559	0.001	38.698	0.002			
M36KH	0.703480	0.000002	0.512999	0.000003	7.04	19.070	0.001	15.567	0.001	38.715	0.003			
M37KH	0.703485	0.000003	0.513005	0.000002	7.16	19.052	0.002	15.553	0.002	38.665	0.005			
M105 KH	0.703468	0.000003	0.512995	0.000002	6.95	19.063	0.001	15.562	0.001	38.705	0.003	0.28	0.00	12.13
M 118aKH	0.703499	0.000003	0.512989	0.000001	6.84	19.051	0.002	15.561	0.002	38.697	0.004	0.28	0.00	12.85
M121aKH	0.703516	0.000003	0.512990	0.000005	6.87	19.079	0.001	15.565	0.001	38.731	0.002			

102

3.8 Appendix:

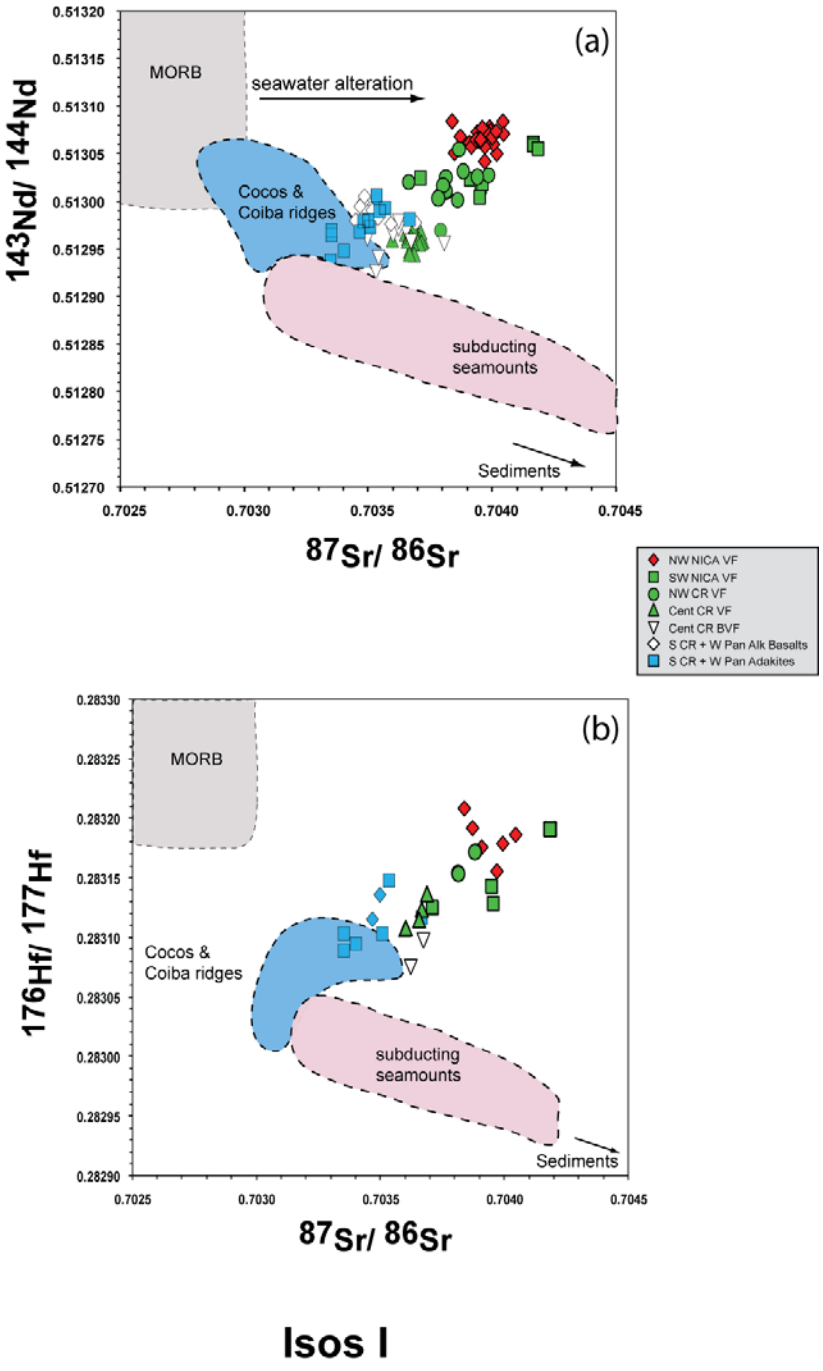

Isos I

Figure Isos I (a-b) **Sr vs. Nd and Hf isotope data for mafic (MgO > 3.15 wt %) southwestern Central American volcanic rock samples from the VF and BVF. Also shown are data for southwestern Costa Rica and western Panama alkali basalt and adakite samples. Data for subducting Seamount province, subducting Cocos and Coiba ridges, Cocos Plate sediments and crust from Feigenson et al. (2004), Werner et al. (2003), Geldmacher et al. (2003, 2008), Heydolph et al. (to be submitted). All errors are reported as 2 sigma of the mean.**

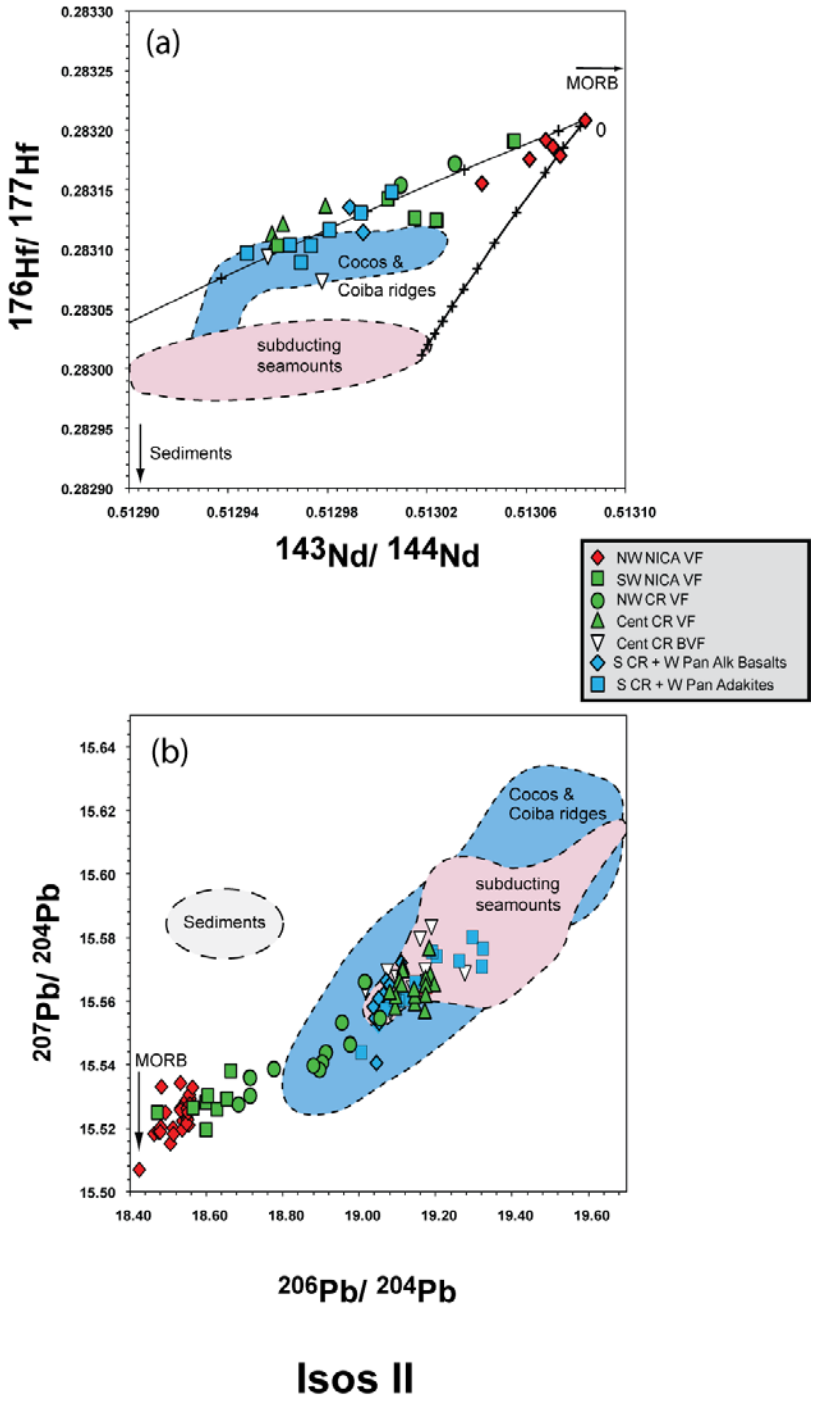

Isos II

Figure Isos II (a-b) **Nd vs. Hf and Pb vs. Pb isotope data for mafic (MgO > 3.15 wt %) southwestern Central American volcanic rock samples from the VF and BVF. Also shown are data for southwestern Costa Rica and western Panama alkali basalt and adakite samples. Data for subducting Seamount province, subducting Cocos and Coiba ridges, Cocos Plate sediments and crust from Feigenson et al. (2004), Werner et al. (2003), Geldmacher et al. (2003, 2008), Heydolph et al. (to be submitted). All errors are reported as 2 sigma of the mean.**

4 Chapter
5 Arc-parallel flow in the mantle wedge beneath Costa Rica and Nicaragua

Kaj Hoernle, David L. Abt, Karen M. Fischer, Holly Nichols, Folkmar Hauff, Geoffrey A. Abers, Paul van den Bogaard, ***Ken Heydolph****, Guillermo Alvarado, Marino Protti & Wilfried Strauch*

nature Vol 451|28 February 2008|doi:10.1038/nature06550

LETTERS

Arc-parallel flow in the mantle wedge beneath Costa Rica and Nicaragua

Kaj Hoernle[1,2], David L. Abt[3], Karen M. Fischer[3], Holly Nichols[1], Folkmar Hauff[2], Geoffrey A. Abers[4]†, Paul van den Bogaard[1,2], Ken Heydolph[1], Guillermo Alvarado[5], Marino Protti[6] & Wilfried Strauch[7]

Resolving flow geometry in the mantle wedge is central to understanding the thermal and chemical structure of subduction zones, subducting plate dehydration, and melting that leads to arc volcanism, which can threaten large populations and alter climate through gas and particle emission. Here we show that isotope geochemistry and seismic velocity anisotropy provide strong evidence for trench-parallel flow in the mantle wedge beneath Costa Rica and Nicaragua. This finding contradicts classical models, which predict trench-normal flow owing to the overlying wedge mantle being dragged downwards by the subducting plate. The isotopic signature of central Costa Rican volcanic rocks is not consistent with its derivation from the mantle wedge[1–3] or eroded fore-arc complexes[4] but instead from seamounts of the Galapagos hotspot track on the subducting Cocos plate. This isotopic signature decreases continuously from central Costa Rica to northwestern Nicaragua. As the age of the isotopic signature beneath Costa Rica can be constrained and its transport distance is known, minimum northwestward flow rates can be estimated (63–190 mm yr^{-1}) and are comparable to the magnitude of subducting Cocos plate motion (~85 mm yr^{-1}). Trench-parallel flow needs to be taken into account in models evaluating thermal and chemical structure and melt generation in subduction zones.

Preferential alignment of the minerals olivine and orthopyroxene occurs as a result of deformation, and produces anisotropy in seismic-wave velocities within the upper mantle. Assuming classical trench-normal 'corner flow' and standard models of crystallographic fabric development, the direction of fast shear-wave polarization will be normal to the arc in the warmer wedge beneath the arc and back-arc, although the fast shear-wave polarization may be parallel to the arc in the cold corner of the wedge beneath the fore-arc[5,6]. Whereas this pattern of seismic anisotropy is observed in some subduction zones[7,8], many display more variable fast directions further from the trench beneath the arc and back-arc, often with a roughly arc-parallel trend[9–12]. The origin of this arc-parallel fast anisotropy, in particular whether it is related to along-arc flow within the mantle wedge or some other process, is vigorously debated[5,6,13–16].

Although arc volcanic rocks from Costa Rica have ocean-island-basalt (OIB)-type compositions similar to those found in Galapagos hotspot rocks[17], the origin of this geochemical signature is controversial. In some models, OIB signatures are contained in the mantle wedge beneath central Costa Rica, reflecting (1) residual Galapagos-type mantle remaining after the formation of the Caribbean large igneous province (CLIP) in the Cretaceous period[1], or flow of OIB-type asthenospheric mantle either (2) from beneath the northwest margin of South America[2] or (3) through a slab window[3] into the mantle wedge beneath central Costa Rica. Alternatively, subduction erosion of older Galapagos and CLIP terranes in the Costa Rican fore-arc may have introduced this signature beneath Costa Rica[4]. The geochemical evidence presented here, however, suggests that the OIB signature is primarily derived from the subducting Galapagos hotspot track.

Central American volcanism results from subduction of the Cocos plate beneath the Caribbean plate (Fig. 1). Normal oceanic crust formed at the East Pacific Rise (EPR) subducts beneath Guatemala

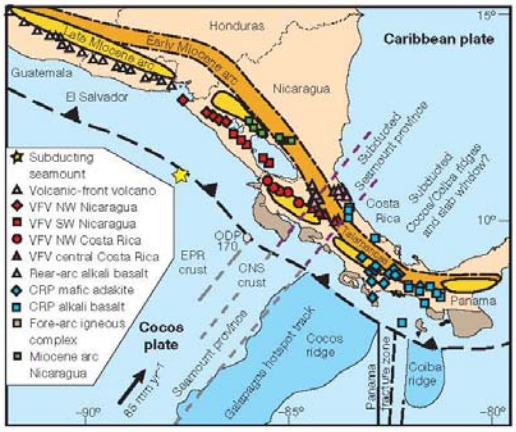

Figure 1 | Reference map of Central America illustrating the subduction of the Galapagos hotspot Seamount province beneath central Costa Rica and the westward migration of the volcanic arc that extends from Costa Rica to southwestern Guatemala. Positions of the arc are shown from the Early Miocene (11–24 Myr ago) to the Late Miocene (6–12 Myr ago) to the Quaternary[30]. The Seamount province of the Galapagos hotspot track is subducting beneath the central Costa Rican volcanic front and Late Pliocene-Holocene (0–2 Myr ago) rear- and back-arc alkali basalts (northeastern occurrences dated at 2 Myr ago). The Cocos and Coiba ridges of the Galapagos hotspot tracks are subducting beneath Pliocene-Holocene mafic adakites and alkali basalts from southeastern Costa Rica and western Panama (CRP), where there has been no volcanic-front volcanism since the Late Miocene. The heavy dashed purple lines project the Seamount province beneath Costa Rica. The boundary between crust formed at the East Pacific Rise (EPR) and the Cocos Nazca (Galapagos) spreading centre (CNS) and the Panama fracture zone are also shown. Volcanic-front volcanoes (VFV) are indicated. A window in the subducting Cocos and Nazca plates may be located beneath southern Costa Rica and western Panama[3].

[1]SFB 574, [2]Leibniz Institute of Marine Sciences (IFM-GEOMAR), University of Kiel, Wischhofstrasse 1-3, Kiel 24148, Germany. [3]Department of Geological Sciences, Brown University, Box 1846, Providence, Rhode Island 02912, USA. [4]Boston University, Department of Earth Sciences, 675 Commonwealth Avenue, Boston, Massachusetts 02215, USA. [5]Observatorio Sismológico y Vulcanológico de Arenal y Miravalles (OSIVAM), Instituto Costarricense de Electricidad (ICE), Apdo. 10032-1000, Costa Rica. [6]Observatorio Vulcanológico y Sismológico de Costa Rica, Universidad Nacional, Apdo. 86-3000, Heredia, Costa Rica. [7]Instituto Nicaragüense de Estudios Territoriales, Apdo. 2110, Managua, Nicaragua. †Present address: Lamont-Doherty Earth Observatory, Columbia University, Palisades, New York 10964, USA.

to northwestern Costa Rica, whereas crust formed at the Cocos-Nazca spreading centre (CNS) with the Galapagos hotspot track on it subducts beneath central Costa Rica to Panama. The Galapagos hotspot tracks (and islands) are chemically zoned[18,19], with the Seamount province having distinctly higher $^{208}Pb/^{204}Pb$ (Figs 1, 2) and lower $^{143}Nd/^{144}Nd$ (Supplementary Fig. 1.1) for a given $^{206}Pb/^{204}Pb$ isotope ratio compared with the Cocos and Coiba ridges.

Radiogenic isotope ratios, which are not fractionated by physical processes such as partial melting and magma differentiation, can be used as tracers to determine the sources contributing to arc magmatism. Along the volcanic front from central Costa Rica to northwestern Nicaragua, Nd isotope ratios increase and Pb isotope ratios decrease continuously (Fig. 2a, b). $^{206}Pb/^{204}Pb$ and $^{208}Pb/^{204}Pb$ isotope data from the volcanic-front rocks also form an excellent linear correlation ($R^2 = 0.997$; Fig. 2c). Although normal arc magmatism ceased in the Late Miocene-Pliocene in southern Costa Rica and western Panama, Pliocene-Quaternary adakitic/alkalic volcanic rocks are widely distributed but volumetrically insignificant[5,20,21]. Lead isotope data from these rocks also form an excellent linear correlation ($R^2 = 0.976$) below, but sub-parallel to, the trend formed by volcanic-front rocks. The highest Pb isotope ratios in the arc rocks occur in the areas situated above the subducting hotspot track, also characterized by radiogenic Pb.

At least three endmembers are required to explain the Pb and Nd isotope data of the Nicaraguan to Panamanian volcanic rocks (see also Supplementary Fig. 1.1). The northwestern Nicaraguan endmember with unradiogenic Pb and radiogenic Nd reflects addition to the depleted mantle wedge of a slab fluid that contains Pb primarily from the subducting crust (as represented by samples from a subducting seamount) (Figs 1, 2). The southern Costa Rica/Panama endmember with radiogenic Pb but intermediate $^{208}Pb/^{204}Pb$ and $^{143}Nd/^{144}Nd$ could be derived from the subducting Cocos/Coiba ridges[3] and/or eroded fore-arc igneous complexes[4], consisting of CLIP basement and accreted early Cenozoic Galapagos seamounts[22–24]. The only source with the appropriate Pb (radiogenic Pb and high $^{208}Pb/^{204}Pb$) and Nd isotopic composition to derive the central Costa Rica endmember is the Seamount province subducting beneath central Costa Rica. Other potential sources for Pb and Nd, such as tectonically eroded Costa Rica fore-arc[4] and input of Galapagos hotspot mantle through a slab window[3] (which would be expected to have a composition similar to the voluminous Cocos/Coiba ridges—representing the primary composition of the Galapagos plume), have isotopic compositions distinct from the Seamount province and thus cannot explain the observed mixing trends.

If the Galapagos seamount slab component has melt-like properties (is a supercritical fluid/hydrous melt), it could readily transport rare-earth elements (for example, La, Nd) and high-field-strength elements (for example, Nb), consistent with the decrease in La/Yb and increase in Ba/La, U/Th and Ba/Th observed in the volcanic-front lavas from central Costa Rica to northwestern Nicaragua[2,25,26] (see Supplementary Information Section 1 for the role of subducted sediments). The transition from a dominantly fluid-like slab component beneath Nicaragua to melt-like slab components in Costa Rica and Panama may be related to the influx of hot mantle through a slab window in the south[3].

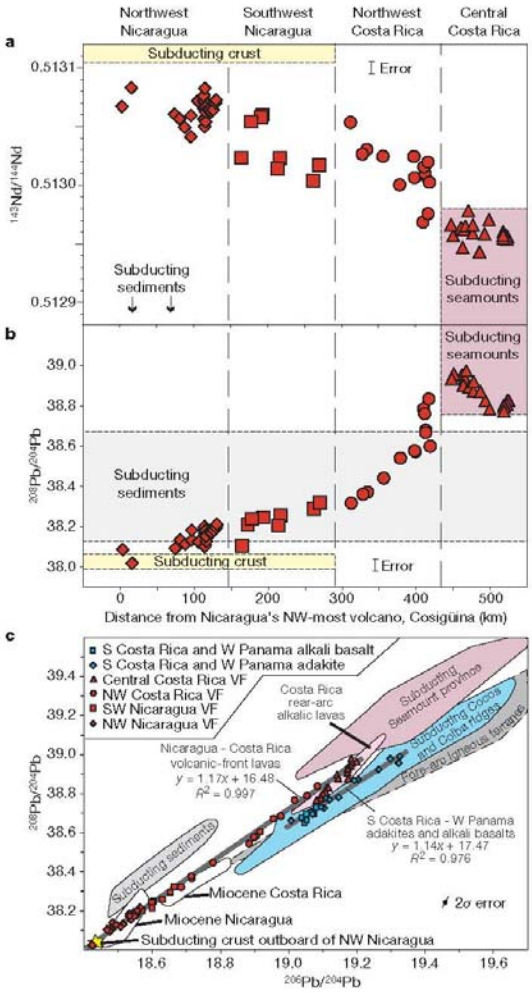

Figure 2 | Systematic variation in lead and neodymium isotopic composition along the volcanic front from Costa Rica to northwest Nicaragua indicates northwestward flow of mantle wedge material. **a**, **b**, Isotope ratios, $^{143}Nd/^{144}Nd$ (**a**) and $^{208}Pb/^{204}Pb$ (**b**), show systematic trends along the arc that indicate mixing of mantle wedge enriched with melts from the subducting Galapagos hotspot Seamount province with mantle wedge enriched with hydrous fluids from the ocean crust subducting beneath Nicaragua. In **c**, Quaternary volcanic front (VF) lavas from Nicaragua and Costa Rica form an excellent linear correlation (longer solid grey line, $R^2 = 0.997$) on the thorogenic Pb isotope diagram. Late Pliocene-Quaternary rear- and back-arc alkalic lavas in northeastern Costa Rica overlap in composition with Costa Rica volcanic-front lavas but extend to more radiogenic compositions, consistent with a greater contribution from a melt-like slab component. Low volume, scattered Pliocene-Quaternary mafic adakites and alkali basalts from southern Costa Rica and western Panama, where there has been no volcanic-front volcanism since the Late Miocene, form a distinct linear array (shorter solid grey line, $R^2 = 0.976$) below but subparallel to the volcanic-front lavas, having lower $^{208}Pb/^{204}Pb$ for a given $^{206}Pb/^{204}Pb$ isotope ratio. Whereas the adakites may represent direct melts of subducted Galapagos rocks, the alkali basalts most probably reflect interaction between carbon-rich fluids/melts from Galapagos material and the overlying mantle wedge. The difference in Pb isotopic composition between the Pliocene-Quaternary central Costa Rica and the southern Costa Rica/western Panama lavas correlates closely with the boundary between the subducting Seamount province and Cocos/Coiba ridges of the chemically zoned Galapagos hotspot track. The subducting Seamount province and the Cocos/Coiba ridges, which have distinct Pb and Nd (Supplementary Fig. 1.1) isotopic compositions[18,19], could serve as the endmembers necessary for generating the distinct isotopic compositions of the central Costa Rica and southern Costa Rica/western Panama lavas, respectively. Fields for (1) fore-arc igneous terranes, which includes CLIP basement from Costa Rica and Panama[22,23,25] and (2) sediments and ocean crust subducting beneath Nicaragua[1,19] are also shown. All errors are reported as 2σ of the mean.

The along-arc variations in volcanic-front isotopic composition indicate that the Galapagos seamount component diminishes in quantity towards northwestern Nicaragua. These trends cannot be produced by upper plate variation. Although CLIP lithosphere underlies Costa Rica, its composition (included in the fore-arc igneous terranes field in Fig. 2c) is distinct from that of the Seamount province[22,23]. The volcanic-front isotopic trends also cannot be explained by systematic changes in the composition of the subducting plate. During ODP Leg 170, gabbro sills with OIB-type geochemical characteristics were drilled about 80 km north of the Seamount province[27], suggesting that the Galapagos hotspot may have affected a larger area than represented by the morphological expression of the hotspot track. However, it is unlikely that the plume spread out 500 km north of the Cocos ridge. When the hotspot track off Costa Rica formed, the CNS was located to the south of the hotspot[19], and plume material would have flowed south towards the ridge (not north). In addition, the gabbro sills from Leg 170 do not have Pb isotopic compositions that plot within the Seamount province, but rather compositions that plot within the Cocos/Coiba ridge field (Supplementary Information Section 1). Finally, a seamount on the Cocos plate subducting beneath central Nicaragua shows no evidence for the presence of Galapagos-type material in this area[19] but rather has the appropriate composition to serve as the depleted Nicaraguan endmember.

As the seamount component only appears to be present on the incoming plate off the Pacific coast of central Costa Rica, this signature must have been introduced into the wedge by a melt-like slab component from the subducting Seamount province and then transported northwest in the mantle wedge in melt pockets (possibly crystallized to form pyroxenite after leaving the slab and reacting with the overlying mantle wedge peridotite). Fluids from the subducting plate beneath Nicaragua flux the wedge, causing melting and mixing with the Galapagos seamount component. As the mantle is transported northwestwards, the seamount component will be progressively flushed out of the wedge, causing a decrease in Pb and increase in Nd isotopic composition.

Seismic anisotropy in the mantle wedge beneath Nicaragua and Costa Rica provides corroborating evidence for arc-parallel flow. Shear-wave splitting was measured in local S phases recorded by a dense temporary deployment of broadband seismometers (Supplementary Fig. 2.1), and a three-dimensional model of anisotropy was obtained (Fig. 3) by tomographically inverting the splitting measurements[28]. Beneath the arc where the Galapagos geochemical signature is observed and further into the back-arc, anisotropy is dominated by roughly arc-parallel alignment of the olivine fast symmetry axis (*a* axis). These *a* axes extend well into the warmer wedge where they should align roughly parallel to flow[6]. A zone of arc-normal *a* axes appears beneath the northwestern end of the Nicaraguan arc where geochemical evidence for the Galapagos seamount component is nearly absent, perhaps suggesting a reduction in arc-parallel flow.

The isotope data allow an along-arc flow rate for the mantle in the wedge to be directly estimated. Given that samples from the Miocene Nicaraguan arc (7–24 Myr old) adjacent to Quaternary southwest Nicaraguan rocks (Fig. 1) have Pb isotope ratios that overlap the range in the Quaternary northwest Nicaraguan volcanic front (Fig. 2), the component with elevated Pb isotope ratios was presumably introduced into the mantle beneath Nicaragua after the Miocene. Igneous rocks from the Miocene arc (6–26 Myr old) in Costa Rica have slightly more radiogenic isotopic compositions than those from Nicaragua, which could reflect interaction with CLIP lithosphere or derivation from subduction of older Galapagos hotspot tracks[24]. The Seamount province composition is not however observed in the Miocene volcanic rocks, providing a maximum age for the appearance of this component of ~6 Myr. Assuming that the oldest part of the subducted Seamount province lies along its boundary with the Panama fracture zone (Fig. 1), it would have passed beneath the central Costa Rican volcanic front 2–3 Myr ago[21] (reversing subduction at a rate of 85 mm yr^{-1}), providing a minimum age of 2 Myr for the appearance of the seamount component beneath the arc.

These dates (2–6 Myr ago) imply that the minimum arc-parallel wedge flow ranges from 63 to 190 mm yr^{-1}, assuming the Galapagos seamount component is transported a distance of 380 km. This distance is measured from the northwesternmost Nicaraguan volcano (Casitas) that shows a clear geochemical influence of the subducting

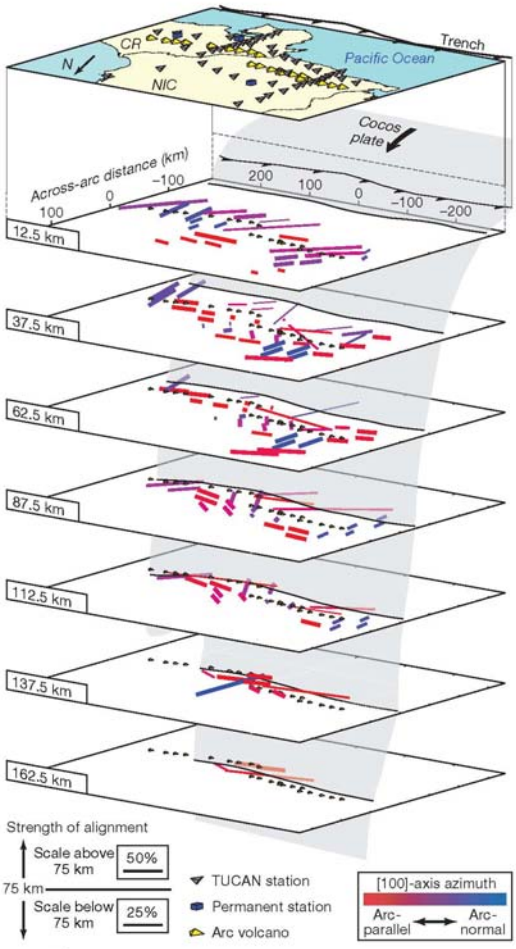

Figure 3 | Model of anisotropy obtained by inverting shear-wave splitting measurements from events in the Nicaragua (NIC)-Costa Rica (CR) subduction zone. The inversion used a tomographic approach[28] (see Methods and Supplementary Information Section 2). The vectors represent well-resolved olivine *a* axes in an olivine-orthopyroxene model, with orientation and colour indicating horizontal azimuth. Vector length corresponds to the strength of anisotropy relative to single-crystal values; note the change in strength scale at 75 km depth. We also invert for *a*-axis dip, but for clarity here we project *a* axes onto map-view planes. Effective block size in the rear- and back-arc is larger. Only well-resolved regions of the model are shown, and vector thickness corresponds to model parameter resolution. The TUCAN seismic array and volcanic arc are shown at the surface, and for reference, the volcanic arc is plotted on each slice through the model. The slab–wedge interface, based on earthquake locations, is shown by grey shading. The top two layers primarily lie within the upper plate; the mantle wedge is located in front of the slab in the layers spanning 50–175 km. Roughly arc-parallel *a* axes dominate well-resolved wedge regions beneath the arc and the rear- and back-arc at depths of 50–150 km, with the exception of a zone of arc-normal *a* axes at the northwestern end of the arc in Nicaragua and one isolated model block deep beneath the back-arc.

Seamount province (more radiogenic Pb and less radiogenic Nd than Cosigüina volcano and the crust subducting beneath Nicaragua) to the location of maximum Pb isotopic composition (greatest amount of Galapagos seamount component) in central Costa Rica. These transport rates are of the order of the Cocos plate subduction rate (~85 mm yr^{-1} off Costa Rica), suggesting that lateral (arc/trench-parallel) flow in the mantle wedge can compete with flow entrained by subduction.

Lead isotope data demonstrate that rapid arc-parallel flow occurs in the mantle wedge beneath Costa Rica and Nicaragua, allowing arc-parallel fast anisotropy to be explained without atypical mechanisms of generating anisotropic fabrics[5,14]. Trench rollback, variations in slab dip, and arc-parallel shearing within the upper plate may all contribute to along-arc wedge flow[9,13,16]. In Costa Rica and Nicaragua, the fore-arc is translating to the northwest, although at less than 15 mm yr^{-1} (ref. 29). Westward migration of the volcanic front since the early Miocene was greatest in Nicaragua and Honduras/El Salvador[30] (Fig. 1) where slab dips are steepest, suggesting differential slab roll-back that could draw wedge material towards northwestern Nicaragua, possibly from a slab window to the south. Collision (indenture) of the thickened Cocos ridge crust with the margin could also have helped drive arc material northwards. Regardless of the mechanism for generating flow, this study demonstrates a rate of arc-parallel flow beneath Costa Rica and Nicaragua that rivals downgoing Cocos plate motion.

METHODS SUMMARY

Nd and Pb isotope analyses were carried out at IFM-GEOMAR by thermal ionization mass spectrometry (TIMS), using a Triton and a MAT262 RPQ^{2+} TIMS, respectively. Over the course of the study, La Jolla produced $^{143}Nd/^{144}Nd = 0.511846 \pm 0.000005$ ($N = 49$) and the long-term reproducibility of NBS 981 ($n = 184$) is $^{206}Pb/^{204}Pb = 16.899 \pm 0.007$, $^{207}Pb/^{204}Pb = 15.437 \pm 0.009$, $^{208}Pb/^{204}Pb = 36.525 \pm 0.028$. Total chemistry blanks were <100 pg for Nd and Pb, and thus are considered negligible.

We solve for a best-fitting model of anisotropy through an iterative, damped, least-squares inversion[28] of 791 local-S splitting measurements from the TUCAN broadband seismic experiment. Anisotropy is described by a hexagonal average of olivine and orthopyroxene elastic coefficients, and parameters in each model block are the azimuth and plunge of the olivine *a* axis and a scalar that controls the strength of anisotropy. A total of 100 iterations were realized, with a moderate relaxation of damping after iteration 40. Model blocks are 25 km on each side, although in back-arc regions constraints were applied after iteration 70 that forced model parameters to be uniform across groups of blocks. Predicted splitting measurements and partial derivatives were calculated at every iteration for each hypocentre–station pair by progressively splitting an initially linearly polarized wavelet to account for the anisotropy encountered in each model block along the phase path.

Full Methods and any associated references are available in the online version of the paper at www.nature.com/nature.

Received 23 July; accepted 5 December 2007.
Published online 21 January 2008.

1. Feigenson, M. D., Carr, M. J., Maharaj, S. V., Juliano, S. & Bolge, L. L. Lead isotope composition of Central American volcanoes: Influence of the Galapagos plume. *Geochem. Geophys. Geosyst.* **5**, Q06001, doi:10.1029/2003GC000621 (2004).
2. Herrstrom, E. A., Reagan, M. K. & Morris, J. D. Variations in lava composition associated with flow of asthenosphere beneath southern Central America. *Geology* **23**, 617–620 (1995).
3. Abratis, M. & Wörner, G. Ridge collision, slab window formation, and the flux of Pacific asthenosphere into the Caribbean realm. *Geol. Soc. Am.* **29**, 127–130 (2001).
4. Goss, A. R. & Kay, S. M. Steep REE patterns and enriched Pb isotopes in southern Central American arc magmas: Evidence for forearc subduction erosion? *Geochem. Geophys. Geosyst.* **7**, Q05016, doi:10.1029/2005GC001163 (2006).
5. Jung, H. & Karato, S.-i. Water-induced fabric transition in olivine. *Science* **293**, 1460–1463 (2001).
6. Kneller, E. A., van Keken, P. E., Karato, S.-i. & Park, J. B-type olivine fabric in the mantle wedge: Insights from high-resolution non-Newtonian subduction zone models. *Earth Planet. Sci. Lett.* **237**, 781–797 (2005).
7. Nakajima, J., Shimizu, J., Hori, S. & Hasegawa, A. Shear-wave splitting beneath the southwestern Kurile arc and northeastern Japan arc: A new insight into mantle return flow. *Geophys. Res. Lett.* **33**, L05305, doi:10.1029/2005GL025053 (2006).
8. Long, M. D. & van der Hilst, R. D. Upper mantle anisotropy beneath Japan from shear wave splitting. *Phys. Earth Planet. Inter.* **151**, 206–222 (2006).
9. Smith, G. P. *et al.* A complex pattern of mantle flow in the Lau backarc. *Science* **292**, 713–716 (2001).
10. Levin, V., Droznin, D., Park, J. & Gordeev, E. Detailed mapping of seismic anisotropy with local shear waves in southeastern Kamchatka. *Geophys. J. Int.* **158**, 1009–1023 (2004).
11. Anderson, M. L., Zandt, G. & Wagner, L. Along-strike mantle flow variations in a segment of the South American subduction zone, Chile and Argentina. *Earth Planet. Sci. Lett.* (submitted).
12. Pozgay, S. H., Wiens, D. A., Conder, J. A., Shiobara, H. & Sugioka, H. Complex mantle flow in the Mariana subduction system: Evidence from shear wave splitting. *Geophys. J. Int.* **107**, 371–386 (2007).
13. Hall, C. E., Fischer, K. M. & Parmentier, E. M. The influence of plate motions on three dimensional back-arc mantle flow and shear wave splitting. *J. Geophys. Res.* **105**, 28009–28033 (2000).
14. Holtzman, B. K. *et al.* Melt segregation and strain partitioning: Implications for seismic anisotropy and mantle flow. *Science* **301**, 1227–1230 (2003).
15. Behn, M. D., Hirth, G. & Kelemen, P. B. Trench-parallel anisotropy produced by foundering of arc lower crust. *Science* **317**, 108–111 (2007).
16. Kneller, E. A. & van Keken, P. E. Trench-parallel flow and seismic anisotropy in the Mariana and Andean subduction systems. *Nature* **450**, 1222–1225 (2007).
17. Reagan, M. K. & Gill, J. B. Coexisting calcalkaline and high-niobium basalts from Turrialba volcano, Costa Rica: Implications for residual titanates in arc magma sources. *J. Geophys. Res.* **94**, 4619–4633 (1989).
18. Hoernle, K. A., Werner, R., Phipps Morgan, J., Bryce, J. & Mrazek, J. Existence of a complex spatial zonation in the Galápagos plume for at least 14.5 Ma. *Geology* **28**, 435–438 (2000).
19. Werner, R., Hoernle, K., Barckhausen, U. & Hauff, F. Geodynamic evolution of the Galapagos hot spot system (Central East Pacific) over the past 20 m.y.: Constraints from morphology, geochemistry, and magnetic anomalies. *Geochem. Geophys. Geosyst.* **4**, doi:10.1029/2003GC000576 (2003).
20. Defant, M. J. *et al.* The geology and geochemistry of El Valle volcano, Panama: Andesite and dacite genesis via contrasting processes. *Contrib. Mineral. Petrol.* **106**, 309–324 (1991).
21. MacMillan, I., Gans, P. B. & Alvarado, G. Middle Miocene to present plate tectonic history of southern Central American volcanic arc. *Tectonophysics* **392**, 325–348 (2004).
22. Hoernle, K., Hauff, F. & van den Bogaard, P. 70 m.y. history (139–69 Ma) for the Caribbean large igneous province. *Geology* **32**, 697–700 (2004).
23. Hauff, F., Hoernle, K. A., van den Bogaard, P., Alvarado, G. E. & Garbe-Schönberg, D. Age and geochemistry of basaltic complexes in Western Costa Rica: Contributions to the geotectonic evolution of Central America. *Geochem. Geophys. Geosyst.* **1**, doi:10.1029/1999GC000020 (2000).
24. Hoernle, K. A. *et al.* The missing history (16–71 Ma) of the Galápagos hotspot: Implications for the tectonic and biological evolution of the Americas. *Geology* **30**, 795–798 (2002).
25. Patino, L. C., Carr, M. J. & Feigenson, M. D. Local and regional variations in Central American arc lavas controlled by variations in subducted sediment input. *Contrib. Mineral. Petrol.* **138**, 265–283 (2000).
26. Carr, M. J., Feigenson, M. D. & Bennett, E. A. Incompatible element and isotopic evidence for tectonic control of source mixing and melt extraction along the Central American arc. *Contrib. Mineral. Petrol.* **105**, 369–380 (1990).
27. Kimura, G. *et al.* SITE 1039 (Ch. 3); SITE 1040 (Ch. 4). *Proc. ODP Init. Rep.* **170**, 45–152 (1997).
28. Abt, D. L. & Fischer, K. M. Resolving three-dimensional anisotropic structure with shear-wave splitting tomography. *Geophys. J. Int.* (submitted).
29. Turner, H. L. *et al.* Kinematics of the Nicaraguan forearc from GPS geodesy. *Geophys. Res. Lett.* **34**, L02302, doi:10.1029/2006GL027586 (2007).
30. Alvarado, G. E. *et al.* in *Central America: Geology, Resources and Hazards* (eds Bundschuh, J. & Avarado, G.) 345–394 (Taylor and Francis, Leiden, 2007).

Supplementary Information is linked to the online version of the paper at www.nature.com/nature.

Acknowledgements Reviewers (J. Walker and S. Schwartz), J. Phipps-Morgan, T. Plank, R. Werner, M. Portnyagin and members of SFB574 and MARGINS are thanked for comments/discussions that helped significantly improve the manuscript. The IRIS PASSCAL programme provided seismometers and technical assistance to the TUCAN experiment. This research was supported by the German Science Foundation Collaborative Research Centre (SFB574) and the National Science Foundation MARGINS programme.

Author Contributions K.H., D.L.A. and K.M.F. collected samples/data, processed and interpreted the data, developed the ideas and wrote the paper, with significant input from G.A.A. and discussions with other co-authors. H.N., F.H. and K.H. generated the geochemical data and P.v.d.B. age data. G.A.A., M.P. and W.S. were key in collecting the seismic data; P.v.d.B., G.A. and H.N. assisted in the collection of the volcanic samples. Central American partners provided geological overviews and logistical support.

Author Information Reprints and permissions information is available at www.nature.com/reprints. Correspondence and requests for materials should be addressed to K.H. (khoernle@ifm-geomar.de).

doi:10.1038/nature06550 nature

METHODS

Sample preparation and isotope analyses. Samples used in this study were cleaned of surficial dirt and then coarsely crushed into chips smaller than 4 cm. The chips were sieved and washed with deionized water, followed by ~12 h drying in a warm (50 °C) oven. Approximately 30–60 g of clean chips were hand-picked under a binocular microscope and ground to sand-sized particles in a mechanized agate mortar and pestle, followed by fine grinding in an agate mill by a shatter box. A subset of 0.5–1.0 mm sized chips was saved for Pb isotope analyses. Sample dissolution and element chromatography were carried out at the Leibniz Institute of Marine Sciences IFM-GEOMAR in Kiel (Germany) in Class 1000 clean rooms that are equipped with Class 100 laminar flow hoods. All reagents used were either double distilled in a PicoTrace Teflon distillery (HCl and HNO_3) or certified ultrapure HF and HBr acids from SEASTAR. An ELGA purifying system provided 18.2 MΩ water. Nd and Pb isotope analyses were carried out on whole rock powders (Nd) and rock chips (Pb) that were leached in hot 2 M HCl (70 °C, 1 h) in order to minimize the effects of alteration and sample handling. About 100 mg of sample was weighed into a Teflon beaker and then dissolved for 2 days in a 5:1 mixture of ultrapure HF and HNO_3 at 150 °C.

The ion chromatography followed established standard procedures[31]. These include a two-pass Pb separation and clean-up using 100 µl Teflon microcolumns filled with Bio-Rad AG 1X8 (100–200 mesh) resin that is equilibrated with 1 M HBr for highest Pb retention and from which Pb is released with 1 ml of 6 M HCl. The rare-earth elements (REEs) are obtained in 6 ml 6 M HCl at the final washout during Rb-Sr separation on quartz glass columns filled with Bio-Rad AG50W-X8 (100–200 mesh) resin. The REEs are then loaded in 0.25 M HCl onto 4 ml quartz glass columns filled with Eichrom Ln-Spec resin (100–150 µm) to obtain the Nd fraction. Pb and Nd isotopic ratios were determined by TIMS at IFM-GEOMAR on a MAT262 RPQ^{2+} and Triton TIMS, respectively. Both instruments operate in static multi-collection mode. Nd isotopic ratios are normalized within each run to $^{146}Nd/^{144}Nd = 0.7219$ and all errors are reported as 2σ of the mean. Over the course of the study, La Jolla produced $^{145}Nd/^{144}Nd = 0.511846 \pm 0.000005$ ($N = 49$) and our in-house Nd-monitor SPEX $^{143}Nd/^{144}Nd = 0.511711 \pm 0.000006$ ($N = 39$). Nd replicate analyses (separate digests) of 4 samples were within the external errors of the standards. The long-term reproducibility of NBS 981 ($N = 184$) is $^{206}Pb/^{204}Pb = 16.899 \pm 0.007$, $^{207}Pb/^{204}Pb = 15.437 \pm 0.009$, $^{208}Pb/^{204}Pb = 36.525 \pm 0.028$. Pb isotope ratios are normalized to published NBS 981 values[32]. Pb replicate analyses (separate digests) of 13 samples were on the average better than 0.022% per AMU. Total chemistry blanks were <100 pg for Nd and Pb and thus are considered negligible.

Shear-wave splitting analysis and tomography method. We analysed shear-wave splitting in local S phases recorded by the TUCAN broadband seismic experiment and by three permanent stations, maintained by the GSN (IRIS), GEOSCOPE (France) and GEOFON (Germany). Over the 20-month deployment, we obtained 791 high-quality splitting measurements (Supplementary Fig. 2.1) using an eigenvalue minimization method[33]. We inverted these local S splitting measurements for a three-dimensional model of anisotropy (Fig. 3 and Supplementary Fig. 2.3).

Here we briefly highlight the key aspects of this technique; the method is described in detail elsewhere[29]. The elastic coefficients of the anisotropic model were assumed to be an average of olivine and orthopyroxene[34–36]. The model was divided into blocks (25 km per side), and parameters in each block are the azimuth and plunge of the olivine *a* axis and a scalar value that controls the strength of anisotropy relative to its single-crystal value. The model in Fig. 3 and Supplementary Fig. 2.3 assumes hexagonal symmetry for the anisotropy, but inversions assuming orthorhombic symmetry yield similar results.

The inversion was conducted using an iterative, damped least-squares approach. The starting model was constructed by prescribing the average fast direction for all phases that sample a block as the olivine *a* axis azimuth in that block. The fabric strength in the starting model was based on the average splitting times from each ray within a block relative to that predicted from the single-crystal elastic coefficients. Synthetic splitting was calculated by propagating, for each ray, an initially linearly polarized wavelet through successive anisotropic blocks along its path and accruing splitting from each block until the phase reached the station[37]. Shear-wave splitting parameters were determined from the resulting waveform using the same method applied to the data[33] and then were used to calculate data–model residuals and partial derivatives.

Inversions were performed using a wide variety of starting models, block sizes and damping parameters. Even when optimal inversion parameters were used, some model blocks in the back-arc remained poorly resolved because of reduced ray coverage. Therefore, effective block size was made larger in back-arc regions to permit interpretation of a larger portion of the model space, albeit at coarser spatial resolution. The size of these larger (non-cubic) model volumes is variable, but is typically 50 km thick and between 50 km and 100 km in each horizontal direction (Supplementary Fig. 2.4).

To test the accuracy with which the *a* axis orientation and fabric strength can be retrieved, inversions of synthetic data predicted by a series of anisotropic target models were carried out using the source–station distribution for the TUCAN shear-wave splitting data set[28]. For target models that vary laterally in better sampled model regions (beneath the fore-arc, arc, and regions of the back-arc near the dense arc-normal lines of stations) with uniform anisotropy elsewhere, *a* axis orientation is retrieved to within 25° on average; *a* axis azimuth is, in general, recovered at high accuracy down to at least 100 km depth, and *a* axis dip recovery is typically good to roughly 75 km. Lateral variations at spatial scales of 50–75 km can be imaged beneath the arc, but retrievable spatial variations are obviously coarser in back-arc regions where individual blocks are grouped into larger volumes (Supplementary Fig. 2.4).

31. Hoernle, K. A. & Tilton, G. R. Sr-Nd-Pb isotope data for Fuerteventura (Canary Islands) basal complex and subaerial volcanics: Applications to magma genesis and evolution. *Schweiz. Mineral. Petrogr. Mitt.* **71,** 3–18 (1991).
32. Todt, W., Cliff, R. A., Hanser, A. & Hofmann, A. W. in *Earth Processes: Reading the Isotopic Code* (eds Basu, A. & Hart, S.) 429–437 (AGU Geophys. Monogr. Ser. 95, American Geophysical Union, Washington DC, 1996).
33. Silver, P. G. & Chan, W. W. Shear wave splitting and subcontinental mantle deformation. *J. Geophys. Res.* **96,** 16429–16454 (1991).
34. Frisillo, A. L. & Barsch, G. R. Measurement of single-crystal elastic constants of bronzite as a function of pressure and temperature. *J. Geophys. Res.* **77,** 6360–6384 (1972).
35. Anderson, O. L. & Isaak, D. G. in *Mineral Physics and Crystallography: A Handbook of Physical Constants* (ed. Ahrens, T. J.) 64–97 (American Geophysical Union, Washington DC, 1995).
36. Abramson, E. H., Brown, J. M., Slutsky, L. J. & Zaug, J. The elastic constants of San Carlos olivine to 17 GPa. *J. Geophys. Res.* **102,** 12253–12263 (1997).
37. Fischer, K. M., Parmentier, E. M., Stein, A. R. & Wolf, E. R. Modeling anisotropy and plate-driven flow in the Tonga subduction zone back arc. *J. Geophys. Res.* **105,** 16181–16191 (2000).

doi: 10.1038/nature06550 nature

SUPPLEMENTARY INFORMATION

Supplementary Information Section 1

The Role of Sediments

The Be and Th isotope systematics of some of the Central Nicaraguan magmas show evidence for the involvement of subducted sediments[38], yet evidence for subducted sediments are not clearly seen in the Pb isotopes. This is likely due to different behavior (decoupling) between highly fluid-mobile Pb and relatively fluid-immobile Be and Th and suggests that fluid-mobile Pb is flushed out of the sediments at shallower depths than fluid-immobile Be and Th. *Rüpke et al.*[39] point out that fluids derived from serpentinite on the downgoing slab beneath Nicaragua are likely to be highly reactive and could mobilize Be (and possibly Th) as they pass through the overlying subducted sediments. The excellent linear correlation on the radiogenic Pb isotope diagram (Fig. 2c) indicates that just two components are necessary to explain the Pb isotopes for Costa Rica and Nicaragua volcanic front volcanoes. Mixing between three components would not generate a binary mixing array unless two components have identical compositions, which is not the case with sediments and depleted MORB-type crust. The other alternative is that one of the components forming the binary array is itself a mixture of multiple components, for example, that we have an integrated slab fluid coming off the slab under Nicaragua containing Pb from the magmatic crust and sediments. This integrated slab fluid could then mix with the mantle wedge containing the Galapagos seamount component; however, due to the very unradiogenic Pb isotopic composition of the depleted endmember of the array (seen at Cosigüina and the incoming plate crust) an integrated slab fluid could not contain much sediment Pb.

Subducting sediments are also likely to be the main source of fluid-mobile elements such as Ba and U[23,38]. Variations in ratios of fluid-mobile to fluid-immobile elements (e.g. Ba/La, U/Th and Ba/Th) in northwest Nicaragua are likely to reflect variable fluid fluxes from the subducting sediments beneath northwest Nicaragua.

Additional References

38. Reagan, M. K., Morris, J. D., Herrstrom, E. A. & Murrell, M. T. Uranium series and beryllium isotope evidence for an extended history of subduction modification of the mantle below Nicaragua. *Geochimica et Cosmochimica Acta* **58**, 4199-4212 (1994).
39. Rüpke, L., Phipps Morgan, J., Hort, M. & Connolly J. A. D. Are the regional variations in Central American arc lavas due to differing basaltic versus peridotitic slab sources of fluids? *Geology* **30**, 1035-1038 (2002).

doi: 10.1038/nature06550 SUPPLEMENTARY INFORMATION

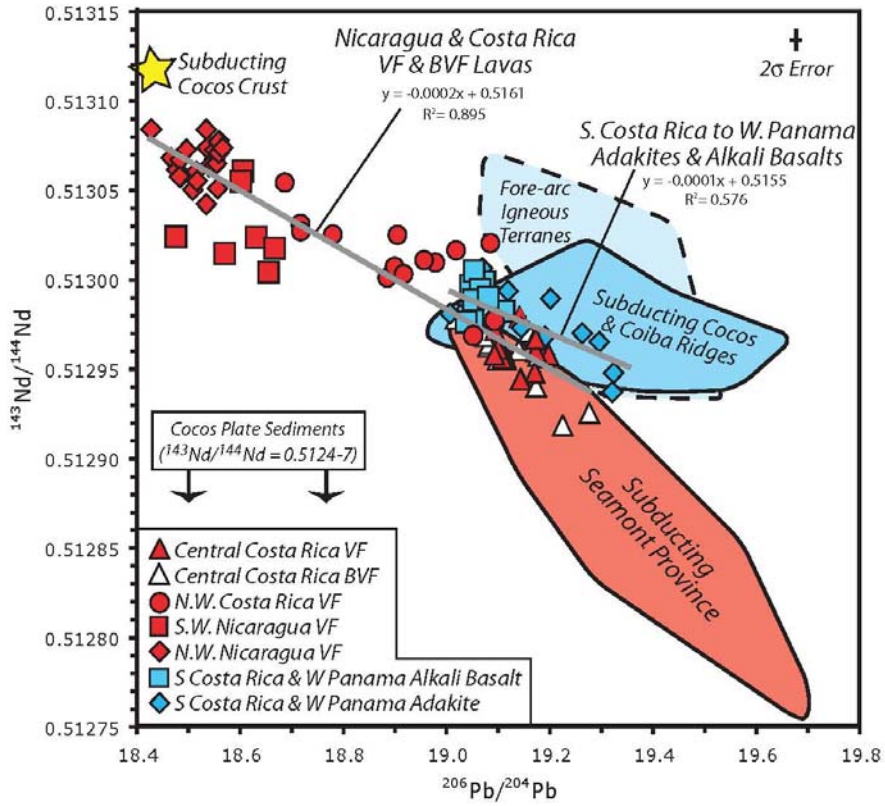

Figure S1.1. Pb vs Nd isotope data for Costa Rica and Nicaragua volcanic front (VF), Costa Rica behind the volcanic front (BVF) alkalic rocks, and southern Costa Rica and western Panama adakites and alkali basalts. At least three endmembers are required to explain the Pb and Nd isotope data of Central American volcanic rocks. The NW Nicaraguan endmember with unradiogenic Pb and radiogenic Nd can be explained by mixing slab fluids from subducting EPR oceanic crust (+/- sediments) with depleted mantle wedge. The southern Costa Rica/western Panama endmember with radiogenic Pb but intermediate $^{208}Pb/^{204}Pb$ and $^{143}Nd/^{144}Nd$ could be derived from the subducting Cocos/Coiba Ridges and/or eroded fore-arc igneous complexes. The only source with the appropriate Pb (radiogenic Pb and high $^{208}Pb/^{204}Pb$) and unradiogenic Nd isotopic composition to derive the central Costa Rica endmember is the Seamount Province subducting beneath Central Costa Rica. Other potential sources for Pb and Nd, such as tectonically eroded Costa Rica fore-arc and input of Galapagos hotspot mantle through a slab window (which would be expected to have a composition similar to the voluminous Cocos/Coiba Ridges – representing the primary composition of the Galapagos plume), have isotopic compositions distinct from the Seamount Province and so cannot explain the observed mixing trends. See Figure 2 caption for additional information and data sources.

doi: 10.1038/nature06550

Table S1.1

Sample #	Sample Location	Lat	Long	$^{143}Nd/^{144}Nd$	2σ	ϵ_{Nd}	$^{206}Pb/^{204}Pb$	2σ	$^{207}Pb/^{204}Pb$	2σ	$^{208}Pb/^{204}Pb$	2σ
NW Nicaragua Volcanic Front												
P-58A	Cosigüina	13.0336	-87.5918	0.513068	0.000003	8.38	18.464	0.001	15.518	0.001	38.091	0.002
P-60	Cosigüina	12.8671	-87.5551	0.513084	0.000003	8.69	18.425	0.001	15.507	0.001	38.023	0.002
P-27A	San Cristobal	12.6811	-87.0278	0.513061	0.000002	8.26	18.475	0.002	15.519	0.002	38.099	0.005
P-13	Casitas	12.6857	-86.9553	0.513057	0.000003	8.18	18.483	0.001	15.533	0.001	38.140	0.002
P2-16	Telica	12.5965	-86.9322	0.513050	0.000002	8.04	18.506	0.001	15.515	0.001	38.118	0.002
P-7A	Telica	12.6073	-86.8332	0.513060	0.000002	8.23	18.513	0.001	15.520	0.001	38.139	0.003
P-9	Telica	12.6051	-86.8361	0.513042	0.000003	7.88	18.532	0.001	15.534	0.001	38.188	0.002
P-43	Cone3	12.5334	-86.6774	0.513051	0.000002	8.05	18.554	0.001	15.521	0.001	38.180	0.003
P-51	Cone2	12.4696	-86.7232	0.513067	0.000006	8.36	18.481	0.001	15.520	0.001	38.114	0.002
P-56G	C. Las Palmitas	12.6072	-86.7329	0.513073	0.000004	8.48	18.493	0.001	15.525	0.001	38.131	0.002
P-4	C. Negro	12.5076	-86.7009	0.513078	0.000006	8.57	18.557	0.002	15.529	0.001	38.205	0.003
P-6	C. Negro	12.5023	-86.7005	0.513066	0.000003	8.34	18.546	0.003	15.529	0.002	38.195	0.006
P2-3a	C. Negro	12.4987	-86.7035	0.513071	0.000003	8.45						
P2-3b	C. Negro	12.4987	-86.7035	0.513072	0.000002	8.47	18.538	0.002	15.522	0.002	38.171	0.005
P2-3d	C. Negro	12.4987	-86.7035	0.513074	0.000003	8.50	18.533	0.002	15.526	0.002	38.172	0.005
P2-11	C. Negro	12.4984	-86.7058	0.513072	0.000003	8.47	18.549	0.002	15.523	0.001	38.184	0.003
P2-13	C. Negro	12.5105	-86.7075	0.513077	0.000004	8.56	18.555	0.001	15.530	0.001	38.205	0.002
P-50	C. Diablo	12.4726	-86.7236	0.513057	0.000002	8.18	18.480	0.001	15.519	0.001	38.107	0.002
P-19	Las Pilas	12.4933	-86.6861	0.513055	0.000002	8.13	18.514	0.003	15.518	0.002	38.133	0.006
P-40A	Cabeza de Vaca	12.5195	-86.6815	0.513084	0.000006	8.69	18.532	0.001	15.526	0.001	38.175	0.002
P-42	Cabeza de Vaca	12.5198	-86.6807	0.513067	0.000003	8.37	18.549	0.002	15.526	0.002	38.187	0.005
P-23	Ojo de Agua	12.5145	-86.6806	0.513063	0.000003	8.30	18.537	0.002	15.520	0.001	38.157	0.003
P-46A	Laguna Asos	12.4402	-86.6716	0.513065	0.000002	8.32	18.550	0.001	15.523	0.001	38.180	0.002
P-47A	C. Buena vista	12.4005	-86.6643	0.513063	0.000002	8.30	18.548	0.001	15.521	0.001	38.176	0.002
P-48B	Cone4	12.3727	-86.6500	0.513065	0.000002	8.33	18.552	0.001	15.525	0.001	38.188	0.002
P-32	Momotombo	12.4278	-86.5808	0.513071	0.000003	8.44	18.557	0.001	15.527	0.001	38.202	0.003
P-34	Momotombo	12.4565	-86.5560	0.513073	0.000003	8.49	18.564	0.001	15.533	0.001	38.217	0.002
SW Nicaragua Volcanic Front												
P2-32d	Nejapa crater	12.2308	-86.3173	0.513024	0.000003	7.53	18.472	0.001	15.525	0.001	38.111	0.003
P2-53	Nejapa	12.0830	-86.3245				18.599	0.004	15.520	0.004	38.215	0.009
P-68B	Masaya	12.0123	-86.1447	0.513061	0.000003	8.25	18.603	0.003	15.530	0.002	38.251	0.006
P-71A	Masaya	12.0027	-86.1699	0.513059	0.000002	8.21						
P2-47	Masaya	12.0870	-86.2620	0.513055	0.000002	8.13	18.597	0.000	15.528	0.000	38.244	0.001
P-63	Cone near Mombacho	11.8402	-85.9952	0.513024	0.000002	7.53	18.628	0.002	15.526	0.002	38.260	0.004
P2-58	Cone near Mombacho	11.8920	-85.9926	0.513015	0.000002	7.35	18.567	0.001	15.526	0.001	38.211	0.003
P-86A	Concepcion	11.5552	-85.6743	0.513004	0.000002	7.15	18.652	0.002	15.529	0.002	38.295	0.005
P-80A	Maderas	11.4963	-85.6245	0.513018	0.000002	7.41	18.663	0.003	15.538	0.003	38.323	0.007

doi: 10.1038/nature06550

Table S1.1 (cont.)

Sample #	Sample Location	Lat	Long	$^{143}Nd/^{144}Nd$	2σ	ϵ_{Nd}	$^{206}Pb/^{204}Pb$	2σ	$^{207}Pb/^{204}Pb$	2σ	$^{208}Pb/^{204}Pb$	2σ
NW Costa Rica Volcanic Front												
CR-44	Orosi	11.0593	-85.4278	0.513054	0.000002	8.12	18.683	0.003	15.528	0.002	38.323	0.005
CR-35	Rincon	10.7543	-85.3740	0.513031	0.000002	7.67	18.714	0.002	15.536	0.002	38.378	0.005
CR-56	Rincon	10.8975	-85.3540	0.513027	0.000003	7.59	18.714	0.002	15.530	0.002	38.367	0.004
P2-118	Miravalles	10.7123	-85.1662	0.513025	0.000002	7.56	18.777	0.001	15.539	0.001	38.447	0.002
CR-30	Canas	10.4690	-85.0674	0.513001	0.000003	7.08	18.882	0.002	15.540	0.002	38.546	0.005
CR-51B	Monteverde	10.3845	-84.9025	0.513007	0.000002	7.20	18.897	0.001	15.539	0.001	38.578	0.002
CR-55	Monteverde	10.2968	-84.8349	0.512969	0.000003	6.46	19.052	0.000	15.554	0.000	38.791	0.001
CR-58	Arenal	10.4798	-84.8538	0.513025	0.000003	7.55	18.903	0.002	15.540	0.002	38.583	0.005
CR-61B	Arenal	10.4834	-84.6883	0.513010	0.000004	7.25	18.976	0.007	15.546	0.005	38.686	0.013
CR-61C	Arenal	10.4834	-84.6883	0.513011	0.000002	7.28	18.954	0.001	15.553	0.001	38.673	0.002
CR-64	Arenal	10.4603	-84.7203	0.513017	0.000004	7.39	19.016	0.004	15.566	0.003	38.768	0.009
CR-71	Chato	10.4570	-84.6419	0.513003	0.000003	7.12	18.914	0.001	15.544	0.001	38.605	0.003
CR-84	Perdidos	10.4259	-84.6797	0.513021	0.000003	7.46	19.083	0.001	15.558	0.001	38.840	0.002
Central Costa Rica Volcanic Front												
P-118	Laguna Rio Cuarto	10.3513	-84.2214	0.512963	0.000002	6.34	19.183	0.004	15.569	0.003	38.960	0.007
P-122	Maar Rio Cuarto	10.3637	-84.2357	0.512965	0.000002	6.37	19.184	0.001	15.569	0.001	38.960	0.002
P-123A	Congo	10.2685	-84.2509	0.512963	0.000002	6.34	19.181	0.002	15.567	0.002	38.942	0.005
P-124	Bosque Alegre	10.3010	-84.2073	0.512966	0.000003	6.40	19.182	0.001	15.577	0.001	38.981	0.002
P-151D	Platanar	10.3027	-84.3883	0.512958	0.000003	6.24	19.198	0.004	15.565	0.003	38.966	0.007
P-119A	Chocosuela	10.2780	-84.2644	0.512948	0.000002	6.04	19.171	0.002	15.557	0.002	38.908	0.005
P-169	Porvenir	10.2907	-84.4237	0.512967	0.000003	6.42	19.174	0.001	15.565	0.001	38.940	0.002
P-109	Poás	10.1951	-84.2305	0.512979	0.000002	6.65	19.141	0.001	15.564	0.001	38.899	0.003
P-112	Redonda cone 2	10.1189	-84.2130	0.512960	0.000002	6.28	19.173	0.001	15.567	0.001	38.879	0.002
P-113	Redonda cone 3	10.1139	-84.2148	0.512967	0.000004	6.42	19.172	0.001	15.562	0.001	38.926	0.003
P-171	Barva	10.0287	-84.0946	0.512959	0.000002	6.26	19.111	0.003	15.562	0.003	38.832	0.006
P-102C	Zurque	10.0676	-84.0058	0.512971	0.000003	6.50	19.093	0.004	15.562	0.003	38.790	0.010
P-139	Cone Oratorio	9.8976	-83.8358	0.512957	0.000002	6.21	19.114	0.001	15.570	0.001	38.833	0.002
P-140	Cone Boqueron	9.8889	-83.8541	0.512955	0.000002	6.18	19.115	0.001	15.571	0.001	38.834	0.001
P-143	Cerro Pasquí	9.9290	-83.8416	0.512958	0.000002	6.24	19.104	0.001	15.567	0.001	38.814	0.002
P-160A	Irazú	9.9783	-83.8526	0.512956	0.000002	6.20	19.108	0.001	15.565	0.001	38.809	0.002
P-162	Irazú	9.9783	-83.8527	0.512961	0.000003	6.30	19.100	0.001	15.566	0.001	38.804	0.002
P2-72	Irazú	9.9807	-83.8537	0.512958	0.000002	6.24	19.093	0.000	15.558	0.000	38.779	0.001
P-96	forearc flow	9.9766	-84.1998	0.512944	0.000004	5.97	19.143	0.001	15.562	0.001	38.877	0.002
P-97A	Turrialba	10.0211	-83.7599	0.512962	0.000002	6.32	19.080	0.002	15.563	0.001	38.769	0.003
P-149A	Turrialba	10.0929	-83.5370	0.512944	0.000002	5.97	19.144	0.001	15.560	0.001	38.880	0.002

doi: 10.1038/nature06550

Table S1.1 (cont.)

Sample #	Sample Location	Lat	Long	$^{143}Nd/^{144}Nd$	2σ	ε_{Nd}	$^{206}Pb/^{204}Pb$	2σ	$^{207}Pb/^{204}Pb$	2σ	$^{208}Pb/^{204}Pb$	2σ
Panama Pliocene-Quaternary Alkaline (<5 My)												
3-12-4-03	island west of Sona	7.4700	-82.2380	0.512983	0.000003	6.72	19.110	0.001	15.572	0.000	38.776	0.001
CP97-1	Chiriquí	8.2170	-81.5870	0.512997	0.000003	7.00	19.045	0.001	15.540	0.000	38.648	0.002
SO96-1	Sona	8.0730	-81.7320	0.512999	0.000003	7.04	19.073	0.001	15.559	0.001	38.698	0.002
M36KH	west of Sona	8.2742	-82.0377	0.512999	0.000003	7.04	19.070	0.001	15.567	0.001	38.715	0.003
M37KH	west of Sona	8.2742	-82.0377	0.513005	0.000002	7.16	19.052	0.002	15.553	0.002	38.665	0.005
M105 KH	Sona	8.2410	-81.7910	0.512995	0.000002	6.95	19.063	0.001	15.562	0.001	38.705	0.003
M 118aKH	Sona	8.1290	-81.4470	0.512989	0.000001	6.84	19.051	0.002	15.561	0.002	38.697	0.004
M121aKH	Sona	8.1880	-81.4880	0.512990	0.000005	6.87	19.079	0.001	15.565	0.001	38.731	0.002
ODP Leg 170 Gabbro Sills												
ODP170-1039c-8R03W/ 3-5cm		9.7436	-86.2016	0.512940	0.000002	5.89	19.623	0.001	15.615	0.001	39.233	0.002
ODP170-1039c-7R03/ 74-76cm		9.7436	-86.2016	0.512925	0.000002	5.60	19.608	0.001	15.626	0.001	39.243	0.002
ODP170-1040c-53R/ 96-98cm		9.8436	-86.3708	0.512960	0.000002	6.27	19.394	0.006	15.627	0.005	39.113	0.013

doi: 10.1038/nature06550

Table S1.1 (cont.)

Sample #	Sample Location	Lat	Long	$^{143}Nd/^{144}Nd$	2σ	ε_{Nd}	$^{206}Pb/^{204}Pb$	2σ	$^{207}Pb/^{204}Pb$	2σ	$^{208}Pb/^{204}Pb$	2σ
Central Costa Rica Behind the Volcanic Front (BVF) - Alkaline (≤2 My)												
CR-85	C. Mercedes	10.9764	-84.3534	0.512918	0.000003	5.47	19.225	0.001	15.564	0.000	38.993	0.001
P-152	Aquas Zarcas Buenos Aires	10.3795	-84.3046	0.512925	0.000002	5.60	19.277	0.001	15.569	0.001	39.096	0.003
P-153	AZ Juan Murillo	10.3899	-84.3241	0.512940	0.000002	5.89	19.173	0.003	15.570	0.002	38.893	0.005
P-154B	AZ Pital	10.4455	-84.2753	0.512964	0.000002	6.36	19.082	0.002	15.556	0.002	38.747	0.005
P-155A	AZ C. Chiles	10.4580	-84.3428	0.512968	0.000002	6.44	19.074	0.002	15.569	0.002	38.785	0.005
P-130A	Rio Colorado	10.7023	-83.6467	0.512971	0.000004	6.49	19.160	0.003	15.580	0.003	38.846	0.007
P-128	Rio San Juan	10.7704	-83.7962	0.512955	0.000003	6.19	19.099	0.002	15.567	0.002	38.782	0.004
P-129	Rio San Juan	10.7755	-83.7776	0.512961	0.000004	6.29	19.140	0.003	15.564	0.003	38.830	0.007
P-138	Puerto Lindo	10.5949	-83.7011	0.512978	0.000003	6.63	19.016	0.002	15.563	0.002	38.702	0.005
P-132B	Tortugero	10.5813	-83.5289	0.512956	0.000004	6.21	19.189	0.001	15.583	0.001	38.911	0.003
P-133	Tortugero	10.5813	-83.5289	0.512957	0.000004	6.23	19.177	0.001	15.566	0.001	38.869	0.002
Southern Costa Rica Pliocene-Quaternary Adakite (<5 My)												
TC-3	Talamanca	9.0907	-83.2715	0.512981	0.000002	6.69	19.006	0.001	15.544	0.001	38.663	0.001
TC-5A	Talamanca	8.8498	-82.9452	0.512973	0.000002	6.53	19.145	0.001	15.566	0.001	38.782	0.001
TC-6A	Talamanca	8.9143	-82.7877	0.512979	0.000002	6.65	19.103	0.000	15.560	0.000	38.727	0.001
TC-7	Talamanca	8.8999	-82.7894	0.512980	0.000002	6.67	19.095	0.000	15.560	0.000	38.734	0.001
TC-8	Talamanca	8.6248	-82.9178	0.512937	0.000002	5.83	19.322	0.004	15.571	0.000	38.958	0.001
Southern Costa Rica Pliocene-Quaternary BVF Alkaline (<5 My)												
P-145	Siquirres	10.0723	-83.5781	0.512980	0.000002	6.67	19.040	0.003	15.555	0.002	38.673	0.006
P-163B	Lomas Azules	10.3559	-83.5850	0.512978	0.000002	6.63	19.050	0.001	15.552	0.001	38.692	0.003
P-164	Lomas Azules	10.3753	-83.5707	0.512976	0.000004	6.60	19.036	0.003	15.558	0.002	38.679	0.006
Southern Costa Rica Miocene Volcanic Front												
EG-1	C. Asuncion	9.5761	-83.7604	0.512968	0.000019	6.43	18.653	0.004	15.523	0.003	38.241	0.007
TC-1	Jaboncillo	9.6019	-83.7880	0.513033	0.000002	7.71	18.725	0.000	15.531	0.000	38.335	0.001
TC-2	Talamanca	9.4646	-83.7095	0.513012	0.000002	7.30	18.623	0.001	15.531	0.001	38.260	0.003
TC-4	Manu de Tigre	9.0320	-83.2911	0.513011	0.000002	7.28	18.817	0.001	15.543	0.001	38.470	0.002
TC-9	Palamar Norte	8.9650	-83.4374	0.513004	0.000003	7.13	18.814	0.001	15.535	0.001	38.425	0.001
Panama Adakites (≤ 1 My)												
M44KH	Barva	9.6690	-82.6210	0.512989	0.000003	6.85	19.202	0.001	15.574	0.001	38.875	0.001
M53KH	Barva	8.7940	-82.5850	0.512948	0.000003	6.04	19.324	0.001	15.577	0.001	38.991	0.002
M55KH	Barva	8.7960	-82.4740	0.512968	0.000003	6.44	19.191	0.001	15.575	0.001	38.869	0.002
M57aKH	Tizingal Volcanic Complex	8.7960	-82.4740	0.512993	0.000002	6.93	19.119	0.001	15.561	0.001	38.770	0.003
M64c KH	Burica	8.1840	-82.8770	0.512965	0.000002	6.38	19.296	0.001	15.580	0.001	38.980	0.002
M65a KH	Chiriquí	8.4700	-82.7100	0.512970	0.000002	6.47	19.263	0.001	15.572	0.001	38.925	0.003
M99a KH		8.3400	-81.8260	0.513006	0.000002	7.18	19.069	0.001	15.557	0.001	38.697	0.002

doi: 10.1038/nature06550 SUPPLEMENTARY INFORMATION

Table S1.2.

Pb Replicate Analyses

Sample	$^{206}Pb/^{204}Pb$	$^{207}Pb/^{204}Pb$	$^{208}Pb/^{204}Pb$
P2-16	18.506	15.515	38.118
P2-16_R	18.507	15.516	38.121
Average (n=2)	*18.506*	*15.516*	*38.120*
2 sigma	*0.001*	*0.001*	*0.003*
2 sigma (ppm/amu)	*19*	*26*	*19*
P-40A	18.532	15.526	38.175
P-40A_R	18.527	15.521	38.160
Average (n=2)	*18.530*	*15.523*	*38.168*
2 sigma	*0.005*	*0.005*	*0.015*
2 sigma (ppm/amu)	*142*	*100*	*99*
P2-53	18.599	15.520	38.215
P2-53_R	18.614	15.539	38.279
Average (n=2)	*18.606*	*15.529*	*38.247*
2 sigma	*0.015*	*0.020*	*0.064*
2 sigma (ppm/amu)	*400*	*421*	*418*
CR-84	19.083	15.558	38.840
CR-84_R	19.087	15.560	38.846
Average (n=2)	*19.085*	*15.559*	*38.843*
2 sigma	*0.004*	*0.001*	*0.006*
2 sigma (ppm/amu)	*103*	*31*	*38*
P-109	19.141	15.564	38.899
P-109_R	19.142	15.555	38.874
Average (n=2)	*19.141*	*15.559*	*38.886*
2 sigma	*0.001*	*0.009*	*0.025*
2 sigma (ppm/amu)	*22*	*200*	*160*
P2-72	19.093	15.558	38.779
P2-72_R	19.093	15.558	38.779
Average (n=2)	*19.093*	*15.558*	*38.779*
2 sigma	*0.001*	*0.000*	*0.000*
2 sigma (ppm/amu)	*19*	*9*	*1*
P-152	19.277	15.569	39.096
P-152_R	19.312	15.581	39.082
Average (n=2)	*19.295*	*15.575*	*39.089*
2 sigma	*0.036*	*0.012*	*0.014*
2 sigma (ppm/amu)	*922*	*264*	*88*
P-154B	19.082	15.556	38.747
P-154B_R	19.074	15.551	38.719
Average (n=2)	*19.078*	*15.554*	*38.733*
2 sigma	*0.008*	*0.005*	*0.028*
2 sigma (ppm/amu)	*206*	*118*	*179*
P-130A	19.160	15.580	38.846
P-130A_R	19.134	15.555	38.771
Average (n=2)	*19.147*	*15.567*	*38.808*
2 sigma	*0.026*	*0.024*	*0.075*
2 sigma (ppm/amu)	*679*	*524*	*484*

doi: 10.1038/nature06550 SUPPLEMENTARY INFORMATION

Table S1.2. Pb Replicate Analyses (cont.)

Sample	$^{206}Pb/^{204}Pb$	$^{207}Pb/^{204}Pb$	$^{208}Pb/^{204}Pb$
P-133	19.177	15.566	38.869
P-133_R	19.166	15.561	38.838
Average (n=2)	*19.172*	*15.563*	*38.854*
2 sigma	*0.012*	*0.005*	*0.031*
2 sigma (ppm/amu)	*302*	*108*	*198*
TC-3	19.006	15.544	38.663
TC-3_R	19.000	15.540	38.643
Average (n=2)	*19.003*	*15.542*	*38.653*
2 sigma	*0.006*	*0.004*	*0.020*
2 sigma (ppm/amu)	*161*	*88*	*131*
TC-5A	19.145	15.566	38.782
TC-5A_R	19.156	15.581	38.830
Average (n=2)	*19.150*	*15.573*	*38.806*
2 sigma	*0.011*	*0.015*	*0.048*
2 sigma (ppm/amu)	*281*	*315*	*307*
TC-7	19.095	15.560	38.734
TC-7_R	19.088	15.554	38.711
Average (n=2)	*19.091*	*15.557*	*38.722*
2 sigma	*0.007*	*0.006*	*0.023*
2 sigma (ppm/amu)	*179*	*134*	*148*
AVERAGE ERRORS (N=13)			
2 sigma (abs)	*0.008*	*0.009*	*0.027*
2 sigma (ppm/amu)	*223*	*186*	*173*

Nd Replicate Analyses

Sample	$^{143}Nd/^{144}Nd$
P-40A	0.513084
P-40A_R	0.513075
Average (n=2)	*0.513079*
2 sigma	*0.000009*
2 sigma (ppm)	*17*
P-152	0.512925
P-152_R	0.512919
Average (n=2)	*0.512922*
2 sigma	*0.000006*
2 sigma (ppm)	*12*
P-132B	0.512956
P-132B_R	0.512948
Average (n=2)	*0.512952*
2 sigma	*0.000008*
2 sigma (ppm)	*15*
TC-5A	0.512973
TC-5A_R	0.512974
Average (n=2)	*0.512973*
2 sigma (abs)	*0.000001*
2 sigma (ppm)	*2*
AVERAGE ERROR (N=4)	
2 sigma	*0.000006*
2 sigma (ppm)	*12*

doi: 10.1038/nature06550 nature

SUPPLEMENTARY INFORMATION

Supplementary Information Section 2

Shear-wave splitting observations

The TUCAN Broadband Seismic Experiment, funded by the NSF-MARGINS program, was in the field from July 2004 through March 2006, and included 48 broadband stations (borrowed from the IRIS/PASSCAL program) in a fore-arc, back-arc, and two cross-arc lines with station spacing of 10-50 km (Fig. S2.1). The very dense cross-arc lines provide excellent resolution in the mantle wedge beneath Costa Rica and Nicaragua.

We measured well-resolved shear-wave splitting parameters in 791 local S waves recorded by the TUCAN array and three permanent global stations (IRIS/GSN station JTS, GEOFON station BOA, and GEOSCOPE station HDC). These data show strong variations in both fast direction and splitting time, but when measurements are broken down in terms of similar paths, coherence emerges, making this dataset a good candidate for tomographic inversion. For example, shallow events that sample the wedge corner produce splitting in which fast directions are arc-normal and then rotate to arc-parallel towards the volcanic arc (Fig. S2.2a). In addition, the majority of measurements to stations in the back-arc line (Fig. S2.2b) show fast directions which are roughly parallel to the arc, with the exception of a prominent group of arc-normal fast directions in the northwest portion of the array and sparser arc-normal measurements in the southeast.

Additional views of the anisotropy model

The three-dimensional anisotropy model shown in this study (Figures 3 and S2.3) is one realization of a damped, linearized, least squares inversion of the shear-wave splitting data. This model minimizes data-model misfit, and contains structure characteristic of most of the inversions obtained during testing (i.e., with different damping, starting model, crystallographic symmetry). Effective block size in the model is intentionally variable to account for less dense sampling of back-arc and deeper model regions. This is accomplished by requiring model perturbations to be equal in certain groups of model blocks (outlined in black in Figure S2.4) in later inversion iterations.

Anisotropy with largely arc-parallel *a*-axes dominates in much of the mantle wedge (depths of roughly 50-150 km), although a zone of arc-normal *a*-axes occurs in the wedge beneath the

doi: 10.1038/nature06550 SUPPLEMENTARY INFORMATION

NW end of the array (right in Fig. S2.3). Arc-parallel anisotropy is also present in the deepest model layer, but lies too close to the slab interface to be clearly attributed to the wedge. Assuming typical development of crystallographic orientation, *a*-axes should align roughly parallel to flow in the wedge beneath the arc and back-arc. In contrast, olivine *a*-axis alignment normal to the flow direction has been observed experimentally at hydrated, low temperature, and high stress conditions[5,40], but should be a factor only in the cold wedge corner[6] trenchward of the slab surface at roughly 70 km depth. In our model, the arc-parallel *a*-axes extend into the mantle wedge well beyond the shallow wedge corner where the B-type olivine fabric may exist[6]. Corroborated by the Pb isotope data, we associate this overall pattern of anisotropy with along-arc flow towards the NW, rather than with anomalous crystallographic preferred orientation fabrics influenced by melt[14]. The rotation of the along-arc *a*-axes to a more arc-normal orientation at the NW end of the arc occurs where geochemical evidence for the Galapagos seamount component is nearly absent. These *a*-axes may represent a transition to more arc-normal flow in the wedge, although this hypothesis cannot be fully tested with existing data due to a drop-off in sampling at the NW end of the TUCAN array.

Additional References

40. Jung, H., Katayama, I., Jiang, Z., Hiraga, T. & Karato, S. Effect of water and stress on the lattice-preferred orientation of olivine, *Tectonophysics* **421**, 1-22 (2006).

doi: 10.1038/nature06550 SUPPLEMENTARY INFORMATION

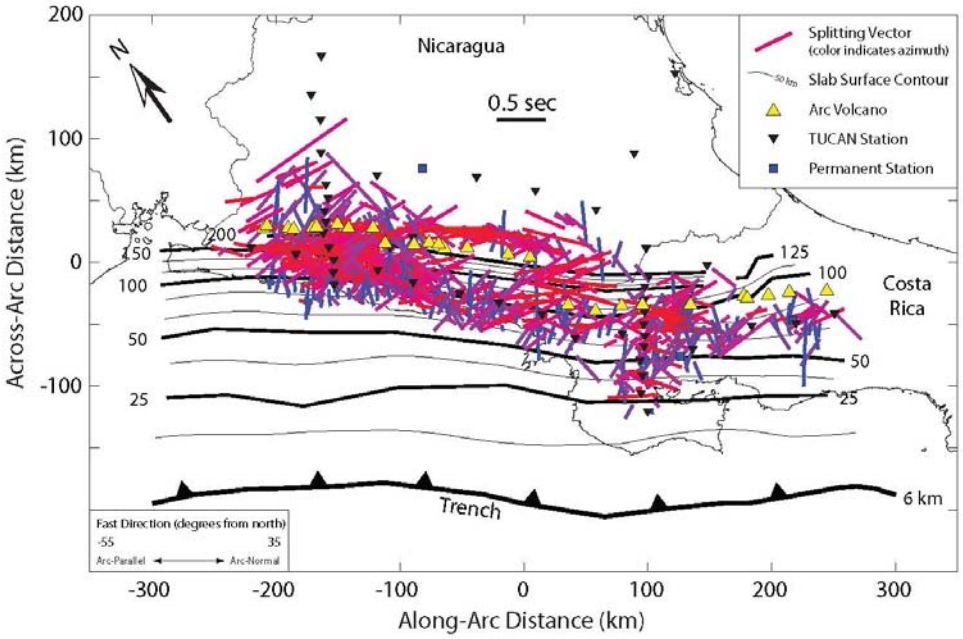

Figure S2.1. Shear-wave splitting measurements, plotted at ray-path midpoints, that were used to invert for the model of anisotropy shown in Figures 3 and S2.3. The vectors overlap, with splitting measurements from deeper events plotting below those from shallow events. The color scheme is used to help distinguish between different fast direction azimuths. When viewed all together, a dominant orientation is difficult to discern, except in the central Nicaraguan back-arc where arc-parallel fast directions are more prevalent.

doi: 10.1038/nature06550 SUPPLEMENTARY INFORMATION

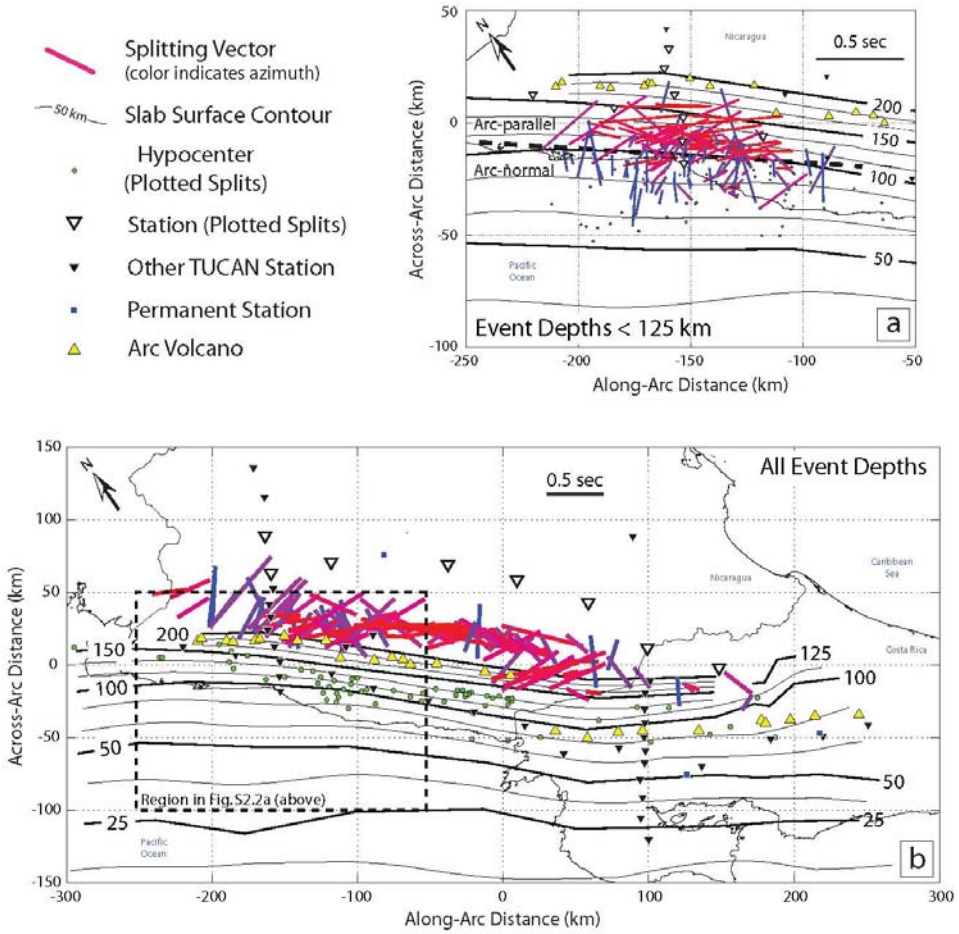

Figure S2.2. Subsets of the shear-wave splitting measurements show greater coherence than the entire dataset (Fig. S2.1). The larger inverted empty black triangles represent the stations at which the splits shown were measured. (a) In NW Nicaragua, for splits from shallow (<125 km) events, a relatively sharp transition (thick dashed line) occurs between arc-normal fast direction closer to the trench and arc-parallel fast directions towards the arc. This pattern is predicted for along-arc flow and B-type fabric in the cold wedge corner[5,6], but is the inverse of what would be expected for 2-D corner flow (i.e., arc-parallel close to the trench and changing to arc-normal in the arc and back-arc). (b) Across the central Nicaraguan back-arc region, fast directions are strongly arc-parallel, while more oblique fast directions are observed to the NW and SE.

doi: 10.1038/nature06550 SUPPLEMENTARY INFORMATION

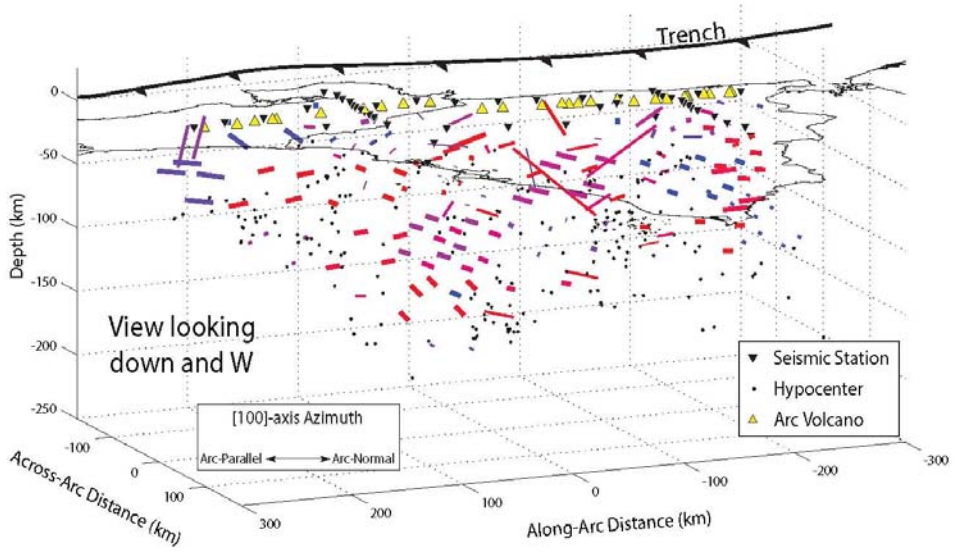

Figure S2.3. Three-dimensional model of anisotropy obtained by inverting local S splitting measurements. Each vector shows the orientation of the olivine *a*-axis in an olivine-orthopyroxene mantle, and its length indicates the strength of anisotropy relative to its single crystal value. Blocks are 25^3 km cubes, although blocks in back-arc regions are made effectively larger by setting their perturbations equal in the later stages of the iterative inversion. Vector thickness corresponds to formal resolution values obtained for the parameters in each block; results are shown only when the resolution of each model parameter in a block exceeds 0.5. Anisotropy vectors at depths of 50-150 km largely lie in the mantle wedge and are roughly oriented parallel to the arc, except in NW Nicaragua.

doi: 10.1038/nature06550 SUPPLEMENTARY INFORMATION

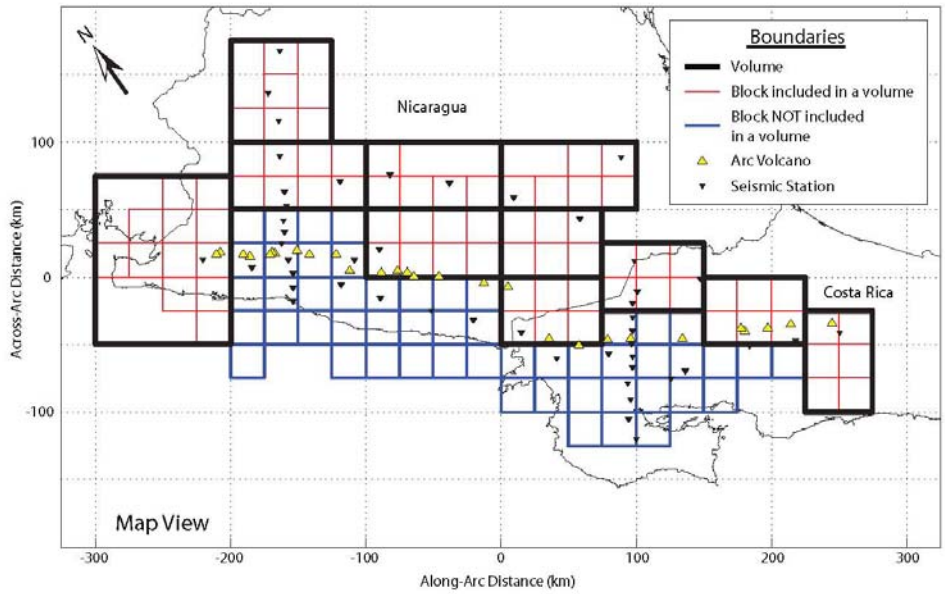

Figure S2.4a. Map-view of individual model blocks (red and blue) and larger back-arc model volumes (black) used in the in the inversion. Beneath much of the fore-arc and arc, model parameters in individual 25^3 km model blocks are well-resolved (blue). Individual model blocks that lack sufficient resolution for interpretation (red) are found in the back-arc regions of the model space, and we force many of these blocks to act as larger model "volumes" (outlined in black). This is accomplished by determining average model parameters for all blocks in a volume at an intermediate iteration, and then requiring that model parameter changes are equal for all blocks in volume in later iterations. The coarsening of model discretization in this manner produces better resolved model parameters for the volume, and allows us to confidently interpret the model in a larger portion of the mantle wedge, although the minimum spatial scale at which anisotropy can be resolved is increased. The lateral extent of these larger volumes does not vary in depth, however the actual number of blocks in each that are sampled by ray paths in the dataset does. In the map view shown here, only blocks sampled by ray paths in the dataset are shown, and in the models resulting from the inversion (Figures 3 and S2.3), only *a*-axes in well-resolved model blocks are displayed.

doi: 10.1038/nature06550

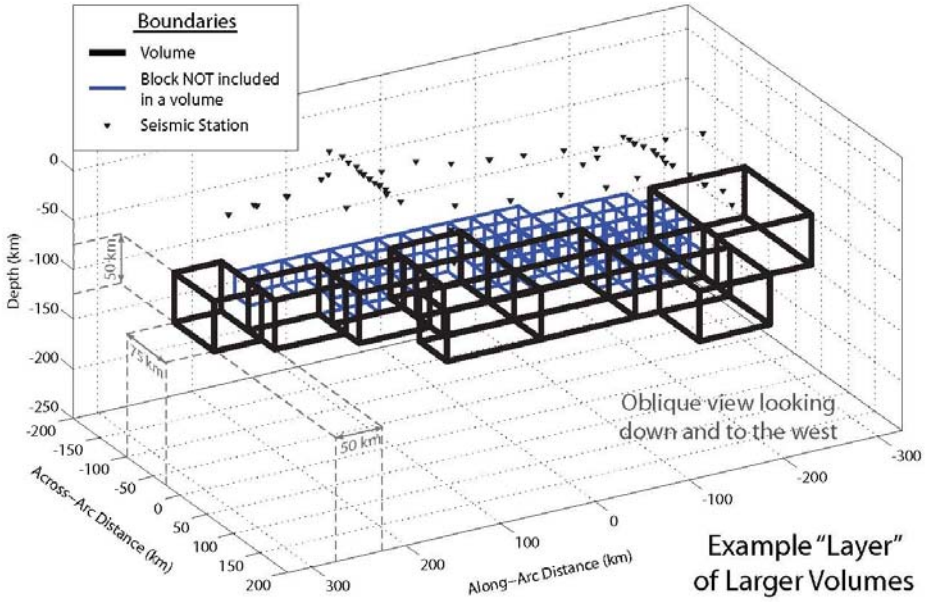

Figure S2.4b. Three-dimensional view of individual model blocks and larger back-arc model volumes used in the inversion. Except for the top layer of 25^3 km model blocks, the larger volumes are each 50 km thick (i.e., containing two layers of blocks) and have different lateral dimensions. The far left block, for example, is 50 km by 75 km. In this view the red blocks are not shown in order to improve visibility of the independent (blue) blocks.

Appendix A

Curriculum Vitae

Dipl. Geol. Ken Heydolph

Born on 24.11.1973 in Kiel

(Schleswig-Holstein)/ Germany
Three children: Ronja (Nov. 2004)
Bente (May 2006)
Mads (June 2009

Address

Eckernförder Str.79
24116 Kiel, Germany

Work Address

Leibniz-Institute of Marine Sciences
IFM-GEOMAR
East Shore Campus, Wischhofstr. 1-3
D-24148 Kiel, Germany
Phone: +49 431 600 2564
Fax: +49 431 600 2924

Referees

Prof. Kaj A. Hoernle,
Leibniz-Institute of Marine Sciences
IFM-GEOMAR
Research Division 4 “Dynamics of the Ocean Floor”
Wischhofstr. 1-3
D-24148 Kiel/ Germany

Tel.: +49 431 6002642; khoernle@ifm-geomar.de

Dr. Reinhard Werner
Leibniz-Institute of Marine Sciences
IFM-GEOMAR
Research Division 4 “Dynamics of the Ocean Floor”
Wischhofstr. 1-3
D-24148 Kiel/ Germany
Tel.: +49 431 6001416; rwerner@ifm-geomar.de

Employment

Jan. 2005	Research assistant at the Collaborative Research Center (SFB) 574 “Volatiles and Fluids in Subduction Zones”, Chair of Prof. Dr. Kaj A. Hoernle at the Leibniz Institute of Marine Sciences, IFM-GEOMAR, Kiel/ Germany
2003 – 2004	Freelancer at Tethys Geoconsulting GmbH at the Leibniz Institute of Marine Sciences, IFM-GEOMAR, Kiel/ Germany (Geochemistry, Chair of Dr. Reinhard Werner)
1999 – 2003	Student assistant at the Leibniz Institute of Marine Sciences, IFM-GEOMAR, Kiel/ Germany (Geochemistry, Chair of Prof. Dr. Hans-Ulrich Schmincke)

Education

Jan. 2005	Ph.D. Geochemistry at the Collaborative Research Center (SFB) 574 “Volatiles and Fluids in Subduction Zones: Climate Feedback and Trigger Mechanisms for Natural Disasters” at the Christian Albrechts University of Kiel
2005	Diploma in Geology/ Palaeontology (supervisor: Prof. Dr. Hoernle, Dr. Werner) Petrology of the Campbell Plateau and the geochemical evolution of the Dunedin Volcano
2002	Pre-diploma in Geology/ Palaeontology
1998 – 2005	Studies of Geology/ Palaeontology Christian-Albrechts-University zu Kiel/ Germany

1995 – 1997	Studies of Material Sciences, Christian-Albrechts- University zu Kiel/ Germany
1995	Abitur, Bildungszentrum Mettenhof, Kiel

Work experiences

work as a research assistant at IFM-GEOMAR

Major and trace elements and Sr-Nd-Hf-Pb-O isotopes in volcanic rocks and minerals
Petrology and geochemistry in subduction zones and intra-plate settings
Petrology and geochemical modeling
Processing of geochemical datasets (e.g. Excel)
Presentation of scientific results on meetings, workshops and conferences
Good skills in graphics
Thorough knowledge of measuring radiogenic isotopes
using TIMS (Triton and MAT 262) and MC-ICPMS
(Axiom) and major and trace element measuring using
EMPA (Cameca and Jeol microrpobes) techniques.
Thorough knowledge of working in clean labs (including chemical separation of Sr, Nd, Pb, Hf)
Skills in XRF, ICP-MS
Experience with Multibeam (SIMRAD) seafloor mapping

additional experiences

June 2007	Co-organizer of the 1. Summer School for Marine Geosciences at the IFM-GEOMAR
Since 2005	supervision of student apprentices
2002 – 2003	scholarship of the German Academic Exchange Service (DAAD) for a study visit in Dunedin, University of Otago, New Zealand

Participation on several seagoing expeditions

2009	Joides Resolution, Exp 324: Shatsky Rise (Testing plume and plate models of oceanic plateau formation at Shatsky Rise,

	northwest Pacific Ocean ; inorganic geochemist (analysis, interpretation and presentation of ICP-AES and XRD data)
2008	RV SONNE, SO199, CHRISP (Christmas Island seamount Province); shift leader for a dredge crew, selection, preparation and detailed description (e.g. petrography, alteration and mineral content) of volcanic and sedimentary rock samples; seafloor mapping using SIMRAD multi echo beam
2003	RV SONNE, SO169, Zealandia (New Zealand microcontinent); selection, preparation and detailed description (e.g. petrography, alteration and mineral content) of volcanic and sedimentary rock samples; seafloor mapping using SIMRAD multi echo beam
2001	RV SONNE, SO160, GARIMAG (Gravity and Magnetic Investigations at the Fossil Spreading Axis of the Galapagos Rise) selection, preparation and detailed description (e.g. petrography, alteration and mineral content) of volcanic and rock samples
1998-2001	several short expeditions with RV Alkor

Publications

Papers

- Hoernle, K., D. L. Abt, K.M. Fischer, H. Nichols, F. Hauff, G.A. Abers, P.v.d. Bogaard, **K. Heydolph**, G. Alvarado, M. Protti, W. Strauch (2008). "Arc-parallel flow in the mantle wedge beneath Costa Rica and Nicaragua." Nature 451(7182): 1094-1097.

- **Heydolph, K**.; Hoernle, K.; Hauff, F.; Bogaard, P.v.d. (to be submitted): Along- and across-arc geochemical variations in northwestern Central America: Increased contribution of enriched lithosphere to lavas along the volcanic front from Nicaragua to Guatemala and behind the volcanic front.

- **Heydolph, K**.; Hoernle, K.; Hauff, (to be submitted): Along-arc geochemical variations in southwestern Central America (Panama to Nicaragua): Source constraints from Hf isotopes

Presentations

- **Heydolph, K**.; Hoernle, K.; Hauff, F.; Bogaard, P.v.d.:
Source components for NW Central American Volcanic Arc lavas

Talk: International Conference and 97th Annual Meeting of the Geologische Vereinigung e.V. (GV): "The Oceans in the Earth System", 01.10.2007

- **Heydolph, K.**; Hoernle, K.; Hauff, F.; Bogaard, P.v.d.:
Continental crust as a source component for NW Central American Arc lavas?

Talk: Goldschmidt Conference 2007, 19.08.2007

- **Heydolph, K.**; Hoernle, K.; Hauff, F.; Bogaard, P.v.d.:
Crustal source components for NW Central American Volcanic Arc lavas

Talk: Workshop to Integrate Subduction Factory and Seismogenic Zone Studies in Central America, 18.06.2007

- **Heydolph, K**.; Hoernle, K.; Hauff, F.; Bogaard, P.v.d.,; Sadofsky, S.:
Potential Source Components for NW Central American Arc Lavas

Talk: LAK 2007: 20th Colloquium on Latin American Earth Sciences, 11.04.2007

- **Heydolph, K.**; Hoernle, K.; Hauff, F.; Bogaard, P.v.d.,; Sadofsky, S.:
Enriched Isotopic Composition of the NW Central American Volcanic Arc: Crustal Contamination or a Sediment Slab Melt?

Talk: Goldschmidt Conference 2006, 27.08.2006

- **Heydolph, K.**; Hoernle, K.; Hauff, F.; Bogaard, P.v.d.:
The potential role of subducted sediment melts on the NW Central American Volcanic Arc volcanism

Talk: Geochemie-Tagung 2006, 14.06.2006